

**STRUCTURAL MODIFICATION OF CLUSIANONE FROM *Garcinia parvifolia* AND *IN VITRO* EVALUATION TARGETING
MICROTUBULE SYSTEM OF RESPIRATORY CARCINOMA CELLS**



SREE VANEESA D/O NAGALINGAM

SCHOOL OF PHARMACY

FACULTY OF SCIENCE

**Thesis submitted to the University of Nottingham for the degree of
Doctor of Philosophy (PhD) in Pharmacy**

ABSTRACT

Clusianone isolated from *Garcinia parvifolia* has been studied for its anticancer properties and cytotoxicity to human respiratory cells. The clusianone was first isolated using solvent extraction, column chromatography, thin layer chromatography and finally recrystallization method through solvent evaporation including seed crystal to induce crystal growth of clusianone. The clusianone was characterized using X-ray crystallography, ESI-MS, NMR and melting point. During the course of this research, clusianone was chemically modified and eight different derivatives abbreviated as CMet, CHyd, CMxA, CMeA, CEtA, CPryl, CGeryl and CDMet were obtained. Some of the chemical methods employed were hydrogenation, methylation, demethylation, ketone reduction *via* addition of amine derivatives and *O*-alkylation to install additional prenyl and geranyl chain into clusianone. Further studies of the role of the clusianone derivatives were presented in its *in vitro* anticancer activity. The anticancer test and cytotoxicity effect were tested using MTT(3-(4,5-dimethylthiazol-2-yl)-2,5-diphenyltetrazolium bromide) assay. Specific normal human and cancer cell lines were used in the assay being MRC5 (lung fibroblast), A549 (lung adenocarcinoma), NP69 (nasopharyngeal epithelial cell and HK1 (squamous carcinoma of the nasopharynx). Preliminary study of clusianone and derivatives showed cytotoxicity effect in dose dependent manner. Based on the results, clusianone and compound CMeA demonstrated good anticancer activity showing IC₅₀ values below 5 μ M against A549 and HK1 cancer cells and at the same time affecting less of the MRC5 and NP69 normal cells. Western blot method was employed to further elucidate the downregulation of the protein expression of β -tubulin including cell cycle regulators Cdk1 and cyclin B1 for clusianone and CMeA derivative treated carcinoma cells. Clusianone and compound CMeA demonstrated potential antimicrotubule agent characteristic since expression of β -tubulin and cell cycle regulators Cdk1/cyclin B1 were downregulated in A549 cells. As for HK1 cells, clusianone downregulated β -tubulin protein without affecting Cdk1 and cyclin B1 expression. In contrast, compound CMeA showed prominent downregulation of β -tubulin, CDK1 and cyclin B1 proteins especially after 48 hours treatment in HK1 cells.

ACKNOWLEDGEMENT

I would like to express my deepest gratitude to my parents, grandparents, sister and brothers for their unconditional love, patience, understanding and support throughout the study. Without their continued support and interest, this thesis would not have been the same as presented here.

In preparing this thesis, I was in contact with many experienced, people, researchers, academicians, and practitioners. They have contributed towards my understanding and thoughts. In particular, I wish to express my appreciation to my supervisor, Dr. Khoo Teng Jin for help, critics and funding for my research. Most important thanks to Ministry of Higher education for sponsoring MyBrain15 scholarship for my postgraduate study. My warm thanks to my cosupervisor Dr. Kok Wai Ling for guidance and exceptional ideas. Thanks to our collaborator from UPM Dr. Mohamed Ibrahim Mohamed Tahir for X-ray crystallography instrumentation utilization and expertise. Many thanks to my friends Chiang Michelle, Suraya Abdul Sani, Tan Hooi Sin, Low Kit Yee, Tan Yew Fung, Kamal, Fasihi and Chua Chong Kuan for your help, guidance, advices and motivation. I'm grateful to those friends who made my daily life a lot more fun and less stressful research environment.

We would like to thank Dr. Alan Khoo Soo-Beng from Institute of Medical Research and Prof. Tsao George Sai-Wah from the University of Hong Kong for providing the NP69 & HK1. My sincere appreciation to Dr. Chew Yen Seng from USM and Dr. Lam Kok Wai from UKM for their help on NMR service. Formal thanks to collaborators from the UK campus Prof. Moody and Dr. Martyn Inman. I would like to thank Miss Renu, pharmacist from Ipoh Specialist Hospital for in depth consultation regarding chemotherapy drugs. My deepest appreciation to administrative staff, senior technicians and technicians in the Faculty of Science for their valuable help. Special thanks to our senior technician, En. Wan Abdul Ghani for having the skills and courage of climbing tree for my plant collection task in Sungai Congkak.

TABLE OF CONTENT

ABSTRACT	i
ACKNOWLEDGEMENT	ii
LIST OF FIGURES	xii
LIST OF TABLES	xiii
LIST OF SCHEMES	xv
LIST OF APPENDICES	xvi
SYMBOLS AND ABBREVIATIONS	xvi
 CHAPTER 1: ANTICANCER COMPOUNDS FROM NATURAL PRODUCTS	
1.0 Cancer	1
1.1 Types of respiratory related carcinoma and its causes	2
1.1.1 Lung cancer	3
1.1.2 Nasopharyngeal cancer	4
1.2 Chemotherapy drugs for cancer treatment	6
1.3 Problem statement	8
1.4 Aim and objective of the research	9
1.5 Research scopes	10
1.6 Significant of the research	11
 CHAPTER 2: LITERATURE REVIEW	
2.0 Clusiaceae family Plants	12
2.1 <i>Garcinia parvifolia</i> (Miq.) Miq	14
2.2 Chemistry of PPAP	17
2.3 Biosynthesis hypothesis of PPAP	18
2.4 Anticancer effects of PPAP from Clusiaceae	22

2.5	Clusianone (29) type B PPAP	27
2.5.1	Isolation and optimization of clusianone (29) from Clusiaceae family Plants	29
2.5.2	Bioactivity of clusianone (29) and its epimer	30
2.5.2.1	Chemopreventive and anticancer activity	30
2.5.2.2	Anti HIV properties	32
2.6	Antimicrotubule agents derived from natural product <i>via</i> chemical modification	33
2.7	Biological and Pharmacological role of microtubule	39
2.7.1	Tubulin function	40
2.7.2	β -tubulin isotypes and roles in cancer cells	41
2.8	Antimicrotubule agents from natural product and mechanism of action	42
2.8.1	The binding site of anti-microtubular drug on β -tubulin	45
2.9	Phases of cell cycle and cell cycle regulators	47
2.9.1	Cdk's and cell cycle regulation checkpoints	49
2.9.2	Cyclin B1-Cdk complex and the G2/M checkpoint	51

CHAPTER 3 : MATERIALS AND METHODS

3.1	General Procedures for chemistry experiments	54
3.1.1	Plant Sample	55
3.1.2	Maceration of <i>Garcinia parvifolia</i> (Miq.) Miq.	55
3.1.3	Extraction and isolation of Clusianone (29) from leaves of <i>Garcinia parvifolia</i> (Miq.) Miq.	56
3.1.4	Recrystallization of clusianone (29)	59
3.2	Preparation of clusianone (29) derivatives	60
3.2.1	Preparation of CMet (53) [(1 <i>S</i> , 5 <i>S</i> , 7 <i>R</i>)-3-benzoyl-4-methoxy-8,8-dimethyl-1,5,7-tris(3-methylbut-2-en-1-yl)bicyclo[3.3.1]non-3-ene-2,9-dione <i>via</i> methylation]	60

3.2.2	Preparation of CHyd (54) [(1 <i>S</i> , 5 <i>S</i> , 7 <i>R</i>)-3-benzoyl-1,5,7-triisopentyl-4-methoxy-8,8-dimethylbicyclo[3.3.1]non-3-ene-2,9-dione]	61
3.2.3	Preparation of CMxA (55) [(1 <i>S</i> , 5 <i>R</i> , 7 <i>R</i>)-3-benzoyl-4-hydroxy-9-(methoxy-imino)-8,8-dimethyl-1,5,7-tris(3-methylbut-2-en-1-yl) bicyclo[3.3.1]non-3-en-2-one]	62
3.2.4	Preparation of CMeA (56) [(1 <i>S</i> , 5 <i>R</i> , 7 <i>R</i>)-3-benzoyl-4-hydroxy-8,8-dimethyl-1,5,7-tris(3-methylbut-2-en-1-yl)-9-(methylimino)bicyclo[3.3.1]non-3-en-2-one]	63
3.2.5	Preparation of CEtA (57) [(1 <i>S</i> , 5 <i>R</i> , 7 <i>R</i>)-3-benzoyl-9-(ethylimino)-4-hydroxy-8,8-dimethyl-1,5,7-tris(3-methylbut-2-en-1-yl)bicyclo[3.3.1]non-3-en-2-one]	64
3.2.6	Preparation of CPryl (58) [(1 <i>S</i> , 5 <i>S</i> , 7 <i>R</i>)-3-benzoyl-8,8-dimethyl-1,5,7-tris(3-methylbut-2-en-1-yl)-4-((3-methylbut-2-en-1-yl)oxy)bicycle[3.3.1]non-3-ene-2,9-dione]	65
3.2.7	Preparation of CGeryl (59) [(1 <i>S</i> , 5 <i>S</i> , 7 <i>R</i>)-3-benzoyl-4-(((<i>Z</i>)-3,7-dimethylocta-2,6-dien-1-yl)oxy)-8,8-dimethyl-1,5,7-tris(3-methylbut-2-en-1-yl)bicycle[3.3.1]non-3-ene-2,9-dione]	66
3.2.8	Preparation of CDMet (60) [(1 <i>S</i> , 5 <i>S</i> , 7 <i>R</i>)-3-benzoyl-4-hydroxy-1,5,7-triisopentyl-8,8-dimethyl bicycle[3.3.1]non-3-ene-2,9-dione]	67
3.3	Summary of synthesis result	68
3.4	X-ray crystallography analysis using crystal software	69
3.5	HPLC method analysis for purity content test	70
3.6	General Procedures for biological experiments	70
3.6.1	Respiratory cell lines for cytotoxicity testing	71
3.6.2	Sub culturing mammalian	72
3.6.3	Cryopreservation of mammalian cells and cell thawing	73
3.6.4	Cell counting	74

3.6.5	MTT 3 - (4,5-dimethylthiazol-2-yl)-2,5-diphenyltetrazolium bromide cell viability assay	75
3.6.4.1	Data analysis for MTT assay	76
3.6.6	Phase contrast inverted microscope study of cell morphology	77
3.6.7	Western Blotting for protein analysis	78
3.6.7.1	Protein extraction from carcinoma cell	78
3.6.7.2	SDS PAGE and immunoblotting	80
3.6.7.3	Densitometry for protein concentration analysis	84

CHAPTER 4 : RESULTS AND DISCUSSION ISOLATION OF CLUSIANONE AND SYNTHESIS OF CLUSIANONE DERIVATIVES

4.1	Isolation and optimization of clusianone (29)	85
4.1.1	Recrystallization of clusianone (29) through crystal seeding and slow evaporation method	87
4.1.2	Characterization of clusianone (29)	89
4.2	Synthesis of clusianone (29) derivatives	99
4.2.1	Synthesis of CMet (53) [(1 <i>S</i> , 5 <i>S</i> , 7 <i>R</i>)-3-benzoyl-4-methoxy-8,8-dimethyl-1,5,7-tris(3-methylbut-2-en-1-yl)bicyclo[3.3.1]non-3-ene-2,9-dione <i>via</i> methylation]	104
4.2.2	Synthesis of CHyd (54) [(1 <i>S</i> , 5 <i>S</i> , 7 <i>R</i>)-3-benzoyl-1,5,7-triisopentyl-4-methoxy-8, 8-dimethylbicyclo[3.3.1]non-3-ene-2,9-dione]	112
4.2.3	Synthesis of CMxA (55) [(1 <i>S</i> , 5 <i>R</i> , 7 <i>R</i>)-3-benzoyl-4-hydroxy -9-(methoxy-imino)-8,8-dimethyl-1,5,7-tris (3-methylbut-2-en-1-yl) bicyclo[3.3.1]non-3-en-2-one]	117
4.2.4	Synthesis of CMeA (56) [(1 <i>S</i> , 5 <i>R</i> , 7 <i>R</i>)-3-benzoyl-4-hydroxy-8,8-dimethyl-1,5,7-tris (3-methylbut-2-en-1-yl) -9-(methylimino)bicyclo[3.3.1]non-3-en-2-one]	123
4.2.5	Synthesis of CEtA (57) [(1 <i>S</i> , 5 <i>R</i> , 7 <i>R</i>)-3-benzoyl-9-(ethylimino)-4-hydroxy-8,8-dimethyl- 1,5,7-tris (3-methylbut-2-en-1-yl)bicyclo[3.3.1]non-3-en-2-one]	129

4.2.6	Synthesis of CPryl (58) [(1 <i>S</i> , 5 <i>S</i> , 7 <i>R</i>)-3- benzoyl-8,8 -dimethyl-1,5,7-tris(3-methylbut-2-en-1-yl)-4-((3-methylbut -2-en-1-yl)oxy)bicycle[3.3.1]non-3-ene-2,9-dione	130
4.2.7	Synthesis of CGeryl (59) [(1 <i>S</i> , 5 <i>S</i> , 7 <i>R</i>)-3-benzoyl -4-(((<i>Z</i>)-3,7-dimethylocta-2,6-dien-1-yl)oxy)-8,8 -dimethyl-1,5,7- tris(3-methylbut-2-en-1-yl)bicycle [3.3.1] non-3-ene-2,9-dione]	135
4.2.8	Synthesis of CDMet (60) [(1 <i>S</i> , 5 <i>S</i> , 7 <i>R</i>)-3-benzoyl -4-hydroxy-1,5,7-triisopentyl-8,8-dimethyl bicycle [3.3.1]non-3-ene-2,9-dione]	140
4.3	TLC analysis for compound CMxA (55), CMeA (56) and CEtA (57)	141
4.4	HPLC analysis of selected compound for purity analysis	143
4.5	Summary of synthesis of clusianone (29) derivatives	145

CHAPTER 5 RESULTS AND DISCUSSION

BIOLOGICAL ACTIVITY OF CLUSIANONE AND DERIVATIVES

5.1	Cytotoxicity testing on respiratory cells lines using MTT assay	148
5.1.1	Cytotoxicity of clusianone (29) against MRC5, A549, NP69 and HK1 cells	151
5.1.2	Cytotoxicity of CMet (53) against MRC5, A549, NP69 and HK1 cells	152
5.1.3	Cytotoxicity of CHyd (54) against MRC5, A549, NP69 and HK1 cells	153
5.1.4	Cytotoxicity of CMxA (55) against MRC5, A549, NP69 and HK1 cells	154
5.1.5	Cytotoxicity of CMeA (56) against MRC5, A549, NP69 and HK1 cells	155
5.1.6	Cytotoxicity of CEtA (57) against MRC5, A549, NP69 and HK1 cells	156
5.1.7	Summary of cytotoxicity results	157

5.2	Morphology changes in treated A549 and HK1 cells	161
5.3	Mode of action pathway studies of clusianone (29) and CMeA (56) treated against A549 and HK1 cells through immunostaining	167

CHAPTER 6 CONCLUSIONS & RECOMENDATION FOR FUTURE STUDIES

6.1	Conclusions	178
6.2	Recommendation for future studies	181

APPENDICES

Appendix A	184
Appendix B	184
Appendix C	185
Appendix D	185
Appendix E	186
Appendix F: Publication	189
Appendix G: Publication	200

REFERENCES	204
-------------------	------------

LIST OF FIGURES

Figure 1.1	The location both adenocarcinoma of the lung and nasopharynx carcinoma	4
Figure 2.1	<i>G. parvifolia</i> tree in Sg.Congkak, Selangor	14
Figure 2.2	Type A,B and C PPAP's	26
Figure 2.3	The sources of anticancer drugs over the period 01/1981-12/2010	33
Figure 2.4	β -tubulin isotypes mRNA expressed in the respective tissues calculated and displayed in bar graphs.	41
Figure 2.5	Polymerization of microtubule	44
Figure 2.6	The different anticancer drug binding sites on microtubule causing disassembly and destabilization of microtubule polymerization.	44
Figure 2.7	Taxol binding site to N-terminal 31 amino acids of β -tubulin using the PrGen software to develop the minireceptor model.	46
Figure 2.8	The cell cycle phases (G ₀ , G ₁ , S, G ₂ and M) and the different stages of M phase during the cell replication.	48
Figure 2.9	The correlation between the cell cycle regulators Cdk1/Cyclin complex in different cell cycle phases.	50
Figure 3.1	Images of <i>G. parvifolia</i> (Miq.) Miq. leaves.	56
Figure 3.2	Isolation of clusianone (29)	58
Figure 3.3	Standard curves using the microassay procedure with BSA standards	79
Figure 3.4	Electro blot transfer of protein on polyacrylamide gel to nitrocellulose membrane using wet transfer method	81
Figure 4.1	Clusianone (29) crystal morphology through solvent evaporation	89
Figure 4.2	Crystal growth through seed crystal	89

Figure 4.3	FT-IR Spectrum of clusianone (29)	90
Figure 4.4	Clusianone (29) in crystal packing unit P2 ₁ 2 ₁ 2 ₁ form	92
Figure 4.5	ESIMS of clusianone (29) from <i>G. parvifolia</i>	94
Figure 4.6	Fragmentation of clusianone (29) predicted from the ESIMS	95
Figure 4.7	¹ H NMR spectra of clusianone (29)	96
Figure 4.8	¹³ C NMR spectra of clusianone (29)	97
Figure 4.9	ESIMS of compound CMet (53)	104
Figure 4.10	¹ H NMR spectra of compound CMet (53)	106
Figure 4.11	¹³ C NMR spectra of compound CMet (53)	107
Figure 4.12	CMet (53) crystal morphology through solvent evaporation	110
Figure 4.13	Compound CMet (53) in crystal packing unit P1 form	110
Figure 4.14	ESIMS of compound CHyd (54)	112
Figure 4.15	¹ H NMR and ¹³ C NMR spectra of compound CHyd (54)	114
Figure 4.16	¹³ C NMR spectra of compound CHyd (54)	115
Figure 4.17	ESIMS of compound CMxA (55)	118
Figure 4.18	¹ H NMR spectra of compound CMxA (55)	120
Figure 4.19	¹³ C NMR spectra of compound CMxA (55)	121
Figure 4.20	ESIMS of compound CMeA (56)	123
Figure 4.21	¹ H NMR spectra of compound CMeA (56)	126
Figure 4.22	¹³ C NMR spectra of compound CMeA (56)	127
Figure 4.23	ESIMS of compound CEtA (57)	129
Figure 4.24	ESIMS of compound CPryl (58)	130
Figure 4.25	¹ H NMR spectra of compound CPryl (58)	132
Figure 4.26	¹³ C NMR spectra of compound CPryl (58)	133
Figure 4.27	ESIMS of compound CGeryl (59)	135
Figure 4.28	¹ H NMR spectra of compound CGeryl (59)	137
Figure 4.29	¹³ C NMR spectra of compound CGeryl (59)	138
Figure 4.30	ESIMS of compound CDMet (60)	140

Figure 4.31	TLC images of compounds CMxA (55), CMeA (56) and CEtA (57)	142
Figure 4.32	Purity percentage of compounds	144
Figure 5.1	Graph showing the change in cell death with increasing clusianone (29) concentration in MRC5, A549, NP69 and HK1 cells after 48 hours treatment.	151
Figure 5.2	Graph showing the change in cell death with increasing CMet (53) concentration in MRC5, A549, NP69 and HK1 cells after 48 hours treatment.	152
Figure 5.3	Graph showing the change in cell death with increasing CHyd (54) concentration in MRC5, A549, NP69 and HK1 cells after 48 hours treatment.	153
Figure 5.4	Graph showing the change in cell death with increasing CMxA (55) concentration in MRC5, A549, NP69 and HK1 cells after 48 hours treatment.	154
Figure 5.5	Graph showing the change in cell death with increasing CMeA (56) concentration in MRC5, A549, NP69 and HK1 cells after 48 hours treatment.	155
Figure 5.6	Graph showing the change in cell death with increasing CEtA (57) concentration in MRC5, A549, NP69 and HK1 cells after 48 hours treatment.	156
Figure 5.7	Morphology changes of carcinoma cell A549 and HK1 cells treated with clusianone (29)	163
Figure 5.8	Morphology changes of carcinoma cell A549 and HK1 cells treated with CMeA (56)	165
Figure 5.9	A549 cells treated at IC ₅₀ of clusianone (29) and protein extraction harvested after 8, 16, 24 and 48 hours for Western blot analysis	169
Figure 5.10	HK1 cells treated at IC ₅₀ of clusianone (29) and protein extraction harvested after 8, 16, 24 and 48 hours for	171

	Western blot analysis.	
Figure 5.11	A549 cells treated at IC ₅₀ of CMeA (56) and protein extraction harvested after 8, 16, 24 and 48 hours for Western blot analysis.	173
Figure 5.12	HK1 cells treated at IC ₅₀ of CMeA (56) and protein extraction harvested after 8, 16, 24 and 48 hours for Western blot analysis.	175

LIST OF TABLES

Table 2.1	Classification of genera in the Clusiaceae	13
Table 3.1	Gradient solvent system for dichloromethane extract	57
Table 3.2	Summary of the synthesis results	68
Table 3.3	Data collection and structure refinement details	69
Table 3.4	List of normal cells and cancer cell tested	71
Table 3.5	Four day routine of MTT assay in the cytotoxicity study	76
Table 3.6	Formulation of stacking gel and resolving gel	80
Table 3.7	Details of monoclonal antibodies used in immunoblotting	83
Table 4.1	X-ray crystallography structure including crystals parameters of clusianone (29)	91
Table 4.2	¹³ C NMR of clusianone (a/b)	98
Table 4.3	¹ H NMR of clusianone (29)	98
Table 4.4	IUPAC names for clusanone (a/b) and derivatives	103
Table 4.5	¹ H NMR of compound CMet (53)	108
Table 4.6	¹³ C NMR of compound CMet (53)	108
Table 4.7	X-ray crystallography structure including crystals parameters of compound CMet (53)	109
Table 4.8	¹ H NMR of compound CHyd (54)	116
Table 4.9	¹³ C NMR of compound CHyd (54)	116
Table 4.10	¹ H NMR of compound CMxA (55)	122
Table 4.11	¹³ C NMR of compound CMxA (55)	122
Table 4.12	¹³ C NMR and ¹ H NMR of compound CMeA (56)	128
Table 4.13	¹³ C NMR and ¹ H NMR of compound CPryl (58)	134
Table 4.13	¹³ C NMR and ¹ H NMR of compound CGeryl (59)	139
Table 4.15	HPLC spectra for selected compound (Absorbance at 254 nm)	143
Table 5.1	IC ₅₀ values of clusianone (29) interpolated from figure	151

	then converted to μM using molecular weight of 502.69.	
Table 5.2	IC_{50} values of CMet (53) interpolated from figure above then converted to μM using molecular weight of 516.712.	152
Table 5.3	IC_{50} values of CHyd (54) interpolated from figure above then converted to μM using molecular weight of 521.75.	153
Table 5.4	IC_{50} values of CMxA (55) interpolated from figure above then converted to μM using molecular weight of 531.73.	154
Table 5.5	IC_{50} values of CMeA (56) interpolated from figure above then converted to μM using molecular weight of 515.73.	155
Table 5.6	IC_{50} values of CEtA (57) interpolated from figure above then converted to μM using molecular weight of 529.75.	156
Table 5.7	Cytotoxicity IC_{50} (μM) of clusianone (29) and derivatives against MRC5, A549, HK1 and NP69 cells.	157

LIST OF SCHEMES

Scheme 2.1	Biosynthesis of MPAPs	20
Scheme 2.2	Proposed cyclization of MPAPs in formation of type A and type B PPAPs	20
Scheme 2.3	Biosynthetic hypothesis of PPAP's	21
Scheme 3.1	Methylation of clusianone (29)	60
Scheme 3.2	Hydrogenation of clusianone (29)	61
Scheme 3.3	Methoxyamine addition of clusianone (29)	62
Scheme 3.4	Methylamine addition of clusianone (29)	63
Scheme 3.5	Ethylamine addition of clusianone (29)	64
Scheme 3.6	Prenylation of hydroxyl group of clusianone (29)	65
Scheme 3.7	Geranylation of hydroxyl group of clusianone (29)	66
Scheme 3.8	Demethylation on CHyd (54)	67
Scheme 4.1 a)	Synthesis reaction of clusianone (29) in tautomer forms and derivatives in tautomer forms obtained	100
Scheme 4.1 b)	Synthesis reaction of clusianone (29) in tautomer forms and derivatives in tautomer forms obtained	101
Scheme 4.1 c)	Synthesis reaction of clusianone (29) in tautomer forms and derivatives in tautomer forms obtained	102
Scheme 4.2	Reaction mechanism for the methylation reaction of Clusianone (29)	105
Scheme 4.3	Addition elimination reaction mechanism of C=O in the formation of oxime compound	117
Scheme 4.4	Reaction mechanism for the methylamine addition reaction to clusianone (29)	125

LIST OF APPENDICES

Appendix A	12% SDS-PAGE showing protein bands of A549 cells stained with Coomassie Blue.	184
Appendix B	A549 cells treated with compound CMeA (56) and proteins transferred from SDS-PAGE to nitrocellulose membrane and incubated with β -tubulin polyclonal antibody.	184
Appendix C	Proteins transferred from SDS-PAGE to nitrocellulose membrane and incubated with β -tubulin monoclonal antibody.	185
Appendix D	Protein quantification method using Quantity One Bio-Rad software and further statistical analysis to quantify total protein stains based on optical density value.	185
Appendix E	Table of total synthetic clusianone (29) derivatives by other synthetic research group and the derivatives tested for anticancer activities.	186
Appendix F	Publication	189
Appendix G	Publication	200

SYMBOLS AND ABBREVIATIONS

δ	Chemical Shifts
δ_H	Proton chemical Shifts
δ_C	chemical Shifts
λ	Wavelength
$[\alpha]_D$	Specific rotation
$[M+H]^+$	Protonated molecular ion
$[M+Na]^+$	Molecular ion with sodium adduct
$[2M+H]^+$	Protonated dimer molecular ion
$[2M+Na]^+$	Dimer molecular ion with sodium adduct
$\mu\text{g/ml}$	Micro gram per microlitre
μL	Microlitre
μM	Micromolar
ax	Axial
calcd.	Calculated
eq	Equatorial
<i>s</i>	Singlet
<i>d</i>	Doublet
<i>t</i>	Triplet
<i>m</i>	Multiplet
hr	Hour
mg	Miligram
mmol	Milimoles
ppm	Parts per million
mAb	Monoclonal antibody
kDa	Kilo Dalton
rel. int.	Relative intensity
v/v	Volume to volume ratio
ACN	Acetonitrile
APS	Ammonium Persulphate
ATP	Adenosine 5' TriPhosphate

BSA	Bovine Serum Albumin
CDK/Cdk	Cyclin Dependent Kinase
DNA	Deoxyribose Nucleic Acid
DMSO	Dimethyl sulfoxide
EC ₅₀	Half maximal effective concentration
EDTA	Ethylenediaminetetraaceticacid
ELISA	Enzyme-Linked Immunosorbent assay
Et ₂ O	Diethyl ether
EtOAc	Ethyl acetate
ESIMS	Electron spray ionisation mass spectrum
FBS	Fetal Bovine Serum
FTIR	Fourier Transform Infrared Spectroscopy
H ₂	Hydrogen gas
H ₂ O	Water
HCl	Hydrochloride Acid
IC ₅₀	Half maximal inhibitory concentration
MgSO ₄	Magnesium Sulphate
Me ₂ SO ₄	Dimethyl sulfide
MIC	Minimum Inhibitory concentration
K ₂ CO ₃	Potassium Carbonate
NSCLC	Non-small cell lung cancer
OD	Optical density
Pd/C	Paladium on carbon
RPMI	Rosewell Park Memorial Institute medium
SDS	Sodium Dodecyl Sulphate
Si gel	Silica gel
TEMED	N', N , N' , N' – Tetramethylethylenediamine
UNMC	University of Nottingham Malaysia Campus
¹ H NMR	Proton-Nuclear Magnetic Resonance
¹³ C NMR	Carbon-13 Nuclear Magnetic Resonance

CHAPTER 1: ANTICANCER COMPOUNDS FROM NATURAL PRODUCTS

1.0 Cancer

Cancer is a disease whereby the normal cells divide uncontrollably resulting in the formation of masses of tissue known as tumours. Consequently, the out of control cell proliferation not only forms into a lump form but may also spread to another organ *via* blood circulatory system leading to metastasis. In this case, the tumour is known as malignant tumour which results in cancer. Tumours which do not metastasize or lack the ability to invade neighbouring tissues are called benign tumours. Benign tumours are non-cancerous since they are self-limiting, non-invasive and have a slower growth rate compared to malignant tumours (Kufe *et al.*, 2003).

The occurrence of cells dividing uncontrollably is linked to the mutations to DNA which subsequently cause damage to the genes which is an essential key component in cell division. There are four types of genes which govern cell division progress and process which are oncogenes initiating cell division, tumour suppressor genes preventing cells from dividing, suicide genes controlling cell death *via* apoptosis and finally DNA-repair genes instructing a cell to repair damaged DNA (Visvader, 2011).

The severity of cancer is classified in stages: 0, I, II, III and IV with the higher scale indicating cancer has progressively moved to a severe stage. Stage 0 indicates patients detected at an early stage of cancer whereby few cells growth is diagnosed. Subsequent stages I, II, III and IV are classified based on the tumour size, aggressiveness related to the growth of cancer and finally to which extent the cancer has spread to the neighbouring tissues or even to

different organs of the patient. Patients diagnosed with a stage IV cancer will go through severe pain due to obstruction of airway or blood vessels, alteration or malfunction of organ, fever, fatigue, weight loss and eventually die (Provencio *et al.*, 2011).

Cancers are now second to cardiovascular diseases with an estimation of 13% of total deaths each year with the most common being: lung cancer (1.4 million deaths), stomach cancer (740,000 deaths), liver cancer (700,000 deaths), colorectal cancer (610,000 deaths) and breast cancer (460,000 deaths) (Lalla *et al.*, 2008). As such, invasive cancer has been the leading cause of death in both developed country and developing country. Based on the demographic changes studies in low-income and middle-income countries, the occurrence of cancer is expected to elevate from 13.3 to 21.4 million cases between 2010 and 2030 (McCormack & Boffetta, 2011).

1.1 Types of respiratory related carcinoma and its causes

Respiratory related cancers and diseases are becoming one of the most alarming health conditions in mankind. Lung cancer is currently the highest incident compared to other types of cancers and also the major cause of death related to cancer cases both in men and women worldwide (Cancer Research UK, 2011). Majority cases of lung cancers are carcinomas that derive from epithelial cells and are known as primary lung cancers. However, failure to provide early treatments will consequently spread the deadly cells *via* metastasis invading nearby tissue or other parts of the body which are known as secondary lung cancer. Some of the causative factors contributing to respiratory related cancers are tobacco smoking, air pollution and haze phenomena by rapid

industrialization, open burning, automobile exhaust, exposure to radon gas and asbestos. Cancer of the lung and bronchus (all cell types), larynx, nasal cavity, paranasal sinuses and nasopharynx are associated with both tobacco smokers and exposure to second-hand tobacco smoke. The carcinogenic agents in the tobacco smokes are polycyclic aromatic hydrocarbons, *N*-nitrosamines, 1,3-butadiene, benzene, aromatic amines and various aldehydes (Cogliano *et al.*, 2011). In this research project, the lung adenocarcinoma cells (A549) and the novel squamous nasopharynx cells (HK1) have been specifically selected since clusianone (29) has never been tested against respiratory carcinoma cell lines. Both A549 and HK1 cells overexpress human growth factor receptor (*EGFR*) (Stabile *et al.*, 2005; Ma *et al.*, 2010).

1.1.1 Lung cancer

Lung cancer can be identified by observing their morphology and appearance under the microscope. Generally, there are two main types of lung cancers commonly known as non-small cell lung cancer and small cell lung cancer. Non-small cell lung cancer (NSCLC) accounts for 80-85% of lung cancers while small cell lung cancer accounts for the remaining 15-20% (Goulart *et al.*, 2001).

Lung adenocarcinoma (**Figure 1.1**) accounts for 40% of the lung cancer cases with 15% and 10% of five years survival rates of these cases respectively, in the United States and Europe (Parkin *et al.*, 2002). Several options are available to treat lung cancer such as surgery, radiation, chemotherapy and targeted therapy. Patients treated with chemotherapy will be treated with two combinations of drugs which are a combination of one platinum based drug and

other commonly used drugs such as paclitaxel, docetaxel, etoposide, vinorelbine, gemcitabine and pemetrexed. This type of chemotherapy is also known as chemotherapeutic drug cocktails. The platinum-based chemotherapy drug used is either cisplatin or carboplatin drug which is widely used in the treatment of advanced non-small cell lung carcinoma (Bareschino *et al.*, 2011).

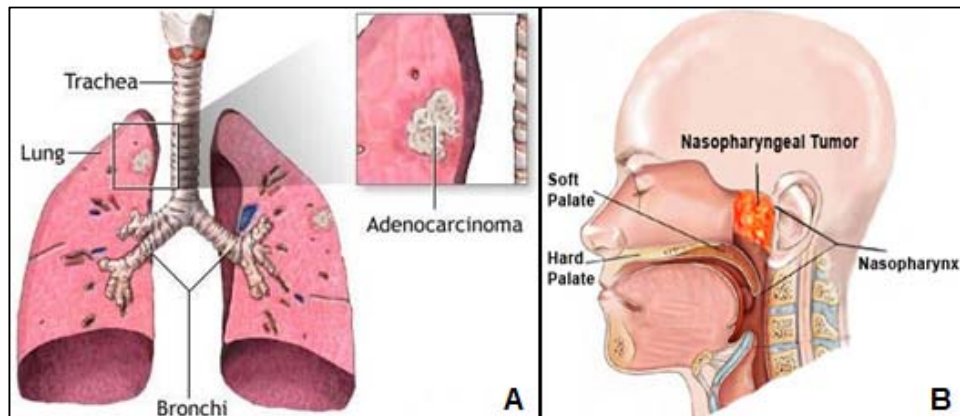


Figure 1.1 The location of both adenocarcinoma of the lung (A) and nasopharynx carcinoma (B) from (Chen, 2012)

1.1.2 Nasopharyngeal cancer

Nasopharyngeal carcinoma (NPC) is a type of malignant neoplasm arising from the mucosal epithelium of the nasopharynx, which is located at the entrance of the Eustachian tube (**Figure 1.1**). It is also generally classified as head and neck cancer type. Nasopharyngeal cancer is very predominant in Southern China (including Hong Kong) and also prevalent in South East Asian countries. The World Health Organization classifies nasopharyngeal carcinoma into three types namely squamous cell carcinoma, non-keratinizing carcinoma

and undifferentiated carcinoma. Elderly generation affected by NPC are most likely to be affected by squamous cell carcinoma. Similarly to lung cancer cells, these nasopharyngeal carcinoma cells have the tendency to metastasize and normally spreads to cervical lymph nodes (Brennan, 2006).

One of the main contributors of NPC is the consumption of salted preserved fish which is consumed in several regions around the world especially in the different areas of Southern China. The over expression of epidermal growth factor receptor (*EGFR*) are observed in some NPC cells and can be linked to being the contributing factor of the cancer (Ma *et al.*, 2010). Some studies confirmed that there is a link between NPC and human leukocyte antigen profile. A study reported the affected siblings in Singapore having a 20-fold risk for NPC because they were identified with a gene locus close to human leukocyte antigen (Parkin *et al.*, 2002). A type of virus known as EBV (Epstein-Barr virus) is also associated with particular forms of NPC including other types of cancers such as Hodgkin's lymphoma and Burkitt's lymphoma (Maeda *et al.*, 2009).

An association between EBV infection and this cancer is complex and not many researches have been conducted to completely understand the link between the EBV and NPC. However, one possible mechanism to link between the salted fish consumption includes the formation of *N*-nitrosamines and other *N*-nitroso compounds during the processing of the fish and/or endogenously after ingestion in the human body. There was also experimental data indicating salted fish extracts which can reactivate EBV in latently infected cells *in vitro* (Secretan *et al.*, 2009).

NPC is treated by using surgery, radiation and chemotherapy and targeted therapy. A number of drugs have been tested and approved for the treatment of NPC such as gemcitabine, capecitabine, oxaliplatin as well as platinum based drug cisplatin. Cisplatin is used together with another drug such as 5-fluorouracil (5-FU) even after radiation therapy for better eradication of the remaining cancer cells in a patient's body. Similarly to the treatment of NSCLC, patients diagnosed with NPC can be treated with targeted therapy utilizing cetuximab monoclonal antibodies (Chan, 2010).

1.2 Natural products for cancer treatment

Terrestrial plants have been used as disease treatment by humans thousands of years ago, ever since our ancestors have been chewing on herbs to relieve from pain or sufferings from diseases. It is estimated that only 10% of the 250,000-300,000 plants all over the world have been investigated for the presence of bioactive compounds (McChesney *et al.*, 2007). By 1992, it was reported that the National Cancer Institute (NCI) managed to screen 33,000 plant extracts and found 3 plant extracts that were active against antitumour activity. In addition to the screening activity, many efforts were also made to improve the methods used to screen the cytotoxicity effect of these plant extracts against various tumour cell lines (Rates, 2001).

By 1995, NCI successfully prepared 40,000 plants extracts and 18,000 extracts were tested for antitumour activity. In addition, the biodiversity of our country tropical rainforest gives us more opportunity to discover the various secondary metabolites which could have potential cancer fighting mechanism.

Over the last few decades, scientists have utilized different methods of synthesis including total synthesis, semi-synthesis and combinatorial chemistry to produce lead compounds that are natural product inspired. This makes structural derivatives selection for the new drug easier since natural product-lead compounds most often possess 'drug-like features'. Some drugs were chemically modified from its originally isolated plant lead compound and showed a stronger effect compared to its original compound when tested against antitumour activity (Rates, 2001).

1.3 Problem statement

The current state of research on clusianone (29) emphasizes the total synthesis of clusianone (29) involving 30-40 reaction steps with low yield production. Furthermore, natural product research in the optimization of clusianone (29) from plant extracts using expensive high speed counter-current chromatography afforded high yield of clusianone (29) with only 90% purity. Unfortunately, the limited supply of high purity (> 98%) clusianone (29) prevented further potential anticancer activity and clusianone (29) derivatives development. The isolation of clusianone (29) from the leaves of *G. parvifolia* has made the optimization method a lot more efficient and sustainable since it was present more abundantly as compared to other parts of Clusiaceae plant. This potentially allowed the discovery of clusianone (29) derivatives as cytotoxic compounds.

To date, potential anticancer pathway studies of clusianone (29) were performed on HepG2 cells which were estrogen receptor (*ER*) positive cells. It was also postulated that clusianone (29) interaction with estrogen receptor (*ER*) may have contributed to apoptosis *via* intrinsic pathway in HepG2 cells. However in this research, male derived lung cells A549 and nasopharyngeal cells HK1 were specifically selected since these cells expressed almost insignificant estrogen receptors (*ER*) compared to cells derived from female cells. These A549 and HK1 cells overexpress human growth factor receptor (*EGFR*). Since type B PPAP compounds have been demonstrating inhibitory activity of tubulin assembly of carcinoma cells, mode of action of clusianone (29) and derivatives were further studied as antimicrotubule agents.

1.4 Aims and objectives of the research

Based on the problem statements, the research has been performed with the following specific objectives:

- 1) Optimization of high purity (> 98%) clusianone (29) from leaves of *G.parvifolia* through recrystallization method.
- 2) To synthesize clusianone (29) derivatives with less than 2 step reaction with more than 50% yield and to characterize the derivatives using ESI-MS, X-ray crystallography, ^1H NMR and ^{13}C NMR spectroscopic methods.
- 3) To evaluate cytotoxicity and study the structure-activity relationship of clusianone (29) and derivatives on MRC5 (lung fibroblast), A549 (lung adenocarcinoma), NP69 (immortalized nasopharyngeal epithelial cell and HK1 (squamous carcinoma of the nasopharynx) using MTT (3-(4, 5-dimethylthiazol-2-yl)-2, 5-diphenyltetrazolium bromide) assay.
- 4) To determine the downregulation of protein expression of β -tubulin, Cdk1 and cyclin B1 by clusianone (29) and potent derivatives treated cancer cells using Western blot method.
- 5) To propose affinity and type of interaction of the inhibitors of clusianone (29) and potent derivative towards microtubule system of cancer cell lines and determine the cell cycle arrest triggered by the inhibitor of clusianone (29) and potent derivative by studying the cell cycle regulators expression.

1.5 Research scopes

There are three main research approaches performed in order to study the potential anticancer pathway of clusianone (29) and derivatives.

The first approach was the extraction, isolation and optimization of the amount of clusianone (29) that can be obtained from the leaves of *G. parvifolia*. The isolation was carried out by successive Si gel gravity column chromatography which involves chlorophyll removal step with the aid of vacuum liquid chromatography. Subsequent fraction purification through recrystallization was to afford high purity (>98%) clusianone (29).

The second approach was to conduct structure modification to clusianone (29) by using straightforward synthetic steps by means of small scale reaction conditions. Characterization of clusianone (29) and derivatives was performed using spectroscopy methods including electron spray ionisation mass spectrometry and nuclear magnetic resonance. Structure elucidation using X-ray diffraction method was employed for compounds obtained in crystal forms. The clusianone (29) derivatives ideally produced in good yield (>50%) were studied for cytotoxic activities.

The third approach was to screen the cytotoxic potential activities of clusianone (29) and potent derivatives against MRC5 (lung fibroblast), A549 (lung adenocarcinoma), NP69 (immortalized nasopharyngeal epithelial cell and HK1 (squamous carcinoma of the nasopharynx) using MTT (3-(4,5-dimethylthiazol-2-yl)-2,5-diphenyltetrazolium bromide) assay. Pathway studies were conducted using Western blot method to investigate the biological property of clusianone (29) and potent derivative as antimicrotubule agents.

Western blot method was employed to further elucidate the downregulation of the protein expression of β -tubulin including cell cycle regulators Cdk1 and cyclin B1 in clusianone (29) and potent derivative treated carcinoma cells.

1.6 Significant of the research

The significant of the research was the development of imine derivative of clusianone (29) which have led to the discovery of potent CMeA (56) as antimicrotubule agent. Most of the published papers on structure-activity relationship of PPAP compounds were addressing hydroxyl group as the main functional group contributing to its potential cytotoxic activity. Focus of this study was to introduce amine functional group into clusianone (29) structure and enhance current clusianone (29) potential anticancer activities. The results obtained from biological tests revealed clusianone (29) as a potential antimicrotubule agent. Furthermore, the research provides information regarding the respiratory carcinoma cell death occurrence by clusianone (29) and CMeA (56). Overall, this research has provided the insights of clusianone (29) and CMeA (56) being a potential antimicrotubule agent since expression of β -tubulin and cell cycle regulators Cdk1 and cyclin B1 were downregulated and consequently signifying cell death *via* apoptosis occurring upon cell cycle arrest at G2/M phase.

CHAPTER 2: LITERATURE REVIEW

2.0 Clusiaceae family plants

Plants in the Clusiaceae family are abundance source of phytochemicals particularly secondary metabolites with various biological activities (Acuña *et al.*, 2009). The major classes of secondary metabolites have been isolated from these plants are xanthones, coumarins and benzophenones. The Clusiaceae comprises of 36 genera and around 1610 species which are mainly distributed throughout the tropics, although plants in a few genera are found in temperate regions. The previously segregated genera *Rheedia*, *Ochrocarpus*, *Pentaphalangium* and *Tripetalum* are now accepted as part of genus *Garcinia* (Table 2.1) (Gustafsson *et al.*, 2014). The presence of latex is a common character of this family. The Clusiaceae is comprised of three subfamilies: the Kielmeyeroideae, the Hypericoideae, and the Clusioideae.

The genus *Garcinia* includes more than 250 species of dioecious trees and shrubs with pantropical distribution, with its center of diversity in Southeast Asia and Madagascar. The floral characters exhibit a high variability in this genus, thus taxonomical issues arise when studying these plants. A broad concept of the genus was supported by a recent molecular phylogenetic study, including a geographically, morphologically, and taxonomically comprehensive sampling (Sweeney, 2008). To date, research has shown that extracts of the *Garcinia* genus particularly *G. mangostana* (Moongkarndi *et al.*, 2004), *G. cowa* (Deharo & Ginsburg, 2011), *G. atroviridis* (Mackeen *et al.*, 2000) and *G. parvifolia* (Syamsudin *et al.*, 2007) exhibit diverse biological

activities such as antibacterial, antioxidant, antiinflammatory, antitumor-promoting, cytotoxic, antimalarial, and antiplasmodial.

Table 2.1 Classification of genera in the Clusiaceae modified from (Gustafsson *et al.*, 2014)

A. Subfamily Kielmeyeroideae Engler	<u>Tribe Calophylleae</u> Choisy <i>Neotatae</i> Maguire <i>Marila</i> Swarzt <i>Mahurea</i> Aublet <i>Kielmeyera</i> Martius <i>Caraipa</i> Aublet <i>Haplocathra</i> Bentham <i>Poeciloneuron</i> Beddome <i>Mesua</i> L. <i>Kayea</i> Wall <i>Mammea</i> L. <i>Calophyllum</i> L.	<u>Tribe Endodesmieae</u> Engler <i>Endodesmia</i> Bentham <i>Lebrunia</i> Staner
B. Subfamily Hypericoideae Engler	<u>Tribe Vismieae</u> Choisy <i>Vismia</i> Vand <i>Harungana</i> Lamarck <u>Tribe Cratoxyleae</u> <i>Bentham</i> <i>Cratoxylum</i> Blume <i>Eliea</i> Cambess	<u>Tribe Hyperiaceae</u> Choisy <i>Hypericum</i> L. <i>Lianthus</i> N.Robson <i>Triadenum</i> Raf. <i>Thornea</i> (Breedlove & Mc.Clintock) <i>Santomasia</i> N.Robson
C. Subfamily Clusioideae Engler	<u>Tribe Clusielleae</u> (P.F.Stevens) <i>Clusiella</i> Planch. & Triana <u>Tribe Clusieae</u> Choisy <i>Clusia</i> L. <i>Dystovomita</i> D'Arcy <i>Tovomita</i> Aublet <i>Chrysochlamys</i> Poepp. <i>Tovomitidium</i> Ducke <u>Tribe Garcinieae</u> Choisy <i>Garcinia</i> L. <i>Penthalangium</i> Warb. <i>Rheedia</i> L. <i>Tripetalum</i> K.Schum. <i>Allanblackia</i> Oliver <i>Ochrocarpus</i> Thouars	<u>Tribe Symhoniae</u> Choisy <i>Pentadesma</i> Sabine <i>Moronobea</i> Aublet <i>Platonina</i> Martius <i>Montrouziera</i> Planch & Triana <i>Lorostemon</i> Ducke <i>Thysanostemon</i> Maguire <i>Symphonia</i> L.f.

2.1 *Garcinia parvifolia* (Miq.) Miq

G. parvifolia's is also known as 'asam kandis' in Malaysia. The species of *Garcinia* is found mainly in Kalimantan, Indonesia including other world tropics such as Thailand, Peninsular Malaysia, Sumatera, Java, Borneo (Sarawak, Brunei, Sabah and Kalimantan), Celebes, Moluccas and New Guinea. It is a sub-canopy tree reaching 25 meters tall with green leaves and yellow/orange fruit (**Figure 2.1**). Young *G. parvifolia* leaves are used in Indonesian cooking and the fruit is edible. The leaves grow to a length of 3.5 cm-17 cm long with the width in the range of 2.0-7.0 cm and petiole length from 0.5-1.5 cm (Lim, 2012).



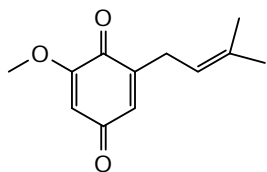
Figure 2.1 (A) *G. parvifolia* tree in Sg.Congkak, Selangor. (B) Pink flower of *G. parvifolia* plant and (C) yellow pale orange fruit of *G. parvifolia* from (Lim, 2012).

Some species have been used as traditional medicines and have been shown to contain isoprenylated xanthenes and bioflavonoids. Crude extracts of some parts of *G. parvifolia* such as roots, stem bark, fruit and leaf, can be dissolved in various organic solvents such as ethanol, hexane, methanol and ethyl acetate. The crude extracts of these plants were screened for anticancer, antibacterial, antioxidant and antiplasmodial activities (Lim, 2012). To date, the leaf extract of *G. parvifolia* has afforded significant amount of novel prenylated depsidones compounds which demonstrated good cytotoxic activity (Xu *et al.*, 2000).

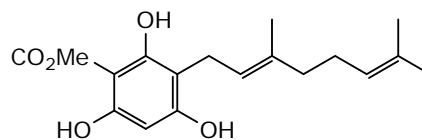
Some studies using the stem bark and root extracts of this plant have shown to have strong bioactivity such as antiplasmodial and antibacterial activities particularly against *Staphylococcus aureus* (Syamsudin *et al.*, 2007). Phytochemical studies on leaves of *G. parvifolia* has led to the further discovery of new benzoquinone derivative namely parvifoliquinone (1) and other six known compounds which include two phloroglucinols, depsidones, flavonoid, xanthone and benzopyran derivative. These compounds were further tested on methicillin- resistant *Staphylococcus aureus* (MRSA) and parvifoliol B (2) showed potential antibacterial activity with a MIC of 32 µg/mL (Rukachaisirikul *et al.*, 2008).

Two known xanthenes, parvixanthenes A (3) and rubraxanthone (4) isolated from *G. parvifolia* exhibited cytotoxic to L1210 murine leukemic cells with the IC₅₀ values in the range of 3-8 µg/mL (Kardono, 2006). Apart from this other compounds isolated from this species includes xanthenes: rubraxanthone (4), triterpenoids: α -amyrin (5) (Ee & Cheow, 2007), daphnifolin (6), benzophenone: isoxanthochymol (7) (Ee *et al.*, 2009). Rubraxanthone (4)

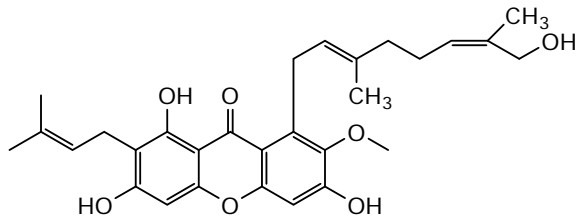
was found to exhibit strong lethal dose activity against the larvae of *Aedes aegypti* and human promyelocytic leukemia cells (HL60).



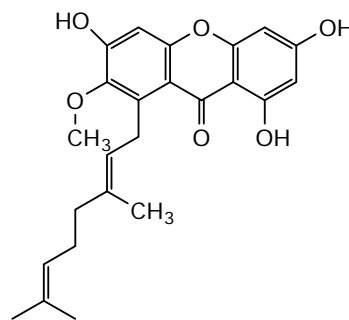
(1)



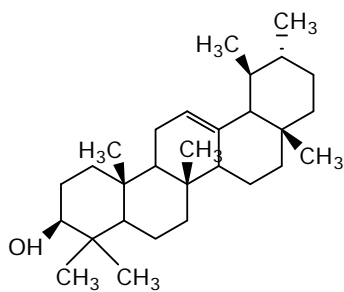
(2)



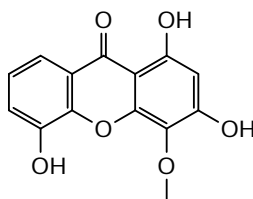
(3)



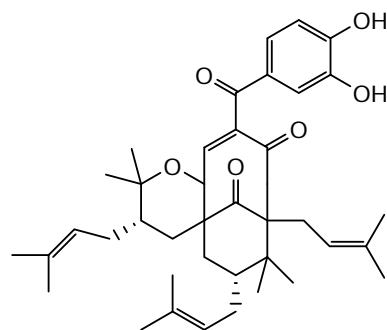
(4)



(5)



(6)



(7)

2.2 Chemistry of PPAP (Polycyclic polyprenylated acylphloroglucinols)

PPAPs consists of a bicyclo[3.3.1]nonane-2,4,9-trione skeleton surrounded by substituents made up of several prenyl and geranyl groups including an acyl group. There are further classified as PPAP type A (8), B (9) and C (10) by the relative position and configuration of the substituents that possesses one common central bicyclo[3.3.1]nonane-2,4,9-trione core as shown in (Figure 2.2) (Biber *et al.*, 2011). Since these benzophenones have a few prenyl groups attached to central bicyclo [3.3.1] nonane-2,4,9-trione, they exert hydrophobicity characteristic and are known to be non-polar phenolic compounds (Ciochina & Grossman, 2006).

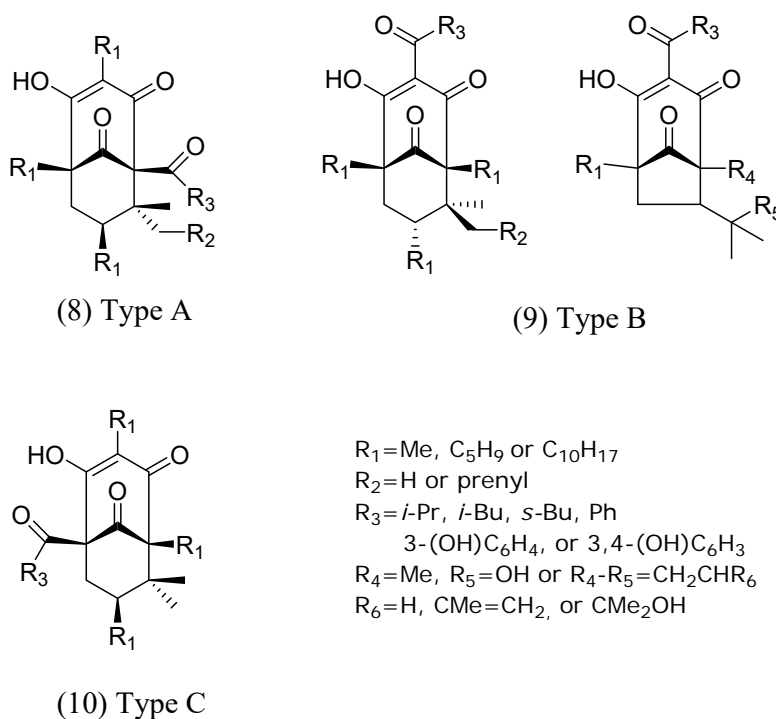
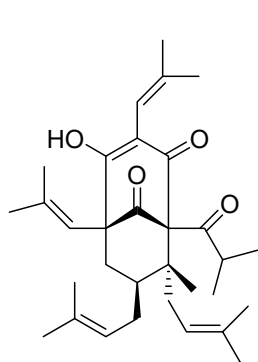
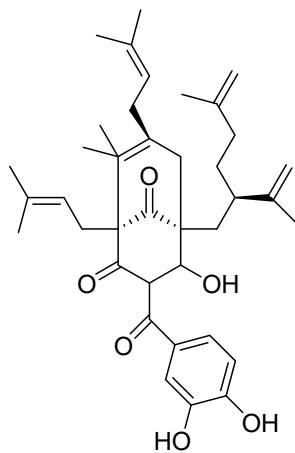


Figure 2.2 Type A, B and C PPAPs extracted from (Ciochina & Grossman, 2006).

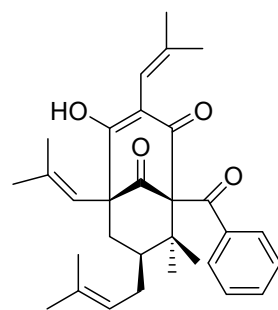
The first PPAP isolated was hyperforin (11), and it is now classified as type A (8) PPAP (Cuesta-Rubio *et al.*, 2001). In 1975, Bystrov and coworkers were able to determine hyperforin's structure and its absolute stereochemistry (Bystrov *et al.*, 1975). The first two type B (9) PPAPs named xanthochymol (12) and isoxanthochymol (7) were isolated in 1973 by Rama Rao and coworkers from fruits of *G. xanthochymus*. The structure given at the time for xanthochymol (12) was monocyclic.



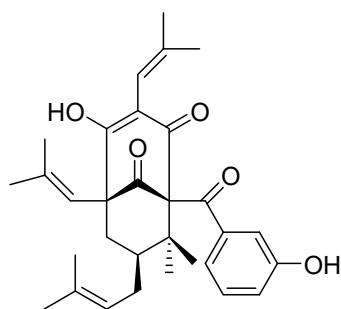
(11)



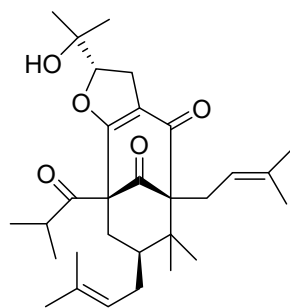
(12)



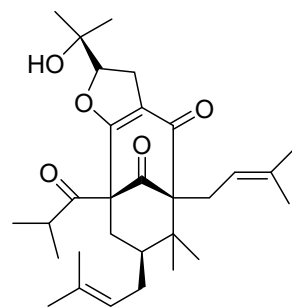
(13)



(14)



(15)



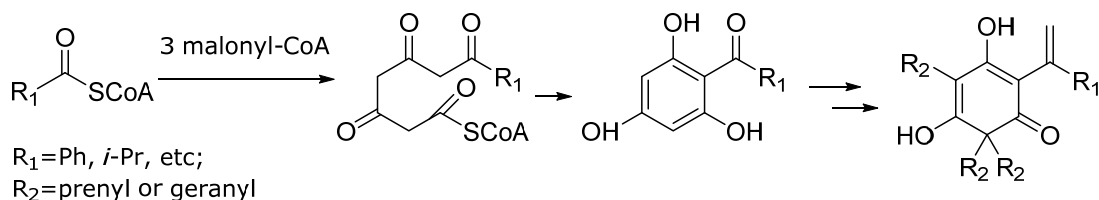
(16)

Type B (9) PPAP clusianone (29) was discovered in crystal forms for the first time in the bark extracts of *Clusia congestiflora*, and the structure was determined using X-ray crystallography in 1976 (McCandlish *et al.*, 1976). Nemorosone (13) and hydroxynemorosone (14) were first isolated by Oliveira who assigned them to be type C (11) PPAP (Oliveira *et al.*, 1996). However in 2001, nemoresone (13) isolation from floral resins of *Clusia rosea* and nemorosone characterization revealed that it had the type A (8) structure where the positions of the bridgehead substituents were different from the previously assigned substituents position (Cuesta-Rubio *et al.*, 2001).

The first type C (11) PPAP was reported by the Lin group in 2004, and they have isolated garcinielliptones M (15) and L (16) from the seeds of *G. subelliptica* (Weng *et al.*, 2004).

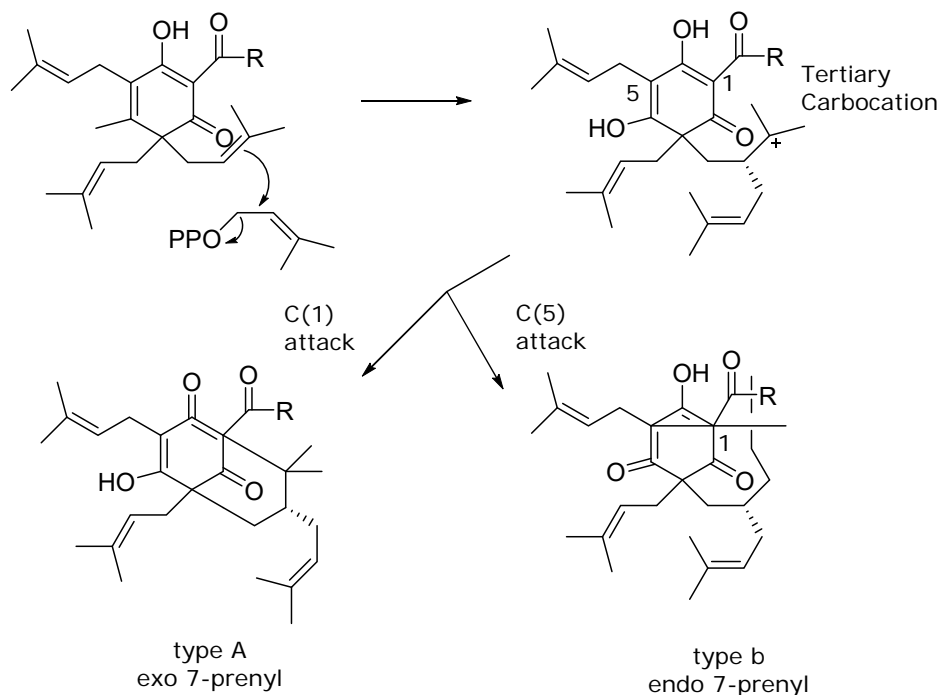
2.3 Biosynthesis hypothesis of PPAP

Phytochemistry *via* labelling experiment and various enzymology studies in plants showed that one acyl-CoA and three malonyl-CoA units are involved in polyketide-type biosynthesis (Adam *et al.*, 2002). Thereafter, acylphloroclucinol is produced by cyclized tetraketide through Dieckmann condensation reaction (**Scheme 2.1**). Subsequent prenylation or geranylation reactions are catalysed by enzyme occurs in order to introduce prenyl and geranyl pyrophosphate to the phloroglucinol compound (Boubakir *et al.*, 2005; Liu *et al.*, 2003; Ciochina & Grossman, 2006).



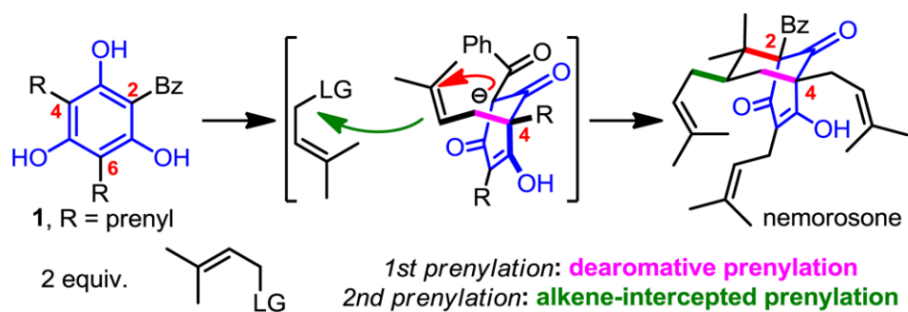
Scheme 2.1 Biosynthesis of MPAPs modified from (Ciochina & Grossman, 2006)

According to Cuesta-Rubio *et al.* (2001), a tertiary carbocation formation is involved in the creation of type A (8) and type B (9) PPAP (**Scheme 2.2**). This tertiary carbocation is formed when the geminal prenyl groups of an MPAP reacts with prenyl pyrophosphate (PPO). Finally, type A (8) PPAP is formed when C(1) attacks the tertiary carbocation and type B is formed when C(5) attacks the tertiary carbocation (Cuesta-Rubio *et al.*, 2001).



Scheme 2.2 Proposed cyclization of MPAPs in formation of type A (8) and type B (9) PPAPs modified from (Ciochina & Grossman, 2006)

The synthetic communities of PPAP compounds are now turning into biosynthetic inspired approach to create new derivatives of PPAP compounds. According to the biosynthetic hypothesis, PPAP compounds are assumed to be derived from three main components with the starting component being a desoxyhumulone substrate as shown in **Scheme 2.3** and additional two prenyl cations. The function of the two prenyl groups is to build the bicyclo [3.3.1] nonane core through two major events which is through dearomative prenylation and alkene-intercepted prenylation. The biosynthetic hypothesis employed in the method development afforded type A (8) PPAP such as nemorosone (13). The research has also successfully synthesize different types of type A (8) and type B (9) PPAP derivatives through both double decarboxylative allylation (DcA) and dearomative conjunctive allylic alkylation (DCAA) (Grenning *et al.*, 2014).



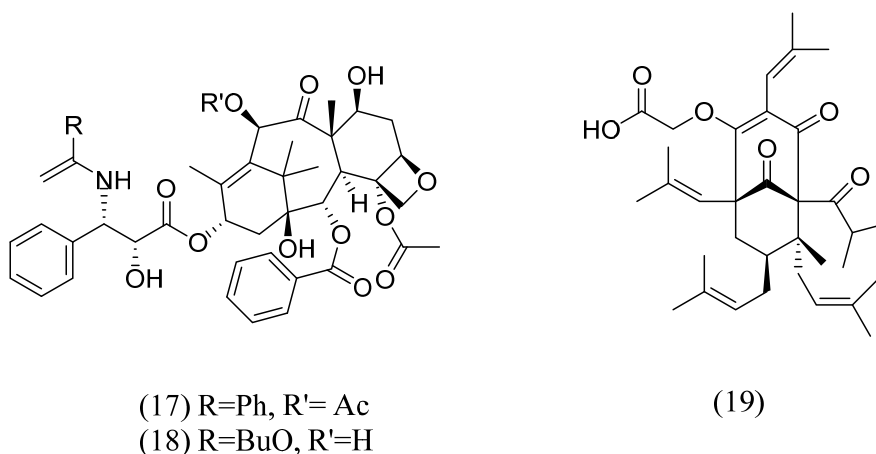
Scheme 2.3 Biosynthetic hypothesis of PPAP's (Grenning *et al.*, 2014)

2.4 Anticancer effects of Polycyclic polyprenylated acylphloroglucinols from Clusiaceae

Hyperforin (11) is a type A PPAP commonly found in the plant of genus *Hypericum*. Hyperforin (11) was isolated from St. John's wort (*Hypericum perforatum*) and the discovery has led scientist to reveal its ability to inhibit tumour cell growth by induction of cell death *via* apoptosis. Interestingly, some research using hyperforin (11) has permitted *in vivo* test to be investigated in rats and *in vitro* test on various human tumour cell lines. Remarkably, IC₅₀ values of the tumor growth of hyperforin (11) on human carcinoma cell lines were between the range of 1-7 μ M while subsequent test on rat tumour cell lines demonstrated IC₅₀ value between the range of 1-9 μ M. The effects of hyperforin (11) were dose dependent generation of apoptotic oligonucleosomes, typical DNA-laddering and apoptosis-specific morphological changes (Schempp *et al.*, 2002).

In vitro hyperforin (11) test against MT-450 mammary carcinoma cell increased the activity of caspase-9 and caspase-3 which were related to proteins expressed during the process programmed cell death. Further *in vitro* test using MT-450 mammary carcinoma cell also compared the activity of both hyperforin (11) and paclitaxel (17) which prevailed that hyperforin (11) solely was responsible for the rapid loss of mitochondrial transmembrane potential and displayed vacuolization of mitochondria when visualized under electron microscope. In addition, isolated mitochondria from MT-450 mammary carcinoma cell revealed that hyperforin (11) was capable of releasing cytochrome c and postulated that hyperforin (11) initiates cell death *via* mitochondria-mediated apoptosis pathway. Most importantly, the results of *in*

vivo test utilising autologous MT-450 breast carcinoma in Wistar rats were profound with hyperforin (11) demonstrating almost comparable cytotoxicity activity to paclitaxel (17) with no effects of acute toxicity (Schempp *et al.*, 2002). In subsequent approach, scientists have also managed to create potent derivative of hyperforin (11) namely Aristoforin (19) and it has shown significant antitumor activity in both *in vitro* MT-450 rat mammary tumour cells and *in vivo* experiments (Gartner *et al.*, 2005; Richard, 2014).

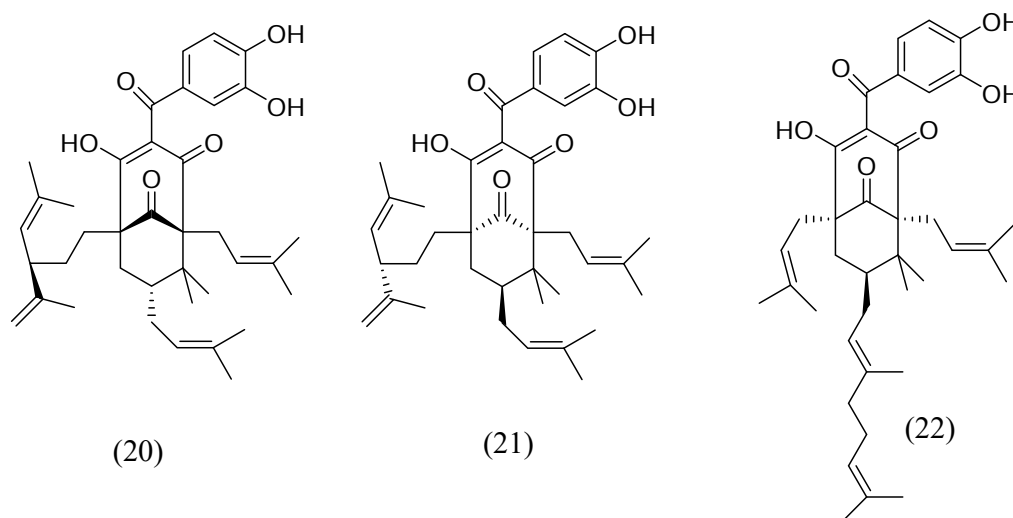


Nemorosone (13), a natural-occurring type A PPAP from *Clusia Rosea*, has gained attention from the natural product community due to its strong anticancer activity on various cancer cell lines such as colon, liver, lung, ovary and breast carcinoma with an interesting molecular mechanism of action. Nemorosone (13) exhibited cytotoxicity activity against neuroblastoma cell line with IC_{50} in the range below 6.5 μ M. Consequently, nemorosone (13) induced DNA damage and caspase-3 activation leading to apoptosis which was observed in a dose dependent manner. Cell cycle analysis using flow cytometry showed that nemorosone treated cells were majority in the G0/G1 fraction and declined in S-phase population (Pardo-Andreu *et al.*, 2011).

To further investigate the cell cycle arrest at G1 to S phase, immunostaining technique utilizing Western blot was employed to study the expression of p21^{Cip1} (cyclin dependent kinase inhibitor). The p21^{Cip1} are essential as regulators of cyclin D/cyclin dependent kinases (Cdk) 4 and cyclin E/cyclin dependent kinases (Cdk) 2 which are important cell cycle regulators in G1 progression to S phase of cell cycle. Based on the Western blot analysis, nemorosone (13) induced the overexpression of p21^{Cip1} in a dose dependent manner indicating cell death *via* cell cycle arrest at G1 to S phase (Díaz-Carballo *et al.*, 2008). Apart from this, studies using cytotoxicity assay revealed that nemorosone (13) exhibit the toxic effect in the range (1–25 μ M) on liver carcinoma (HepG2) cells. In order to study mechanism of action of nemorosone (13), mitochondrial were isolated from rat liver cells. The results indicated that nemorosone caused early mitochondrial impairment along with ATP depletion (Pardo-Andreu *et al.*, 2011).

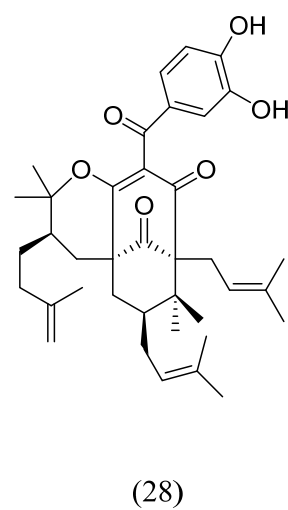
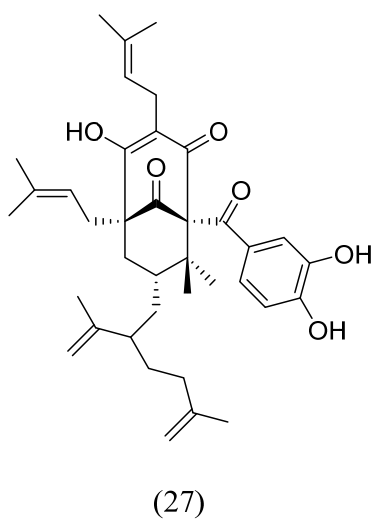
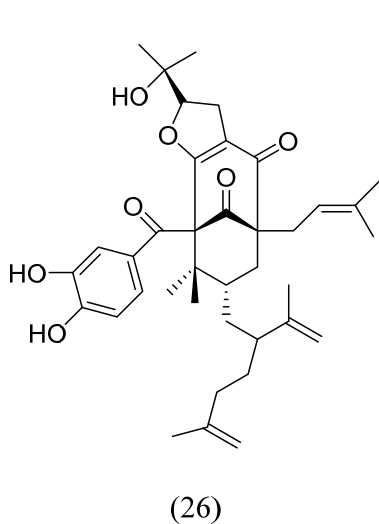
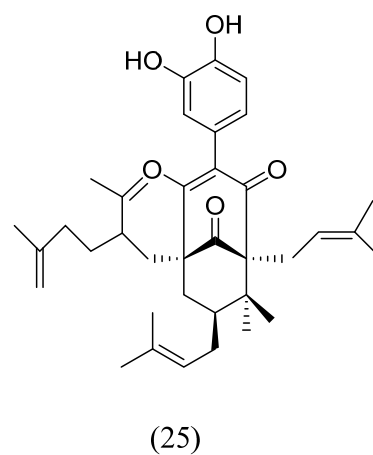
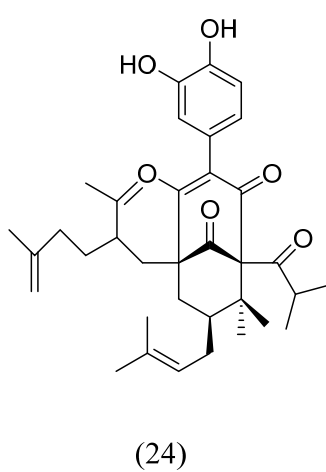
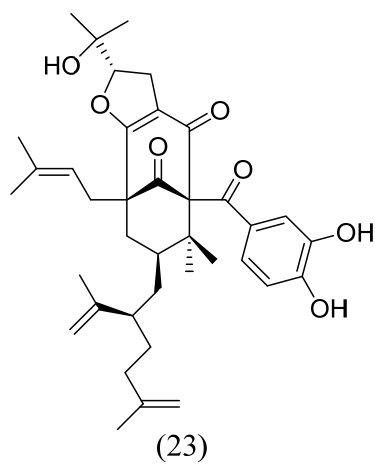
Garcinol (20) and xanthochymol (12) are two most prominent type B PPAP with various bioactivity have been studied and cited for its anticancer bioactivity over the past few years (Pan *et al.*, 2001; Matsumoto *et al.*, 2003; Hong *et al.*, 2007; Protiva *et al.*, 2008; Padhye *et al.*, 2009; Zhang *et al.*, 2011). Most of these including animal model experiments indicate garcinol (20) induced cell cycle arrest at G1 phase. Type B PPAP compound such as xanthochymol (12), guttiferone E (21), garcinol (20) and oblongifolin A (22) have been tested for tubulin assembly assay and remarkably xanthochymol demonstrated significant activity almost comparable to taxol (17) in tubulin assembly inhibition test in nasopharyngeal carcinoma (KB) cells (Roux *et al.*, 2000). It is noticed that oblongifolin (22) showed weak inhibition activity

against tubulin assembly assay compared to garcinol (20) (Hamed *et al.*, 2006). Garcinol's (20) effect on some cancer lines have been linked with the increase in the activity of caspase-3, possibly inducing apoptosis (Matsumoto *et al.*, 2003; Hong *et al.*, 2007). Apart from caspase activation, type B PPAP compounds have been associated with the same mechanism as that of paclitaxel (17), but at a lower potency (Roux *et al.*, 2000).



As for type C PPAP, garcinielliptones FB (23) was isolated from *Garcinia subelliptica* and has shown moderate activity against liver (IC_{50} = 6.8 μ g/mL), breast (IC_{50} = 6.3 μ g/mL) and colon (IC_{50} = 11.2 μ g/mL) cancer cell lines (Wu *et al.*, 2008). In addition, the extraction and column chromatography fractionation of fruit extracts of *Garcinia subelliptica* afforded six new polyisoprenylated benzophenoids (\pm)-garcinialiptinone A (24), B (25), C (26) and D (27) and several known compound xanthochymol (12), isoxanthochymol (7) and cycloxanthochymol (28). All compounds were tested against non-small lung carcinoma (A549), prostate carcinoma (DU145), and nasopharyngeal

carcinoma (KB) cell lines together with paclitaxel as a drug control. The cytotoxicity data showed that all the polyisoprenylated benzophenoids compounds had significant IC_{50} value in between the range 4-5 $\mu\text{g/mL}$ although it is 2000-fold less effective than paclitaxel (Zhang *et al.*, 2011).



2.5 Clusianone (29) type B PPAP (Polycyclic polyprenylated acylphloroglucinols)

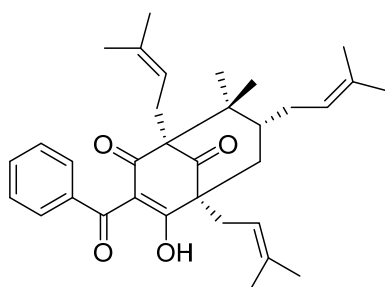
Clusianone (29) is a polycyclic polyprenylated acylphloroglucinols (PPAP) isolated from the plants of the Clusiaceae (Guttiferae) family which has gained significant interest to study its potential bioactivity. Naturally occurring clusianone (29), exhibited anti-HIV (Piccinelli *et al.*, 2005) and anti-cancer properties (Ito *et al.*, 2003; Reis *et al.*, 2014).

First reported in 1976, clusianone (29) was isolated from the roots of *Clusia congestiflora* and X-ray diffraction analysis has firmly established the equatorial orientation of the 3-methyl-2-butenyl group at C-7 position (McCandlish *et al.*, 1976). Subsequent isolation of clusianone (29) from *Clusia sandiensis* (Monache *et al.*, 1991) and *Clusia spiritu-santensis* (Oliveira *et al.*, 1996) reported the NMR spectroscopy of clusianone (29) and its methyl derivative respectively which leads to the contradictory NMR data for clusianone (29). Unfortunately, due to the complexity of the data and the unavailability of authentic sample of clusianone (29), no report was made of the C (7) stereochemistry.

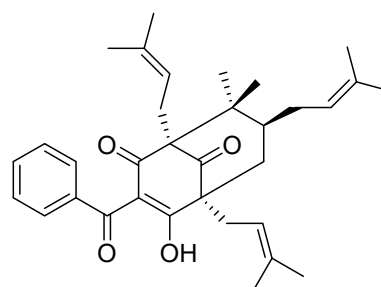
Santos and coworkers isolated 7-epiclusianone (30) from *Rheedia gardneriana* and reported its NMR (Santos *et al.*, 2001) including X-ray crystal structure (Santos *et al.*, 1998), showing the C(7) exo isomerism. The absolute structure of (+)-7- epi-clusianone (30) possessing the C-7 prenyl group at axial orientation while comparing to clusianone (29) that was isolated in 1976 had C-7 prenyl group established at equatorial position.

Finally, in 2005, both tautomeric pairs of clusianone (29) and epi-clusianone (30) were isolated from the fruits of *Clusia torresii* (Piccinelli *et al.*,

2005). The structures were solved by NMR spectroscopy and the report confirmed that the compound isolated from *Clusia sandiensis* in 1991 was actually epiclusianone (30). In this study, the clusianone (29) were isolated from the leaves of *G. parvifolia* collected from tree in a reserved forest Sungai Congkak Selangor (Nagalingam *et al.*, 2013).



(29)



(30)

Over the last decade, attempts to study the bioactivity of clusianone (29) which includes cancer chemopreventive activity and HIV activity has gained much interest from the international chemical community to make research breakthrough in the total synthesis of clusianone (29) (Njardarson, 2012). These growing evidence has consequently led the chemist community to explore various methods in the total synthesis of clusianone (29) (Tsukano *et al.*, 2007; Ahmad *et al.*, 2007; Nuhant *et al.*, 2007; Qi & Porco, 2007; Garnsey *et al.*, 2011; Boyce & Porco, 2014; Horeischi *et al.*, 2015). However, further structure-activity relationship of naturally occurring clusianone (29) derivatives has never been reported. Therefore, the novelty of this research was emphasized on the structure-activity relationship of clusianone (29) which was approached *via* novel synthesis method which was to modify the naturally occurring clusianone (29) through chemical synthetic routes.

2.5.1 Isolation and optimization of clusianone (29) from Clusiaceae family

Plants

In this research, the leaves of *G. parvifolia* were used to isolate clusianone (29) (Nagalingam *et al.*, 2013). The isolation of clusianone (29) from the leaves of *G. parvifolia* has made the optimization of the compound a lot more efficient and sustainable since it was present more abundantly as compared to those clusianone (29) isolated from dried stem barks of *G. assigu* (Ito *et al.*, 2003) and roots of *Hypericum hypericoides* (Christian *et al.*, 2008). Exploitation of some plants may result in the extinction of the plant species which also leads to the loss of the genes governing the biosynthesis pathway required for the production of interesting phytochemicals present in secondary metabolite forms (Rates, 2001).

To date optimization of clusianone (29) from the male flowers of *Clusia fluminensis* was carried out using high speed counter current chromatography (HSCCC) (Silva *et al.*, 2012). It was reported that the presence of clusianone (29) was 37% of the resin composition of the flowers (Bittrich *et al.*, 2000). However, the fact that the clusianone (29) were isolated from flowers clearly indicates that this plant collection could only be obtained during the flowering season. One point to be taken note was the fact that the isolation of clusianone (29) throughout the history has proven that this compound could exist in the various parts of the targeted Clusiaceae plant which covers the fruits (Piccinelli *et al.*, 2005), flowers (Bittrich *et al.*, 2000; Silva *et al.*, 2012), leaves (Nagalingam *et al.*, 2013), roots (McCandlish *et al.*, 1976; Christian *et al.*, 2008), stems and barks (Ito *et al.*, 2003).

2.5.2 Bioactivity of clusianone (29) and its epimer

2.5.2.1 Chemopreventive and anticancer activity

Clusianone (29) exhibited chemopreventive activity as reported by Ito and coworkers (Ito *et al.*, 2003). Clusianone (29) isolated from *Garcinia assigu* was treated to Raji cells. Treatment of the clusianone (29) on Epstein-Barr virus early antigen (EBV-EA) activation induced by 12-O-tetradecanoylphorbol-13-acetate (TPA) in Raji cells showed potential chemopreventive activity when compared to glycyrrhetic acid, a known anti-tumor promoter (Ito *et al.*, 2003).

Clusianone (29) and other polyprenylated acylphloroglucinols (PPAPs) such as nemorosone (13) are known cytotoxic compounds. Simpkins screened synthetic clusianone (29) for cytotoxicity in cervix carcinoma (HeLa), breast carcinoma (MCF7) and pancreatic carcinoma (MIA-PaCa-2) cell lines. The IC_{50} was evaluated using the resazurin assay. Both enantiomers of clusianone (29) were evaluated separately with (-)-clusianone giving the lower IC_{50} values (more potent) than (+)-clusianone (29). Clusianone (29) was most potent in cervix carcinoma cells: IC_{50} 3.0 (\pm 1.1) μ M for (-)-clusianone. The IC_{50} values ranged from 3.0 to 8.3 μ M for the three cancer cell lines (Simpkins *et al.*, 2012).

It has been by protonophoric mitochondrial uncoupling; efflux of mitochondrial proposed by Reis *et al.* (2014) that clusianone (29) causes its cytotoxicity effects in HepG2 (hepatocarcinoma) cells protons from the internal membrane space into the mitochondrial matrix resulting in dissipation of membrane potential. At low concentrations necrosis predominated as the main route of cell death possibly due to depleted ATP levels; at higher concentrations mitochondria-mediated apoptosis dominated. This method of cytotoxicity was

similar to that identified for nemorosone (13) which is a regioisomer of clusianone (29) (Pardo-Andreu *et al.*, 2011).

However, the extent of protonophoric and cytotoxic activity is less for clusianone (29) than nemorosone (13). HepG2 cell death was preceded by a concentration-dependent mitochondrial membrane potential dissipation and decreased mitochondrial ATP levels, suggesting that the cytotoxic function of clusianone (29) includes early mitochondrial impairment, which could then lead to apoptosis *via* the intrinsic pathway. It has been suggested that nemorosone (13) is most active as an anticancer agent against estrogen receptor (*ER*) positive cells, most likely due to its antiestrogenic activity (Camargo *et al.*, 2013).

Since HepG2 cells express *ER*, the nemorosone (13) and clusianone (29) interaction with this receptor could also contribute to HepG2 cell death. It has been demonstrated that the removal of the 3-hydroxyl substituent from estradiol significantly decreases receptor binding (Chernayaev *et al.*, 1975). Similarly, nemorosone (13) and clusianone (29) contain a hydroxyl group capable of mimicking the hydroxyl group in the ring of estradiol, which interacts with the receptor, these compounds could conceivably bind to and compete for the estrogen receptor. Thus, a lower binding capacity of clusianone (29) to this receptor could be expected due to the presence of an intramolecular hydrogen bond involving the hydroxyl group with the juxta-posed carbonyl group at C15 (Reis *et al.*, 2014).

2.5.2.2 Anti HIV properties

Clusianone (29) has not only become of interest as a potential anti-cancer agent. There has been a lot of work investigating its anti-HIV properties. When tested in HIV infected C8166 human T lymphoblastoid cells both clusianone (29) and 7-epiclusianone (30) were active against gp120 at very low concentrations (EC_{50} 0.02-2.0 μ M); however, this was also associated with increased toxicity to uninfected C8166 cells. Clusianone (29) acts at the attachment and fusion part of the HIV infection cycle as it prevents the gp120-CD4 interaction between the virus and the host cell (Piccinelli *et al.*, 2005). A further study of the anti-HIV activity of individually synthesized enantiomers of clusianone (29) showed very similar IC_{50} values for (+)-clusianone and (-)-clusianone (29) of 1.53 and 1.13 μ M, respectively (Garnsey *et al.*, 2011).

2.6 Antimicrotubule agents derived from natural product *via* chemical modification

Natural product compounds have been an inspiration to medicinal chemist because these molecules possess drug likeliness and biological friendliness compared to totally synthetic molecules. Scientist has utilized different methods of synthesis including total synthesis, semi-synthesis and combinatorial chemistry to produce lead compounds that are natural product inspired (**Figure 2.3**). Particularly synthesis and molecular modelling researchers prefer using natural product drug as a template, making them a reliable candidate to further drugs development studies. Some of the natural plant-lead compound such as taxol (17), xanthochymol (12), and guttiferone (21) were further chemically modified and remarkably the efforts lead to the discovery of a more potent lead compound in tubulin assembly inhibition activity.

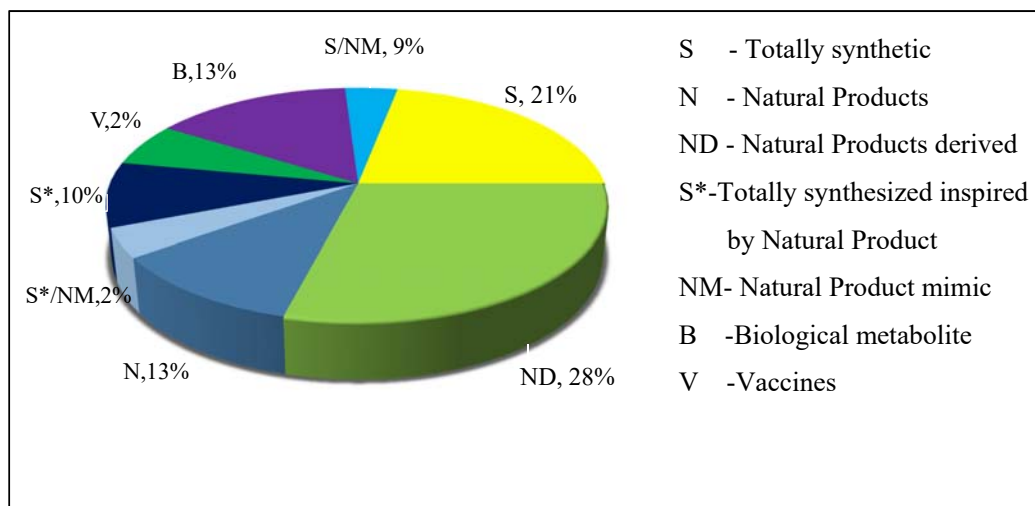
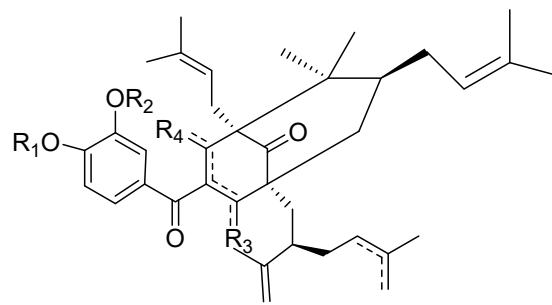
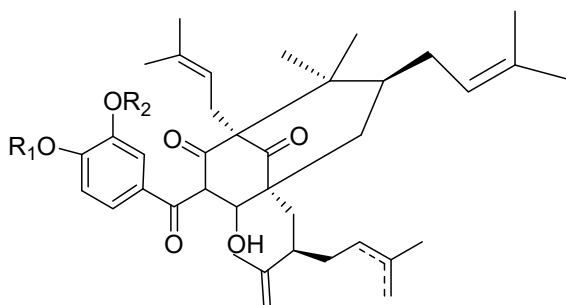


Figure 2.3 The sources of anticancer drugs over the period 01/1981-12/2010 extracted from (Cragg & Newman, 2013).

To date, structure-activity relationship studies through chemical modification on type B PPAP compound as mixture form of xanthochymol (12) and guttiferone (21) have been studied. These compounds were claimed to be inseparable but exist as major compounds estimated about 40% of the crude extract of *G. pyrifera*. The research successfully synthesized 14 types of various derivatives of both naturally occurring xanthochymol (12) and guttiferone (21) in mixture forms through hydrogenation, esterification of enol by methylation and cyclization, partial dimethylation and hydroxyl modification of the benzoyl group. Further to this, the compounds (31-45) were tested against nasopharynx (KB) cells and also on microtubule disassembly assay. The studies revealed that methylation of the catechol groups and hydroxyl group results in the loss of the activity of microtubule assembly inhibition assay unless only one of the enol group was methylated. In addition, hydrogenation of all the double bonds has led to the loss of microtubule assembly inhibition activity meanwhile glycosylated compound (44) through OH modification of one of the catechol groups showed interesting microtubule assembly inhibition activity. However, one point to be noted is the microtubule assembly inhibition activity has no relation to its cytotoxic activity on KB cells (Roux *et al.*, 2000).



(31) $R_1=R_2=H$

(40) $R_1=Me, R_2=H$

(41) $R_1=R_2=H$

(42) $R_1=H, R_2=Me$

(43) $R_1=Et, R_2=H$

(44) $R_1=Beta\text{-D-Glc}, R_2=H$

(34) $R_1=R_2=H, R_3=OMe, R_4=O$

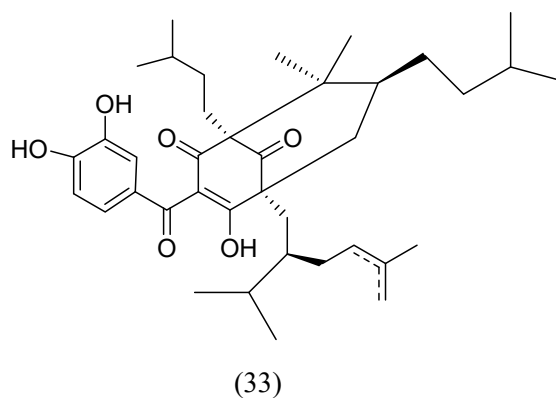
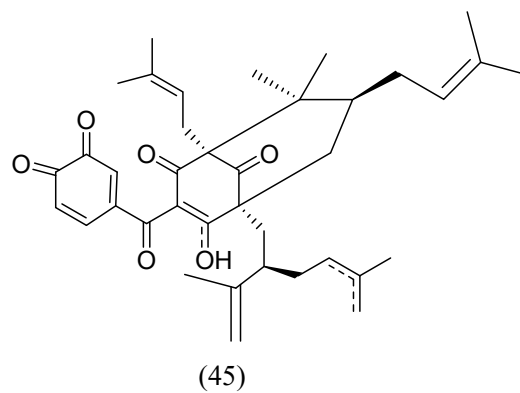
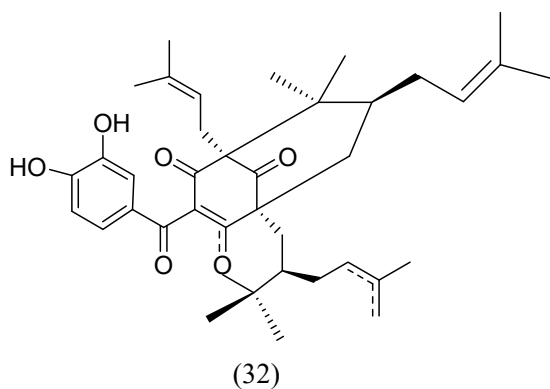
(35) $R_1=R_2=H, R_3=O, R_4=OMe$

(36) $R_1=Me, R_2=H, R_3=OMe, R_4=O$

(37) $R_1=Me, R_2=H, R_3=O, R_4=OMe$

(38) $R_1=R_2=Me, R_3=OMe, R_4=O$

(39) $R_1=R_2=Me, R_3=O, R_4=OMe$



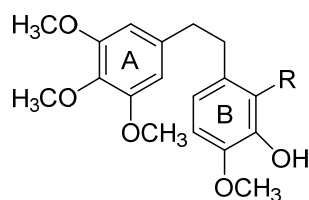
One of the phenomenal drug discoveries in natural product is paclitaxel (Taxol) (17), a naturally occurring diterpene alkaloid isolated from the bark of Pacific Yew, *Taxus brevifolia*. The drug taxol (17) has been approved by Food and Drugs Administration (FDA) and currently commercialized by Bristol-Myers Squibb (BMS) for the treatment of ovarian cancer, breast cancer, advanced kaposi sarcoma, non-small lung cancer, head and neck cancer. However, the initial efforts to obtain taxol (17) were hindered by the low yields and the most critical factor was that the yew trees have to be harvested in order to move forward with large scale extraction of the limited supply of stem barks. Consequently, the relative shortage, slow growth and development of the *Taxus* trees made the efforts non-sustainable (Fu *et al.*, 2009).

Successively, scientist manage to semi-synthesize taxol (17) by the conversion of the relatively abundant baccatins to paclitaxel (17) (Baloglu & Kingston, 1999). In addition, the non-sustainable efforts were solved by isolating paclitaxel (17) and its precursors from fresh branches and leaves instead of barks (Witherup *et al.*, 1990; Eric *et al.*, 2000; Zu *et al.*, 2008). Significantly, the abundance of renewable resources such as leaves and branches instead of using the tree bark provides a good alternative for the commercial production of paclitaxel (17).

Subsequent attempts led to the search for other taxane derivatives produced from abundant sources and major accomplishment achieved *via* semi-synthesis method with the discovery of docetaxel (Taxotere) (18) by Bissery and co-worker at the French Centre national de la recherche scientifique (CNRS). Docetaxel (18) is a semi-synthesis product derived from an inactive taxane precursor which can be isolated from the abundantly present yew species

such as the European Yew, *Taxus baccata*. Docetaxel (18) has better solubility in water compared to taxol (17) which makes it easier to be administered to patients (Bissery *et al.*, 1991). Moreover, docetaxel (18) is almost 100 fold more potent anticancer agent than taxol (17) in phosphorylating Bcl-2 (B-cell Lymphoma 2) which was related to the differential pro-apoptotic activity in cancer cells (Gligorov & Lotz, 2004). Bcl-2 is important protein regulators involved in the programmed cell death. Research also revealed that docetaxel (18) has a longer retention time in a cell as compared to taxol (17) since it has greater cellular uptake into tumour cells and slower efflux from tumour cells (Herbst & Khuri, 2003).

Interestingly, combretastatin (46) has exhibited good inhibitory activity against the microtubule dynamics of cancer cells. Combretastatin (46) a class of natural phenol isolated from *Combretum caffrum* possess varying ability to cause vascular disruption in tumors. Some of the most potent combretastatin which is currently being investigated in phase-I/II clinical trials known is phosphate prodrug (CA-4). Combretastatin (CA-4) (47) acts as a microtubule formation inhibitor by binding to the β -tubulin sub units of microtubules and causes destabilization of tubulin cytoskeleton. Structure-activity relationship (SAR) studies of combretastatin have led to the identification of the configuration and functional group which is fundamental in increasing its bioactivity as antimicrotubule agent. The SAR studies of this benzophenone derivatives have significant findings which concluded that the introduction of an amino group at the ortho position of the benzophenone ring has increased the cytotoxicity activity (Hsieh *et al.*, 2003).



(46) R= OH, Combretastatin (CA-1)

(47) R= H, Combretastatin (CA-4)

Clusianone (29) could be a good lead compound to create a better anticancer entity since its *in vitro* anticancer activity has been proven on some cancer cells such as cervix carcinoma, pancreatic carcinoma, breast carcinoma and hepatocarcinoma (Simpkins *et al.*, 2012; Reis *et al.*, 2014). As such in this research, the simple chemical modification method was employed to further develop clusianone (29) derivatives which could have higher inhibitory activity towards cancer cell proliferation. Simultaneously, the approach allows structure activity-relationship of clusianone to be studied since clusianone (29) is a potential anticancer agent. The chemical modification on naturally occurring clusianone (29) allows the study the structure-activity relationship of clusianone (29) against anticancer activity since reasonable amount of clusianone (29) has been obtained.

2.7 Biological and Pharmacological role of microtubule

Microtubules are essential in cell mitosis for all eukaryotic cells and also are required for the maintenance of cell structure, motility and cytoplasmic motion within the cell. Microtubules are structurally hollow cylindrical tubes of about 30 nm in diameter which are made up of 13 subunits that are called protofilaments or tubulin. Tubulin exists as a dimer of two alternating protein monomers: α -tubulin and β -tubulin and has a molecular weight of 55 kDa (Ludueno, 1998).

During mitosis, the microtubule rapidly reassembles and disassembles to form mitotic spindle allowing cell division to occur. There are currently eight types of α -tubulin and eight types of β -tubulin isoforms (Verdier-Pinard *et al.*, 2009; Leandro-García *et al.*, 2010). Besides that, guanosine-5'-triphosphate (GTP) is also essential energy carrier substrate which binds at the minus end of microtubule cap and function to stabilize the microtubule dynamics. The tubulin-GTP subunits were slowly hydrolysed using its derivative guanylyl-(a,b)-methylene-diphosphonate (GMPCPP) and later discovered that this reaction caused major catastrophe to microtubule dynamics by triggering rapid disassembly to the structure (Caplow & Shanks, 1996).

During the prometaphase of mitosis, microtubule assembly occurs actively elongating from centrosome and are essential components in the correct alignment and positioning of chromosomes at their kinetochores to the spindle after nuclear-envelope breakdown. In the subsequent metaphase stage, congression happens whereby microtubule has elongated timely for the complex movements and at this point all chromosomes are aligned along the equator of the cell. Next, the microtubule plays a role in the synchronous

separation of the sister chromatids towards opposite sides of the cell in anaphase. Finally, telophase occurs, microtubules disassembles and shortens towards the centrosome at the opposite pole of the cells (O'Connor, 2008).

In summary, microtubules emanating from each of the centrosomes positioned at the opposite poles make vast growing and shortening with excursions growth for long distances (typically 5–10 μm), then shorten almost completely, and then regrow again for the next cell cycle phase to take place. The absence of microtubule will cause catastrophe during anaphase stage as chromosomes are unable to achieve a bipolar attachment to the spindle. Consequently causing cell cycle arrest at prometaphase/metaphase stage leading to apoptosis since parent cell is unable to divide/duplicate into two genetically identical daughter cells (Caplow & Shanks, 1996).

2.7.1 Tubulin function

Tubulin having a molecular weight of 100 kDa is found to be present as 10% protein in brain and 3-4% as total protein in cells. Tubulin isotypes formation becomes even complex when it undergoes postranslational modification such as phosphorylation, detyrosination, acetylation, polyglutamylation and polyglycylation. The variation in either the tubulin or the subunit tubulin isoforms are crucial in acknowledging the type of interaction with microtubule associated proteins (MAP), dynein motors and kinesin (Janke & Bulinski, 2011). In other words, these combination of MAPs and β -tubulin isoforms results in a complex “tubulin code” which directs the mechanism governing the microtubule dynamics and hence altering the microtubule architecture (Verdier-Pinard *et al.*, 2009).

2.7.2 β -tubulin isotypes and roles in cancer cells

The different types of β -tubulin isotypes can be distinguished by the variation that occurs at the end part specifically the last 15 sequences of the β -tubulin C-terminal (Luduena, 1998). The differences in β -tubulin isotypes in mammalian cells are associated with tissue specific function and some β -tubulin isotypes are expressed more in certain types of both normal and cancer cells (Burkhart *et al.*, 2001). The various expression of β -tubulin isoforms patterns present in the cell will control the mechanism of inhibition of the microtubule dynamics which eventually implicate cell division (Leandro-García *et al.*, 2010). Specific isotope such as the β 1-tubulin, β 3-tubulin and β 2c-tubulin are often linked to tumours (**Figure 2.10 B**). In some chemotherapeutic trials, the studies prevailed that the β 3-tubulin and β 1-tubulin isotypes are resistance to the drugs such as paclitaxel (Magnani *et al.*, 2006; Kavallaris, 2010).

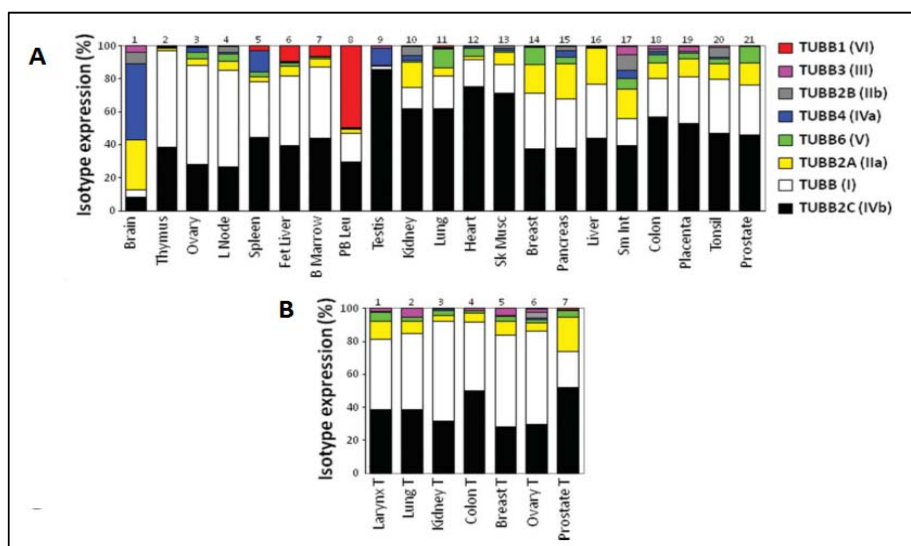


Figure 2.4 β -tubulin isotypes mRNA expressed in numerous human tissues calculated by percentage and displayed in bar graphs. (A) The eight β -tubulin isotypes mRNA fractions in nontumoral tissues and (B) The eight β -tubulin isotypes mRNA fractions in tumoral tissues. The diagram is modified from (Leandro-García *et al.*, 2010).

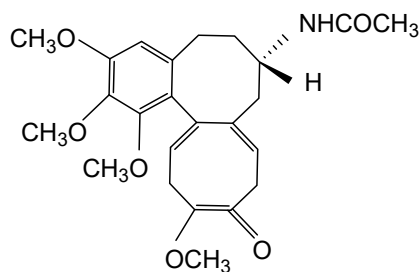
These β -tubulin isotypes generally group with its identical isoforms in order to attract cluster of MAP's which then combines together to initiate or complete a specialised task (Caplow & Shanks, 1995). This characteristic of the β -tubulin isotypes leads to an ideal drug mechanism hypothesis and a target for scientist to discover new drug for chemotherapeutic treatment of cancer cells (Ohishi *et al.*, 2007; Jirásek *et al.*, 2009; Narvi *et al.*, 2013).

2.8 Antimicrotubule agents from natural product and mechanism of action

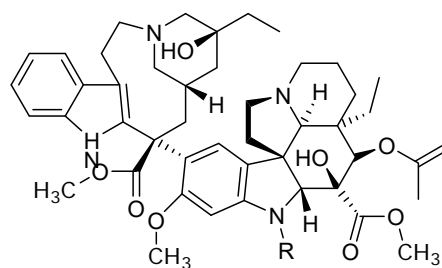
Over the past decades, scientists around the world have studied drugs derived from plants as antimicrotubule agents such as vinca alkaloids and colchicines (52). One of the types of interaction these drugs works is by acting as a microtubule-stabilizing agent which enhance microtubule polymerization at high concentrations preventing disassembly progression after anaphase stage. Examples of antimicrotubule agents includes the paclitaxel (17), docetaxel (18), vinblastine (48), vincristine (49), epothilones (50), laulimalide (51) and polyisoprenyl benzophenones (Dumontet & Jordan, 2010).

To date, researchers have significantly showed the tubulin binding site of taxol (17). The binding occurs at the β -tubulin protein at the *N*-terminal 31 amino acids sequence (Dumontet & Jordan, 2010). This mechanism of action was distinctive from the binding sites of other mitotic drugs such as vinca alkaloids and colchicine (52). Even though the mechanism of action of these antimicrotubule agents might differ but eventually all these compounds disrupts the normal dynamic reorganization of the microtubule network required for mitosis and cell proliferation and ultimately leading to G2/M cell cycle arrest (Figure 2.5 & Figure 2.6).

Therefore, the next approach of this research was to study the mechanism of action of clusianone (29) and derivatives against microtubule dynamics of cancer cells. The β -tubulin protein was selected for protein analysis using immunostaining technique since β -tubulin isotypes expression contributes to some characteristics of tumour and most importantly being the major component of microtubule entity. The Western blot methodology allowed β -tubulin expression in carcinoma cells to be studied at different time point after treatment with clusianone (29) and derivatives.

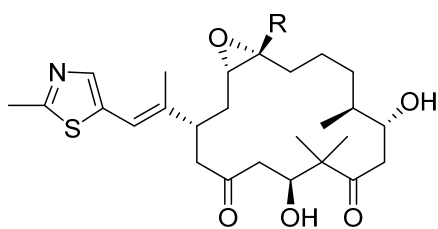


(52)

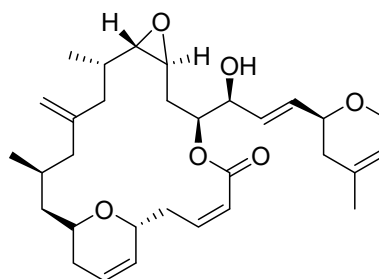


(48) R= CH₃

(49) R=CHO



(50)



(51)

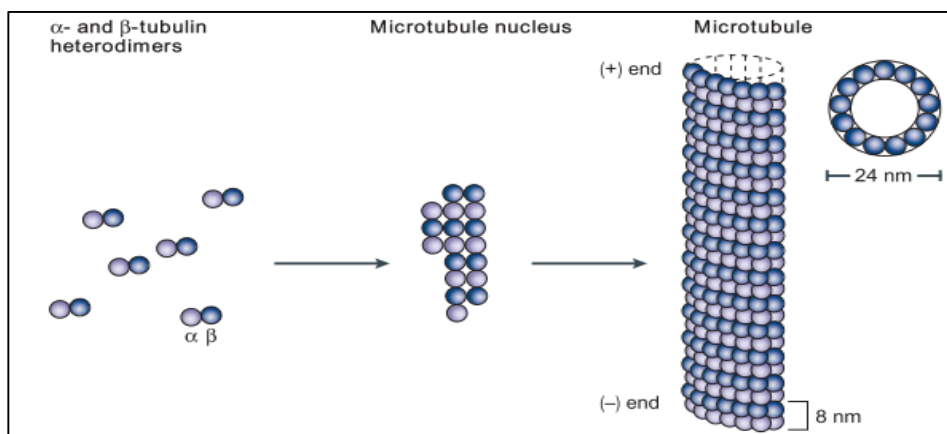


Figure 2.5 Polymerization of microtubule extracted from (Jordan & Wilson, 2004).

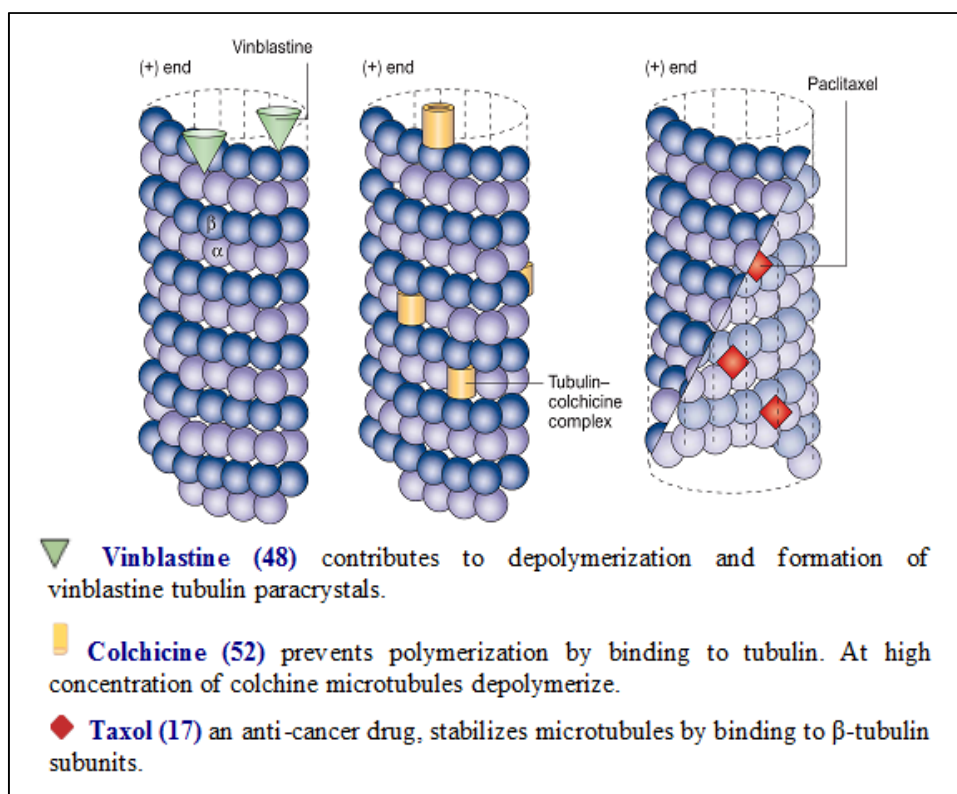


Figure 2.6 The different anticancer drug binding sites on microtubule causing disassembly and destabilisation of microtubule polymerization modified from (Jordan & Wilson, 2004).

2.8.1 The binding site of anti-microtubular drugs on β -tubulin

Taxol and derivatives binding site to beta tubulin protein has been discovered using photoaffinity labelling and electron crystallography methods (Rao *et al.*, 1994; Rao *et al.*, 1999). Similar experiments using electron crystallography was carried out to determine the binding site of epothilone to the receptor site of β -tubulin protein. The findings from the experiment revealed that the interaction of both taxol and epothilone are both independent to the promiscuous binding pocket of the specific *N*-terminal of β -tubulin protein (Nettles *et al.*, 2004). This has prompted some researchers to aim the specific binding site of the drugs to the *N*-terminal 31 amino acids of β -tubulin *via* molecular modelling studies to establish new sets of derivatives that could possibly be a more potent anticancer drug.

The molecular modelling studies approach was combined with quantitative structure-activity relationship studies to create drug entity that was presumed to have pharmacophoric element which enhances the binding properties to the protein of interest. The studies also include the binding domain properties such as lipophilic and hydrophobic characteristic of the specific sites of protein receptor domain sites. Numerous taxol and epothilones derivatives were studied and new methods to synthesize the compound were established. (Snyder *et al.*, 2001; Maccari *et al.*, 2003; Renzulli *et al.*, 2006). Other microtubule stabilizing agents such as colchicines, laulimalide and peloruside were also studied using molecular docking studies to determine the β -tubulin-binding interaction in an independent manner (Pineda *et al.*, 2004).

In one of the molecular modelling approach to study taxol binding site to microtubule, it was discovered several different moieties results in the interaction (**Figure 2.7**). These interactions involve lipophilic domain filled by C3' phenyl, C12 methyl, and C4 acetyl group. In addition to this, there is an interaction between C7 hydroxyl and oxetane group of taxol with polar cluster region defined by (Thr276, Ser277 and Arg278). The domain existing between C3' benzamido and C2 benzoyl is occupied by His229. The studies also revealed that hydrogen bonds contacts were present at C2 benzoyl, C2' hydroxyl, C3' amido and C7 hydroxy group (Renzulli *et al.*, 2006).

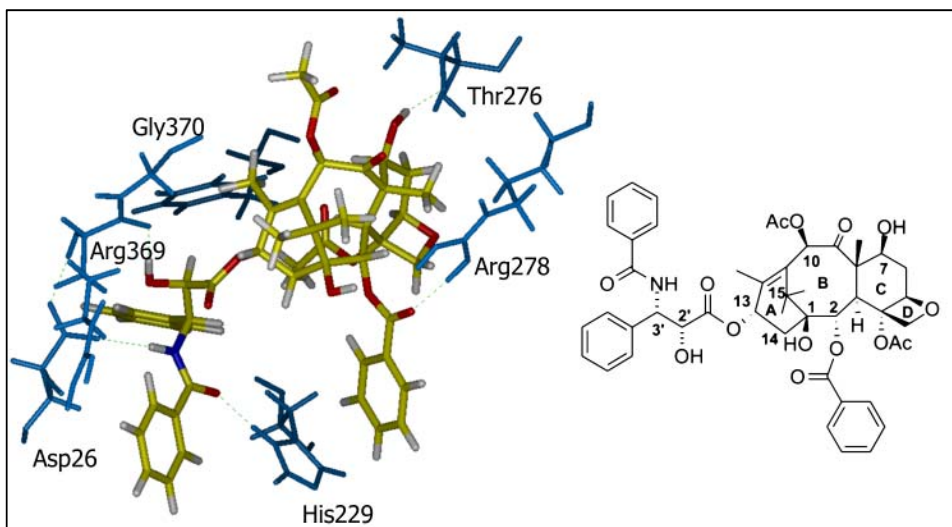


Figure 2.7 Taxol binding site to N-terminal 31 amino acids of β -tubulin using the PrGen software to develop the minireceptor model modified from (Renzulli *et al.*, 2006).

2.9 Phases of cell cycle and cell cycle regulators

The cell cycle refers to a cascade of cellular events leading to the division and duplication of cells (**Figure 2.8**). In eukaryotes, the cell cycle can be divided into two periods: the interphase and the mitotic (M) phase. The interphase consists of three phases: gap phase I (G1), responsible for the synthesis of organelles in most cells; synthesis phase (S), during which DNA is replicated; and gap phase II (G2), which is a period in preparation for cell division (O'Connor, 2008).

During the initiation and progression of each phase, cell cycle regulators are involved and these cell regulators are heterodimeric enzymes made up of cyclin dependent kinases (Cdk's) subunits and cyclin subunits. Cdk4 and Cdk6 together with cyclin D regulate the early stage of G1 phase. During the transition from G1 phase to S phase cyclin E-Cdk2 complex is required while cyclin A-Cdk2/ essential for the progression of S phase. The M phase leads to segregation of chromosomes and results in two daughter cells, which is the end point of cell division. Cyclin B1-Cdk1 regulates the entry and exit of M phase (Williams & Stoeber, 2012).

Sometimes, cells become quiescent or senescent after mitosis; this phase of is known as G0. The progression and completion of each phase are activated by the previous phase. Theoretically, cells will undergo G1 phase for continuous growth after the completion of mitosis. However, in multi-cellular eukaryotes cells very often enter G0 from G1 if they are nonproliferative. The time span of G0 can be very long, even indefinite in the case of neuron cells and cell types which are fully differentiated. It is also a phase for cellular responses to DNA damage with affected cells becoming senescent, rendering them at a metabolic

active state but unable to divide. It is an alternative to programmed cell death, apoptosis (Williams & Stoeber, 2012).

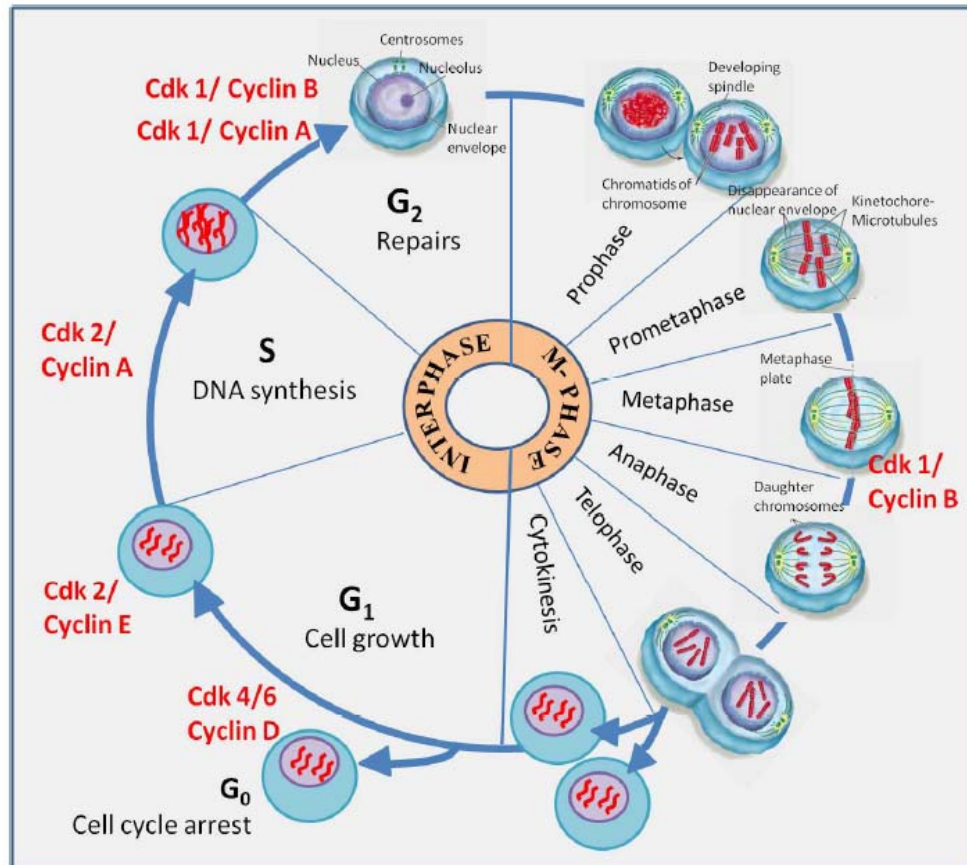


Figure 2.8 The cell cycle phases (G₀, G₁, S, G₂ and M) and the different stages of M phase during the cell replication. In M-phase, the cell goes through 5 phases: prophase, prometaphase, metaphase, anaphase and telophase for separation of chromosomes and finally, the cytoplasm is divided through cytokinesis to form two daughter cells. The regulatory factors (cyclin and cyclin-dependent kinases - Cdk) which control the cell cycle are also indicated from (O'Connor, 2008).

2.9.1 Cdk's and cell cycle regulation checkpoints

Cyclin dependent kinases (Cdks) enzyme proteins are classified as a family of serine/threonine kinases having the molecular weight within the range of 34 to 40 kDa. Specifically, Cdk's are fundamental components in the modification of numerous protein substrate required for cell cycle initiation and progression. Most importantly, Cdk's are actively involved in substrate phosphorylation by transporting phosphate groups from ATP to specific amino acid sequence. The number and types of Cdk's in a living organism depend on the nature of eukaryotic cells. In fact in yeast, there was only one Cdk present compared to four types of Cdk's found in vertebrates. Cdk's are inactive until it is being associated with cyclin also known as regulatory partners triggering the activation of a heterodimer cyclin-Cdk complex. The cyclin-Cdk complex phosphorylates large numbers of substrate in the cell resulting in the onset of the various specific cell cycle (Morgan, 1997).

Several checkpoints are present in the eukaryotic cell cycle to confirm the occurrence of cell phase's proceeds or progresses after adequate growth and conscientious DNA replication. Cdk's is a key component in cell regulation and also play a major role in the regulation of transcription and mRNA processing including biochemical process in cells which includes neuronal signalling, golgi membrane trafficking, cell death, cell differentiation and retinal phosphodiesterase regulation. The Cdk's function solely relies on its cyclin counter partner. At each checkpoint of the cell cycle, various proteins are involved in a series of carefully coordinated biochemical reactions and these proteins includes the different Cdk and cyclin complex formation for the onset of each phase in the cell cycle (Satyanarayana & Kaldis, 2009).

Throughout the progression of cell cycle and cell division, both synthesis and degradation of cyclin occur actively (**Figure 2.9**). The synthesis of cyclin stimulates the formation of cyclin-Cdk complex which then send a signal to the cell to either move to the next phase of cell cycle or regulates the progression within the particular cell cycle phase. Eventually, cell signalling to exit certain cell cycle phases happens with the deactivation of Cdk when cyclins start to degrade. In other words, cyclin levels very much influence the formation of cyclin-Cdk complex formation. The relationship between cyclin and Cdk is inseparable since the degradation of cyclin causes Cdk's to lose their phosphorylating capability. Similar to Cdk's there are numerous cyclins with various functions in eukaryotic cells (Furuno *et al.*, 1999; Khodjakov & Rieder, 2009; Hochegger *et al.*, 2008).

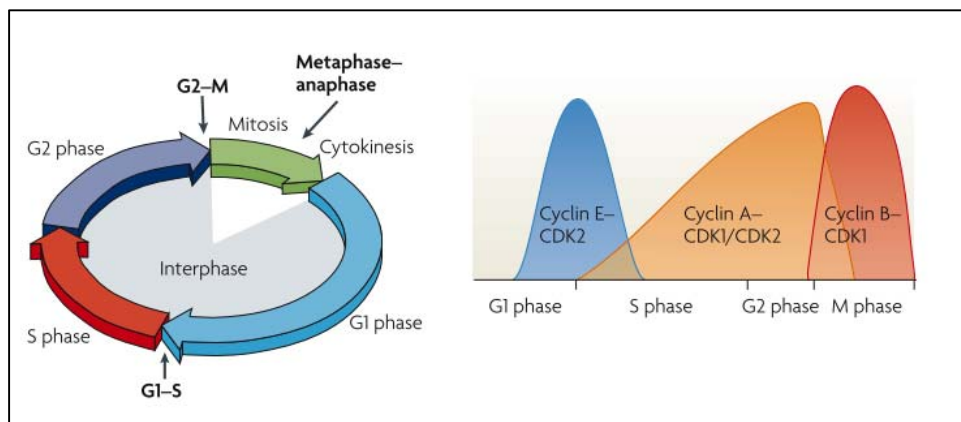


Figure 2.9 The correlation between the cell cycle regulators cyclin-Cdk complex in different cell cycle phases from (Hochegger *et al.*, 2008).

2.9.2 Cyclin B1-Cdk complex and the G2/M checkpoint

Antimicrotubule agents interfere with the mitosis phase of the cell cycle specifically on the *Spindle Assembly Checkpoint* (SAC), inducing a mitotic arrest and normally leads to cell death. During mitosis phase, the involvement of numerous protein kinases has been discovered in this molecular mechanism of mitotic progressions such as CDK family (Cdk), Polo Like Kinases family (PLKs), Aurora kinases and NIMA (Never In Mitosis A) family. Additionally, there are also kinases molecules involved in mitotic exit network, *Spindle Assembly Checkpoint* (SAC) and finally in the cytokinesis completion (Nigg, 2001). The cyclin B1/Cdk1 complex is the key component to specifically regulate and initiate the mitosis phase of the cell and plays the role of phosphorylating proteins that are essential for nuclear envelope breakdown, chromatin condensation, spindle assembly and centrosome separation (Nurse, 1990; Lindqvist *et al.*, 2007).

These cyclin B1-Cdk1 complex exist in both cytoplasm and nuclear envelope synchronizing the events in mitosis such as nuclear envelope breakdown and centrosome separation. Apart from this, cyclin B1/Cdk1 complex stimulates mitochondrial fission activity with the onset of G2/M transition (Taguchi *et al.*, 2007). There are also studies reporting substantial amount of cyclin B1/Cdk1 complex remaining in the cytoplasm during mitosis including active cyclinB1/Cdk1 complex found in cytoplasm and nucleus during prophase (Gavet & Pines, 2010).

The cyclin B1/Cdk1 complex are also present and essential in other components of cells such as cytoskeleton microtubule (Vasquez *et al.*, 1999; Liakopoulos *et al.*, 2003; Moore & Miller, 2007), actin (Yamashiro *et al.*, 1991;

Yamashiro *et al.*, 2001) and intermediate filament networks (Chou *et al.*, 1991; Yamaguchi *et al.*, 2005), caspases (Allan & Clarke, 2007), the Golgi apparatus (Lowe *et al.*, 1998; Draviam *et al.*, 2001; Wang *et al.*, 2003; Preisinger *et al.*, 2005) and nucleolus (Klein & Grummt, 1999; Sirri *et al.*, 2002). In addition to this, G1/S and G2/M checkpoints are energy-sensitive and require pronounced bioenergy supply for de novo synthesis of biomasses needed for cell-cycle phase transitions (Sweet & Singh, 1999).

The molecular mechanisms determining the balance between these responses are not well understood. However, exquisite control of cyclin B1/Cdk1 complex activity during the cell cycle to peak at metaphase is necessary for a successful G2/M transition (Allan & Clarke, 2007; Clute & Pines, 1999). To date, Wang *et al.* (2014) conducted experiments using isolated mitochondria from mouse liver tissues and the research revealed that cyclin B1/Cdk1 complex proteins were found to relocate in the matrix of mitochondria, and an increased influx of mitochondrial cyclin B1/Cdk complex was associated with elevated mitochondrial bioenergetics in G2/M transition. As a result, mitochondria-targeted cyclin B1/Cdk1 increases mitochondrial respiration with enhanced oxygen consumption and ATP generation, which provides cells with efficient bioenergy for G2/M transition and shortens overall cell-cycle time (Wang *et al.*, 2014).

In summary, cyclin B1/Cdk1 complex has been a target for scientist to discover antimitotic anticancer drugs. The strategy is to investigate mitotic cell death (MCD) pathway which involves cell cycle regulators dysregulation. Undoubtedly, further investigation of the effect of clusianone (29) and derivatives on Cdk1 and cyclin B1 expression using immunostaining studies was

carried out in this research. The potential anticancer pathway selected is novel since there were no studies so far which showed the effects of clusianone (29) in mitotic phase specifically targeting mitotic spindle protein β -tubulin and G2/M phase cell cycle regulators cyclin B1/Cdk1 complex.

CHAPTER 3 : MATERIALS AND METHODS

3.1 General Procedures for extraction and chemical synthesis experiments

Plant extracts and synthesized compound solvents are evaporated *in vacuo* at 40 °C with Buchi Rotary Unit (USA). Melting points of compounds were determined using Stuart's (SMP100) melting point apparatus. Isolation and reactions were monitored on thin layer chromatography (TLC) 0.25 mm Merck silica gel plates (60 F₂₅₄), and compounds were visualized with UV light. Column chromatography was carried out using Merck silica gel (70-230 mesh). Purity quantification studies on selected compounds were performed using high performance liquid chromatography (HPLC) with series 600 Link Interface Perkin Elmer (USA) on Series 200 UV/Vis detector, autosampler and pump.

The mass spectrometer used for the Open Access analyses was a Bruker MicroTOF, which was a time of flight mass spectrometer (University of Nottingham, UK) on Electro Spray Ionisation (ESI) mode. ¹H NMR and ¹³C NMR spectra (500 and 125 MHz respectively) were recorded on a Bruker 500 UltraShield (Nottingham University UK Campus). Raw data were processed using MestReNova LITE NMR processor. IR spectra were recorded on a Perkin-Elmer series 1600 spectrometers as KBr pellet for solid samples. X-ray crystallography analysis on single crystal was carried out using Oxford Diffraction Xcaliber Eos Gemini with copper k α radiation at the Department of Chemistry of Universiti Putra Malaysia.

3.1.1 Plant Sample

The leaves of *G. parvifolia* (Miq.) Miq (UNMC 45) were collected from trees in a reserved forest Sungai Congkak, Selangor (GPS coordinate: N 03° 12'49.8", E101°50'71.1", elevation: 234 m) (**Figure 3.1**). The plant authenticity was verified and deposited with voucher number PID 271210-13 at School of Pharmacy, The University of Nottingham Malaysia Campus herbarium and Forest Research Institute Malaysia (FRIM) by a co-worker (Ching, 2013).

3.1.2 Maceration of *G. parvifolia* (Miq.) Miq.

Dried and powdered leaves of *G. parvifolia* (Miq.) Miq leaves (1000 g) were extracted by maceration. In the first step, 400 g of the powdered leaves were placed in a 5 L Erlenmeyer flask. The flask was filled with 3 L of hexane solvent and swirled from time to time. After three days the solvent was filtered, evaporated and then dried using a rotary evaporator under reduced pressure at 40 °C in water bath. The maceration procedure was repeated three times and with the same duration of three days. From 1000 g of powdered leaves macerated, a total of 80 g of hexane extract was obtained (Sarker *et al.*, 2006).



Figure 3.1 (A) Images of *G. parvifolia* (Miq.) Miq. Leaves (10-15 cm). (B) Images of leaves dried in trays.

3.1.3 Extraction and isolation of clusianone (29) from leaves of *G. parvifolia* (Miq.) Miq.

The hexane extract (5 g) from leaves was chromatographed on silica gel (70-230 mesh) in a column (8 × 100 cm) and eluted with diethyl ether of about 1L. The solvent was removed under reduced pressure using rotatory evaporator at 40 °C in water bath. This part of the extract contains major portion of chlorophyll since it was obtained from leaves. Therefore, in the next step, the chlorophyll was removed. The dry weight of the diethyl ether extract was approximately 5 g. First, the diethyl ether extract was mixed with silica gel: activated charcoal in a proportion of 1:3:1, respectively and placed in a column with a porous frit. The material was eluted with hexane (300 mL) followed by dichloromethane *in vacuo* (Sargenti & Vichnewski, 2000).

The hexane and dichloromethane fractions after chlorophyll removal were further chromatographed on silica gel (70-230 mesh). The two extracts weighed approximately 2 g of dry weight each. Both the extracts were chromatographed on a column (4 × 100 cm) and eluted with solvent gradient mixtures (200 mL of each mixture) as shown in the table below. To isolate the compound, the dichloromethane dried fraction (4.8 g) was further chromatographed on silica gel (70-230 mesh) and eluted with mixtures of cyclohexane/chloroform and chloroform/methanol of increasing polarity (**Table 3.1**). A total of 122 fractions were collected in 20 mL vials. Thin layer chromatography (TLC) profiling was performed on all the fractions collected and compared with the standard clusianone (29) isolated previously by a co-worker (**Figure 3.2**). Clusianone (29) spot appears at $R_f = 0.45$ (Cyclohexane/chloroform = 1/1). Thereafter, the targeted fractions F51—F60 which showed the presence of clusianone (29) *via* TLC profiling were crystallized *via* slow methanol evaporation.

Table 3.1 Gradient solvent system for dichloromethane extract

Solvent	Ratio
Cyclohexane: chloroform	7:3
	6.5:3.5
	6:4
	1:1
	4:6
	3:7
	2:8
	1:9
	100%
Chloroform	
Chloroform: Methanol	8:2

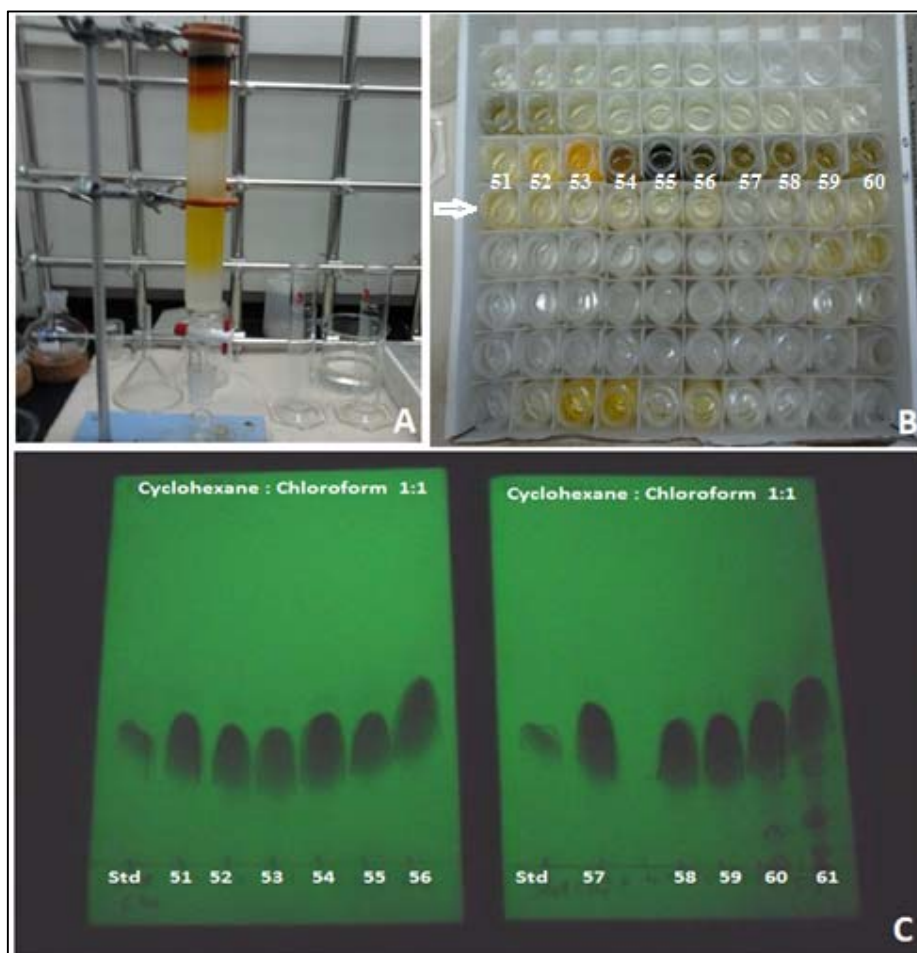


Figure 3.2 Isolation of clusianone (29) (A) Column chromatography to separate clusianone (29) from dichloromethane fraction. (B) Dichloromethane fractions collected in scintillation vial after subjected to gradient solvent system column chromatography. (C) Fractions collected in scintillation vials are spotted on TLC plate to detect the presence of clusianone (29) with standard clusianone (29) as reference.

3.1.4 Recrystallization of clusianone (29)

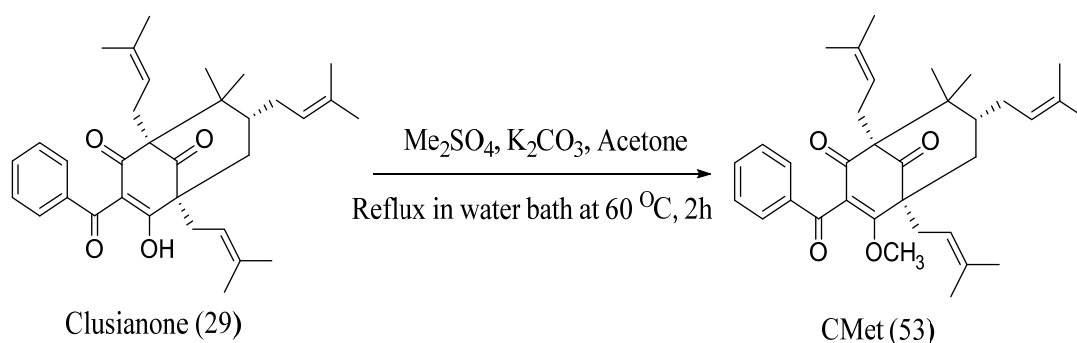
The targeted fractions F51—F60 which showed presence of clusianone (29) were recrystallized several times with methanol to give yellow crystalline solid (100 mg, 0.05%) over a period of 10 days. Further to this method, the seeding technique was used to promote the growth of diffraction-quality crystals whereby the supersaturated solution was induced with a small crystal of the compound obtained from the previous isolation (Sunagawa, 2005). The solution was then left to evaporate through slow evaporation including vapour diffusion under controlled temperature below room temperature. These crystals were stored at 2 -8 °C (Nagalingam *et al.*, 2013). Clusianone $C_{33}H_{42}O_4$: Yellow crystals; m.p. 90-92 °C; ESI-MS m/z , $[M+H]^+$: 503.3147 calcd. for 503.3167 (rel. int. %) = 503 (100), 435 (23), 379 (4.5), 343 (1.9), 311 (4.6), 235 (1.7).

3.2 Preparation of clusianone (29) derivatives

3.2.1 Preparation of CMet (53)

[(1*S*, 5*S*, 7*R*)-3-benzoyl-4-methoxy-8,8-dimethyl-1,5,7-tris(3-methylbut-2-en-1-yl)bicyclo[3.3.1]non-3-ene-2,9-dione]

Clusianone (29) (100 mg, 0.20 mmol) was dissolved in acetone (2.0 mL) and then K_2CO_3 (100 mg, 0.10 mmol), and Me_2SO_4 (0.10 mmol) were sequentially added (**Scheme 3.1**). The mixture was stirred under reflux in water bath at 60 °C for 2 hours under the argon atmosphere (Ahmad *et al.*, 2007). The reaction was monitored using TLC with dyeing agent vanillin-sulphuric acid and along with the aid of heat exposure from hot gun on to the surface of the TLC (Rosen *et al.*, 1952). The mixture was cooled to room temperature and the residue was removed by filtration. The solvent was removed *in vacuo*. The residue was purified by column chromatography on Si gel (light petroleum/EtOAc = 9/1) to give CMet (53) as white solids (91 mg, 90%); mp 108-110 °C; ESI-MS *m/z*: $[M+H]^+$ calcd. for $C_{34}H_{44}O_4$ 517.3318 found 517.3316 (rel. int. %) = 517 (100), 449 (40.6), 393 (5.3), 357 (4.2), 325 (4.0).

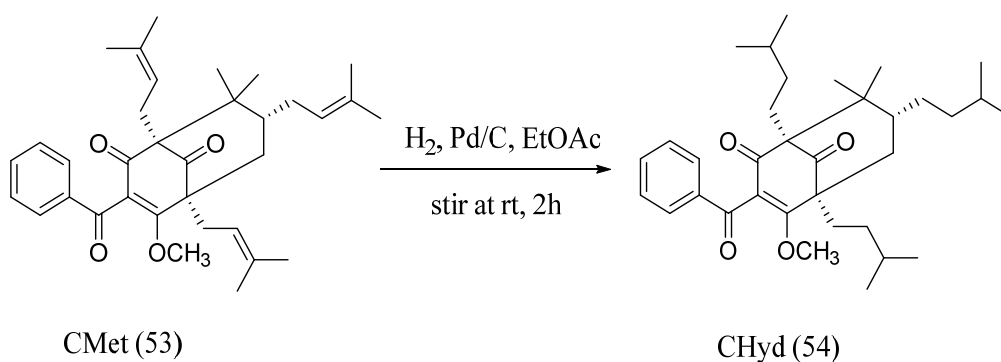


Scheme 3.1 Methylation of clusianone (29)

3.2.2 Preparation of CHyd (54)

[(1*S*, 5*S*, 7*R*)-3-benzoyl-1, 5, 7-triisopentyl-4-methoxy-8, 8-dimethylbicyclo[3.3.1] non-3-ene-2, 9-dione]

CMet (53) (20 mg, 0.03 mmol) was dissolved in EtOAc (0.5 mL) and palladium on carbon (8 mg, 0.0075 mmol) was added simultaneously. The mixture was stirred and hydrogenated at room temperature for 2 hours using hydrogenation apparatus affixed to the condenser (**Scheme 3.2**). The reaction was monitored using TLC with dyeing agent potassium permanganate-sulphuric acid (Wusteman *et al.*, 1964). The catalyst was then removed by filtration using celite (Roux *et al.*, 2000). The filtrate was then purified by column chromatography on Si gel (light petroleum/ EtOAc = 9/1) to provide CHyd (54) (16.3 mg, 80%) as brown wax; ESI-MS m/z : $[M+Na]^+$ calcd. for $C_{34}H_{50}O_4Na$ 545.3607 found 545.3607 (rel. int. %) = 545 (100), 523 (13.4), 429 (2.8), 413 (5.5), 385 (3.4), 341 (3.3), 310 (6.0), 226 (4.0).

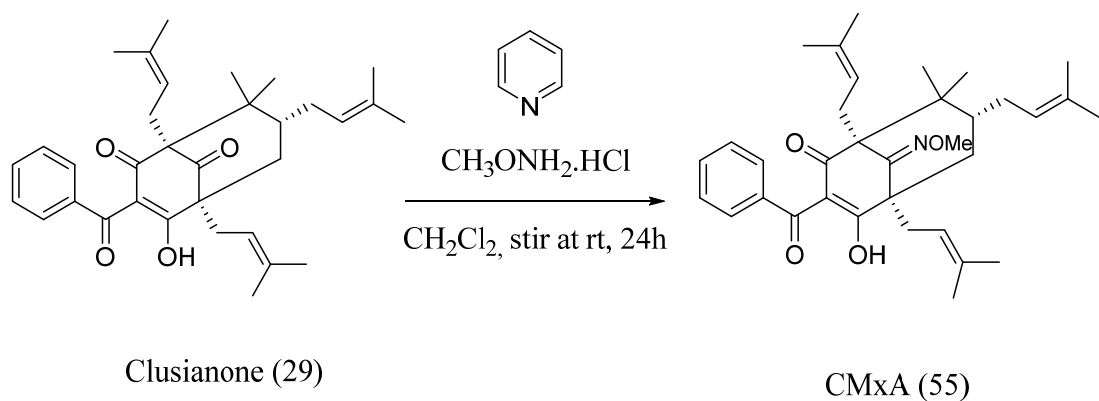


Scheme 3.2 Hydrogenation of CMet (53)

3.2.3 Preparation of CMxA (55)

[(1*S*, 5*R*, 7*R*)-3-benzoyl-4-hydroxy-9-(methoxyimino)-8,8-dimethyl-1,5,7-tris(3-methylbut-2-en-1-yl)bicycle[3.3.1]non-3-en-2-one]

Clusianone (29) (15 mg, 0.03 mmol) was dissolved in dichloromethane (1.0 mL). Methoxyamine HCl (4.5 mg, 0.05 mmol) and pyridine (0.01 mL) were then sequentially added dropwise (**Scheme 3.3**). The mixture was stirred under room temperature for 24 hours. The reaction was monitored using TLC sprayed with Dragendoff reagent (Munier, 1953). Once the reaction completed, the mixture was washed with 5% HCl (3 × 10 mL) to remove the pyridine (Blatt, 1939). The combined organic layer was dried over MgSO₄ and concentrated *in vacuo*. The filtrate was purified by column chromatography on Si gel (cyclohexane/chloroform = 1/1) and afforded CMxA (55) (11.5 mg, 76%) as colorless wax; ESI-MS *m/z*: [M+H]⁺ calcd. for C₃₄H₄₆NO₃ 532.3423 found 532.3423 (rel. int. %) = 532 (100), 500 (4.3), 429 (2.3), 385 (2.6).

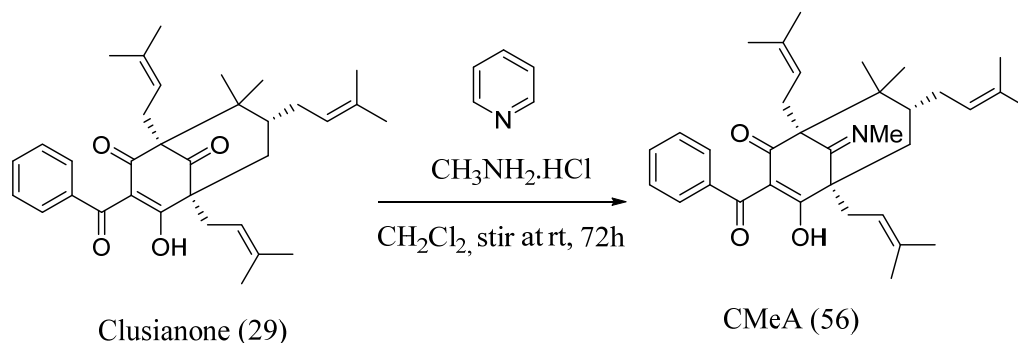


Scheme 3.3 Methoxyamine addition of clusianone (29)

3.2.4 Preparation of CMeA (56)

[(1*S*, 5*R*, 7*R*)-3-benzoyl-4-hydroxy-8,8-dimethyl-1,5,7-tris (3-methylbut-2-en-1-yl)-9-(methylimino)bicyclo[3.3.1]non-3-en-2-one]

Clusianone (29) (15 mg, 0.03 mmol) was dissolved in dichloromethane (1.0 mL). Methylamine HCl (3.5 mg, 0.05 mmol) and pyridine (0.01 mL) were then sequentially added dropwise (**Scheme 3.4**). The mixture was stirred under room temperature for 72 hours. The reaction was monitored using TLC sprayed with Dragendoff reagents (Munier, 1953). After the reaction completed, the mixture was washed with 5% HCl (3 × 10 mL) to remove the pyridine (Blatt, 1939). The combined organic layer was dried over MgSO₄ and concentrated *in vacuo*. The filtrate was purified by column chromatography on Si gel (cyclohexane/chloroform = 1/1). The purification provided CMeA (56) (11.25 mg, 75%) as colorless wax; ESI-MS *m/z*: [M+H]⁺ calcd. for C₃₄H₄₆NO₃ 516.3478 found 516.3423 (rel. int. %) = 517 (100), 498 (1.7), 490 (2.0), 448 (1.1).

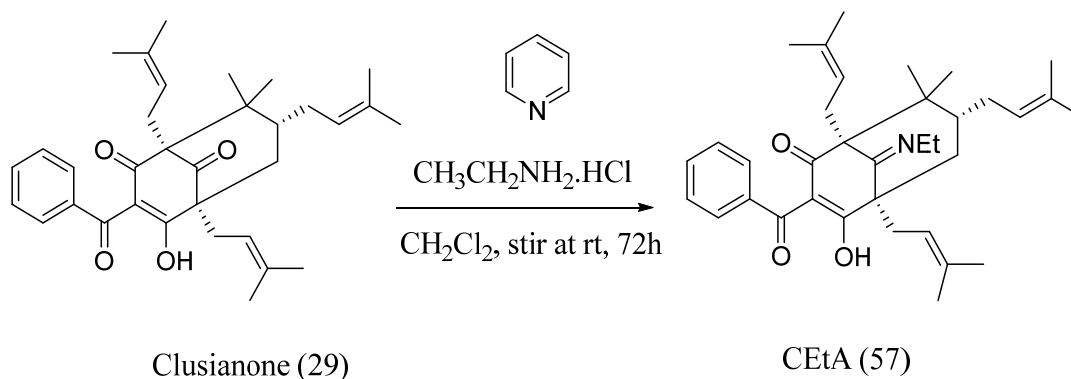


Scheme 3.4 Methylamine addition of clusianone (29)

3.2.5 Preparation of CEtA (57)

[(1S, 5R, 7R)-3-benzoyl-9-(ethylimino)-4-hydroxy-8,8-dimethyl-1,5,7-tris(3-methylbut-2-en-1-yl)bicyclo[3.3.1]non-3-en-2-one]

Clusianone (29) (15 mg, 0.03 mmol) was first dissolved in dichloromethane (1.0 mL). Ethylamine HCl (4.0 mg, 0.05 mmol) and pyridine (0.01 mL) were then sequentially added dropwise (**Scheme 3.5**). The mixture was stirred under room temperature for 72 hours. The reaction was monitored using TLC sprayed with Dragendoff reagents (Munier, 1953). After the reaction completed, the mixture was washed with (3 × 10 mL) of 5% HCl to remove the pyridine (Blatt, 1939). The combined organic layer was dried over MgSO₄ and concentrated *in vacuo*. The filtrate was purified by column chromatography on Si gel (cyclohexane/chloroform = 1/1) to obtain CEtA (57) (11.3 mg, 75.3%) as colorless wax; ESI-MS *m/z*: [M+H]⁺ calcd. for C₃₄H₄₆NO₃ 530.3634 found 530.3621 (rel. int. %) = 530 (100), 526 (0.5), 505 (0.6), 504 (1.9).

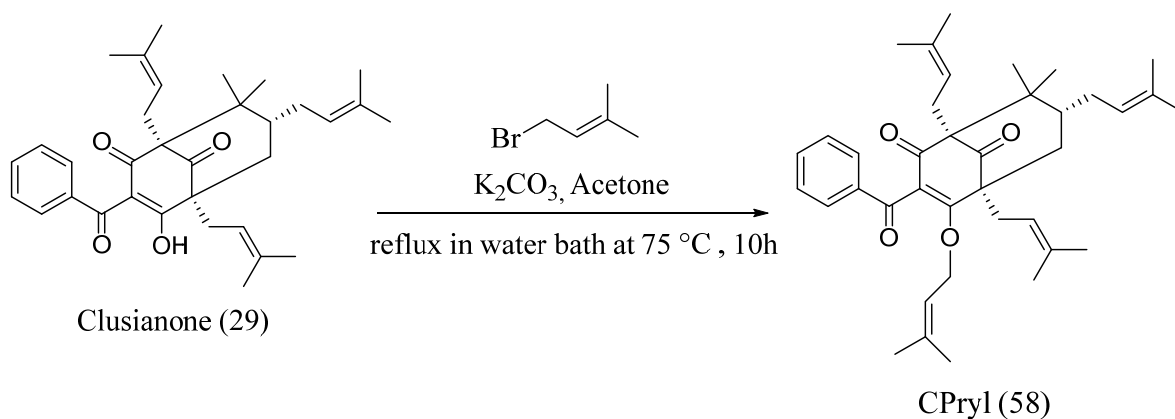


Scheme 3.5 Ethylamine addition of clusianone (29)

3.2.6 Preparation of CPryl (58)

[(1*S*,5*S*,7*R*)-3-benzoyl-8,8-dimethyl-1,5,7-tris(3-methylbut-2-en-1-yl)-4-((3-methylbut-2-en-1-yl)oxy)bicyclo[3.3.1]non-3-ene-2,9-dione]

Clusianone (29) (10 mg, 0.02 mmol), 3, 3-dimethylallyl bromide (0.02 mmol) and anhydrous K₂CO₃ (10 mg) was stirred in acetone (2.0 mL) and refluxed in water bath at 75 °C (Rullah *et al.*, 2014) (**Scheme 3.6**). The refluxed reaction was monitored using TLC and after 10 hours, the mixture in the round bottom flask was cooled to room temperature. Thereafter, the reaction mixture was filtrated and evaporated *in vacuo*. The residue was purified by column chromatography on Si gel (light petroleum/EtOAc = 9/1) to give CPryl (58) as colorless wax (4.3 mg, 43%); ESI-MS *m/z*: [M+H]⁺ calcd. for C₃₈H₅₀O₄ 571.3787 found 571.3829 (rel. int. %) = 571 (52.0), 503 (100), 435 (58.9), 379 (15.0), 343 (5.9), 275 (2.6), 311 (8.4).

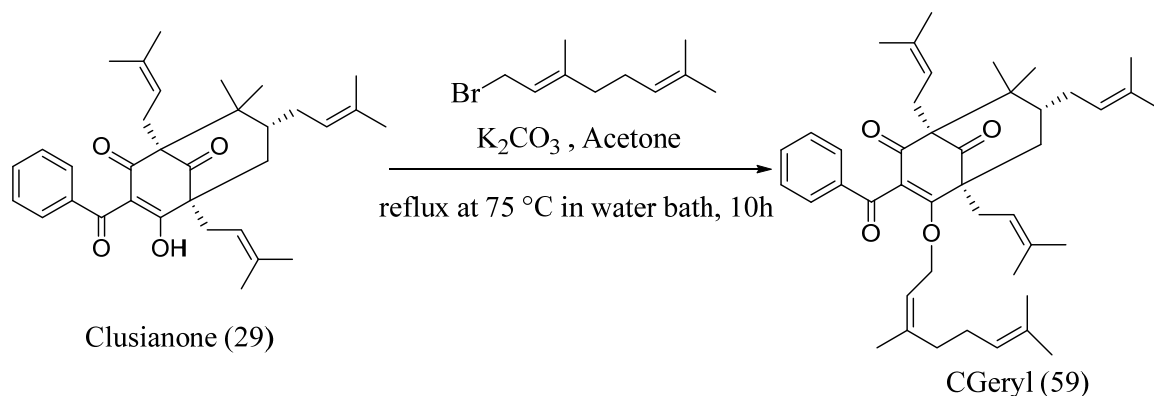


Scheme 3.6 Prenylation of hydroxyl group of clusianone (29)

3.2.7 Preparation of CGeryl (59)

[(1*S*, 5*S*, 7*R*)-3-benzoyl-4-(((*Z*)-3,7-dimethylocta-2,6-dien-1-yl)oxy)-8,8-dimethyl-1,5,7-tris(3-methylbut-2-en-1-yl)bicycle [3.3.1] non-3-ene-2,9-dione]

Clusianone (29) (10 mg, 0.02 mmol), geranyl bromide (0.02 mmol) and anhydrous K₂CO₃ (10 mg) was stirred in acetone (2.0 mL) and refluxed in water bath at 75 °C (Rullah *et al.*, 2014) (**Scheme 3.7**). The refluxed reaction was monitored using TLC and after 10 hours, the mixture was cooled to room temperature. Thereafter, the reaction mixture in a round bottom flask was filtrated and evaporated *in vacuo*. The residue was purified by column chromatography on Si gel (light petroleum/EtOAc = 9/1) to afford CGeryl (59) as yellow wax (2.8 mg, 28%); ESI-MS *m/z*: [M+H]⁺ calcd. for C₄₃H₅₉O₄ 639.4413 found 639.4458 (rel. int. %) = 639 (11), 571 (3.3), 541 (4.0), 503 (100), 435 (63.9), 379 (9.4), 343 (6.4), 311 (8.1), 167 (6.7), 149 (19.5).

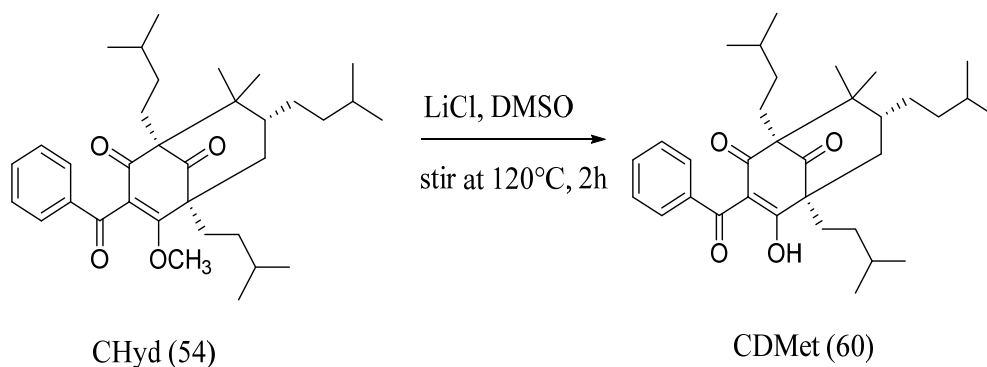


Scheme 3.7 Geranylation of hydroxyl group of clusianone (29)

3.2.8 Preparation of CDMet (60)

[(1*S*, 5*S*, 7*R*)-3-benzoyl-4-hydroxy-1,5,7-triisopentyl-8,8-dimethylbicyclo[3.3.1]non-3-ene-2,9-dione]

To a solution of CHyd (54) (9 mg, 0.0045 mmol) in DMSO (0.50 mL) was added with LiCl (1.5 mg, 0.035 mmol) and the resulting solution was stirred for 2 hours at 120 °C as shown in **Scheme 3.8** (Rodeschini *et al.*, 2006). The mixture was cooled to room temperature and then diluted with H₂O (2 mL). The mixture was then extracted with Et₂O and the combined organic layer was dried over anhydrous MgSO₄. The product was spotted on TLC (light petroleum/EtOAc, 90/10) which showed presence of 4 spots. The residue upon purification by column chromatography on Si gel (light petroleum/EtOAc = 9/1) afforded (60) in 5.0 % yield as brown wax; *R*_f = 0.35 (light petroleum/ EtOAc = 9/1); ESI-MS *m/z*: [M+H]⁺calcd. for C₃₃H₄₉O₄ 509.3630 found 509.3618 (rel. int. %) = 509 (100), 413 (1.7), 271 (2.3).



Scheme 3.8 Demethylation on CHyd (54)

3.3 Summary of synthesis results

Several clusianone (29) derivatives were prepared by using synthetic routes in small scale conditions. The derivatives were prepared utilising synthetic steps of less than four. The products obtained were methylated CMet (53), hydrogenated CHyd (54), oxime added CMxA (55), two primary amines added CMeA (56), CEtA (57) including prenylation and geranylation of clusianone (29) hydroxyl group which gave compound CPryl (58) and CGeryl (59) respectively. The deprotected CHyd (54) to produce compound CDMet (60) was also reported. The percentage yield of products are listed in **Table 3.2**.

Table 3.2 Summary of synthesis results steps taken and percentage product yield.

Product	Reaction steps from clusianone (29)	Overall yield (%)
CMet (53)	1	90.0%
CHyd (54)	2	80.0%
CMxA (55)	1	76.0%
CMeA (56)	1	75.0%
CEtA (57)	1	75.0%
CPryl (58)	1	43%
CGeryl (59)	1	28%
CDMet (60)	3	5.0%

3.4 X-ray crystallography analysis using crystal data software

The X-ray diffraction data also known as the crystallographic information file (CIF) obtained for clusianone (29) and CMet (53) were further refined using several crystal software such as enCIFer 1.4, CRYSTALS 14.23, CAMERON and Mercury 3.3. This software encompasses computing details such as cell refinement (**Table 3.3**), crystal structure in packing unit and various characteristics of intermolecular and intramolecular bonds present in the crystal structure.

Table 3.3 Data collection and structure refinement details

Data collection	
Type of diffractometer	Oxford diffraction Gemini
Radiation source	Cu K α radiation
Data collection temperature	100K
θ range for 19011 reflections used in lattice determination	3-71°
Structure solution and refinement	
Structure solution program	CrysAlis PRO (Agilent 2011)
Primary solution method	Direct methods
Secondary solution method	Direct fourier map
Hydrogen placement	Geometric position
Structure refinement program	CRYSTALS
Refinement method	Full matrix least squares on F ²
Treatment of hydrogen method	Riding
Goodness-of-fit o F ²	0.034
Final R indices [I>2 σ (I),5269 reflections]	0.084

3.5 Modified HPLC method analysis for purity content test

HPLC analysis of selected clusianone (29) derivatives was performed on a series 600 Link Interface Perkin Elmer (USA) HPLC instrument with Polaris C18 (5 μ m C18 column (4.6 x 150 mm)). Elution of the compounds was monitored at an absorbance of 254 nm using an isocratic gradient of 85:15 (ACN : H₂O) over 10 minutes followed by an increasing linear gradient from 85:15 (ACN : H₂O) to 100% acetonitrile over 15 minutes, followed by an isocratic gradient of 85:15 (ACN : H₂O) for an additional 15 minutes (flow rate of 1 mL/min). The injection volume was kept at minimum which was 5 μ L from each sample with concentration of 1 mg/mL. Methods were modified from previous co-worker (Ching, 2013).

3.6 General Procedures for biological experiments

Samples were spectrophotometrically measured at 540 nm using Varioskan Flash and SkanIt Software (Thermo Scientific, USA). Phase contrast inverted microscope to study the cell morphology (FEI, Quanta) with Nikon ECLIPSE TS100. BioRad Mini-PROTEAN[®] cell for handcast gels and (Sodium Dodecyl Sulfate Polyacrylamide gel electrophoresis) SDS-PAGE to run vertical mini gel electrophoresis. XCell SureLock[®] Mini-Cell Invitrogen wet transfer system used for transferring the protein on gel membrane to nitrocellulose membrane. GS800 Densometer to scan the nitrocellulose membrane after staining with TMB solution in order to detect the targeted protein presence and intensity.

3.6.1 Respiratory cell lines for cytotoxicity testing

Cytotoxicity testing's were conducted on selected panel of respiratory cells of both normal and carcinoma cells. The clusianone (29) and clusianone derivatives (53-57) were evaluated for anticancer activity against human respiratory mammalian cells as stated in the **Table 3.4**.

Table 3.4 List of normal and cancer cells tested.

Cell line code	Description and type of cell
MRC5	Lung fibroblast (normal cells) established from normal lung tissue of a 14-week-old male foetus (Jacobs <i>et al.</i> , 1970).
A549	Lung adenocarcinoma (carcinoma cells) established from cell culturing of cancerous lung tissue in the explanted tumour of 58-year-old Caucasian male (Giard <i>et al.</i> , 1973).
NP69	Immortalized nasopharyngeal epithelial cell (normal cells) established from biopsies from the nasopharynx of patients (Tsao <i>et al.</i> , 2002).
HK1	Squamous carcinoma of the nasopharynx (carcinoma cells) established from a recurrent squamous carcinoma of a 58 year old Chinese male after going through 17 and a half years of radiation therapy (Huang <i>et al.</i> , 1980).

3.6.2 Sub culturing mammalian cell

The human lung cells were obtained from ATCC (Rockville, MD) and the nasopharyngeal cells were from collaborator Prof. Tsao George Sai-Wah from the University of Hong Kong with proper agreement on material transfer. MRC5 (passage 10-20), A549 (passage 10-20) and HK1 (passage 20-30) were grown in T-25 flask in growth medium consist of RPMI with L-glutamine (with phenol red), 10% (v/v) FBS, 1% (v/v) 100 units/mL of penicillin/streptomycin and incubated at 37 °C in 5% CO₂ atmosphere.

The cells were split when it reaches 80-90% confluence and provided the morphology indicates healthy cells according to the recommended ATCC protocol (No. CCL-171 and CCL-185). The confluent cells in the flask were rinsed with 3 mL of PBS prior to incubation with 1 mL of trypsin-EDTA (0.05% (v/v) Trypsin, 0.53 mM EDTA.4Na) for 5 minutes at 37 °C. The cells were detached and dispersed from the flask surface by tapping gently and shaking the flask. The cell detachment was confirmed with inverted microscope. Thereafter, 3 mL of RPMI with 10% (v/v) FBS medium was added to prevent further proteolysis and the cell suspension was spun down in a centrifuge for 5 minutes at 1800 rpm (Eppendorf centrifuge 5810R). The supernatant was removed and the cell pellet was resuspended in 1 mL RPMI . Finally, 0.25 mL of this suspension was then added to 5 mL medium in a clean T-25 flask.

As for the NP69 cells (passage 60-90), the growth medium used was Keratinocyte-SFM and the methods were modified using protocol from Keratinocyte-SFM Cat.No.17005 , 0.25% (v/v) Bovine Pituitary Extract, 0.0014% (v/v) recombinant epidermal growth factor, 0.5% (v/v) of penicillin/streptomycin and incubated at 37 °C in 5% CO₂ atmosphere. The

trypsinization method was similar to the other cells except that the deactivation of trypsin after the cell detachment was using 3 mL solutions consisting of 98% (v/v) PBS and 2% (v/v) FBS. The cell suspension was spun down in a centrifuge for 5 minutes at 1800 rpm. The supernatant was removed and the cell pellet was resuspended in 1 mL of the keratinocyte medium with supplements as mentioned earlier. Finally, 0.25 mL of this suspension was then added to 5 mL keratinocyte medium with supplements in a clean T-25 flask.

3.6.3 Cryopreservation of mammalian cells and cell thawing

Cells were harvested and pelleted by centrifugation as described in **section 3.6.1**. After the removal of the supernatant, the cell pellets were resuspended with freezing media which consist of 90% (v/v) FBS and 10% (v/v) DMSO except for NP69 cell pellet which was resuspended with freezing medium consisting 75% (v/v) FBS, 10% (v/v) DMSO and 15% (v/v) Bovine Pituitary Extract. Cells were pipetted into cryovials and placed in a Nalgene™ Cryo Freezing Container which was kept at -80 °C overnight before being transferred to a -150 °C cold liquid nitrogen tank for long-term storage. Normally cells with low passage number are stored in liquid nitrogen tank (Statebourne biorack 750).

To re-establish cell cultures, cells were thawed briefly at 37 °C in a water bath. Once the contents are thawed partially, the vial was removed from the water bath and wiped with 70% (v/v) ethanol to avoid contaminations. The cells were then resuspended in 1ml of the cells growth medium before being transferred to T-25 cell culture flasks. As for the subsequent passages, some cells

were transferred to T-75 flasks and some were cryopreserved to replenish stores of stock cells.

3.6.4 Cell counting

The number of cells seeded in 96 well plates or 6 well plates has to be consistent and accurately calculated using haemocytometer. Therefore, cell counting was performed in the resuspended cell suspension prior to cell seeding into its respective plates. Firstly, the cells were harvested and centrifuged as described in **section 3.6.1**. After the cells were resuspended in 1mL of the growth medium, 50 μ L of the cell suspension was mixed and resuspended with 50 μ L of 0.4% (v/v) trypan blue solution. Next, 10 μ L of this suspension was pipetted and gently delivered between the coverslip and well region of the haemocytometer. Viable cells exclude trypan blue while dead cells stained blue. The numbers of unstained cells were counted in the middle square of the haemocytometer. The calculation of the cell per mL was calculated using the formula below. From the total number of the viable cells calculated in 1 mL media, the seeding of the cells was done using dilution ratio factor to provide 10000 cells in each 100 μ L media pipetted into the 96 well plates.

Total number of cell

= Average number of cells in one large square \times * dilution factor \times 10^4

*dilution factor is usually 2 (1:1/ 50 μ L:50 μ L dilution with trypan blue), but may need to further dilute (or concentrate) cell suspensions.

10^4 = conversion factor to convert 10^{-4} mL to 1 mL which was related to volume of one square of the well of the haemocytometer.

3.6.5 MTT (3-(4,5-dimethylthiazol-2-yl)-2,5-diphenyltetrazolium bromide cell viability assay

All stock cultures except the NP69 cultures were grown in T25 flask with RPMI with 10% v/v FBS medium. As for the NP69 cell, the cultures are grown in keratinocyte-SFM together with the supplement of bovine pituitary extract (BFE) and human recombinant (EGF). Freshly trypsinized cell suspension after spun down at 1800 rpm for 5 min were seeded into 96-well plates at densities of 10000 cells in 100 μ L medium per well. After one day of culture, the medium was removed from each well and were subjected to different concentration of compounds starting from 0 μ g/mL – 200 μ g/mL.

The compounds were dissolved in DMSO and diluted further with RPMI medium for all the cultures, except the NP69 which was diluted with keratinocyte-SFM which serves as a stock solution. The DMSO concentration used was not more than 0.1% (v/v). The different concentration of compound was prepared by serial dilution of the stock solution. The plates were then incubated for 48 hours to test its cytotoxicity level. Docetaxol (18) was used as a positive control. The docetaxol was dissolved in sodium chloride buffer. The well containing the untreated cells serves as negative control.

After the respective incubation period, all the media in each individual well were aspirated prior to treatment of MTT (3-(4,5-dimethylthiazol-2-yl)-2,5-diphenyltetrazolium bromide) assay (Mosmann 1983). Next, MTT tetrazolium salt was prepared in accordance to formulation of 5 mg/mL in PBS, stored in the dark at 4 °C and filtered sterile; before it was diluted 1:10 into respective RPMI/Keratinocyte-SFM. Subsequent step involves the addition MTT containing medium to each well in a volume of 100 μ L and the plates were then

covered with aluminium foil and incubated at 37 °C for an additional 4 hours. After labelling the cells with MTT for 4 hours, 75 µL medium was carefully aspirated out from each well. Finally, 50 µL of DMSO was added to each well. The plate was then incubated at 37 °C for 10 minutes. Absorbance reading was set at 540 nm using microplate reader and the absorbance was further analysed (Gerlier & Thomasset, 1986).

Table 3.5 Four day routine of MTT assay in the cytotoxicity study

Day	Cell activities
Day 1	Cell counting and seeding/plating cells
Day 2	Treatment with different concentration of compound
Day 3	-
Day 4	MTT assay – adding MTT, MTT formazan solubilisation and absorbance measurement

3.6.5.1 Data analysis for MTT assay

Absorbance readings from the MTT assay were converted into percentage cell death using the following equation:

$$\left[\frac{(\text{Control-Blank})\text{Abs} - (\text{Treated cell-Blank})\text{Abs}}{(\text{Control - Blank})\text{Abs}} \right] = \text{The \% of cell death}$$

Abs = Absorbance at 540 nm

The results of three independent experiments were obtained and the values were presented as mean \pm standard deviation. One-way analysis of variance (ANOVA) test was applied to analyse P value. *P*-values less than 0.05 were considered as statistically significant. The mean \pm standard deviation of the MTT assays was plotted as a dose-response graph in Graphpad Prism 6. The IC₅₀ values were interpolated from the graph. The standard error of the mean was calculated to show the reproducibility of the three MTT assays.

3.6.6 Phase contrast inverted microscope study of cell morphology

The 96 well plates were seeded with the carcinoma cells (A549 and HK1) at a density of 10^5 cells in 100 μ L of RPMI with 10% (v/v) FBS. The plate was incubated at 37 °C and 5% CO₂ for 24 hours. The medium was aspirated from all wells and then the cells were treated with 100 μ L compounds solution at different concentrations 1-10 μ g/mL, and RPMI as a control. The plate was incubated for 48 hours. Images of both cell lines captured at the varying strengths of clusianone (29) using an optical microscope connected to a computer at 10 \times magnifications. The media were aspirated out of the well to improve the image quality and cell images treated at different concentrations of the compounds were captured using Nikon ECLIPSE TS100.

3.6.7 Western Blotting for protein analysis for clusianone (29) and derivatives anticancer pathway studies

3.6.7.1 Protein extraction from carcinoma cell

The protein extraction was done using the PRO-PREPTM protein extraction solution (iNtRON Biotechnology, Seongnam Korea) and method was modified using suppliers protocol. Cells were grown in 6 well plate at a density of 10^6 cells in 2 mL per well. After the time point treatment which covers 8, 16, 24 and 48 hours with clusianone (29), cells were harvested by trypsinisation and washed in phosphate buffered saline (PBS) and centrifuge at 2000 rpm (Eppendorf centrifuge 5810R) for 5 min. After washing cells with PBS, cells were counted and approximately 5×10^6 transferred to 2 mL tube. The cell pellet was harvested by centrifuging the tube at 13,000 rpm for 5 minutes (Eppendorf centrifuge 5452).

The remnants were removed using a pipette and thereafter the cells were resuspended in 400 μ L of PRO-PREPTM solution. The cell lysis was then induced by incubation for 20 minutes in freezer at -20 °C. The sample containing lysed cells in PRO-PREPTM solution were then centrifuged at 13,000 rpm for 5 minutes (Eppendorf centrifuge 5452) and subsequently the supernatant was transferred to a fresh 2 mL tube. The Bradford method was conducted to measure the Bovine Serum Albumin (BSA) protein concentration in each of the sample treated at different time points and the method was modified from the Quick Start Bradford protein assay protocol (Bradford, 1976). The simple method involves adding 4 μ L of the samples into the same 96 well plate followed by 200 μ L of Bradford Reagent.

After incubating 5 minutes in the dark, the readings were taken at 595 nm using microplate readers. The protein solutions were assayed in triplicate. As for the Bovine Serum Albumin (BSA) standard protocol, the method was prepared equally similar with the sample preparation whereby the linear range BSA concentration (125-1500 $\mu\text{g/mL}$) was assayed in a microplate assay. To determine the protein concentration of unknown sample (8, 16, 24 and 48 hours) treatment, BSA standard curve was created by plotting the 595 nm values (y-axis) versus their concentration in $\mu\text{g/mL}$ (x-axis). Protein concentrations in cell lysate from each sample were then determined using the formulation generated by BSA standard curve as shown in (Figure 3.3).

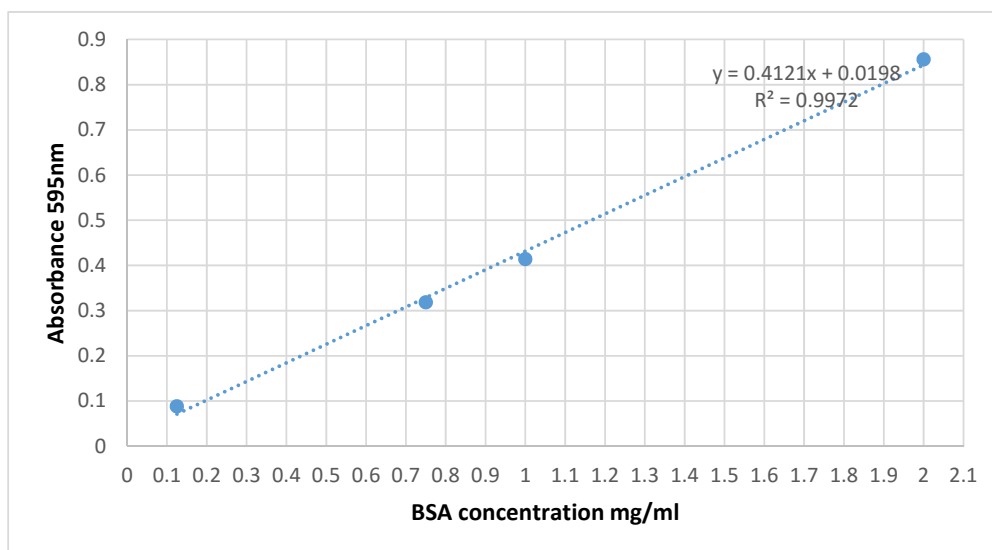


Figure 3.3 Standard curve using the microassay procedure with BSA standards.

3.6.7.2 SDS PAGE and immunoblotting

The samples were diluted in loading buffer 94% (v/v) SDS, 10% (v/v) 2-mercaptophenol, 20% (v/v) glycerol, 0.004% (v/v) bromophenol blue, 0.125 M Tris HCl) and heated at 90 °C for 10 minutes. All the samples were loaded on the well including the Rainbow marker Protein ladder (Fisher Scientific). Proteins were separated by SDS-PAGE as shown in **Table 3.6** with 4-12% (v/v) gradient gel (BioRad Mini-PROTEAN®) at 120V. The proteins were then transferred to nitrocellulose membrane (0.45 µm) using wet transfer method by running the electro blot at 25V for 80 minutes (XCell SureLock® Mini-Cell Invitrogen) (**Figure 3.4**).

Table 3.6 Formulation of stacking gel and resolving gel

Chemical/Material	Stacking gel (4%)	Resolving gel (12%)
30% (v/v) Acrylamide	0.66 mL	4.00 mL
0.5M Tris HCl	1.26 mL	-
1.5M Tris HCl	-	2.5 mL
10% (v/v) SDS	50 µL	100 µL
Purified water	3 mL	3.35 mL
Tetramethylethylenediamine (TEMED)	7.5 µL	7.5 µL
10% (v/v) APS	25 µL	50 µL
Total Volume	5 mL	10 mL

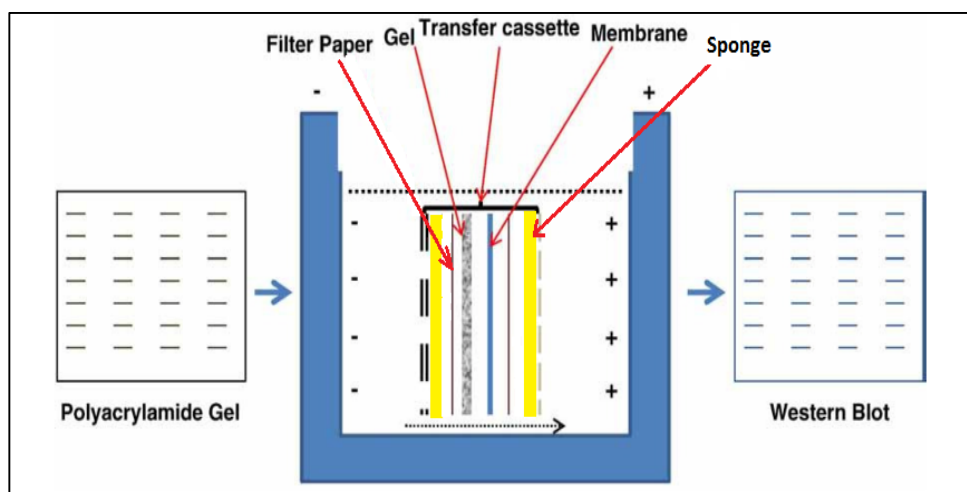


Figure 3.4 Electro blot transfer of protein from polyacrylamide gel to nitrocellulose membrane using wet transfer method edited and modified from (MacPhee, 2010)

Thereafter, proper concentration of protein was prepared for SDS-PAGE analysis. Selection of gradient gel of SDS-PAGE was essential in the separation and migration of protein bands. In this research, better protein band separation was observed when gel gradient of 4-12% was used instead of single gradient gel (**Table 3.6 & Appendix A**). As for the molecular weight marker, rainbow marker with molecular range from 11.0 kDa to 170.0 kDa was selected since all targeted proteins for the research (β -tubulin, Cdk-1, Cyclin B1 and GAPDH) are between 30.0 kDa to 60.0 kDa molecular weight as shown in (**Table 3.7 & Appendix B**).

Next, the membrane was soaked in 20 mL of blocking buffer (PBS-Tween containing 10% v/v non-fat milk) for 3 hours with gentle agitation at 50 rpm at room temperature using shaker. Subsequent step involves overnight

incubation with gentle agitation using orbital shaker with the membrane immersed in primary antibody. The primary antibody solution was freshly prepared according to the manufacturer's recommended dilution as shown in **Table 3.7**. The primary antibody was diluted with blocking buffer (PBS-Tween containing 5% (v/v) non-fat milk). The next step involves washing the membrane in 10 mL PBS-Tween for three times within 5 minutes interval. The membrane was then incubated for 3 hours with secondary antibody of HRP conjugate solution at 1:2000 dilutions with gentle agitation using horizontal shaker. The secondary antibody was diluted in blocking buffer (PBS-Tween containing 5% (v/v) non-fat milk). After 3 hours, the membrane was washed three times with PBS-Tween with 5 minutes interval and rinsed thoroughly with distilled water prior to staining.

Finally, the membrane was stained with TMB substrate for detection of the targeted protein. The monoclonal antibodies mAb against the following proteins were used for immunoblotting: Cdk-1, Cyclin B1, β -tubulin and GAPDH. GAPDH was used as a loading control (Aldridge *et al.*, 2009). Secondary antibodies were chosen according to the primary antibodies used (goat anti-rabbit or anti-mouse IgG antibody linked to HRP) (Narvi *et al.*, 2013; Cang *et al.*, 2014).

Table 3.7 Details of monoclonal antibodies used in immunoblotting

Antibodies	Host species	Molecular weight	Dilution factor	Supplier
β -tubulin	Rabbit	55 kDa	1:1000	Cell Signalling
Cdk-1	Rabbit	34 kDa	1:10000	abcam
Cyclin B1	Rabbit	58 kDa	1:3000	abcam
GAPDH	Mouse	40.2 kDa	1:10000	abcam

The selections of antibodies are decisive in detection of specific band relevant to targeted protein and generally, antibodies are categorized as monoclonal and polyclonal antibodies. Polyclonal antibodies are derived from animal B cells such as mice, rabbits, sheep, goats and donkeys. These antibodies consist of immunoglobulin molecule that binds to different epitopes on an antigen. This action differs in monoclonal antibodies by which it binds to a single epitope within an antigen. Monoclonal antibodies contain homogenous cloned immunoglobins made by fusing antibody producing B cells from the spleen of the immunized animal (rabbit, mouse or rat) with an immortalized cell.

As a result, polyclonal antibodies tends to develop higher cross reactivity which results in higher background bands since it interacts with multiple epitopes. During the course of immunoblot evaluation, it was noticed that the use of β -tubulin polyclonal antibody resulted in higher background bands as shown in **Appendix C**. Therefore, monoclonal antibodies are always a better choice of primary antibodies in western blot analysis since it detects one target epitope and result in less background bands (Kalyuzhny, 2011).

3.6.7.3 Densitometry for protein concentration analysis

The densitometry was an important device in capturing images of agarose gel and nitrocellulose membrane. After staining the nitrocellulose with TMB substrate, images of the membrane were captured using Quantity One Bio-Rad software. The imaging software was also used to analyse the protein concentration based on the intensity of the band appearing on the nitrocellulose membrane.

The user guide version 4.2.1 (PIN 4000 126-10 Rev A) were used to analyse the signals detected in each band. Small boxes are placed around the protein band appearing on single lanes. The placement of this rectangle strips allows multiple single proteins signals to be quantified. Relative quantification was given by the optical density value (defined as $\Sigma(\text{each pixel value} - \text{background})$) which was determined for equal sized boxes drawn around bands, with background values taken below each band of interest to account for non-specific antibody staining in the lane (**Appendix D**). Any values which were too high were taken as a warning and rectangle strips were placed until correlation between the rest of the bands on the same lane was observed. At the same time, it was noticed that background values were almost negligible and did not significantly deviate values of the data. Since each experiment to target Cdk-1, Cyclin B1, β -tubulin and GADPH were done in duplicate, the mean optical density from both experiments were calculated.

CHAPTER 4 RESULTS AND DISCUSSION

ISOLATION OF CLUSIANONE AND CHEMICAL SYNTHESIS OF CLUSIANONE DERIVATIVES

4.1 Isolation of clusianone (29) from leaves of *G. parvifolia* (Miq.)Miq

The hexane extract has been identified to contain the non-polar phenolic compound clusianone (29). Initial step of maceration of leaves was performed over 3 days then repeated 3 times subsequently to optimize the concentration of the compound of interest. However, the same maceration process also increased the concentration of waxes, oily substances and chlorophyll in the hexane extract. For removing chlorophyll from hexane extract, a mixture with Si gel together with activated charcoal was then subjected to a gravity column chromatography and the diethyl ether eluent was collected. Thereafter, fractionations were followed by subjecting two different solvents first with hexane followed by dichloromethane to the mixture in a column chromatography (Sargenti & Vichnewski, 2000).

This technique was used to decolorize the extract because coloured pigments in plants such as chlorophyll which was abundant in leaf extract were adsorbed on the surface of the carbon particle. The coloured compounds adsorb more strongly to the surface of activated charcoal binding sites. A potential disadvantage of this method was that the desired compound clusianone (29) might be adsorbed by the activated carbon and low recovery occurred when excessive carbon was added. Therefore, the coloured pigments and compound still exist in hexane and dichloromethane fraction and it was separated and fractionated through gradient elution column chromatography. The fractions collected in vials were then spotted on thin layer chromatography (TLC) after evaporation. The fundamental of TLC profiling was based on the standard

clusianone (29) spotted and with R_f value of 0.45 in (Cyclohexane/chloroform = 1/1). This was to target the particular scintillation vials containing compound of interest for recrystallization and at the same time to detect the fractions required for further recrystallization work through impurity removal (Sarker *et al.*, 2006).

To date, the isolation of clusianone (29) from dried roots of *Hypericum hypericoides* and stem barks of *Garcinia assigu* has produced 0.02% and 0.0021% respectively from its dried plant materials (Christian *et al.*, 2008; Ito *et al.*, 2003). The optimization of clusianone (29) from the leave extract of *G. parvifolia* afforded 0.05% yield from the dried plant material and further purity test carried out using HPLC showed > 98% purity. This method proves to be sustainable as a source of producing clusianone (29) compared to usage of non-renewable plant sources such as roots and stem barks since the yield was higher. However, the yields were not as promising as reported in the floral resins of *Clusia fluminensis*. Clusianone (29) was quantified using HPLC method and it was estimated that 37% of the male flowers composition were reported to comprise of clusianone (29) (Bittrich *et al.*, 2000).

Further to this report, subsequent attempt using high speed counter current chromatography (HSCCC) to optimize clusianone (29) from *Clusia fluminensis* was carried out and fractions obtained were subjected to both TLC and GC-MS for purity content analysis. The yield was indeed satisfactory with 6.93% (49.3 mg) of clusianone (29) presence in fraction obtained from the dried floral resins (711.3 mg) meanwhile the purity analysis showed that clusianone obtained *via* HSCCC were only 90.32% pure (Silva *et al.*, 2012).

4.1.1 Recrystallization of clusianone (29) by crystal seeding and slow evaporation method

Clusianone (29) was crystallized through two major events which were nucleation and crystal growth *via* slow solvent evaporation (**Figure 4.1**). Two main factors affecting the crystal morphology were temperature and supersaturation level of the solution. Recrystallization method was employed to separate out the foreign molecules that were present in the fraction that was collected previously (Sunagawa, 2005).

Further to this, recrystallization technique can be used to refine crystal from traces of impurities specifically using crystal seeding technique. Clusianone (29) crystal seeds nucleated from previous crystallization were introduced into supersaturated solution and acts as a heterogeneous point for the occurrence of further crystallization of similar compound (**Figure 4.2**). Hence, allowing only clusianone (29) related target molecule to crystallize isomorphously on the clusianone (29) crystal seed. As such the growth of such crystal features is called epitaxial since it is known to be single domain crystallography lattice which enhances the purity of the crystal compound (Bergfors, 2003).

Recrystallization method has afforded high purity clusianone (29) crystals (>98%) formed in $P2_12_12_1$ space group. One of the publications arising from this thesis which reports the clusianone (29) in crystalline $P2_12_12_1$ space group was essential particularly for furthering its potential therapeutic effects as anticancer drug (Nagalingam *et al.*, 2013) (**Appendix F**). The rationale behind this was the purity requirements set by ICH (International Conference on Harmonization of Technical Requirements for Pharmaceutical on Human Use)

for potential drug development (Guideline, 2009). The previous reports on clusianone (29) have never mentioned this polymorph state in crystalline $P2_12_12_1$ space group as discussed in the next subheading.

Polymorphism occurrences may cause a difference in pharmacological effect in terms of the stability and solubility of clusianone (29) (Bauer, 2008). Consequently, the efforts to produce high purity clusianone (29) in crystalline form (500 mg) consumed months of effort in order to guarantee the quality and purity of the novel derivatives which were produced *via* structural modification of clusianone (29).

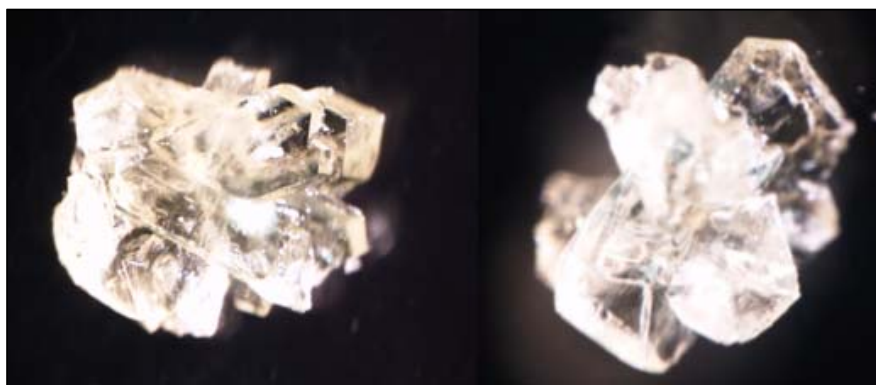


Figure 4.1 Clusianone (29) crystal morphology through solvent evaporation

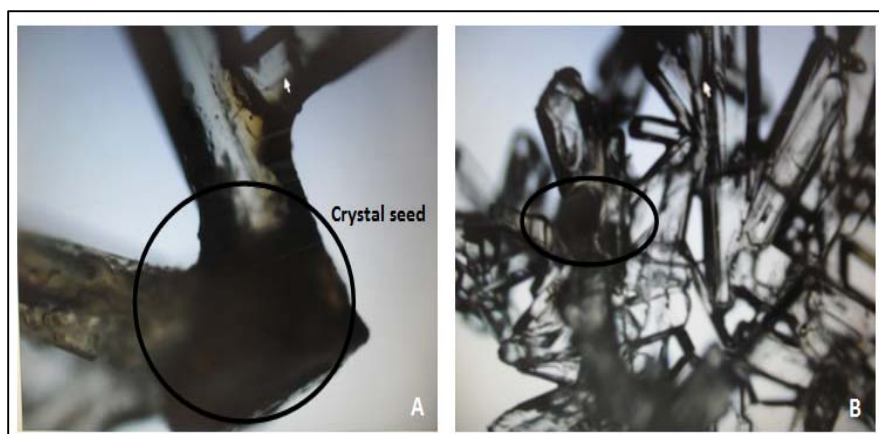


Figure 4.2 Crystal growths through seed crystal (A) 100 \times magnification (B) 40 \times magnification.

4.1.2 Characterisation of clusianone (29)

Clusianone (29) structure was characterized using FT-IR (**Figure 4.3**), single crystal diffractometer (**Table 4.1 & Figure 4.4**), ESIMS (**Figure 4.5 & Figure 4.6**), ^{13}C NMR (**Figure 4.8 & Table 4.2**), ^1H NMR (**Figure 4.7 & Table 4.3**), melting point device and polarimeter. The IR spectra of clusianone (29) showed absorptions at 3488 cm^{-1} for hydroxyl groups and 1726 cm^{-1} for carbonyl groups.

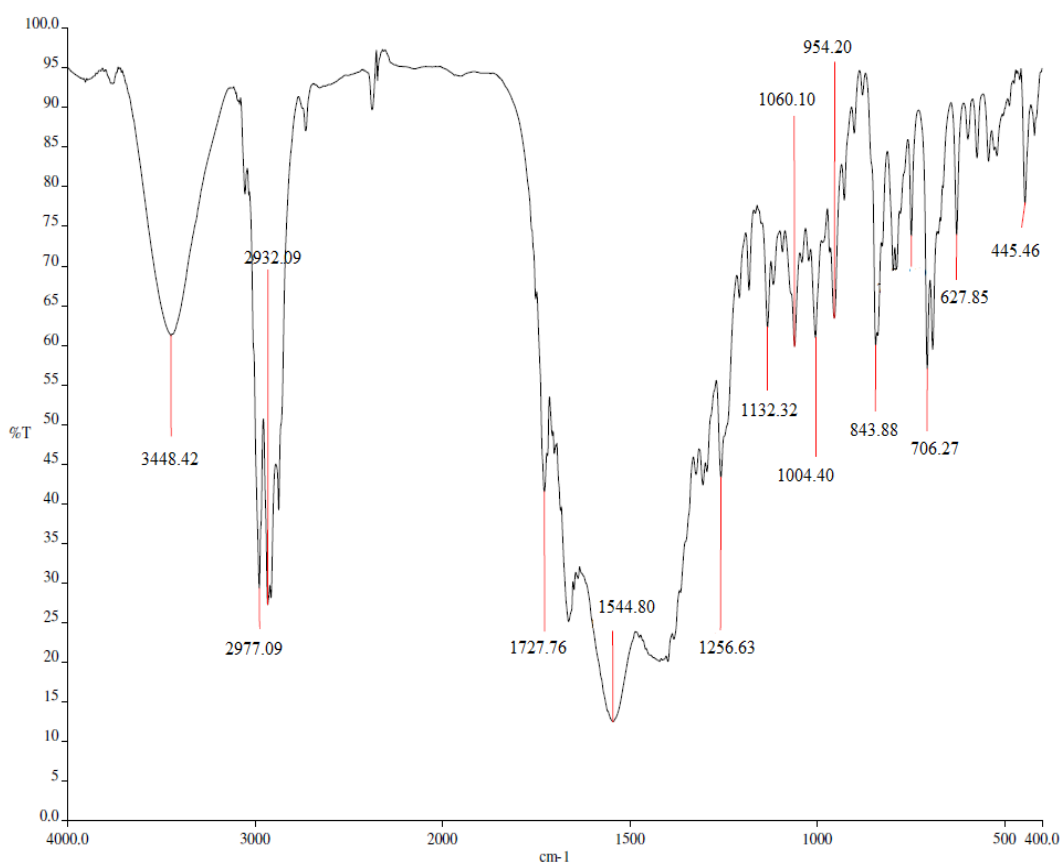
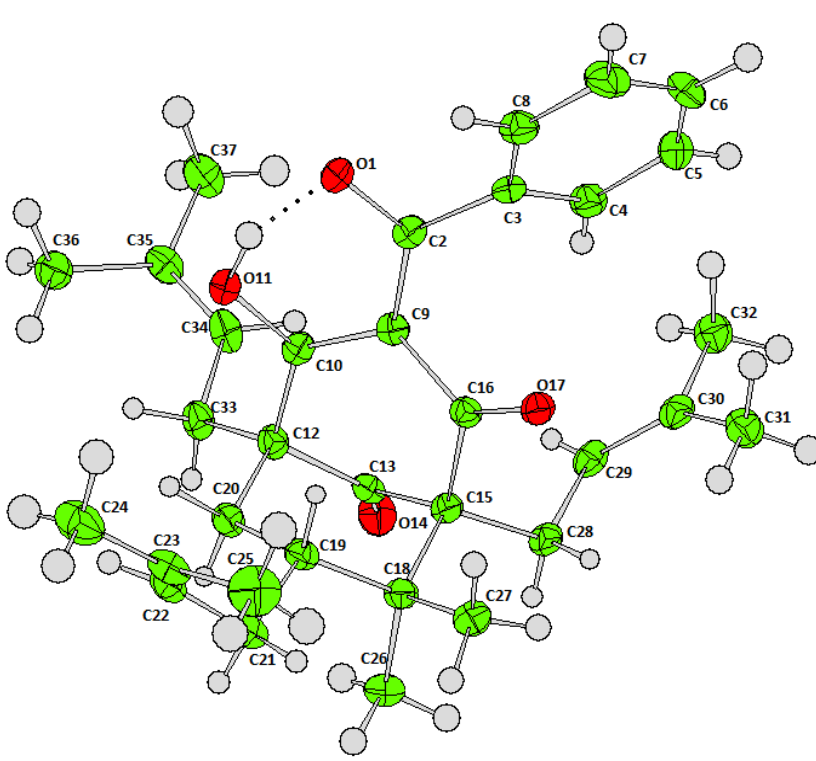


Figure 4.3 FT-IR Spectrum of clusianone (29) isolated from *G.parvifolia*

Clusianone (29) crystallizes in orthorhombic with space group $P2_12_12_1$ form having melting point of 365-366K (Table 4.1 & Figure 4.4). X-ray crystallography data was compared with the first report made for clusianone (29) isolated from *Clusia congestiflora* by McCandlish *et al.* (1976).

Table 4.1 Ortep structure including crystals parameters of clusianone

Clusianone $C_{33}H_{42}O_4$	
	
Mr	: 502.69
Melting point	: 365K
Cell parameter	: a= 9.2035, b= 13.4629, c= 22.9607
Cell angle	: $\alpha = \beta = \gamma = 90^\circ$
Volume	: 2844.96
Crystal shape	: orthorhombic
Space group	: $P2_12_12_1$
Crystal colour	: yellow

A few concerns related to the melting point and crystal space group of clusianone (29) were discovered as the data obtained were not consistent and contradicts when cross-checked with several literature reviews on clusianone (29). The melting point and space group of clusianone (29) by McCandlish *et al.* (1976) was reported as 150-152 °C and *Pna*21 respectively meanwhile our laboratory result showed clusianone (29) melting point in the range of 90-92 °C and crystal space group was $P2_12_12_1$ (**Figure 4.4**).

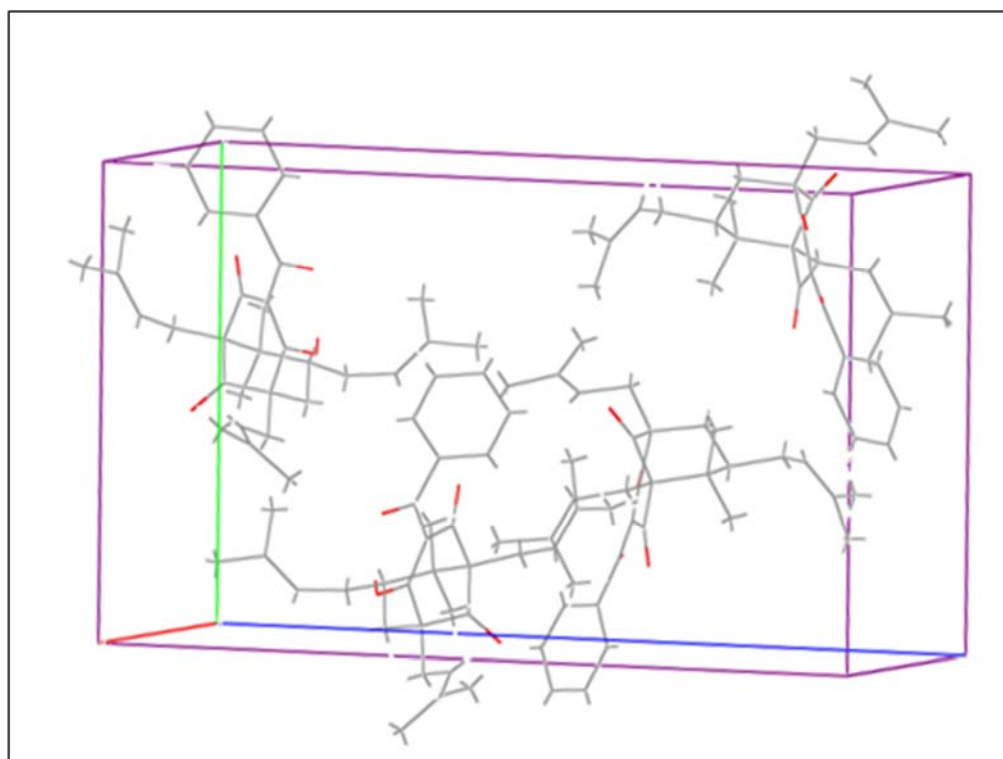


Figure 4.4 Clusianone (29) in crystal packing unit $P2_12_12_1$ form

The X-ray crystallography data comparison was also cross checked with literature related to clusianone's epimer known as 7-epiclusianone (30) in two separate reports (Santos *et al.*, 1998; Christian *et al.*, 2012). Unexpectedly, both the melting point and crystal space group of clusianone (29) were similar to its epimer and this made the data published by McCandlish *et al.* (1976) questionable. A few hypotheses were made based on the findings and additional test conducted to analyse and support the hypothesis. The different solvent used for the recrystallization method might have caused the polymorphism to occur whereby the crystals obtained by McCandlish *et al.* (1976) were crystallized in 95% ethanol solution.

The lack of detail on the specific rotation of clusianone (29) isolated by McCandlish *et al.* (1976) led us to test clusianone (29) crystal using polarimetry since naturally occurring clusianone (29) could also exist in both *S*-(+)-clusianone and *R*-(-)-clusianone enantiomer forms. The specific rotation $[\alpha]_{20}$ value was +51.94° indicating clusianone (29) isolated from *G. parvifolia* was in *S*-(+)-clusianone absolute configuration form. All these findings together with intramolecular and intermolecular bonding of clusianone in orthorhombic space group $P2_12_12_1$ were reported and published in Section E of Acta Crystallography (Nagalingam *et al.*, 2013) (**Appendix F**).

Clusianone (29) was confirmed with ESIMS (**Figure 4.5**) with adduct H^+ having base peak of (m/z 503.3147, 100%) for the $[M+H]^+$. From the ESIMS of clusianone (29), it was proposed that fragmentation of clusianone (29) yielded ions resulting from successive elimination of prenyl side chain at C5 and C7. As such, ESIMS fragment ions m/z 435 (23.3%) was a result of loss of prenyl chain at C5 $[M+H-68]^+$. Consequently, the fragments at m/z 435 resulted in two ions, one from a loss of isobutene chain at m/z 379 (4.5%) and the other at m/z 311(4.6%) occurring through the opening of bicyclo-[3.3.1]-nonane. The fragments proposed were as per shown in (**Figure 4.6**).

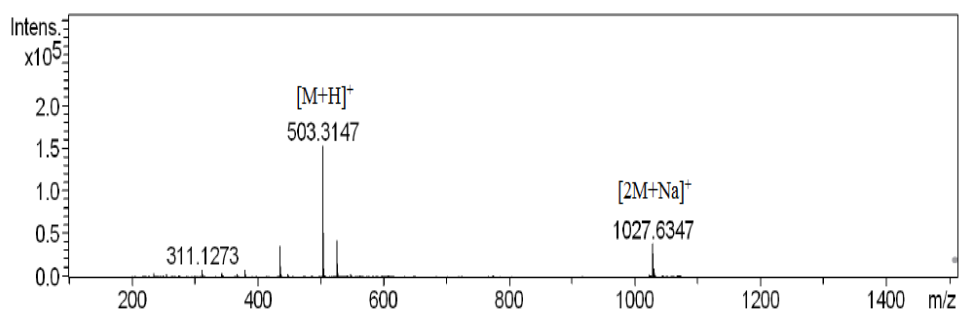


Figure 4.5 ESIMS of clusianone (29) from *G. parvifolia*

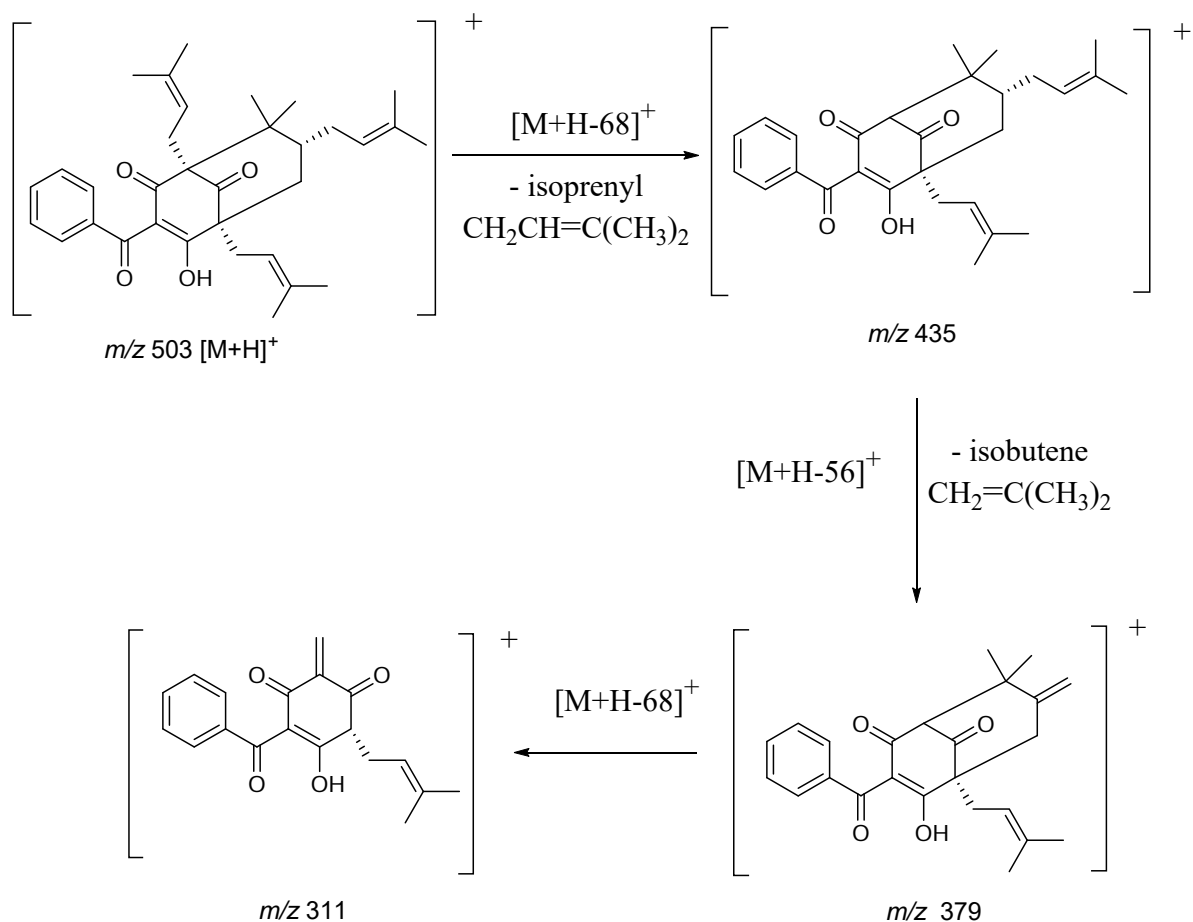


Figure 4.6 Fragmentation of clusianone (29) predicted from the fragments ion based on ESIMS

As for the 1H NMR and ^{13}C NMR interpretation, the 1H NMR (**Figure 4.7 & Table 4.3**) and ^{13}C NMR (**Figure 4.8 & Table 4.2**) details were corroborated with previously published report for clusianone (29) compound structure confirmation (Piccinelli *et al.*, 2005).

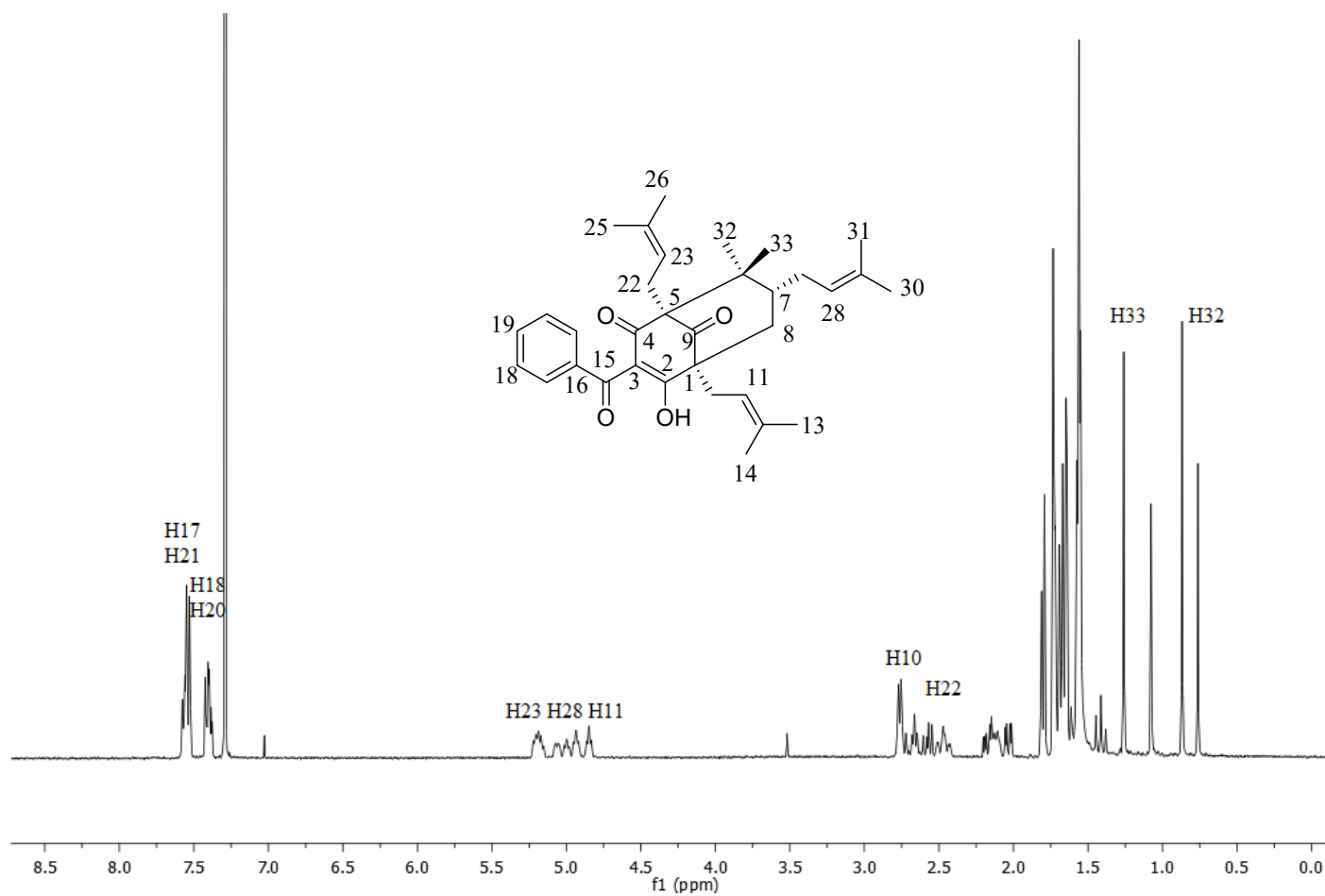


Figure 4.7 ^1H NMR spectrum of clusianone (29)

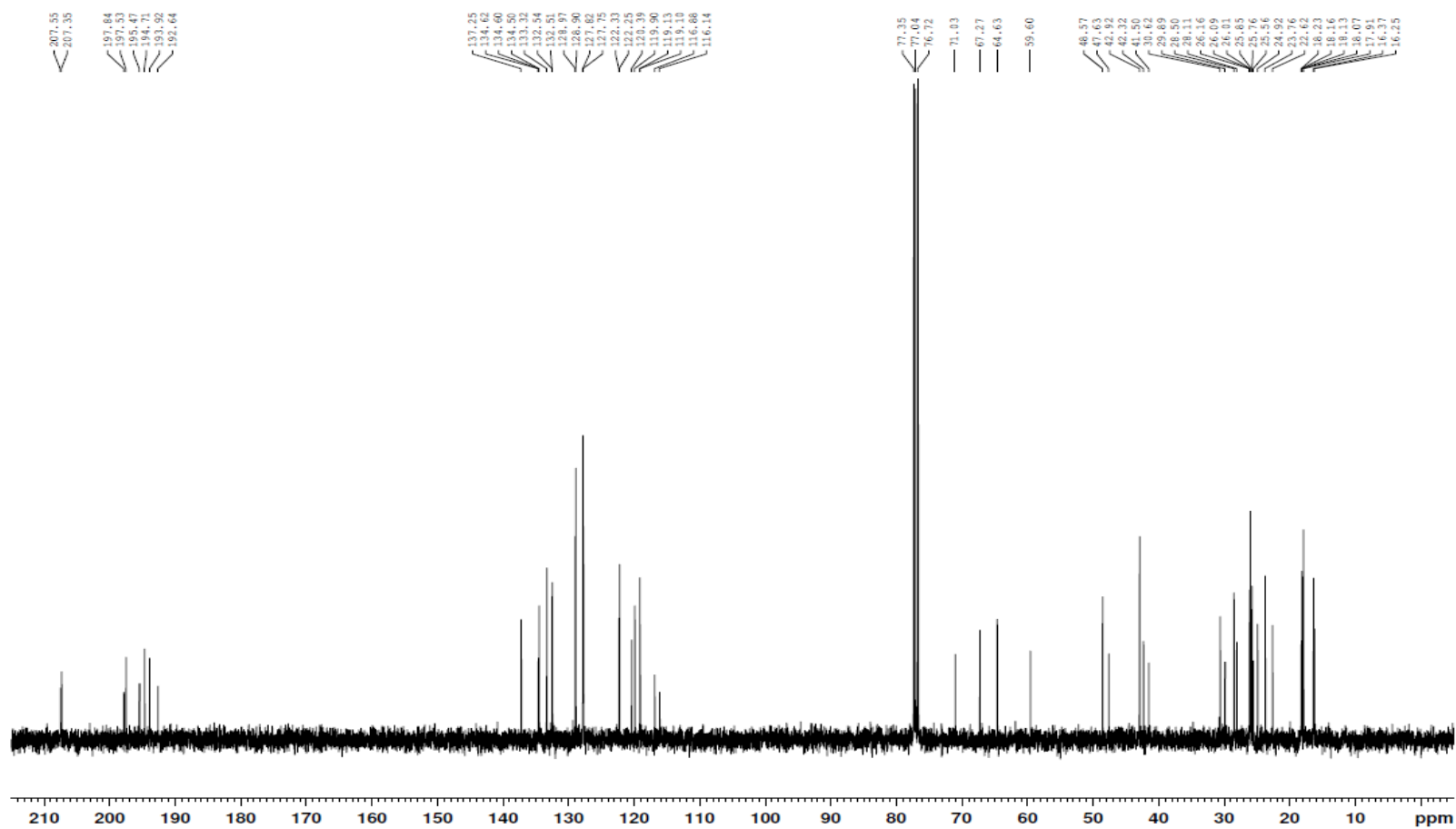


Figure 4.8 ^{13}C NMR spectrum of clusianone (29)

Table 4.2 ^1H NMR of clusianone (29) **Table 4.3** ^{13}C NMR of clusianone (29)

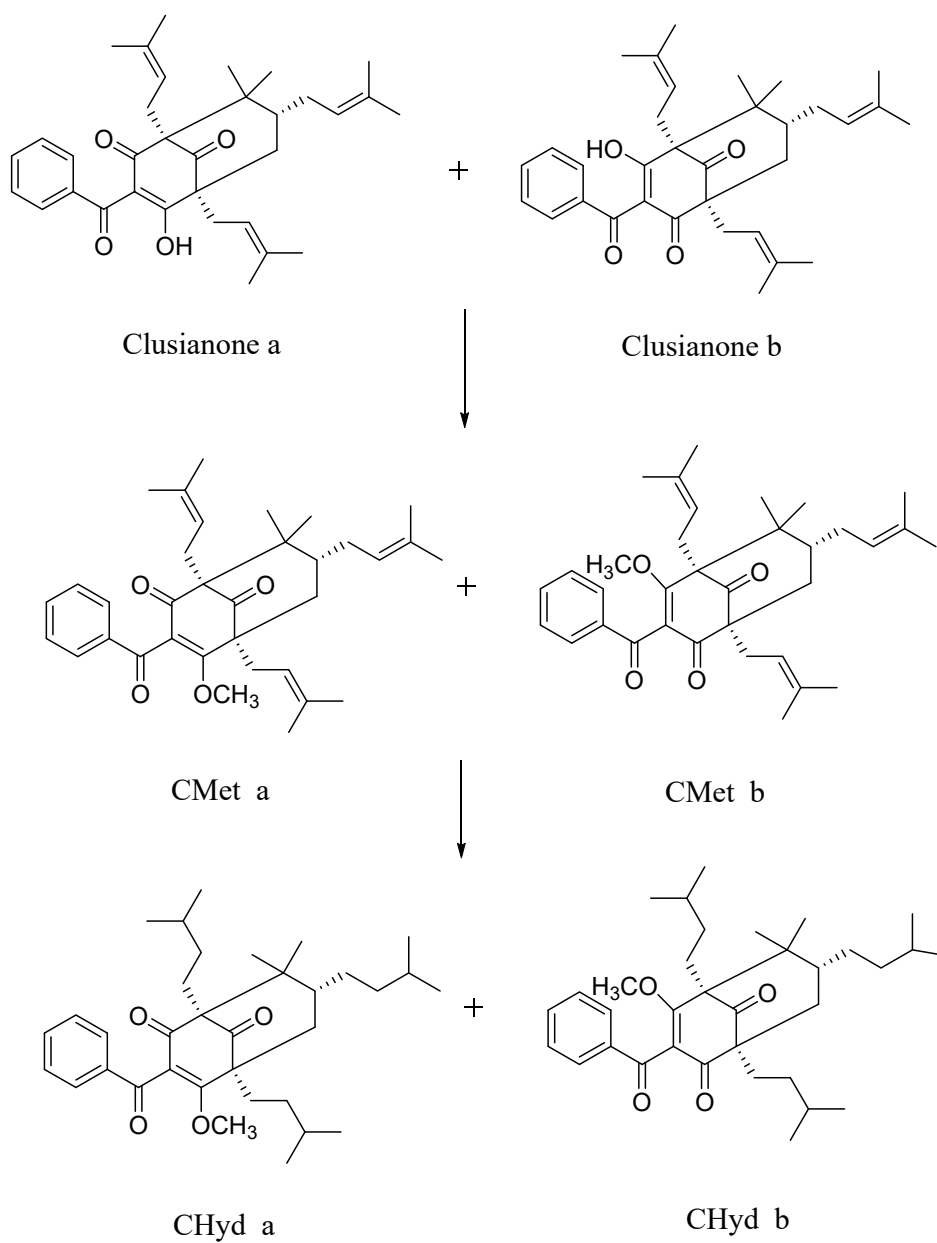
Proton assignment	δ ^1H NMR (J_{H-H} in Hz) (ppm)		Carbon assignment	δ ^{13}C NMR (ppm)	
	clusianone a	clusianone b		clusianone a	clusianone b
1	-	-	1	71.0	67.2
2	-	-	2	192.6	194.7
3	-	-	3	116.8	116.1
4	-	-	4	195.4	193.9
5	-	-	5	59.6	64.6
6	-	-	6	47.6	48.5
7	1.57	1.54	7	42.3	42.3
8ax	1.56, (t, 8Hz)	1.44, (t, 8Hz)	8	41.5	42.9
8eq	2.15, m	2.00, dd (t, 12Hz)	9	207.3	207.5
9	-	-	10	25.5	24.9
10	2.69, m	2.75, m	11	119.1	119.1
11	4.85, m	4.93, m	12	134.5	134.5
12	-	-	13	18.0	18.0
13	1.72, s	1.69, s	14	25.7	25.7
14	1.64, s	1.61, s	15	197.8	197.5
15	-	-	16	137.2	137.2
16	-	-	17,21	128.9	128.9
17,21	7.38, (d, 7.6Hz)	7.40, (d, 7.6Hz)	18,20	127.8	127.8
18,20	7.55, (t, 7.6Hz)	7.55, (t, 7.6Hz)	19	132.5	132.5
19	7.53, (t, 7.6Hz)	7.53, (t, 7.6Hz)	22	29.8	30.6
22	2.66, m	2.66, m	23	120.3	119.9
23	5.17, m	5.19, m	24	134.5	134.5
24	-	-	25	18.1	18.1
25	1.66, s	1.66, s	26	26.0	26.0
26	1.79, s	1.79, s	27	28.1	28.5
27	1.93, m	2.19, m	28	122.2	122.3
28	5.00, m	5.07, m	29	133.3	133.3
29	-	-	30	18.1	17.9
30	1.56, s	-	31	26.0	26.0
31	1.61, s	-	32	16.2	16.3
32	0.76, s	0.87, s	33	22.6	23.7
33	1.08, s	1.26, s			

*Structures of clusianone a and clusianone b on page 99

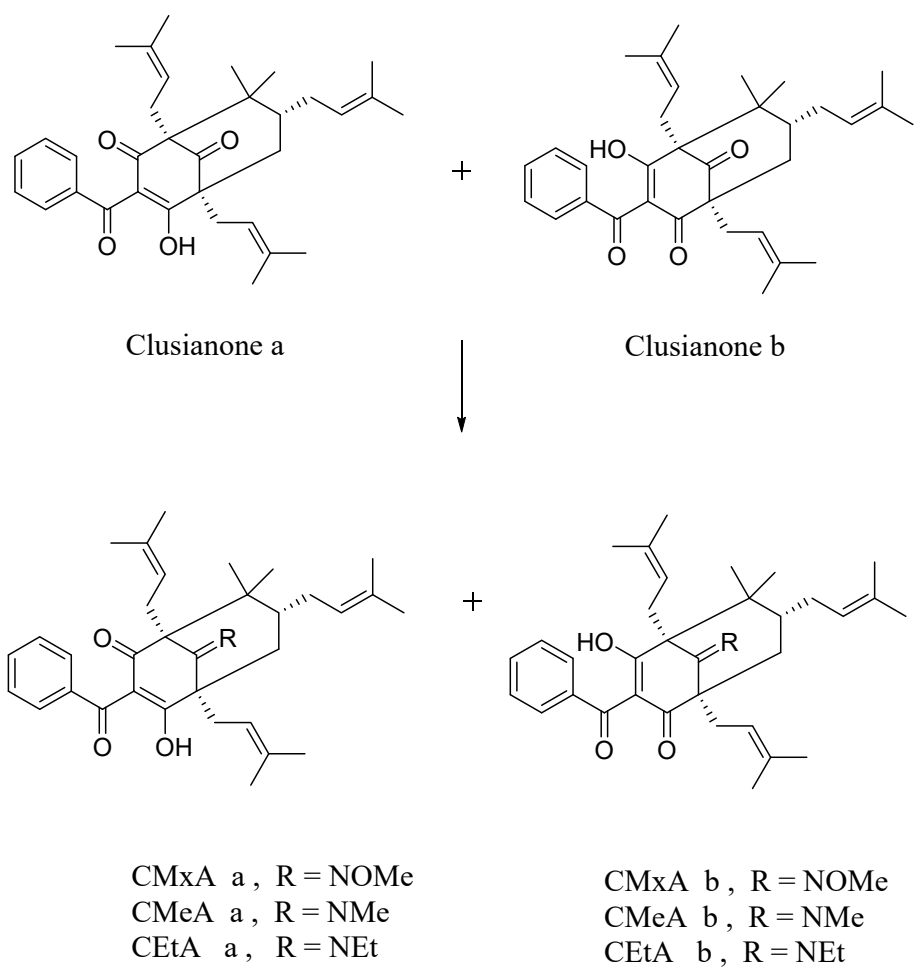
4.2 Synthesis of clusianone (29) derivatives

The synthesis of clusianone (29) derivatives was to study the structure-activity relationship of clusianone (29) and its derivatised compounds against selected respiratory cancer and normal cell lines. Eight clusianone (29) derivatives were prepared on a scale of 10-100 mg and purified using Si gel column chromatography. These successful reactions were also repeated three times to assess reproducibility and feasible synthetic plan with good yield (>75%) afforded methylated CMet (53), hydrogenated CHyd (53), oxime added CMxA (55) including two primary amines added CMeA (56) and CEtA (57) derivatives. Other reactions produced compound CPryl (58) and CGeryl (59) both with yield below 50%. Apart from this, reaction to deprotect by removing the methyl group on compound CHyd (54) gave very low overall yield 5.0% of compound CDMet (60). The overall synthesis reactions together with the expected products are illustrated in **Scheme 4.1** and IUPAC names, the abbreviated name including molecular weight are shown in **Table 4.4**.

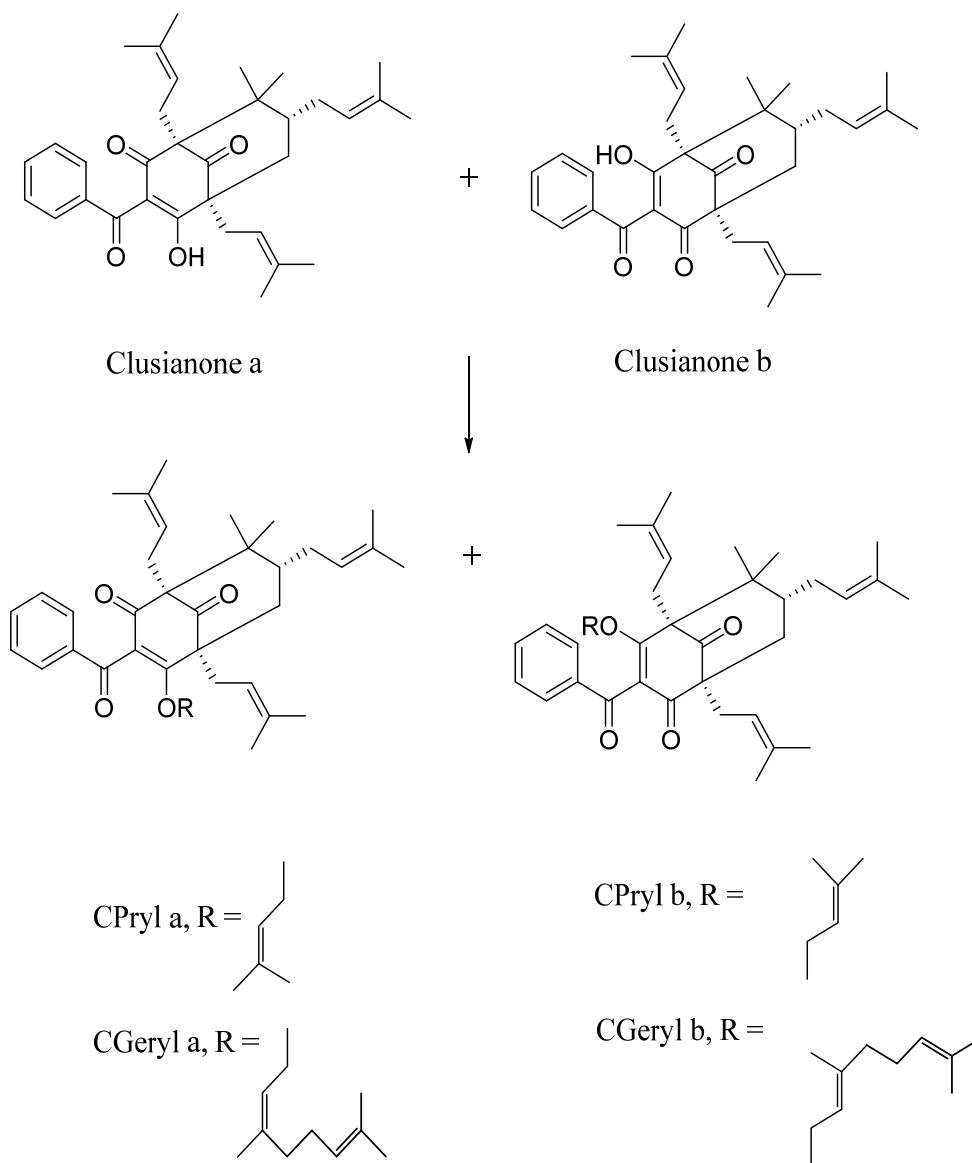
The main objective was to study the importance of existing functional group that was present in clusianone (29) and also to integrate other functional groups which could lead to a better anticancer entity. Synthesis reactions yielded two tautomer's product since clusianone (a/b) used as starting material exists in its tautomer forms (**Scheme 4.1**). Clusianone (29) derivatives were mainly characterized using ESIMS, ^1H NMR and ^{13}C NMR spectroscopy results being compared to clusianone (29) spectroscopy results shown as ESIMS (**Figure 4.5 & Figure 4.6**), ^1H NMR (**Figure 4.7 & Table 4.3**) and ^{13}C NMR (**Figure 4.8 & Table 4.2**).



Scheme 4.1 a) Synthesis reaction of clusianone (29) in tautomer forms and derivatised product in tautomeric forms.



Scheme 4.1 b) Synthesis reaction of clusianone (29) in tautomer forms and derivatised product in tautomeric forms.



Scheme 4.1 c) Synthesis reaction of clusianone (29) in tautomer forms and derivatised product in tautomeric forms.

Table 4.4 IUPAC names for clusianone (a/b) and derivatives (a/b)

Compound	Molecular Formula	IUPAC name
Clusianone a	C ₃₃ H ₄₂ O ₄	(1 <i>S</i> , 5 <i>S</i> , 7 <i>R</i>)-3-benzoyl-4-hydroxy-8,8-dimethyl-1,5,7-tris(3-methylbut-2-en-1-yl)bicyclo[3.3.1]non-3-ene-2,9-dione
Clusianone b	C ₃₃ H ₄₂ O ₄	(1 <i>R</i> , 5 <i>R</i> , 7 <i>R</i>)-3-benzoyl-4-hydroxy-6,6-dimethyl-1,5,7-tris(3-methylbut-2-en-1-yl)bicyclo[3.3.1]non-3-ene-2,9-dione
CMet a	C ₃₄ H ₄₄ O ₄	(1 <i>S</i> , 5 <i>S</i> , 7 <i>R</i>)-3-benzoyl-4-methoxy-8,8-dimethyl-1,5,7-tris(3-methylbut-2-en-1-yl)bicyclo[3.3.1]non-3-ene-2,9-dione
CMet b	C ₃₄ H ₄₄ O ₄	(1 <i>R</i> , 5 <i>R</i> , 7 <i>R</i>)-3-benzoyl-4-methoxy-6,6-dimethyl-1,5,7-tris(3-methylbut-2-en-1-yl)bicyclo[3.3.1]non-3-ene-2,9-dione
CHyd a	C ₃₄ H ₅₀ O ₄	(1 <i>S</i> , 5 <i>S</i> , 7 <i>R</i>)-3-benzoyl-1,5,7-triisopentyl-4-methoxy-8,8-dimethylbicyclo[3.3.1]non-3-ene-2,9-dione
CHyd b	C ₃₄ H ₅₀ O ₄	(1 <i>R</i> , 5 <i>R</i> , 7 <i>R</i>)-3-benzoyl-1,5,7-triisopentyl-4-methoxy-6,6-dimethylbicyclo[3.3.1]non-3-ene-2,9-dione
CMxA a	C ₃₄ H ₄₅ NO ₄	(1 <i>S</i> , 5 <i>R</i> , 7 <i>R</i>)-3-benzoyl-4-hydroxy-9-(methoxyimino)-8,8-dimethyl-1,5,7-tris(3-methylbut-2-en-1-yl)bicyclo[3.3.1]non-3-en-2-one
CMxA b	C ₃₄ H ₄₅ NO ₄	(1 <i>R</i> , 5 <i>S</i> , 7 <i>R</i>)-3-benzoyl-4-hydroxy-9-(methoxyimino)-6,6-dimethyl-1,5,7-tris(3-methylbut-2-en-1-yl)bicyclo[3.3.1]non-3-en-2-one
CMeA a	C ₃₄ H ₄₅ NO ₃	(1 <i>S</i> , 5 <i>R</i> , 7 <i>R</i>)-3-benzoyl-4-hydroxy-8,8-dimethyl-1,5,7-tris(3-methylbut-2-en-1-yl)-9-(methylimino)bicyclo[3.3.1]non-3-en-2-one
CMeA b	C ₃₄ H ₄₅ NO ₃	(1 <i>R</i> , 5 <i>S</i> , 7 <i>R</i>)-3-benzoyl-4-hydroxy-6,6-dimethyl-1,5,7-tris(3-methylbut-2-en-1-yl)-9-(methylimino)bicyclo[3.3.1]non-3-en-2-one
CEtA a	C ₃₅ H ₄₇ NO ₃	(1 <i>S</i> , 5 <i>R</i> , 7 <i>R</i>)-3-benzoyl-9-(ethylimino)-4-hydroxy-8,8-dimethyl-1,5,7-tris(3-methylbut-2-en-1-yl)bicyclo[3.3.1]non-3-en-2-one
CEtA b	C ₃₅ H ₄₇ NO ₃	(1 <i>R</i> , 5 <i>S</i> , 7 <i>R</i>)-3-benzoyl-9-(ethylimino)-4-hydroxy-6,6-dimethyl-1,5,7-tris(3-methylbut-2-en-1-yl)bicyclo[3.3.1]non-3-en-2-one
CPryl a	C ₃₈ H ₅₀ O ₄	(1 <i>S</i> , 5 <i>S</i> , 7 <i>R</i>)-3-benzoyl-8,8-dimethyl-1,5,7-tris(3-methylbut-2-en-1-yl)-4-((3-methylbut-2-en-1-yl)oxy)bicyclo[3.3.1]non-3-ene-2,9-dione
CPryl b	C ₃₈ H ₅₀ O ₄	(1 <i>R</i> , 5 <i>R</i> , 7 <i>R</i>)-3-benzoyl-6,6-dimethyl-1,5,7-tris(3-methylbut-2-en-1-yl)-4-((3-methylbut-2-en-1-yl)oxy)bicyclo[3.3.1]non-3-ene-2,9-dione
CGeryl a	C ₄₃ H ₅₉ O ₄	(1 <i>S</i> , 5 <i>S</i> , 7 <i>R</i>)-3-benzoyl-4-(((<i>Z</i>)-3,7-dimethylocta-2,6-dien-1-yl)oxy)-8,8-dimethyl-1,5,7-tris(3-methylbut-2-en-1-yl)bicyclo[3.3.1]non-3-ene-2,9-dione
CGeryl b	C ₄₃ H ₅₉ O ₄	(1 <i>R</i> , 5 <i>R</i> , 7 <i>R</i>)-3-benzoyl-4-(((<i>E</i>)-3,7-dimethylocta-2,6-dien-1-yl)oxy)-6,6-dimethyl-1,5,7-tris(3-methylbut-2-en-1-yl)bicyclo[3.3.1]non-3-ene-2,9-dione
CDMet	C ₃₃ H ₄₈ O ₄	(1 <i>S</i> , 5 <i>S</i> , 7 <i>R</i>)-3-benzoyl-4-hydroxy-1,5,7-triisopentyl-8,8-dimethyl bicyclo[3.3.1]non-3-ene-2,9-dione

4.2.1 Synthesis of CMet (53)

[(1*S*, 5*S*, 7*R*)-3-benzoyl-4-hydroxy-8,8-dimethyl-1,5,7-tris(3-methylbut-2-en-1-yl)bicyclo[3.3.1]non-3-ene-2,9-dione]

Synthesis method approach on clusianone (29) was first initiated by methylation reaction to facilitate subsequent hydrogenation of clusianone (29) since too many side reactions occurred during direct hydrogenation of clusianone (29) including trials of synthesis in basic conditions. The approach was similar to the methylation reaction carried out by Simpkins group using K_2CO_3 and Me_2SO_4 in acetone under refluxed condition (Ahmad *et al.*, 2007).

This single step method was completed in two hours and the reaction was feasible at a larger scale using 100 mg of clusianone (29) as starting material with 90% yield of CMet (53) recovery from Si gel column chromatography purification. This made the next step of obtaining CHyd (54) feasible with sufficient amount of CMet (53) as a precursor compound for hydrogenation reaction. The ESIMS (**Figure 4.9**) showed a base peak at m/z 517.3316 (100%) for the $[M+H]^+$.

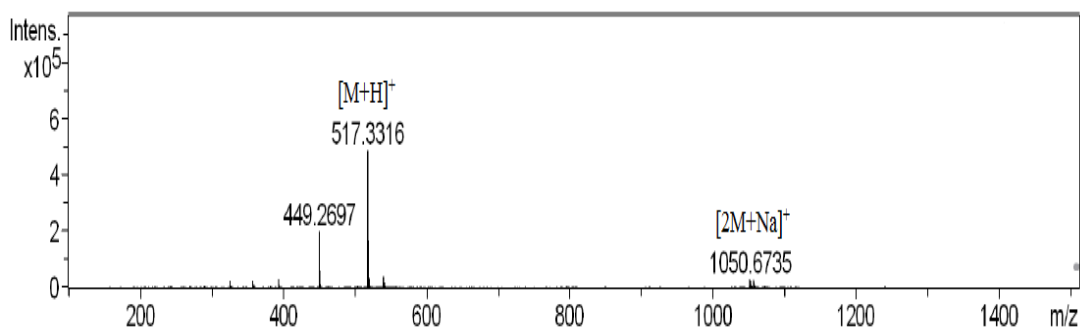
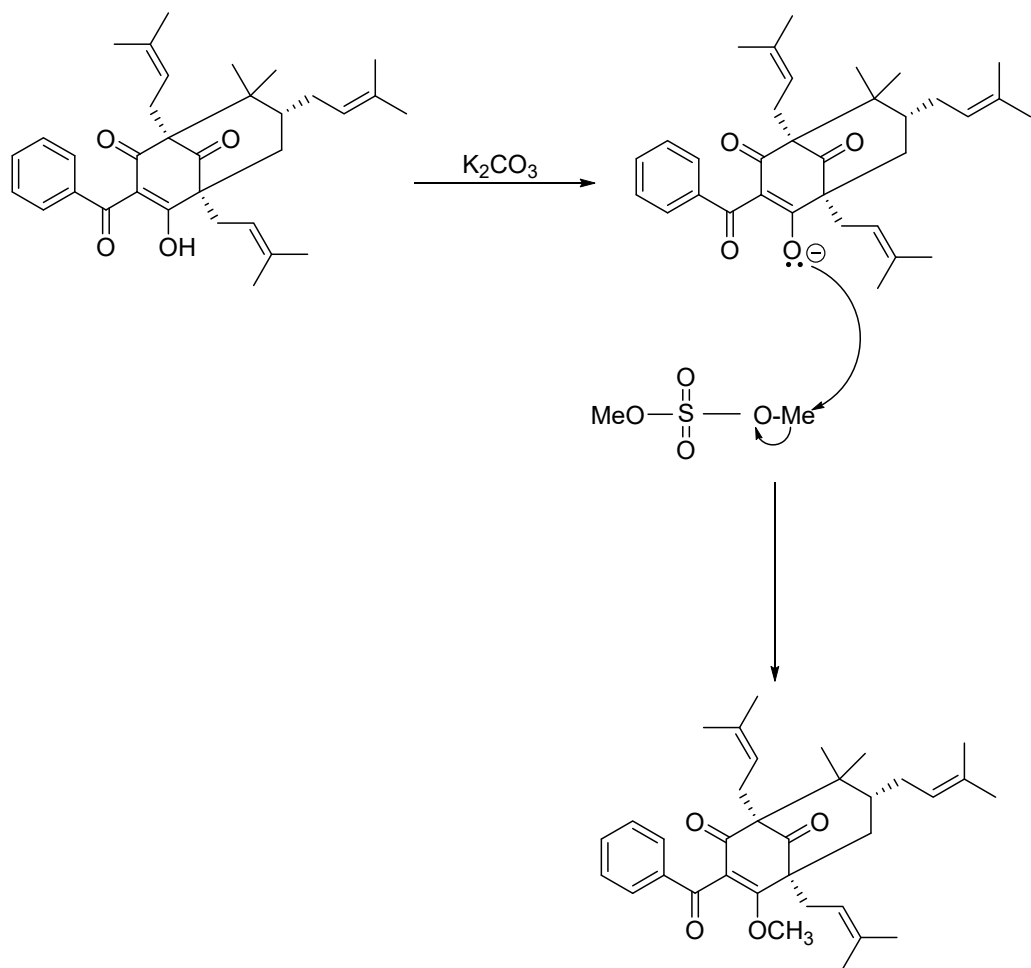


Figure 4.9 ESIMS of compound CMet (53)

The reaction mechanism of methylation on clusianone (29) is illustrated in **Scheme 4.2**. The methyl group presence was confirmed with NMR spectroscopic data. The ^1H NMR (**Figure 4.10** & **Table 4.5**) and ^{13}C NMR (**Figure 4.11** & **Table 4.6**) showed the methyl group was observed at δ_{H} 3.65 (s, 3H) and δ_{C} 60.49 respectively. The chemical shifts for both ^1H NMR and ^{13}C NMR corresponding to methyl group for CMet (53) were corroborated to the previously reported methylated clusianone (29) *via* diazomethane treatment (Oliveira *et al.*, 1996).



Scheme 4.2 Reaction mechanism for methylation of clusianone (29)

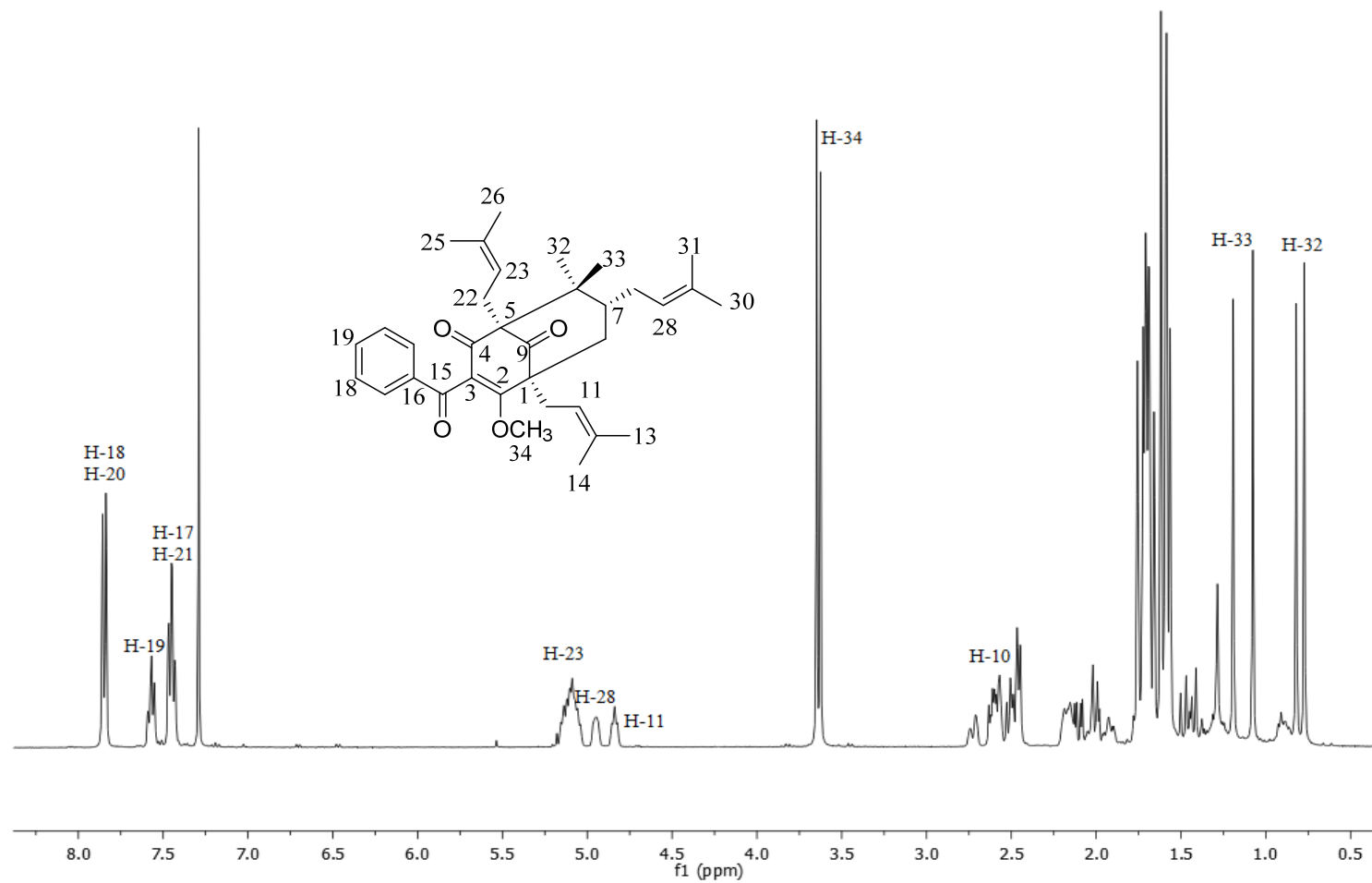


Figure 4.10 ^1H NMR spectrum of compound CMet (53)

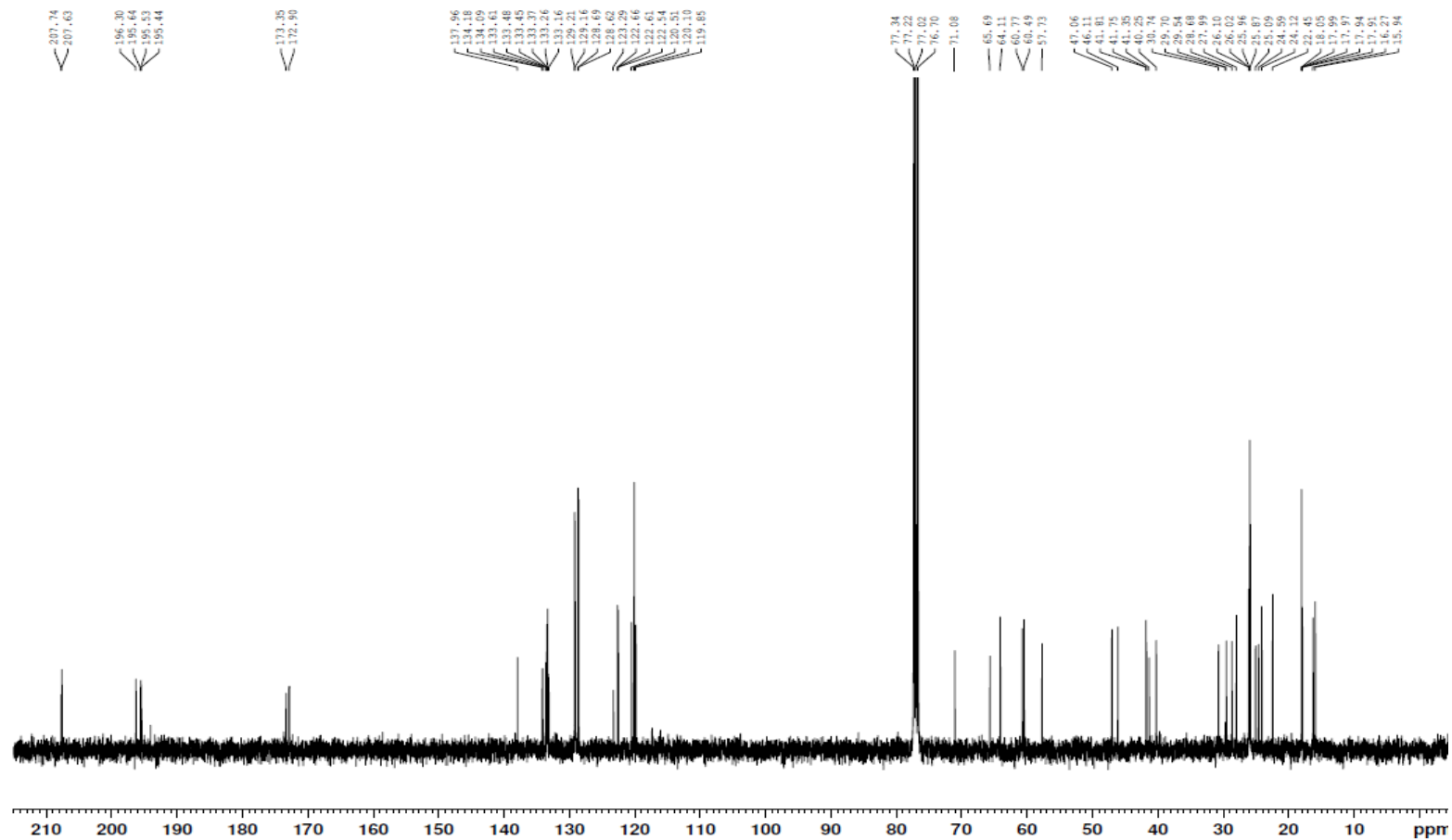


Figure 4.11 ^{13}C NMR spectrum of compound CMet (53)

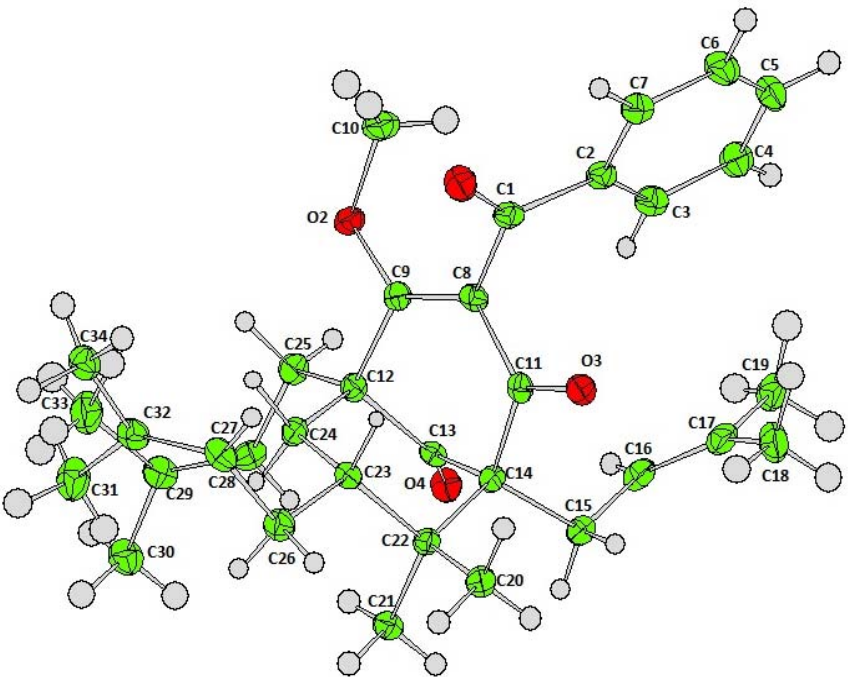
Table 4.5 ^1H NMR of CMet (53) **Table 4.6** ^{13}C NMR of CMet (53)

Proton assignment	δ ^1H NMR (J_{H-H} in Hz) (ppm)		Carbon assignment	δ ^{13}C NMR (ppm)	
	CMet a	CMet b		CMet a	CMet b
1	-	-	1	71.0	65.6
2	-	-	2	173.3	172.9
3	-	-	3	119.8	119.8
4	-	-	4	196.3	196.3
5	-	-	5	64.3	64.3
6	-	-	6	47.0	47.0
7	1.62	1.62	7	41.8	41.7
8ax	1.71, (t, 8Hz)	1.71, (t, 8Hz)	8	40.2	40.2
8eq	2.15, m	2.11, dd (t, 12Hz)	9	207.7	207.6
9	-	-	10	25.0	24.5
10	2.59, m	2.59, m	11	120.1	120.1
11	4.82, m	4.82, m	12	134.1	134.0
12	-	-	13	17.9	17.9
13	1.62, s	-	14	25.8	25.8
14	1.66, s	-	15	195.6	195.5
15	-	-	16	137.9	137.9
16	-	-	17,21	129.2	129.1
17,21	7.85, (d, 7.6Hz)	7.85, (d, 7.6Hz)	18,20	128.6	128.6
18,20	7.43, (t, 7.6 Hz)	7.43, (t, 7.6 Hz)	19	133.3	133.2
19	7.55, (t, 7.6Hz)	7.55,(t, 7.6Hz)	22	29.7	29.5
22	2.57, m	-	23	120.5	120.5
23	5.09, m	5.09, m	24	134.1	134.0
24	-	-	25	17.9	17.9
25	1.65, s	1.69, s	26	26.1	26.0
26	1.78, s	1.78	27	27.9	28.6
27	1.93, m	2.19, m	28	122.5	122.6
28	4.94, m	4.94, m	29	133.6	133.4
29	-	-	30	17.9	17.9
30	1.41, s	1.45, s	31	25.9	25.9
31	1.56, s	1.59, s	32	16.2	15.9
32	0.77, s	0.82, s	33	22.4	24.1
33	1.08, s	1.19, s	34	60.7	60.4
34	3.63, s	3.65, s			

*Structures of CMet a and CMet b on page 99

CMet (53) formed single crystal through slow evaporation method in methanol solvent. Further to this, the excellent yield also afforded large white crystals upon recrystallization using slow methanol evaporation in scintillation vials. CMet (53) single crystal was further characterized using single X-ray crystallographic analysis (**Table 4.7**, **Figure 4.12** & **Figure 4.13**).

Table 4.7 ORTEP diagram including crystals parameters of compound CMet (53)

Compound CMet (53) $C_{34}H_{44}O_4$	
	
Mr	: 516.72
Melting point	: 383K
Cell parameter	: a=10.1811, b= 11.0948, c= 13.1334
Cell angle	: α = 87.57°, β = 82.46°, γ = 89.81°
Volume	: 1469.38
Crystal shape	: triclinic
Space group	: P1
Crystal colour	: white

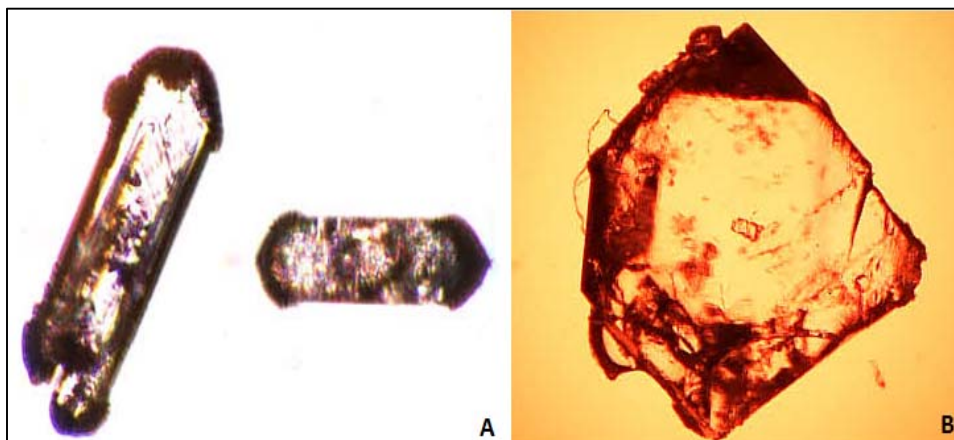


Figure 4.12 (A) CMet (53) crystal morphology through solvent evaporation. (B) Growth banding observed in single crystal of CMet (53).

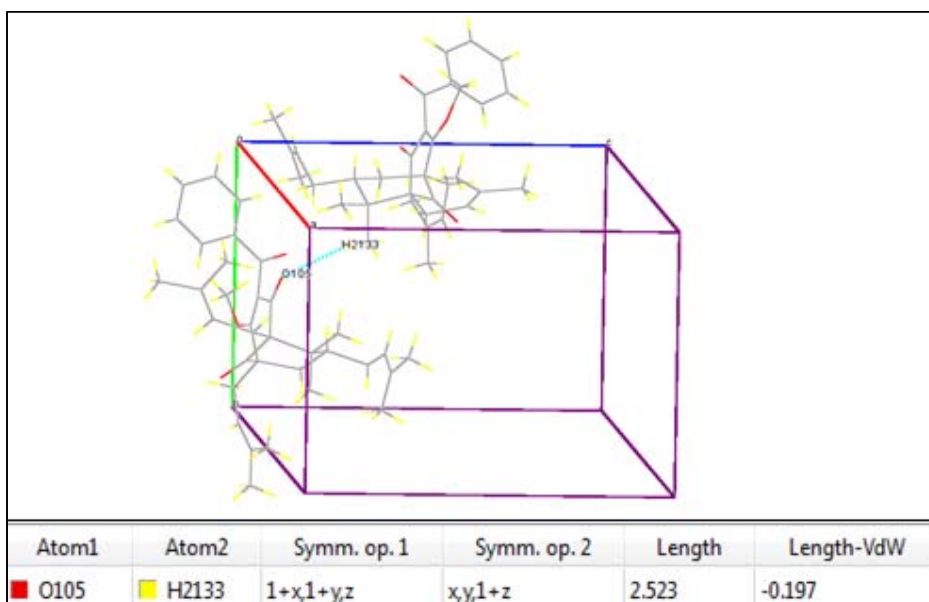


Figure 4.13 Compound CMet (53) in crystal packing unit P1 form

To date, CMet (53) crystals were obtained by diazomethane treatment of clusianone (29) isolated from *Clusia spiritus-santensis* (male) and the x-ray diffraction analysis reported the ORTEP stereoview of crystal compound. CMet (53) compound characterization using MS and NMR was reported previously. The report did not cover the crystal properties and characteristic such as space group, shape, cell parameters, bond lengths and intramolecular interactions including intermolecular interactions (Oliveira *et al.*, 1996). The melting point of CMet (53) obtained was 110 °C which contradicts the melting point (123-125 °C) reported by Oliveira *et al.* (1996).

As for the synthesis community, CMet (53) has been an important intermediate in total synthesis of clusianone (29) which involves 20 to 40 reaction steps. CMet (53) was the precursor compound involved in the final step of producing clusianone (29) (Ahmad *et al.*, 2007; Qi & Porco, 2007; Garnsey *et al.*, 2011). In this research, X-ray diffraction analysis showed CMet (53) crystallizes in triclinic system with *P1* space group. The presence of strong intermolecular hydrogen bond between the O105 atom and H2133 could be also the reason for the higher melting point value compared to clusianone (29) possessing supramolecular layers in the *ab* plane were stabilised by weak C—H···O interactions (**Figure 4.13**). Currently, there is no information regarding the crystal structure of CMet (53) in literature. Since CMet (53) was a fundamental component in total synthesis of clusianone (29), the X-ray diffraction analysis data for CMet (53) obtained from this research is considered valuable information reported in this thesis.

4.2.2 Synthesis of CHyd (54)

[(1*S*, 5*S*, 7*R*)-3-benzoyl-1,5,7-triisopentyl-4-methoxy-8,8-dimethylbicyclo[3.3.1]non-3-ene-2,9-dione]

Successively, hydrogenation of CMet (53) afforded 80% yield of CHyd (54) in a single step. Although there are several options of opening alkene double bonds, catalytic hydrogenation using palladium on activated charcoal has been an effective and fast way of obtaining the desired product CHyd (54). This method has been previously employed by other synthetic researchers studying structure-activity relationship of PPAP compounds such as xanthochymol and hyperforin (Roux *et al.*, 2000; Gartner *et al.*, 2005). Another method employed to hydrogenate CMet (53) using Wilkinson catalyst, $\text{ClRh}(\text{PPh}_3)_3$ was not successful (Trost *et al.*, 2006). Compound CHyd (54) was confirmed with ESIMS (m/z 545.3607, 100%) for the $[\text{M}+\text{Na}]^+$ (**Figure 4.14**).

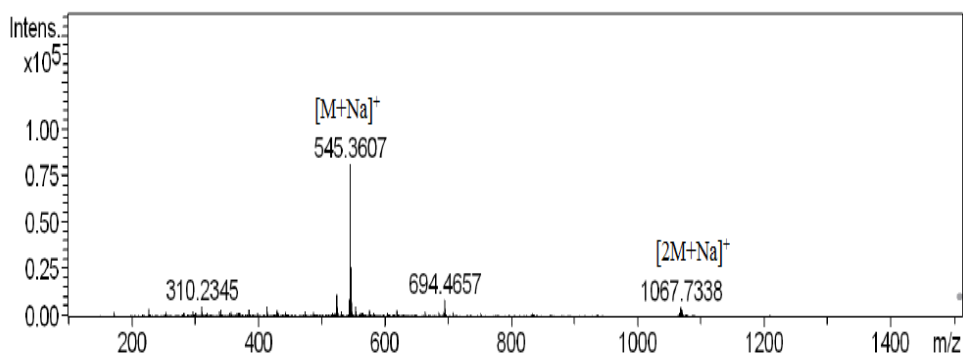


Figure 4.14 ESIMS of compound CHyd (54)

The ^1H NMR signals corresponding to H-11, H-23 and H-28 of compound CMet (53) observed at δ 5.07, δ 5.11 and δ 5.08 respectively was not observed in compound CHyd (54) (**Figure 4.15 & Table 4.8**). The deshielding was due to the presence of electronegative alkene in tetraprenyl group which increases the ^1H chemical shifts at about 5.0 ppm. As for the ^{13}C NMR signals, (**Figure 4.16 & Table 4.9**) for compound CHyd (54) of the carbon of C-11, C-12, C-23, C-24, C-28 and C-29 were found at highfield range between δ 30.0 to δ 35.0. In contrast to those in compound CMet (53), ^{13}C NMR signals were found in the range between δ 120.0 to δ 134.0. To date, there were no reports of compounds having a structure similar to CHyd (54) and hence, CHyd (54) is a newly reported clusianone (29) derivative and this was the first time hydrogenation has been carried out for clusianone (29) *via* CMet (53) as a precursor.

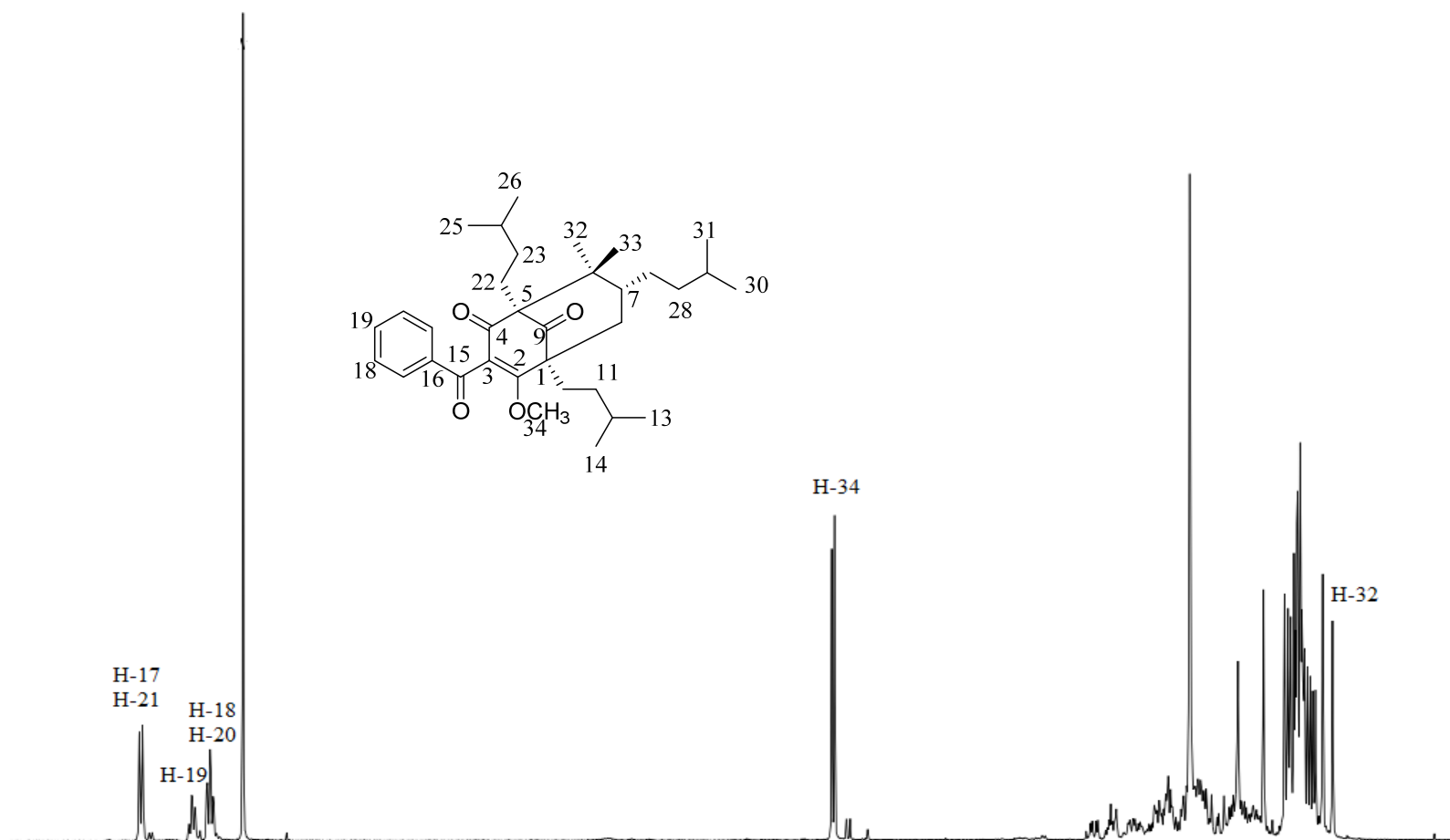


Figure 4.15 ^1H NMR spectrum of compound CHyd (54)

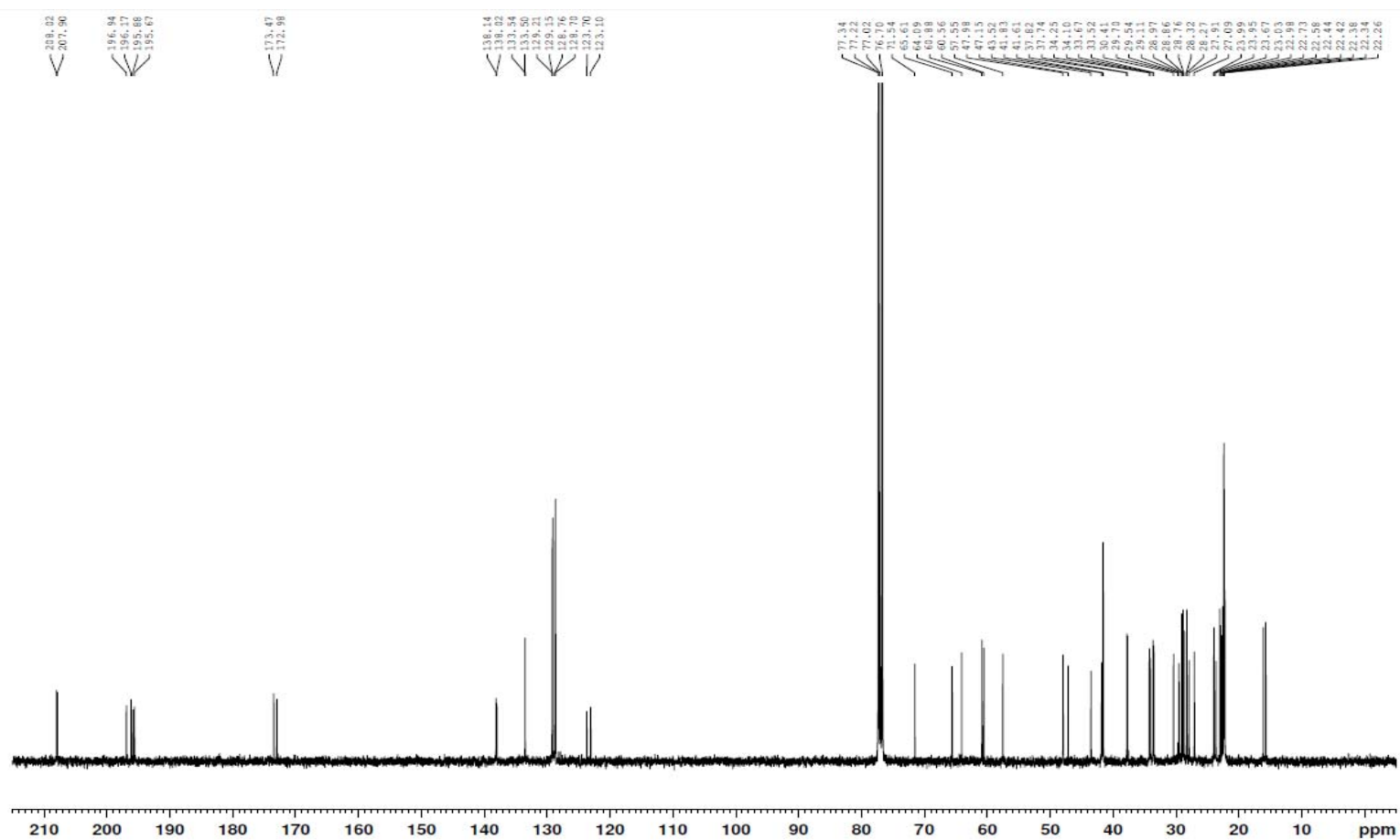


Figure 4.16 ^{13}C NMR spectrum of compound CHyd (54)

Table 4.8 ^1H NMR of CHyd (54)**Table 4.9** ^{13}C NMR of CHyd (54)

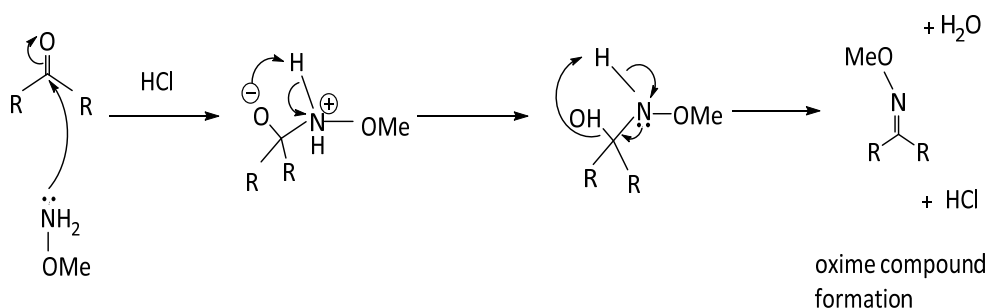
Proton assignment	δ ^1H NMR (J_{H-H} in Hz) (ppm)		Carbon assignment	δ ^{13}C NMR (ppm)	
	CHyd a	CHyd b		CHyd a	CHyd b
1	-	-	1	71.5	65.6
2	-	-	2	172.9	173.4
3	-	-	3	123.1	123.7
4	-	-	4	196.1	196.9
5	-	-	5	57.5	57.5
6	-	-	6	47.1	47.9
7	1.56, m	1.56, m	7	41.6	41.8
8ax	1.59, (t, 8Hz)	1.59, (t, 8Hz)	8	43.5	43.5
8eq	2.05, m	2.15, dd (t, 12Hz)	9	207.9	208.0
9	-	-	10	27.0	27.0
10	1.29, m	1.29, m	11	29.7	29.7
11	1.22, m	1.25, m	12	34.1	34.2
12	1.37, m	1.40, m	13	22.4	22.4
13	0.96, s	0.98, s	14	27.9	27.9
14	0.91, s	0.93, s	15	195.6	195.8
15	-	-	16	138.0	138.1
16	-	-	17,21	129.1	129.2
17,21	7.90, (d, 7.6Hz)	7.90, (d, 7.6Hz)	18,20	128.7	128.7
18,20	7.49, (t, 7.6Hz)	7.49, (t, 7.6Hz)	19	133.5	133.5
19	7.60, (t, 7.6Hz)	7.60, (t, 7.6Hz)	22	29.5	29.1
22	1.13, m	1.13, m	23	33.5	33.6
23	2.02, s	2.05, m	24	34.1	34.2
24	1.31, m	1.31, m	25	22.7	22.9
25	0.82, s	0.83, s	26	28.2	28.3
26	0.79, s	0.81, s	27	28.8	28.9
27	1.94, m	2.02, m	28	33.5	33.6
28	1.54, s	1.54, s	29	37.8	37.7
29	1.44, m	1.48, m	30	22.7	22.5
30	0.83, s	0.85, s	31	23.0	23.6
31	0.86, s	0.88, s	32	22.3	22.4
32	0.71, s	0.74, s	33	16.2	16.4
33	1.00, s	1.13, s	34	60.5	60.8
34	3.72, s	3.74, s			

*Structures of CHyd a and CHyd b on page 99

4.2.3 Synthesis of CMxA (55)

[(1*S*, 5*R*, 7*R*)-3-benzoyl-4-hydroxy-9-(methoxyimino)-8,8-dimethyl-1,5,7-tris(3-methylbut-2-en-1-yl)bicyclo[3.3.1]non-3-en-2-one]

Reduction of ketone was envisioned since clusianone (29) has ketone groups on bicyclo [3.3.1] nonane-2, 4, 9-trione skeleton. However, benzoyl group was electron withdrawing and ketone reduction at C-15 will not occur and acts as hindrance to the ketone reduction of either at C-2 or C-4. Hence, ketone reduction at C-9 was successfully carried out using acidic condition using dichloromethane solvent together with methoxyamine HCl as starting material. To date, ketone reduction at C-9 has never been reported in PPAP compounds and all PPAP compounds possess ketone group at C-9 position of the [3.3.1] nonane-2,4,9-trione skeleton. Oximation of clusianone (29) reaction afforded CMxA (55) which involves the modification of C-9 ketone of clusianone (29) to an oxime substituent. The ketone reduction was successful *via* nucleophilic addition under mild acidic condition. The synthesis of CMxA (55) was easily achieved in one step with 75% yield.



Scheme 4.3 Addition elimination reaction mechanism of C=O in the formation of oxime compound CMxA (55)

The mechanism of this reaction was preceded by addition-elimination reaction of the carbonyl group at C-9. The nucleophilicity of nitrogen on the methoxyamine was increased by the presence of oxygen. Successive proton transfer allows for elimination of water (**Scheme 4.3**). Pyridine was added to stabilize the HCl in the reaction. After 48 hours, the mixture was extracted with 5% HCl to remove the pyridine. The organic layer was dried over MgSO_4 to remove the presence of H_2O produced as by product in the reaction and further purified using Si gel column chromatography.

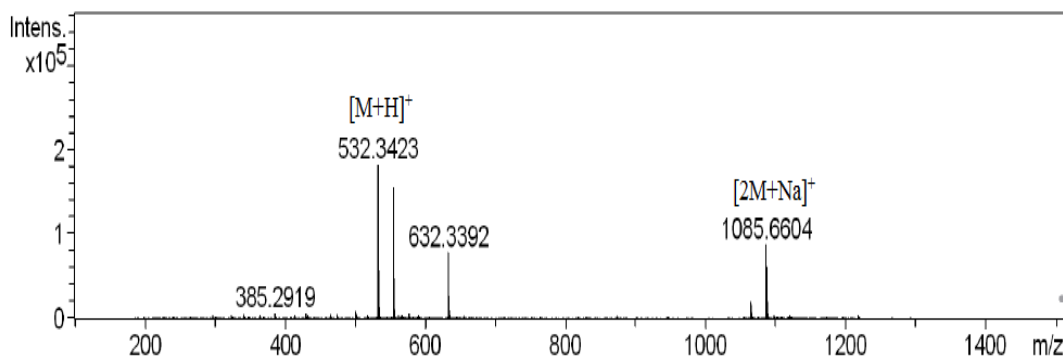


Figure 4.17 ESIMS of compound CMxA (55)

Compound CMxA (55) was confirmed with ESIMS (**Figure 4.17**) with adduct H^+ and Na^+ having base peak of (m/z 532.3423, 100%) for the $[\text{M}+\text{H}]^+$ and (m/z 554.3231, 85.9%) for the $[\text{M}+\text{Na}]^+$ respectively. The methyl group of C-34 was confirmed from its ^1H NMR (**Figure 4.18** & **Table 4.10**) corresponding to the methoxy group were observed at δ_{H} 4.10 (s, 3H) meanwhile ^{13}C NMR (**Figure 4.19** & **Table 4.11**) at δ_{C} 62.55.

The ^{13}C NMR signal of C-9 ($\text{C}=\text{N}$) attached to oxime group was represented at δ_{C} 153.0 since the $\text{C}=\text{N}-\text{O}-\text{CH}_3$ was less electronegative than $\text{C}=\text{O}$. Other signals related to C-1 and C-5 observed at δ 64.1 and δ 39.5 were shielded due to the effect of oximation which was noticed in the chemical shifts of ^{13}C NMR of compound CMxA (55) (**Table 4.11**). This was because generally in six membered heterocycles, decrease in electronegativity of a particular group in the ring skeleton shields the α -carbon (Parthiban *et al.*, 2008).

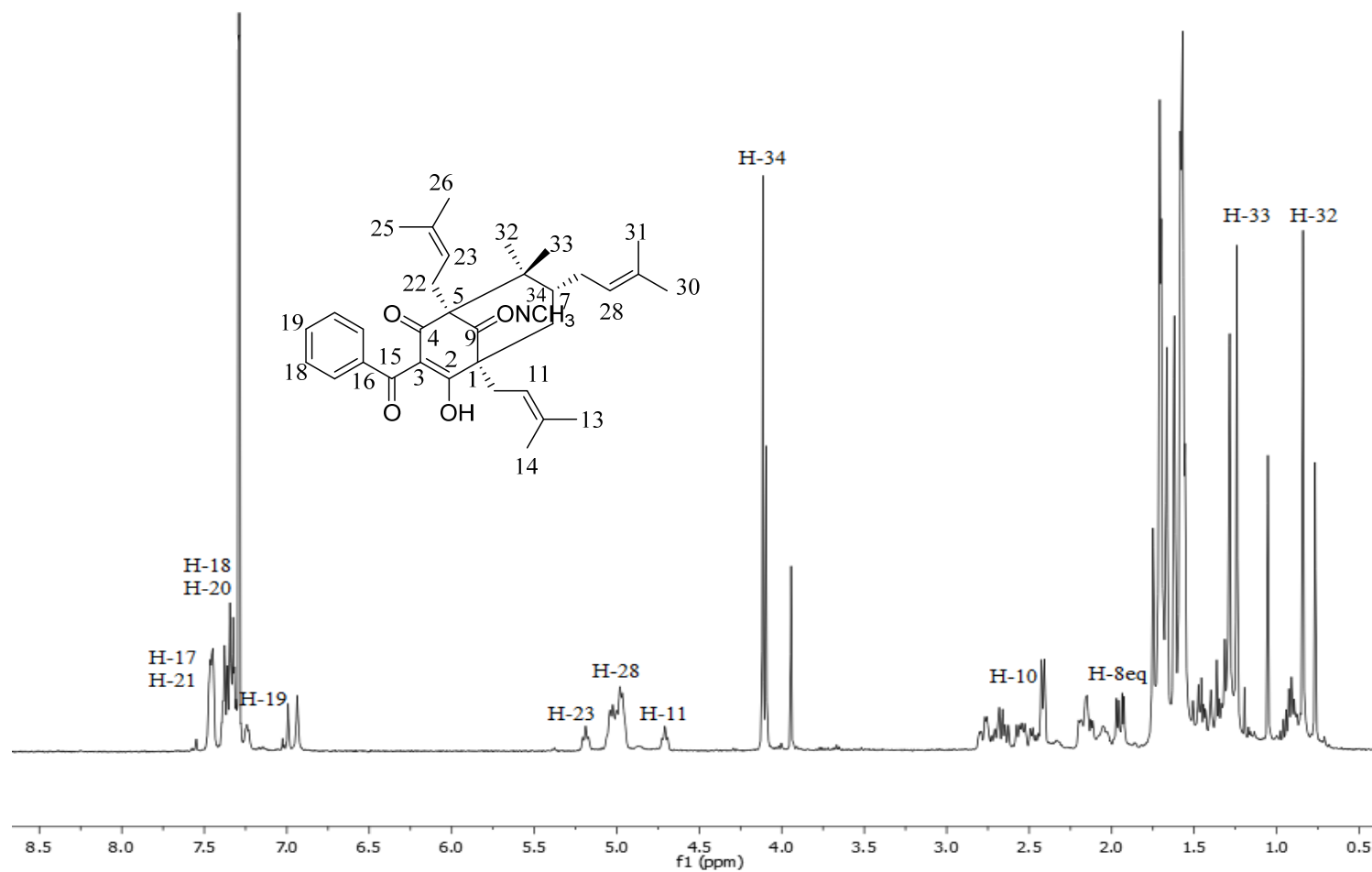


Figure 4.18 ^1H NMR spectra of compound CMxA (55)

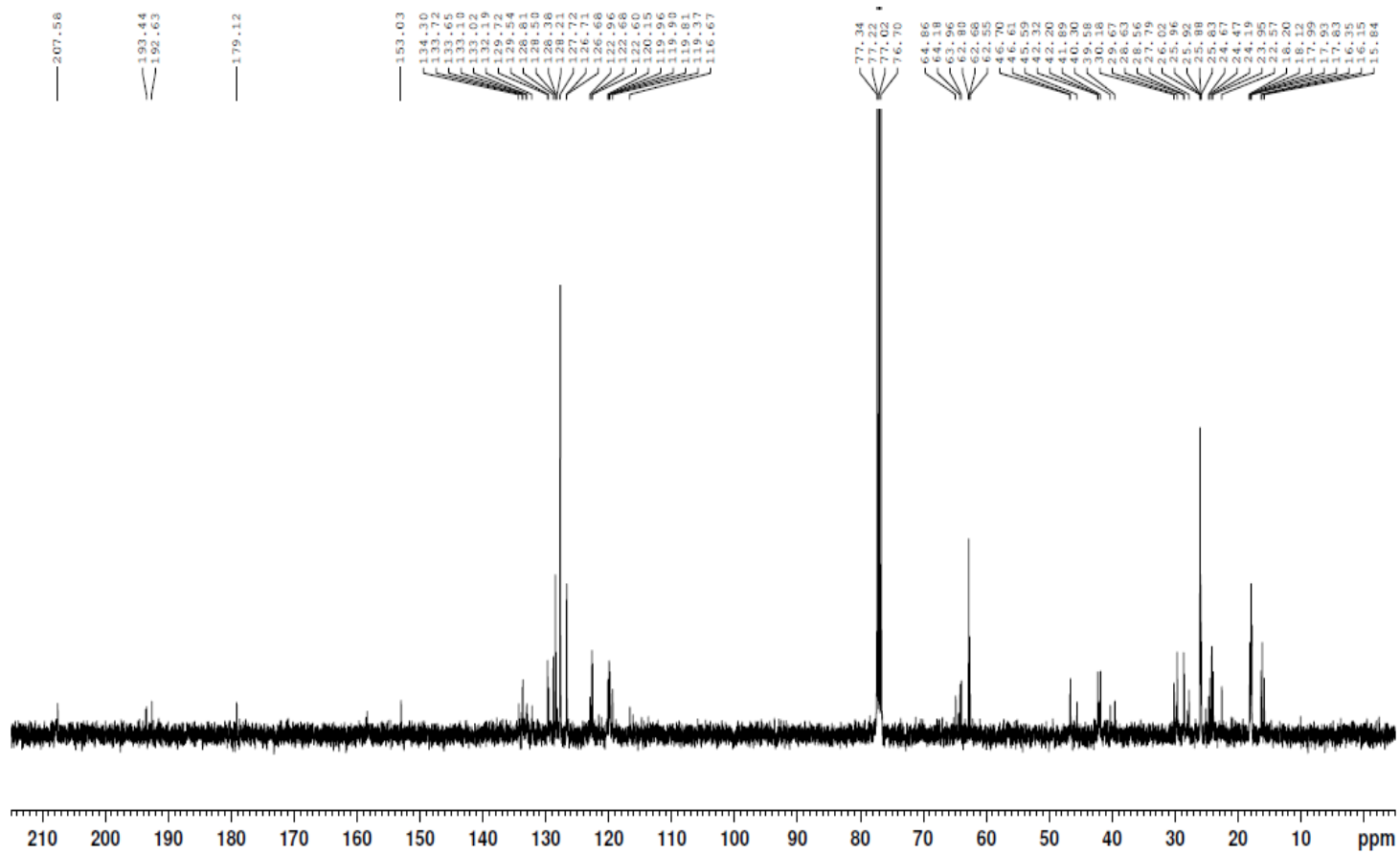


Figure 4.19 ^{13}C NMR spectra of compound CMxA (55)

Table 4.10 ¹H NMR of CMxA (55) **Table 4.11** ¹³C NMR of CMxA (55)

Proton assignment	δ ¹ H NMR (J_{H-H} in Hz) (ppm)		Carbon assignment	δ ¹³ C NMR (ppm)	
	CMxA a	CMxA b		CMxA a	CMxA b
1	-	-	1	64.1	64.8
2	-	-	2	179.1	207.5
3	-	-	3	116.6	116.6
4	-	-	4	192.6	193.4
5	-	-	5	39.5	39.5
6	-	-	6	40.3	40.3
7	1.56	1.56	7	42.2	42.2
8ax	1.57, (t, 8Hz)	1.46, (t, 8Hz)	8	46.6	46.7
8eq	2.16, m	1.96, dd (t, 12Hz)	9	153.0	-
9	-	-	10	24.4	24.1
10	2.74, m	2.76, m	11	119.3	119.9
11	4.75, m	4.75, m	12	132.1	133.0
12	-	-	13	15.8	16.2
13	1.70, s	1.70, s	14	25.8	25.8
14	1.68, s	1.68, s	15	207.5	-
15	-	-	16	133.7	134.3
16	-	-	17,21	128.5	128.8
17,21	7.46, (d, 7.6Hz)	7.46, (d, 7.6Hz)	18,20	128.2	128.3
18,20	7.36, (t, 7.6Hz)	7.36, (t, 7.6Hz)	19	129.5	129.7
19	7.24, (t, 7.6Hz)	7.24, (t, 7.6Hz)	22	29.6	30.1
22	2.66, m	2.66, m	23	119.9	120.1
23	5.19, m	5.19, m	24	132.1	133.0
24	-	-	25	17.8	17.9
25	1.66, s	1.66, s	26	25.9	25.9
26	1.75, s	1.75, s	27	27.7	28.5
27	2.54, m	2.56, m	28	122.6	122.9
28	4.99, m	4.99, m	29	133.1	133.6
29	-	-	30	18.1	18.2
30	1.56, s	1.56, s	31	23.9	24.1
31	1.62, s	1.62, s	32	15.8	16.1
32	0.76, s	0.84, s	33	22.5	-
33	1.05, s	1.19, s	34	62.55	62.6
34	4.10, s	4.11, s			

*Structures of CMxA a and CMxA b on page 100

4.2.4 Synthesis of CMeA (56)

[(1*S*, 5*R*, 7*R*)-3-benzoyl-4-hydroxy-8,8-dimethyl-1,5,7-tris(3-methylbut-2-en-1-yl)-9-(methylimino)bicyclo[3.3.1]non-3-en-2-one]

Next, synthesis of clusianone (29) derivative by installing amine groups to carbonyl C-9 of clusianone (29) was envisaged since most antimicrotubule agents such as taxol, epothilone and vinca alkaloids contains amine groups in the structure (Lucas & Moody, 2010). Reduction of clusianone (29) with methylamine HCl gave imine compound CMeA (56) in 75% yield. The ^1H NMR (Figure 4.21 & Table 4.12) corresponding to the N-CH₃ group were observed at δ_{H} 2.82 (s, 3H). The imine C9 (C=N) bond was shown in ^{13}C NMR (Figure 4.22 & Table 4.12) chemical shifts at δ_{C} 83.17 ppm. The ESIMS (Figure 4.20) showed a base peak at m/z 516.3423 (100%) for the $[\text{M}+\text{H}]^+$.

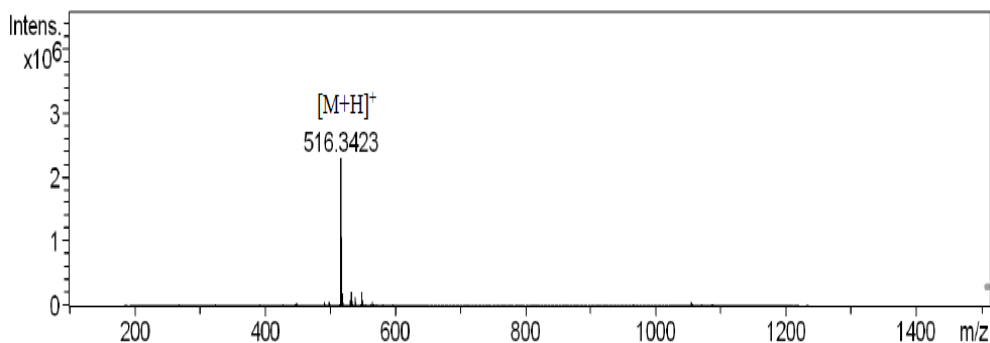
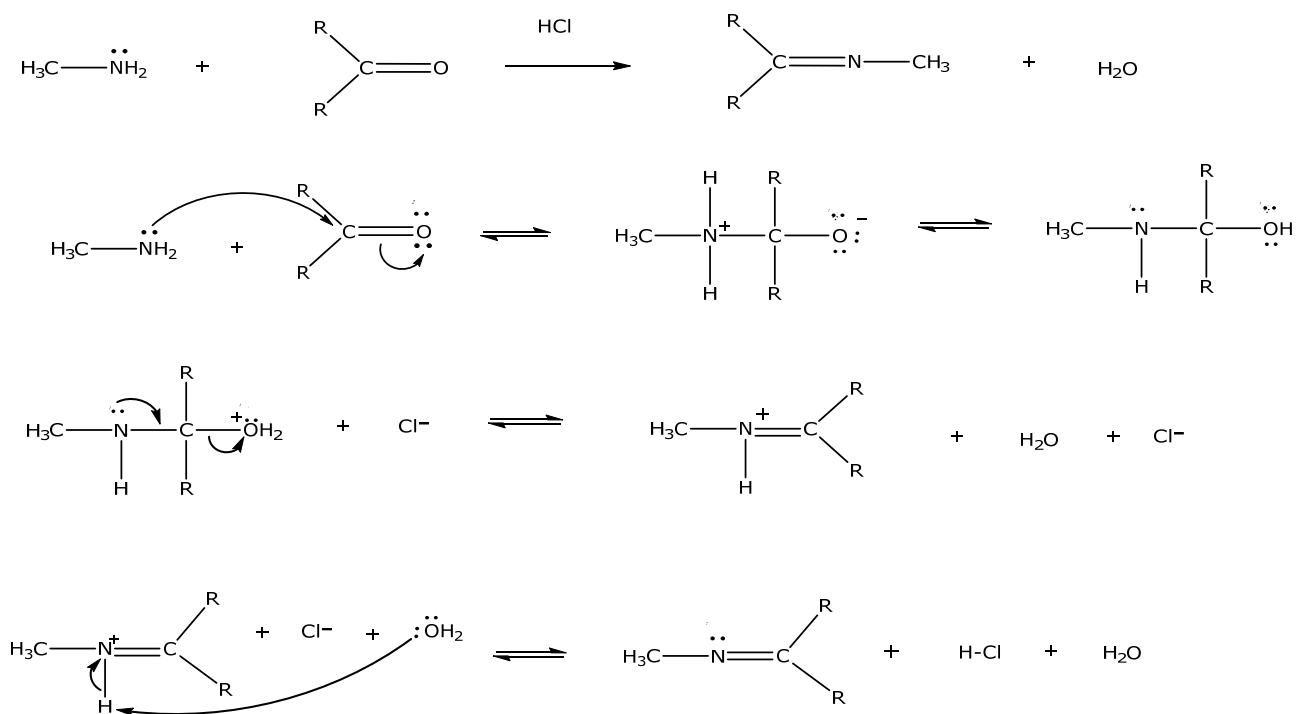


Figure 4.20 ESIMS of compound CMeA (56)

Thereafter, the addition of bulkier amine compound such as aminopiperidine to the carbonyl group of C-9 was envisioned. However, the reaction was unsuccessful and subsequent reaction with the addition of simple primary amines such as ethylamine was conducted. The reaction was successful and afforded formation of imine compound CEtA (57). The reaction mechanism of imine compound was similar to oxime compound whereby two major step occurs with carbonyl addition of an amine being the first step and dehydration elimination of water molecule as the second step to yield the C=N double bond. HCl acts as a catalyst in the formation of the imine compound formation otherwise; the reaction occurs very slowly (**Scheme 4.4**).

Based on the previously published report, it was postulated that hydroxyl group in clusianone was responsible for cytotoxic effect in liver carcinoma (Reis *et al.*, 2014). Thus the next strategy was to create clusianone (29) derivative with additional hydroxyl group. The ketone reduction to carbonyl group of C-9 to be substituted with hydroxyl group was carried out using weak reducing agent NaBH₄. The reaction indicated no signs of desired product formation upon mass spectrum analysis. A second method was also introduced, this time using a much stronger reduction agent in the form of DIBAL. Unfortunately, this reaction gave complex mixtures as a result of side reactions which lead to difficulty in the isolation process.



Scheme 4.4 Reaction mechanism of the methylamine addition to clusianone (29)

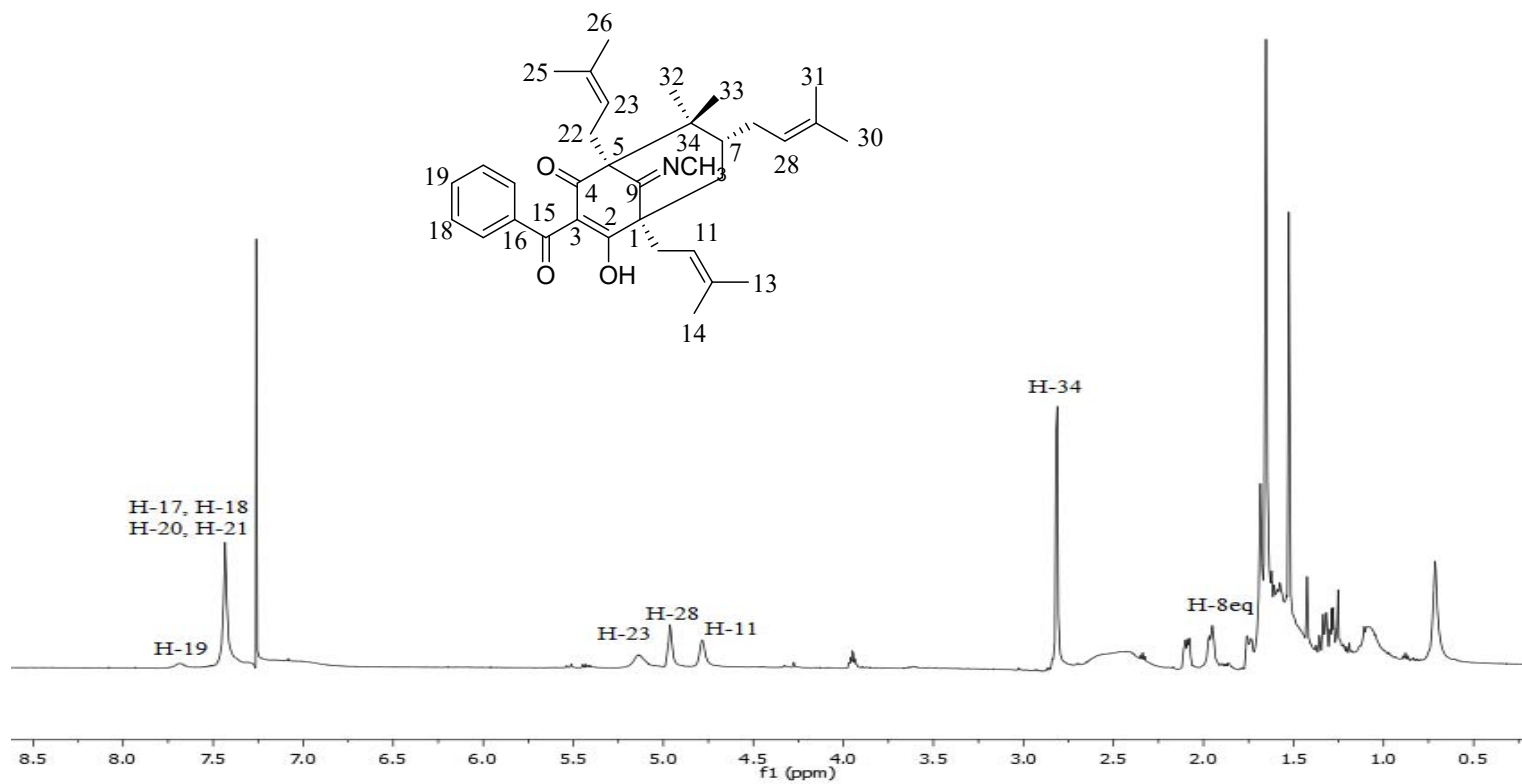


Figure 4.21 ^1H NMR spectra of compound CMeA (56)

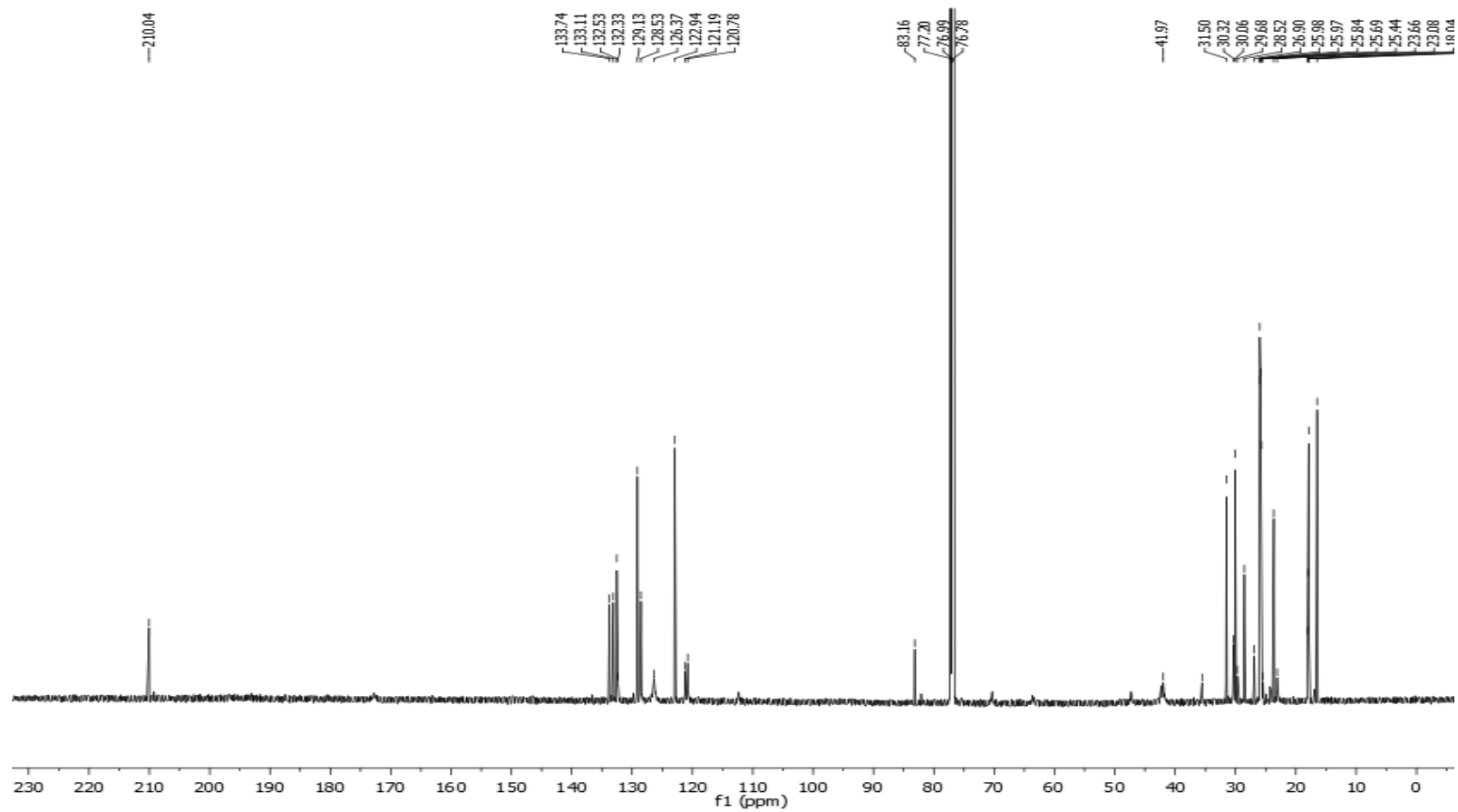


Figure 4.22 ^{13}C NMR spectra of compound CMeA (56)

Table 4.12 ^{13}C NMR and ^1H NMR of compound CMeA (56)

Carbon assignment	δ ^{13}C NMR (ppm) CMeA a/b	Proton assignment	δ ^1H NMR ($J_{\text{H-H}}$ in Hz) (ppm)	
			CMeA a	CMeA b
1	70.3	1	-	-
2	210.0	2	-	-
3	120.7	3	-	-
4	210.0	4	-	-
5	47.3	5	-	-
8	41.9	6	-	-
7	42.3	7	1.58, m	1.54, m
6	30.0	8ax	1.60, (t, 8Hz)	1.60, (t, 8Hz)
9	83.1	8eq	1.95, m	1.97, dd (t, 12Hz)
10	25.4	9	-	-
11	121.2	10	2.42, m	2.42, m
12	133.7	11	4.96, m	4.96, m
13	17.8	12	-	-
14	25.6	13	1.73, s	1.73, s
15	132.3	14	1.68, s	1.68, s
16	132.5	15	-	-
17,21	128.5	16	7.43, (t, 7.6Hz)	7.43, (t, 7.6Hz)
18,20	126.4	17,21	7.43, (t, 7.6Hz)	7.43, (t, 7.6Hz)
19	132.5	18,20	7.69, (t, 7.6Hz)	7.69, (t, 7.6Hz)
22	29.6	19	-	-
23	121.2	22	2.44, m	2.44, m
24	133.7	23	4.96, m	4.96, m
25	17.9	24	-	-
26	25.9	25	1.65, s	1.65, s
27	28.5	26	1.76, s	1.76, s
28	122.9			
29	133.1	27	2.09, m	2.09, m
30	18.0	28	4.80, m	4.80, m
31	25.8	29	-	-
32	16.4	30	1.54, s	1.54, s
33	23.0	31	1.62, s	1.62, s
34	35.5	32	0.71, s	0.87, s
		33	1.05, s	1.10, s
		34	2.82, s	2.81, s

*Structures of CMeA a and CMeA b on page 100

4.2.5 Synthesis of CEtA (57)

[(1*S*, 5*R*, 7*R*)-3-benzoyl-9-(ethylimino)-4-hydroxy-8,8-dimethyl-1,5,7-tris(3-methylbut-2-en-1-yl)bicyclo[3.3.1]non-3-en-2-one]

Compound CEtA (57) was confirmed with ESIMS (**Figure 4.23**) with adduct H^+ and Na^+ having base peak of (m/z 530, 100%) for the $[\text{M}+\text{H}]^+$ and (m/z 552, 24%) for the $[\text{M}+\text{Na}]^+$ respectively (**Figure 4.23**). Unfortunately, the reaction product was unstable and sensitive to certain organic solvents. Therefore, compound ^1H NMR and ^{13}C NMR of CEtA (57) could not be established. In addition, HPLC analysis was carried out to see the purity percentage of CEtA (57) to determine degradation of products due to the low stability of the product under normal environment and atmosphere. The mechanism of reaction was similar to imine compound CMeA (56) in **Scheme 4.4** but with ethylamine HCl ($\text{CH}_3\text{CH}_2\text{NH}_2\cdot\text{HCl}$) as the starting material.

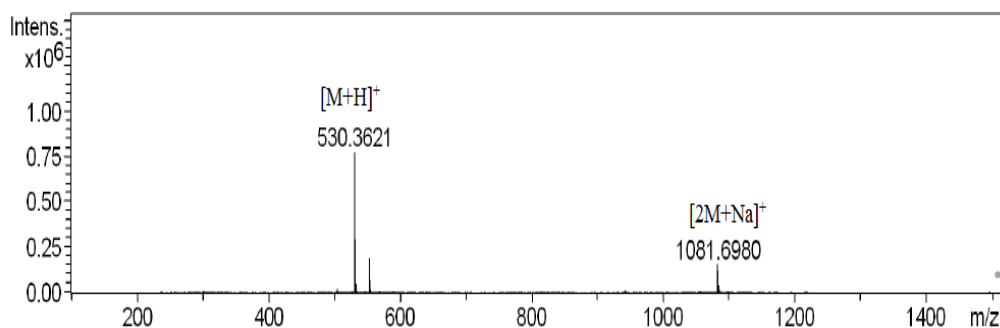


Figure 4.23 ESIMS of compound CEtA (57)

4.2.6 Synthesis of CPryl (58)

[(1*S*, 5*S*, 7*R*) -3-benzoyl-8,8-dimethyl-1,5,7-tris(3-methylbut-2-en-1-yl)-4-((3-methylbut-2-en-1-yl)oxy)bicyclo[3.3.1]non-3-ene-2,9-dione]

Prenyl groups in PPAP compounds were often reported to be responsible for activity against carcinoma cell lines. In addition, PPAP compound such as hyperforin (11) and its derivative Aristoforin (19) which possesses four prenyl compounds surrounding its bicyclo[3.3.1]nonane-2,4,9-trione core structure have shown remarkable antitumor activity both *in vitro* and *in vivo* (Gartner *et al.*, 2005; Richard, 2014). As such, the next envision was to employ the *O*-alkylation method to install prenyl group to the hydroxyl group of clusianone (29). The reaction to install additional prenyl group to clusianone (29) successfully produced compound CPryl (58). The product CPryl (58) was in moderate yield of 43% having molecular ion peak at m/z 571 for the $[M+H]^+$ (Figure 4.24).

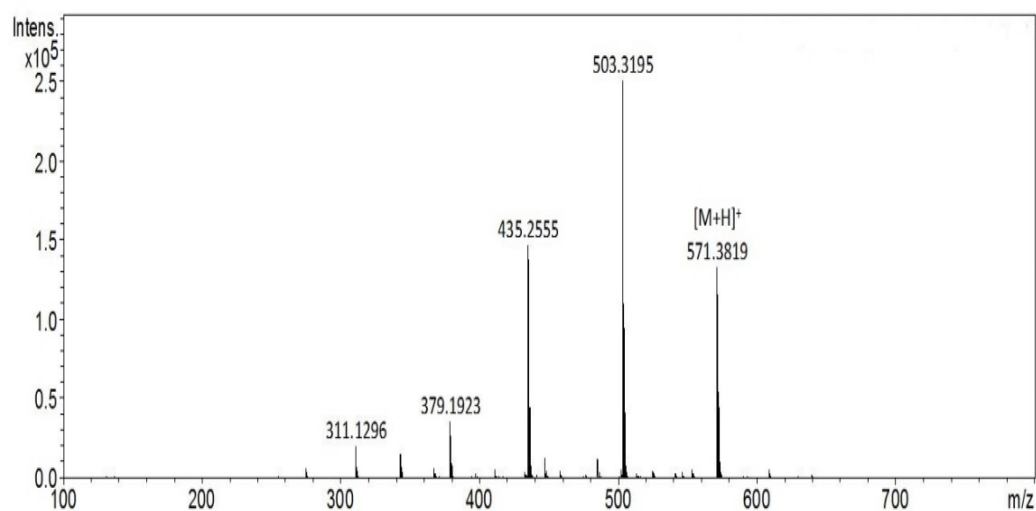


Figure 4.24 ESIMS of compound CPryl (58)

From the ESIMS of CPryl (58), it was proposed that fragmentation of CPryl (58) yielded ions resulting from successive elimination of prenyl side chain at C2 and C7. As such, ESIMS fragment ions m/z 503 was a result of the loss of a prenyl chain at C2 $[M+H-68]^+$ and consecutive elimination of another prenyl chain at C7 has led to the fragmentation of ions with m/z 435 (**Figure 4.24**).

The reaction was predicted to yield two tautomer's product of CPryl (58a) and CPryl (58b) since clusianone (a/b) used as starting material exists in its tautomer forms (**Scheme 4.1 c**). The ^1H NMR signals corresponding to H-35 of compound CPryl (58) was observed at δ 5.16 (**Figure 4.25 & Table 4.13**). This signal arises due to the additional prenyl chain (C_5H_9) added to clusianone (29). In addition ^1H NMR signals corresponding to H-34 were observed at δ 4.12 (s, 2H). As for the ^{13}C NMR signals, detailed interpretations of the data relevant to the correlation of the carbons in the additional prenyl chain were shown in **Figure 4.26 & Table 4.13**. The ^{13}C NMR signal of C-34 was observed at δ_c 65.4 attributed to the additional prenyl chain.

An important point to be note in interpreting the NMR signals of CPryl (58), the ^1H NMR signals corresponding to H-35 and H-23 have overlapped and these signals appear as multiplets resembling sextets. However, these were overlapped triplet signals arising from the respective ^1H NMR signals of H-35 and H-23.

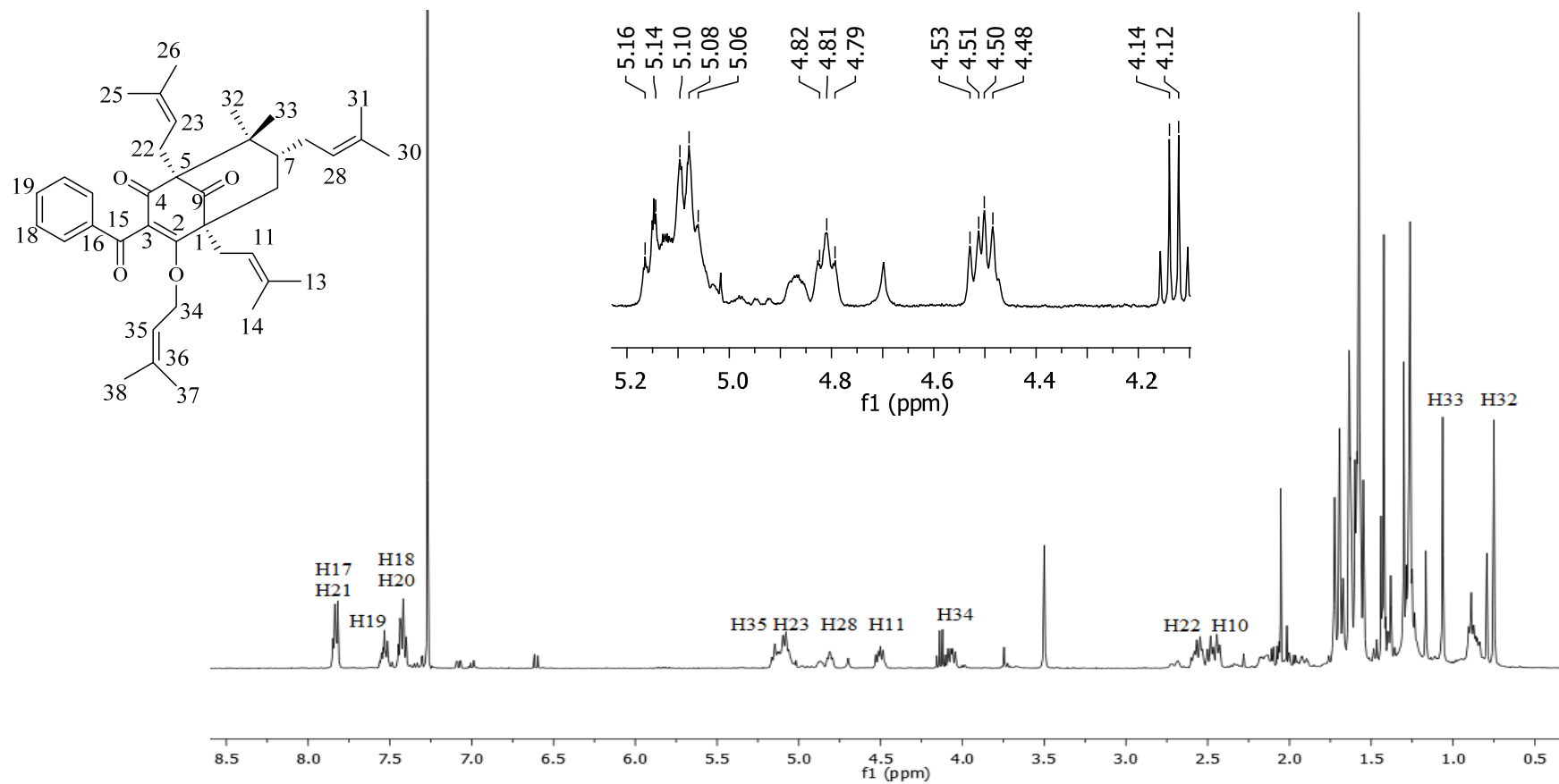


Figure 4.25 ^1H NMR spectrum of compound CPryl (58)

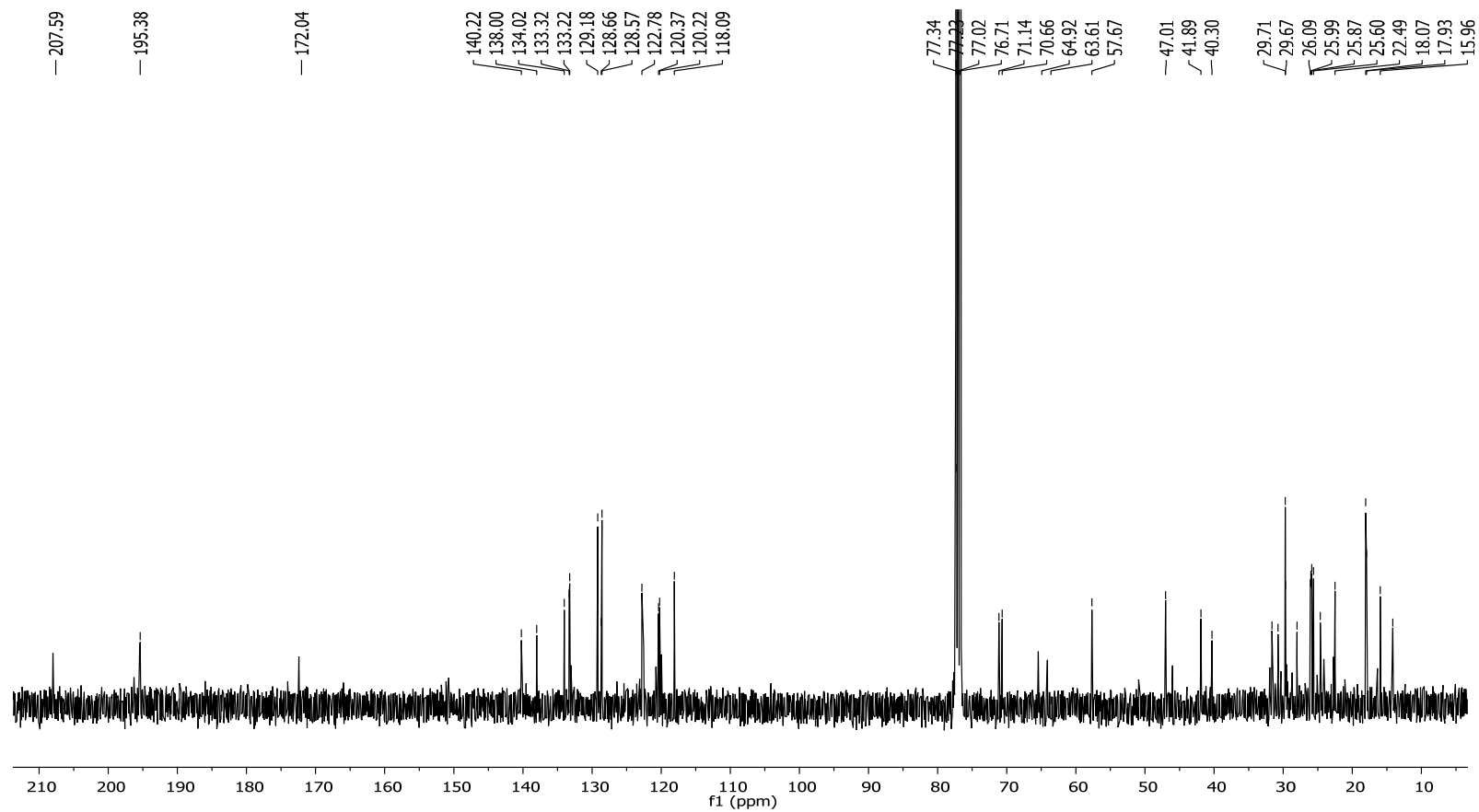


Figure 4.26 ¹³C NMR spectra of compound CPryl (58)

Table 4.13 ^{13}C NMR and ^1H NMR of compound CPryl (58)

Carbon assignment	$\delta^{13}\text{C}$ NMR (ppm) CPryl a/b	Proton assignment	$\delta^1\text{H}$ NMR ($J_{\text{H-H}}$ in Hz) (ppm)	
			(CPryl a)	(CPryl b)
1	57.6	1	-	-
2	172.6	2	-	-
3	120.3	3	-	-
4	195.4	4	-	-
5	71.1	5	-	-
6	40.3	6	-	-
7	47.0	7	1.58, m	1.54, m
8	30.7	8ax	1.57, (t, 8Hz)	1.57, (t, 8Hz)
9	207.9	8eq	2.01, m	2.05, dd (t, 12Hz)
10	25.6	9	-	-
11	120.2	10	2.58, m	2.58, m
12	133.2	11	4.51, m	4.50, m
13	16.0	12	-	-
14	25.8	13	1.72, s	1.72, s
15	195.2	14	1.69, s	1.67, s
16	138.0	15	-	-
17,21	128.5	16	7.41, (t, 7.6Hz)	7.43, (t, 7.6Hz)
18,20	126.4	17,21	7.82, (t, 7.6Hz)	7.83, (t, 7.6Hz)
19	129.2	18,20	7.51, (t, 7.6Hz)	7.52, (t, 7.6Hz)
22	29.6	19	-	-
23	122.8	22	2.48, m	2.48, m
24	134.0	23	5.08, m	5.08, m
25	18.1	24	-	-
26	25.9	25	1.63, s	1.63, s
27	28.0	26	1.67, s	1.67, s
28	120.4	27	2.42, m	2.42, m
29	133.3	28	4.81, m	4.81, s
30	17.9	29	-	-
31	25.0	30	1.54, s	1.54, s
32	22.5	31	1.62, s	1.62, s
33	23.0	32	0.75, s	0.79, s
34	65.4	33	1.06, s	1.16, s
35	118.1	34	4.12, s	4.14, s
36	140.2	35	5.16, m	5.16, m
37	14.1	36	-	-
38	22.5	37	1.56, s	1.56, s
		38	1.59, s	1.59, s

*Structures of CPryl a and CPryl b on page 101

4.2.7 Synthesis of CGeryl (59)

[(1*S*, 5*S*, 7*R*)-3-benzoyl-4-(((*Z*)-3,7-dimethylocta-2,6-dien-1-yl)oxy)-8,8-dimethyl-1,5,7-tris(3-methylbut-2-en-1-yl)bicyclo[3.3.1]non-3-ene-2,9-dione]

Interestingly type B of PPAP compound such as oblongifolin (22) has been tested for tubulin activity and results revealed that this compound interacts by inhibiting tubulin assembly activity at a cellular level (Hamed *et al.*, 2006). Since oblongifolin (22) compound possesses geranyl group, the subsequent reaction was to insert a geranyl group to the hydroxyl group of clusianone (29). The product CGeryl (59) was in low yield at 28% having molecular ion peak at m/z 639 for the $[M+H]^+$ (**Figure 4.27**). Based on the ESIMS of CGeryl (58), there was clear indication of fragmentation patterns of CPryl (58) which yielded ions resulting from successive elimination of geranyl and prenyl side chains at C2 and C5 respectively. As a result, ESIMS fragment ions m/z 503 was a result of loss of geranyl chain at C2 $[M+H-136]^+$ and consecutive elimination of another prenyl chain at C5 has led to the fragmentation of ions with m/z 435 (**Figure 4.27**).

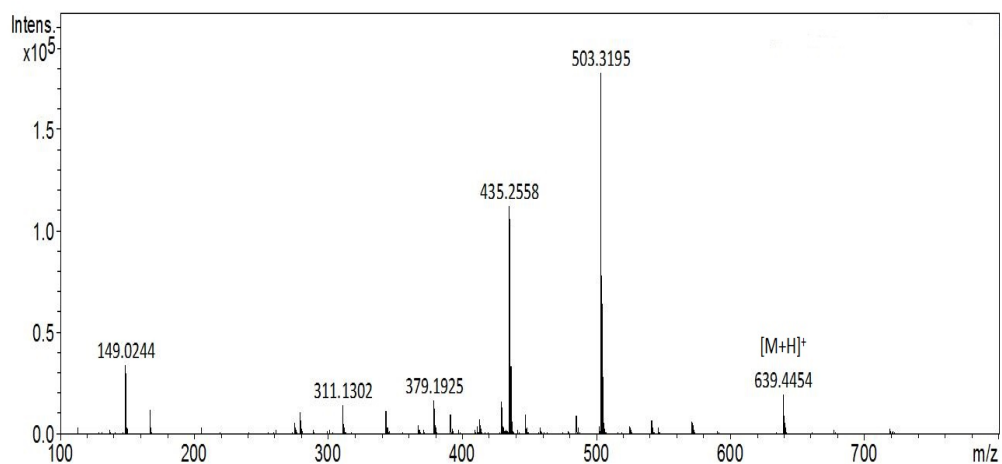


Figure 4.27 ESIMS of compound CGeryl (59)

It was noticed that the presence of more signals of ^1H NMR arising in the downfield region of δ 4.0 to 6.0 ppm (**Figure 4.28**) for compound CGeryl (59). The deshielding effect was due to the presence of electronegative alkene chains which were present in geranyl ($\text{C}_{10}\text{H}_{17}$) and prenyl (C_5H_9) chains in CGeryl (59). The ^1H NMR spectrum of compound CGeryl (59) as shown in **Figure 4.28** showed proton signals of H-35 and H-40 at δ 5.57 and δ 5.54 respectively attributed to the presence geranyl chain (**Figure 4.28 & Table 4.14**). The presence of geranyl chain was confirmed by both ^1H NMR and ^{13}C NMR signals which were observed at δ_{H} 4.03 (s, 2H) and δ_{C} 68.2 respectively. The ^{13}C NMR signals and detailed interpretations of the data relevant to the correlation of the carbons in compound CGeryl (59) were shown in **Figure 4.29 & Table 4.14**.

In addition, the reaction was predicted to yield two tautomer's CGeryl (59a) and CGeryl (59b) since clusianone (a/b) used as starting material exists in its tautomeric forms (**Scheme 4.1 c**). In this circumstances, the additional ^1H NMR signals arising in the region of δ 4.0 to 6.0 ppm were evidence of the consequences of the enolizable 1,3-diketone system in clusianone (29) producing CGeryl (59) also in two tautomeric forms. On the basis of these consideration, some of these triplet signals exhibited two sets of ^1H NMR signals arising from proton attached to prenyl chain (H-28 and H-11) of either compound CGeryl (59a) or CGeryl (59b) (**Figure 4.28 & Table 4.14**). Additionally, the ^1H NMR triplet signals corresponding to H-35 and H-40 have overlapped and these signals appear as multiplets resembling quartet (**Figure 4.29**).

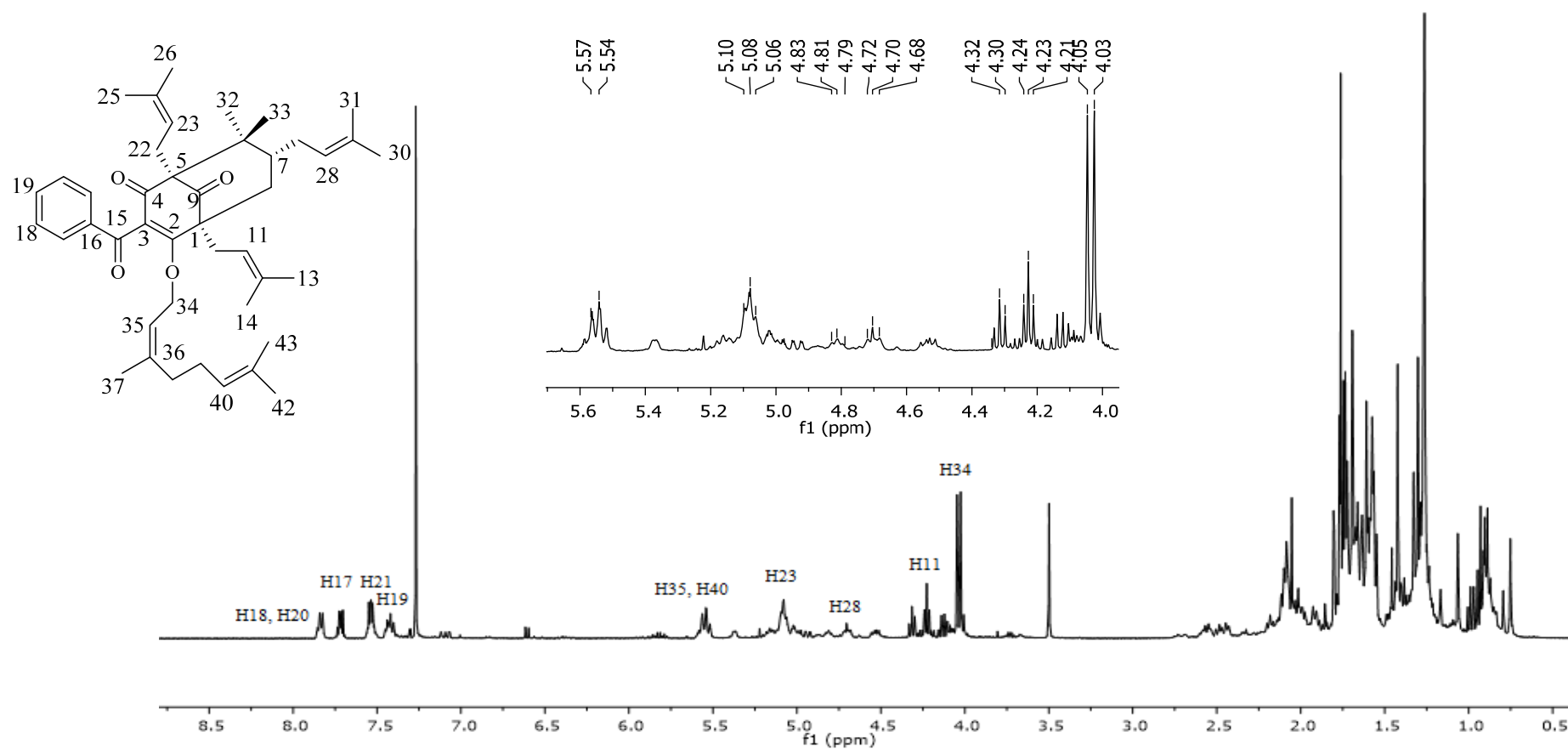


Figure 4.28 ^1H NMR spectrum of compound CGeryl (59)

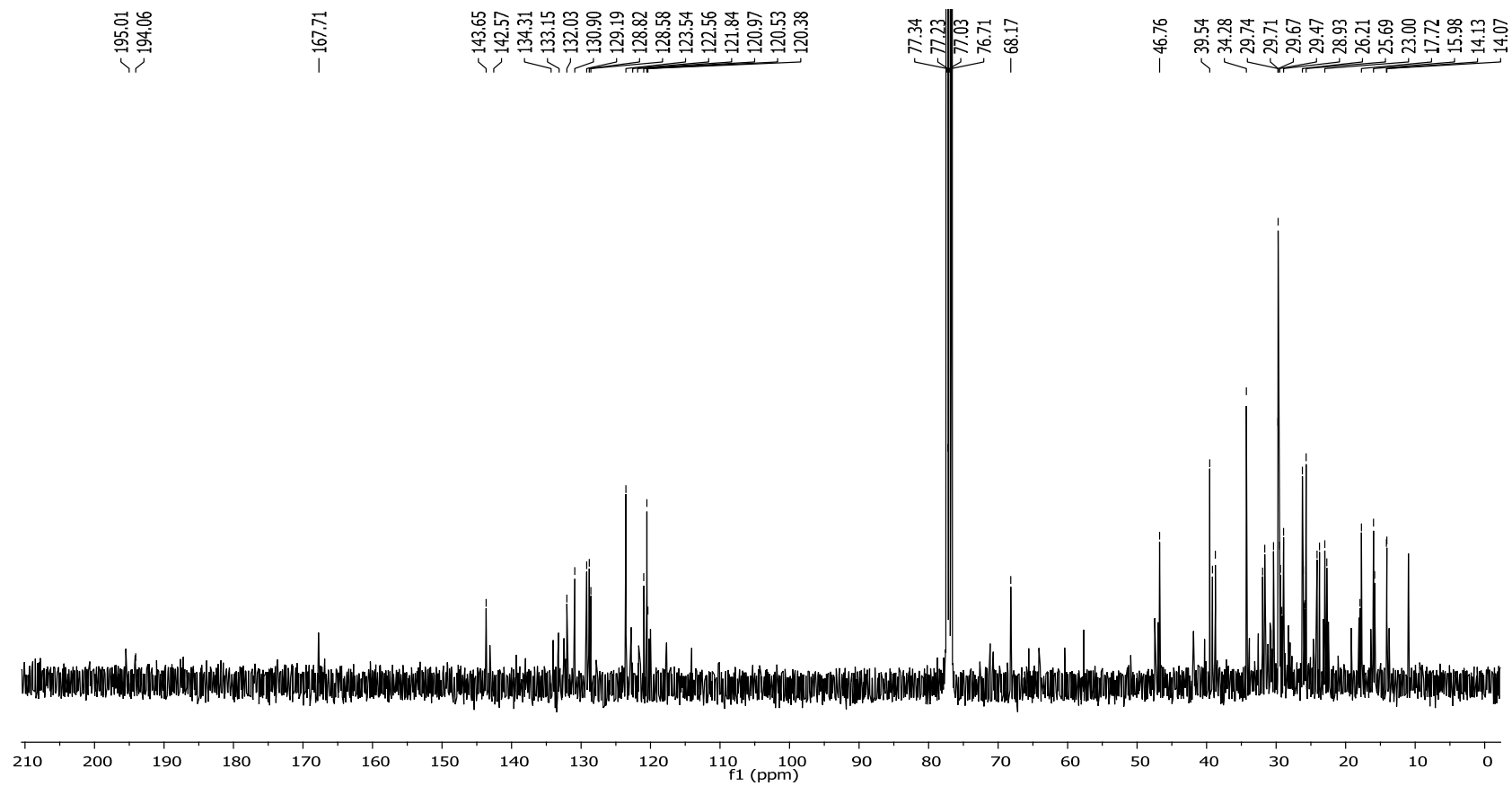


Figure 4.29 ^{13}C NMR spectra of compound CGeryl (59)

Table 4.14 ^{13}C NMR and ^1H NMR of compound CGeryl (59)

Carbon assignment	δ ^{13}C NMR (ppm) CGeryl a/b	Proton assignment	δ ^1H NMR ($J_{\text{H-H}}$ in Hz) (ppm)	
			CGeryl a	CGeryl b
1	58.4	1	-	-
2	143.7	2	-	-
3	120.5	3	-	-
4	193.0	4	-	-
5	72.1	5	-	-
8	39.1	6	-	-
7	46.8	7	1.57, m	1.57, m
6	30.4	8ax	1.60, (t, 8Hz)	1.60, (t, 8Hz)
9	195.0	8eq	1.95, m	2.05(overlapped)
10	24.1	9	-	-
11	120.4	10	2.44, m	2.44, m
12	130.9	11	4.23, m	4.30, m
13	16.0	12	-	-
14	25.7	13	1.69, s	1.69, s
15	167.8	14	1.76, s	1.76, s
16	18.1	15	-	-
17,21	128.8	16	7.53, (t, 7.6Hz)	7.71, (t, 7.6Hz)
18,20	128.6	17,21	7.82, (t, 7.6Hz)	7.84, (t, 7.6Hz)
19	129.2	18,20	7.40, (t, 7.6Hz)	7.40, (t, 7.6Hz)
22	29.7	19	-	-
23	123.5	22	2.55, m	2.55, m
24	132.0	23	5.07, m	5.07, m
25	18.0	24	-	-
26	26.2	25	1.61, s	1.61, s
27	28.9	26	1.76, s	1.76, s
28	121.0	27	2.09, m	2.09, m
29	130.9	28	4.70, m	4.81, s
30	17.9	29	-	-
31	23.8	30	1.30, s	1.33, s
32	22.7	31	1.42, s	1.46, s
33	23.7	32	0.75, s	0.79, s
34	68.2	33	1.06, s	1.17, s
35	117.6	34	4.03, s	4.05, s
36	143.1	35	5.57, m	5.57, m
37	14.0	36	-	-
38	34.3	37	1.64, s	1.66, s
39	26.0	38	2.05, m	2.05, m
40	124.0	39	2.05, m	2.05, m
41	133.0	40	5.54, m	5.54, m
42	22.5	41	-	-
43	14.1	42	1.74, s	1.74, s
		43	1.76, s	1.76, s

*Structures of CGeryl a and CGeryl b on page 101

4.2.8 Synthesis of CDMet (60)

[(1*S*, 5*S*, 7*R*)-3-benzoyl-4-hydroxy-1,5,7-triisopentyl-8,8-dimethylbicyclo[3.3.1]non-3-ene-2,9-dione]

Demethylation reaction was carried out to deprotect CHyd (54) using previously published method (Ahmad *et al.*, 2007). In this report, Krapcho-type conditions (LiCl, DMSO, 120 °C) used afforded 50% of the desired yield. Unfortunately, the same reaction performed on CHyd (54) gave (60) in 5.0 % yield. Based on the ESIMS result, it indicated that base peak at 509.3618 corresponds to the mass of $[M+H]^+$. However, further attempts to increase the yield of the product by extending the stirring duration was not conducted due to the paucity of precursor compound CHyd (54).

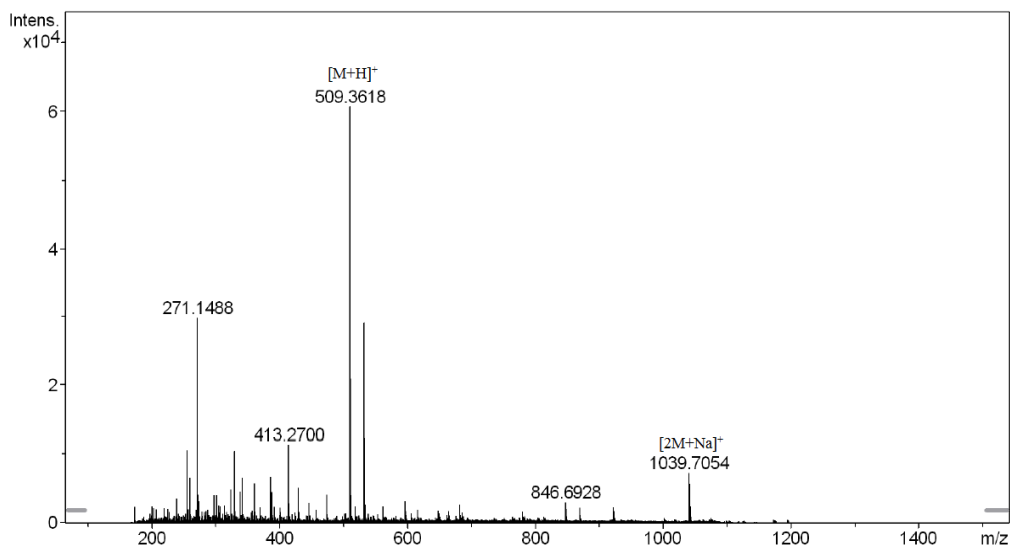


Figure 4.30 ESIMS of compound CDMet (60)

4.3 TLC analysis for compound CMxA (55), CMeA (56) and CEtA (57)

Crystallization efforts on compound CMxA (55) and CEtA (57) were not fruitful. The main factor was the formation of by-products through degradation along the process when the compounds were subjected to several organic solvents such as ethanol, methanol, chloroform and dichloromethane. In addition, exposure to atmosphere while waiting for the crystallization to occur *via* slow solvent evaporation method, indicate that these products were air sensitive in solution forms. Therefore, the presence of by-products through degradation had suppressed the formation of crystallization. Further purity test using TLC profiling and HPLC analysis were necessary to determine the existence of possible by-product formation due to instability of the compounds.

TLC profiles of clusianone (29) added with oxime and imines were shown in (Figure 4.31). The orange stains on TLC after spraying with Dragendoff reagent confirmed the presence of nitrogen element in the products. The black circles indicated starting material clusianone (29) or product CMxA (55), CMeA (56) and CEtA (57). White circles spots indicate by-products through degradation formed for compounds when viewed under UV light at short wavelength (254 nm).

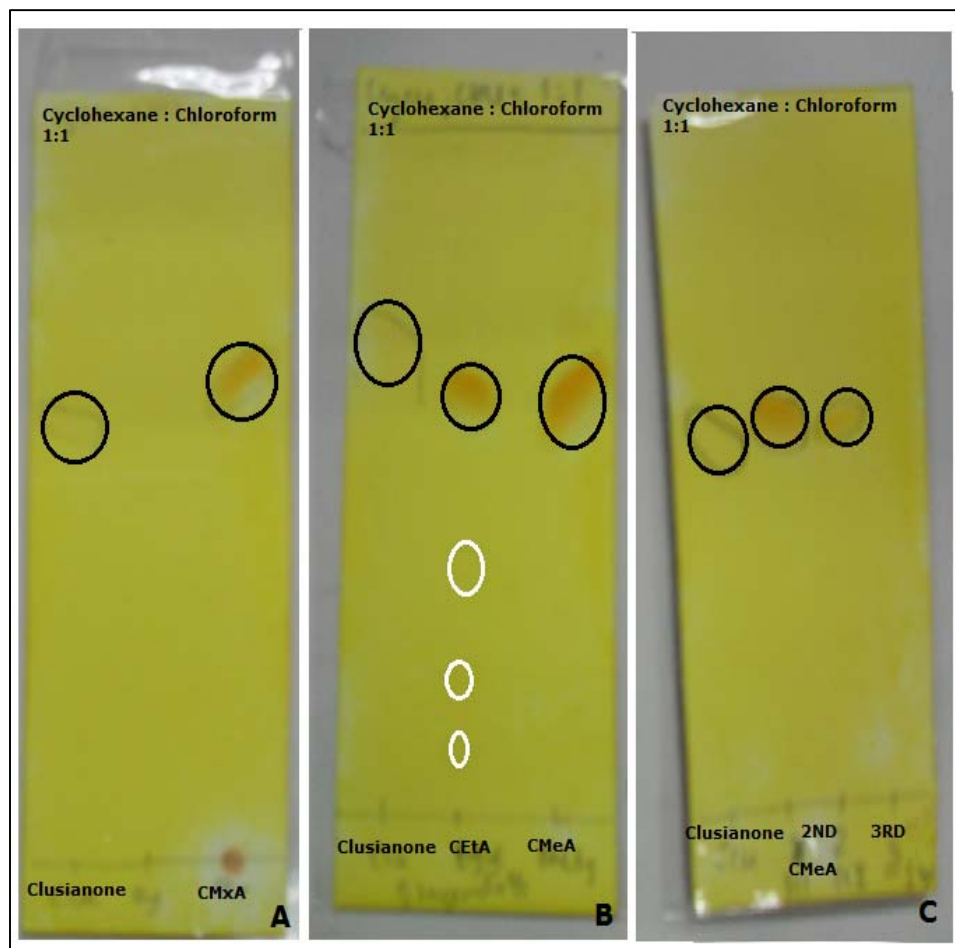


Figure 4.31 TLC images of compounds CMxA (55), CMeA (56) and CETA (57) after reaction and purification through column chromatography. (A) CMxA (55) formed stained orange with Dragendoff dyeing agent compared to the starting material clusianone (29) not stained. (B) CETA (57) and CMeA (56) formed stained orange with Dragendoff dyeing agent compared to the starting material clusianone (29) not stained. (C) CMeA formed from second and third trial of reaction.

4.3 HPLC analysis of selected compound for purity content analysis

The additions of oxime and amine functional groups to C-9 of clusianone (29) *via* ketone reduction were feasible in a single step. However some of these samples CMxA (55) and CEtA (57) showed susceptibility to degradation when being exposed to atmospheric moisture and also to organic solvents after purification *via* column chromatography. This occurrence of degradation in the sample was noticed after a period of time when compounds were dissolved using various solvents such as methanol, chloroform and dichloromethane.

Purity profiling is crucial and requires critical attention from drug companies. Earlier the degradation of product was screened using TLC to see by-product spots appearance under short wavelength (254 nm). Thereafter, HPLC works were carried out to determine and quantify purity percentage of compounds while taking into account by-products presence. Only compound CMxA (55), CMeA (56) and CEtA (57) were selectively analysed for purity studies. Purity content was determined using HPLC analysis (**Table 4.13 & Figure 4.32**).

Table 4.15 HPLC spectra for selected compound (Absorbance at 254 nm)

Compound	Purity percentage (%)
Clusianone (29)	98.7
CMxA (55)	86.2
CMeA (56)	95.1
CEtA (57)	74.3

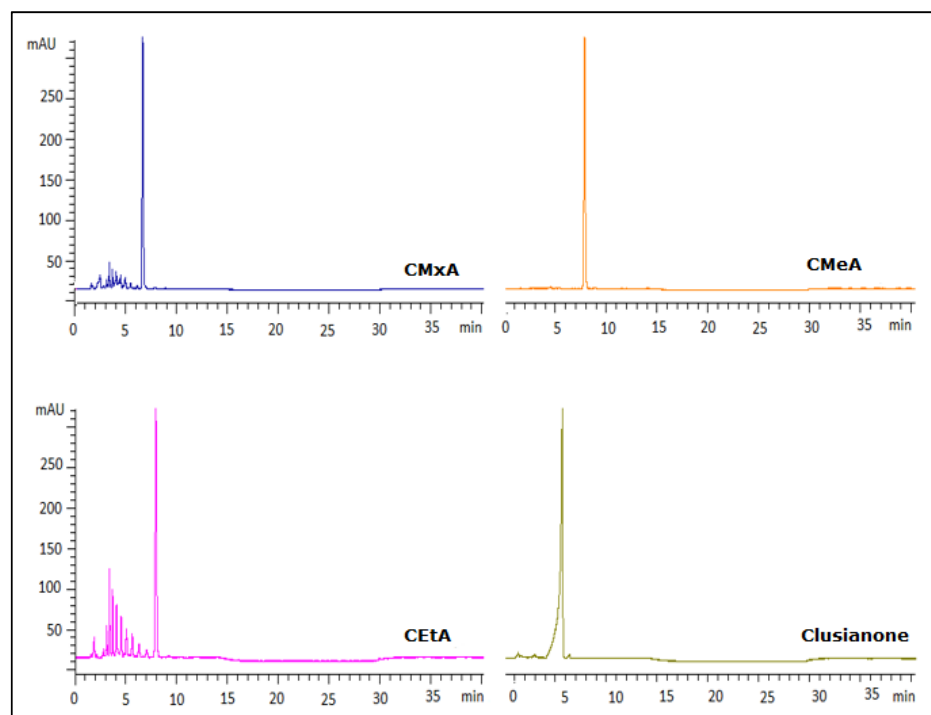


Figure 4.32 HPLC Purity analysis of compounds

Therefore, after product purification through column chromatography of compound CMxA (55), CMeA (56) and CEtA (57), it is advisable that these compounds should be kept in a well closed scintillation vials, away from light sources and stored under refrigeration at 2-8°C. In addition, it is recommended to apply nitrogen gas as inert environment for storage to avoid any further degradation when stored in a closed scintillation vials.

4.5 Summary of synthesis of clusianone (29) derivatives

Based on the synthesis results, eight derivatives of clusianone (29) abbreviated as CMet (53), CHyd (54), CMxA (55), CMeA (56), CEtA (57), CPryl (58), CGeryl (59) and CDMet (60) were obtained *via* chemical modification of clusianone (29). Nevertheless, all these derivatives were synthesized using high purity (>98%) clusianone (29) crystals produced through recrystallization methods. Interestingly, the highlight of the synthetic reaction step involves the ketone reduction on C-9 of naturally occurring clusianone (29) to afford imine derivative namely CMeA (56). To date, there was no information in naturally occurring PPAP compounds literature about the integration of nitrogen element into the core structure of bicyclo [3.3.1] nonane-2,4,9-trione.

The next approach was to prepare sufficient amount of clusianone (29) derivatives for biological testing. The high yield (>75%) of CMet (53), CHyd (54), CMxA (55), CMeA (56), CEtA (57) makes these derivatives feasible candidates for cytotoxicity screening, structure-activity relationship studies (SAR) interpretation and further antimicrotubule activity studies as described in Chapter 5. The yield after modification limits the number of biological experiments to be performed. Under this circumstances, small scale synthesis reactions were conducted with less than 2 reaction steps in order to produce high yield derivatives as outlined in the thesis objective and research scopes. This research aim was to produce high yield synthesised derivatives combined with economically viable methods which would contribute to medical values of these compounds.

On the other hand, the purity profiling utilizing HPLC analysis for compound CMxA (55) and CEtA (57) having purity percentage of 86.2% and 74.3% respectively indicated these two compounds were not suitable candidates for further therapeutic intervention (Guideline, 2009). Therefore, clusianone (29) derivatives CMet (53), CHyd (54) and CMeA (56) were the only ones selected to be reported and published in *Planta Medica Letters* (Nagalingam *et al.*, 2016) (**Appendix G**). This is the first time a concise report on chemical modification on naturally occurring clusianone (29) has been established including in-depth structure-activity relationship studies (SAR) against normal and carcinoma respiratory cell lines.

Selection of the next synthesis reaction step to produce the novel derivatives were focused based on envisaging the functional group that will lead to the development of ultimate antimicrotubule agent as outlined in the objective of the thesis. Concurrently, the synthesis and cytotoxicity screening of some of the derivatives such as CMet (53) and CHyd (54) were conducted as a preliminary results for structure-activity relationship studies (SAR). As such, it was revealed that alteration of prenyl and hydroxyl group leads to significant loss in cytotoxicity activity in these preliminary SAR studies in all four respiratory cell lines that will be described explicitly in Chapter 5. Previous report on total synthesis of clusianone derivatives involves 15-30 synthesis routes to afford clusianone with additional methyl esters (61) (62) (68), trifluoroethyl esters (63), phenyl sulfones (64) (65) (66) (67) and bromobenzoate group (69) (**Appendix E**). It was revealed that the modification of either prenyl chain or the hydroxyl group despite the various functional group installed has led in lower potency or loss in anticancer activity (Zhu *et al.*, 2014).

Further to this, compound CPryl (58) and CGeryl (59) were developed to study the significant of the additional prenyl and geranyl chains as compared to a hydroxyl group of clusianone (29) in the hope of creating the future lead compounds with stronger inhibitory interaction in the domains of microtubule structure. The presence of additional prenyl and geranyl chain surrounding the bicyclo [3.3.1] nonane-2,4,9-trione is also postulated to increase the lipophilicity of the compounds. Hence, enhancing stronger affinity of the compound to the cell membranes for optimum pharmacological effect (Rullah *et al.*, 2014). Due to time restraints in the current synthesis reaction trial, the yield of CPryl (58) and CGeryl (59) have not been optimised and cytotoxicity screening for CPryl (58) and CGeryl (59) have yet to be investigated.

CHAPTER 5 RESULTS AND DISCUSSION

BIOLOGICAL ACTIVITY OF CLUSIANONE AND DERIVATIVES

5.1 Cytotoxicity testing on respiratory cells lines using MTT assay

The discovery of bioactive phytochemicals often leads to the cytotoxicity test to determine bioactivity in cancer cells and most importantly the impact of these compounds on normal cells. These assays affect the different parts of the treated cells and are used in measuring various aspects of the compound toxicity. There are several cytotoxicity tests that have been used by NCI over the past few decades such as tetrazolium assay (MTT and XTT) and sulforhodamine B assay (SRB). SRB assay has been selected as the most reliable method by NCI since cytotoxicity test conducted by NCI was performed in larger scale with a wide range of cell line panels (Boyd, 1995; Shoemaker, 2006). However this nontetrazolium SRB assay involves many washing steps compared to MTT assay (Keepers *et al.*, 1991). Besides, the SRB assay is used to determine the cellular protein content unlike MTT assay determined metabolic activity of cells, which is related to mitochondrial action.

Synthetic clusianone (29) has been tested using reazurin test against cervix carcinoma (HeLa), breast carcinoma (MCF7) and pancreatic carcinoma (MIA-PaCa-2) cell lines (Simpkins *et al.*, 2012). Reazurin and MTT assays evaluate the metabolic activity in the mitochondria in the cells and both assays were claimed to be high quality and reliable for high throughput screening (Hamid *et al.*, 2004). MTT assay is an enzyme based method which measures the cell viability through bioreduction process in the cell. MTT is associated with mitochondrial succinate dehydrogenase and involves the reduction of

pyridine nucleotides NADH to NADPH. During the event of bio-reduction, tetrazolium salt MTT changes into insoluble form known as formazan which is purple in color. The faster cells proliferate or perhaps the more cell viability detected, the more formazan crystals are formed, this increases the intensity of the purple coloration (Mosmann, 1983; Berridge *et al.*, 1996). Therefore, in this research MTT assay has been selected since recent studies on clusianone (29) on HepG2 cells showed that clusianone (29) exhibited early mitochondrial impairment (Reis *et al.*, 2014). Furthermore, MTT assay is less time consuming, cheap, easy to perform, non-destructive and relatively reliable. Most importantly it measures the metabolic activity of the cells and not necessarily the viability of the cells (Berridge *et al.*, 1996).

During the MTT assay method optimization, two main factors were taken into consideration, firstly the concentration of DMSO used for the treatment of cell and secondly the cell number in each well. Colon cancer was not affected when subjected up to 10 % DMSO (Haumeil & Rnaud, 2002) while Burkitt's lymphoma cells were easily affected at 1.5% DMSO treatment (Lin *et al.*, 1995). It was reported that 1.0% DMSO in lung adenocarcinoma (CL1-5) induces cell cycle arrest at G1 phase eventually leading to apoptosis (Wang *et al.*, 2012). The optimization test to determine the safe concentration of DMSO subjected to both lung and nasopharyngeal cells revealed 0.4% DMSO caused zero effect on the cell growth. As such, 0.1% DMSO concentration was selected in stock solution as suggested by previous studies to avoid any effects of cell death due to DMSO (Chippendale *et al.*, 2012).

The seeding number for each well was followed as per NCI recommendation between 5000 to 20,000 cell per well (Boyd, 1995). However,

after optimization, 10,000 cells per well was chosen as the cell density since the absorbance reading were more stable and cell growth including cell morphology was consistent in each well when observed under the inverted phase microscope.

The screening of cytotoxicity of clusianone (29) and its derivatives performed using quantitative colorimetric MTT assay against MRC5, A549, HK1 and NP69 cells. Cytotoxicity screening test was also performed against normal cell lines to validate compound inhibitory activity in cancer cells without significantly affecting the viability of the normal cell.

Absorbance was measured at 540 ± 5 nm and the absorbance used for the cell death percentage was subtracted with the blank absorbance to deduct the interference from other sources in the cell media or DMSO. The IC_{50} values were concentration of compounds that causes 50% of cell death at 48 hours and were averaged from the three sets of experiments. The IC_{50} values were determined using the interpolation method in GraphPad Prism 6 from the resulting dose response plot (Boyd, 1995). Separate graphs were displayed to view and study the pattern of cytotoxicity effect of clusianone (29) and derivatives against these 4 different cell lines.

5.1.1 Cytotoxicity of clusianone (29) against MRC5, A549, NP69 and HK1 cells

The cytotoxicity values IC_{50} of clusianone (29) against all the cells were between 1.5-5.5 μM (**Table 5.1**). A clear cell death trend was seen after 5.0 μM (**Figure 5.1**) since no cell viability was detected after 48 hours of treatment with clusianone (29). Clusianone (29) cytotoxicity was higher in A549 carcinoma cell line (3.06 μM) compared to HK1 carcinoma cell lines (5.35 μM). Apart from that, clusianone (29) was less toxic to both MRC (4.16 μM) and NP69 (3.66 μM) normal cells compared to A549 (3.06 μM) carcinoma cells.

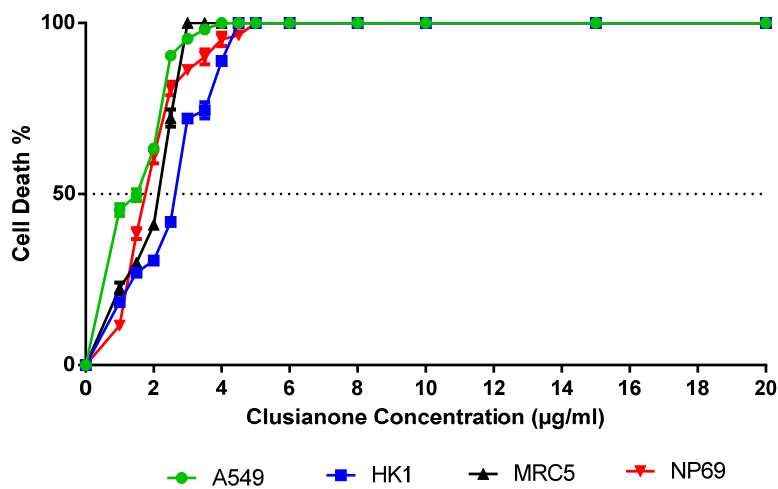


Figure 5.1 Graph showing the change in cell death with increasing clusianone (29) concentration in MRC5, A549, NP69 and HK1 cells after 48 hours treatment. Each point represents the mean \pm standard deviation from three independent experiment (n=3) $P < 0.05$.

Table 5.1 IC_{50} values of clusianone (29) interpolated from **Figure 5.1** then converted to μM using molecular weight of 502.69. Docetaxel (18) IC_{50} values were used as the positive control.

Cell type	MRC5	A549	NP69	HK1
IC_{50} Clusianone ($\mu g/mL$)	2.09	1.54	1.84	2.69
IC_{50} Clusianone (μM)	4.16	3.06	3.66	5.35
IC_{50} Docetaxol (μM)	0.006	0.006	0.006	0.006

5.1.2 Cytotoxicity of CMet (53) against MRC5, A549, NP69 and HK1 cells

Compound CMet (53) was inactive since there were no signs of cell death which occurred below 10 μM (**Figure 5.2**). Besides, CMet (53) IC_{50} values against all the cell line occurred in a wide range from 60-120 μM (**Table 5.2**). Even though CMet (53) was less toxic to normal cells MRC5 and NP69, the CMet (53) was considered ineffective as anticancer potential compound since carcinoma cell death occurred at a very high CMet (53) dose.

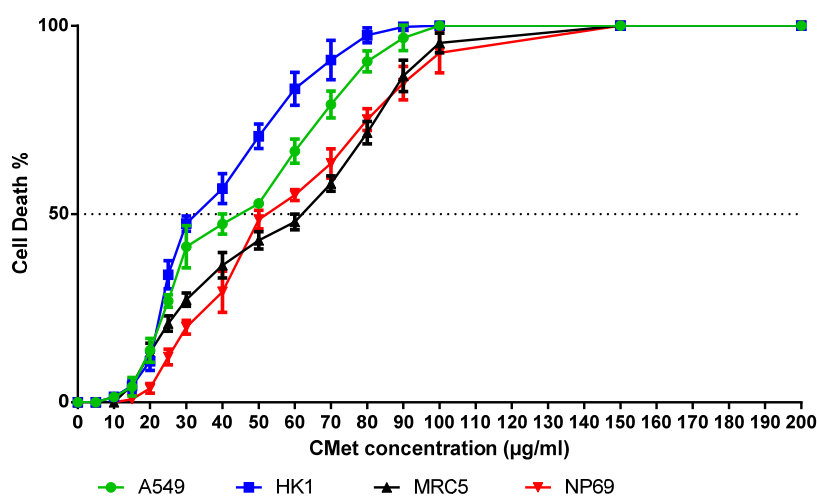


Figure 5.2 Graph showing the change in cell death with increasing compound CMet (53) concentration in MRC5, A549, NP69 and HK1 cells after 48 hours treatment. Each point represents the mean \pm standard deviation from three independent experiment ($n=3$) $P < 0.05$.

Table 5.2 IC_{50} values of CMet (53) interpolated from **Figure 5.2** then converted to μM using molecular weight of 516.712. Docetaxel (18) IC_{50} values were used as the positive control.

Cell type	MRC5	A549	NP69	HK1
IC_{50} Compound CMet ($\mu\text{g/mL}$)	62.20	44.80	52.20	32.40
IC_{50} Compound CMet (μM)	120.38	86.70	101.02	62.70
IC_{50} Docetaxol (μM)	0.006	0.006	0.006	0.006

5.1.3 Cytotoxicity of CHyd (54) against MRC5, A549, NP69 and HK1 cells

Similar to CMet (53), the CHyd (54) prevailed its cell death effect against all the cell lines above 10 μM treatments (**Figure 5.3**). The IC_{50} values of CHyd (54) were between the range of 40.0 to 70.0 μM (**Table 5.3**). In addition to this, CHyd (54) exhibit high toxicity against MRC5 normal cells compared to A549 carcinoma cells with IC_{50} values of 47.15 μM and 57.70 μM respectively. Meanwhile, IC_{50} cytotoxicity values of NP69 and HK1 cells were almost the same with 68.80 μM and 65.55 μM respectively.

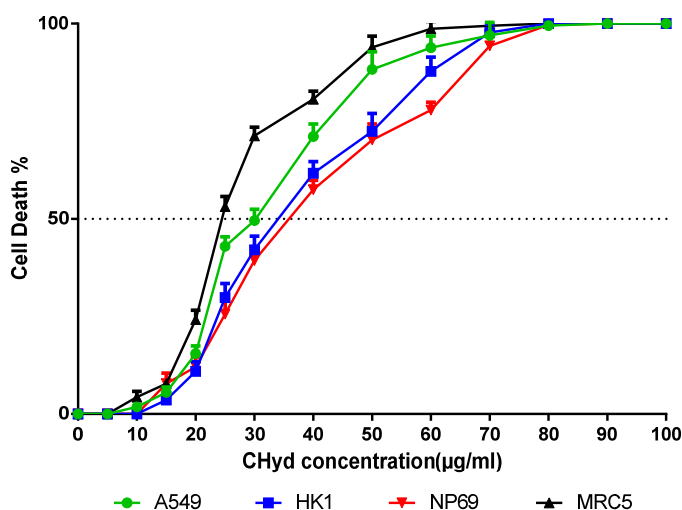


Figure 5.3 Graph showing the change in cell death with increasing compound CHyd (54) concentration in MRC5, A549, NP69 and HK1 cells after 48 hours treatment. Each point represents the mean \pm standard deviation from three independent experiment ($n=3$) $P < 0.05$.

Table 5.3 IC_{50} values of CHyd (54) interpolated from **Figure 5.3** above then converted to μM using molecular weight of 521.75. Docetaxel (18) IC_{50} values were used as the positive control.

Cell type	MRC5	A549	NP69	HK1
IC_{50} Compound CHyd ($\mu\text{g/mL}$)	24.6	30.1	35.9	34.2
IC_{50} Compound CHyd (μM)	47.15	57.70	68.80	65.55
IC_{50} Docetaxol (μM)	0.006	0.006	0.006	0.006

5.1.4 Cytotoxicity of CMxA (55) against MRC5, A549, NP69 and HK1 cells

As for compound CMxA (55), IC_{50} values indicate cell death below 10 μ M against all the respective cells (**Figure 5.4** & **Table 5.4**). The IC_{50} values of CMxA (55) was considered active against HK1 cells (4.85 μ M). However, it was observed that toxicity related to normal cells were rather high with 5.12 μ M in NP69 cells. The toxicity effect was even higher in MRC5 cells (2.82 μ M) compared to A549 cells (7.67 μ M).

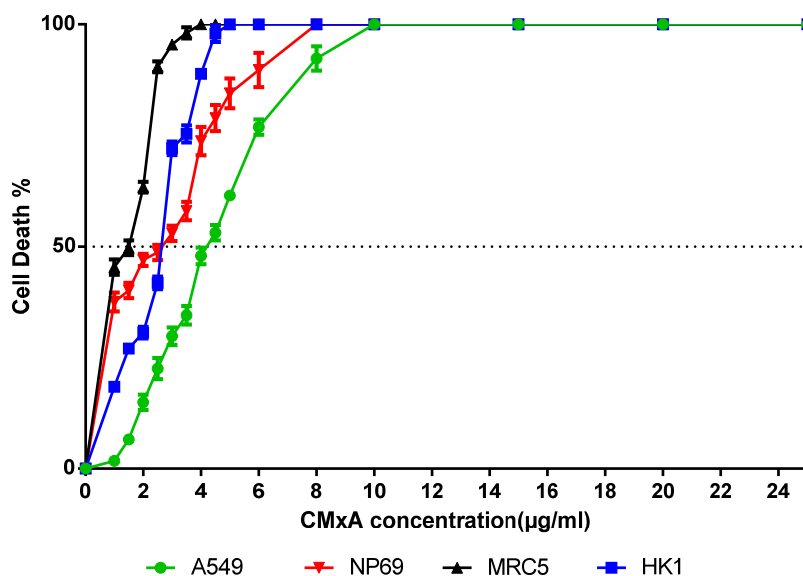


Figure 5.4 Graph showing the change in cell death with increasing compound CMxA (55) concentration in MRC5, A549, NP69 and HK1 cells after 48 hours treatment. Each point represents the mean \pm standard deviation from three independent experiment (n=3) $P < 0.05$.

Table 5.4 IC_{50} values of CMxA (55) interpolated from **Figure 5.4** above then converted to μ M using molecular weight of 531.73. Docetaxel (18) IC_{50} values were used as the positive control.

Cell type	MRC5	A549	NP69	HK1
IC_{50} Compound CMxA (μ g/mL)	1.50	4.08	2.72	2.58
IC_{50} Compound CMxA (μ M)	2.82	7.67	5.12	4.85
IC_{50} Docetaxol (μ M)	0.006	0.006	0.006	0.006

5.1.5 Cytotoxicity of CMeA (56) against MRC5, A549, NP69 and HK1 cells

Interestingly, IC₅₀ values of compound CMeA (56) were almost comparable with clusianone (29). The IC₅₀ values of CMeA (56) for both carcinoma cells were less than 4 µM (**Figure 5.5** & **Table 5.5**). In particular, CMeA (56) IC₅₀ value against HK1 cells was 3.43 µM. Most importantly both the IC₅₀ values against MRC5 and NP69 normal cells were above 10 µM. Thus indicating less toxicity of CMeA (56) compared to the rest of the compounds.

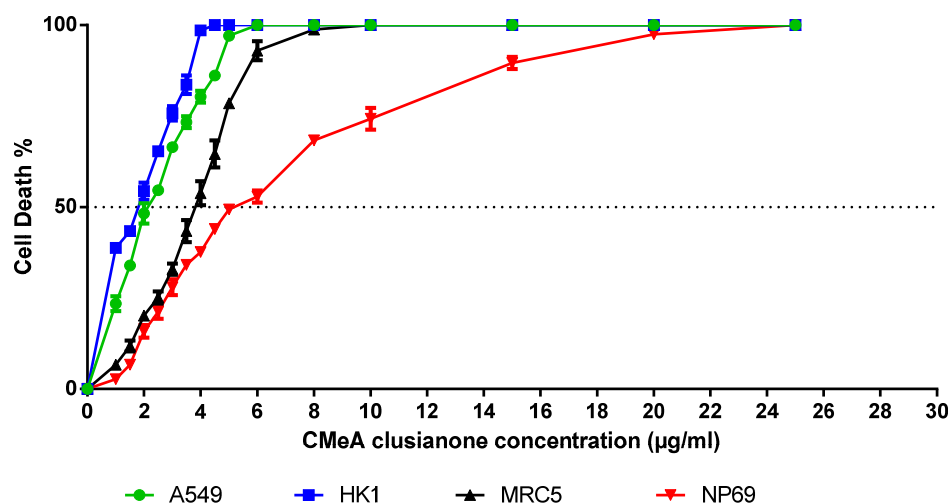


Figure 5.5 Graph showing the change in cell death with increasing compound CMeA (56) concentration in MRC5, A549, NP69 and HK1 cells after 48 hours treatment. Each point represents the mean \pm standard deviation from three independent experiment (n=3) $P < 0.05$.

Table 5.5 IC₅₀ values of CMeA (56) interpolated from **Figure 5.5** then converted to µM using molecular weight of 515.73. Docetaxel (18) IC₅₀ values were used as the positive control.

Cell type	MRC5	A549	NP69	HK1
IC ₅₀ Compound CMeA (µg/mL)	5.26	2.11	5.17	1.77
IC ₅₀ Compound CMeA (µM)	10.20	4.09	10.02	3.43
IC ₅₀ Docetaxol (µM)	0.006	0.006	0.006	0.006

5.1.6 Cytotoxicity of CEtA (57) against MRC5, A549, NP69 and HK1 cells

The IC₅₀ values of CEtA (57) were all observed above 10 µM for all the four types of cells (**Figure 5.6** & **Table 5.6**). Based on the result both carcinoma cells A549 and HK1 cells IC₅₀ values were below 15 µM while normal cells NP69 and MRC cells IC₅₀ values were above 15 µM.

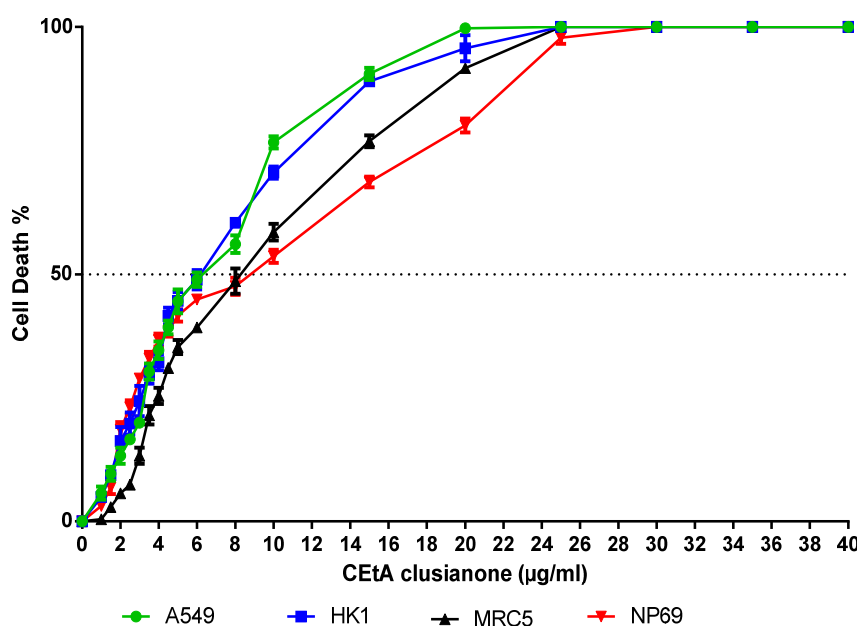


Figure 5.6 Graph showing the change in cell death with increasing compound CEtA (57) concentration in MRC5, A549, NP69 and HK1 cells after 48 hours treatment. Each point represents the mean \pm standard deviation from three independent experiment (n=3) $P < 0.05$.

Table 5.6 IC₅₀ values of CEtA (57) interpolated from **Figure 5.6** above then converted to µM using molecular weight of 529.75. Docetaxel (18) IC₅₀ values were used as the positive control.

Cell type	MRC5	A549	NP69	HK1
IC ₅₀ Compound CEtA (µg/mL)	8.19	6.27	8.87	6.63
IC ₅₀ Compound CEtA (µM)	15.46	11.84	16.74	12.52
IC ₅₀ Docetaxol (µM)	0.006	0.006	0.006	0.006

5.1.7 Summary of cytotoxicity results

The results of the MTT bioassay were summarised in (Table 5.7). Clusianone (29) tested on A549 and MRC cells showed IC₅₀ values of 3.06 μ M and 4.16 μ M respectively indicating that the cytotoxicity effect of clusianone (29) was higher 26.44% in lung carcinoma compared to normal lung fibroblast cell lines. Meanwhile, the IC₅₀ values of clusianone (29) against HK1 and NP69 were 5.35 μ M and 3.66 μ M respectively resulting in higher 31.58% toxicity of clusianone (29) in normal epithelial nasopharyngeal cells compared to its effect on nasopharyngeal carcinoma cells.

Table 5.7 Cytotoxicity IC₅₀ (μ M) of clusianone (29) and derivatives against MRC5, A549, HK1 and NP69 cells.

Compound	MRC5	A549	NP69	HK1
Clusianone (29)	4.16	3.06	3.66	5.35
CMet (53)	120.38	86.70	101.02	62.70
CHyd (54)	47.15	57.70	68.80	65.55
CMxA (55)	2.82	7.67	5.12	4.85
CMeA (56)	10.20	4.09	10.02	3.43
CEtA (57)	16.49	11.84	16.74	12.52
Docetaxol (18) ^a	0.006	0.006	0.006	0.006

^aDocetaxol (18) control *MRC5 (lung fibroblast) , A549 (lung adenocarcinoma), NP69 (immortalized nasopharyngeal epithelial cell) and HK1 (squamous carcinoma of the nasopharynx) .

Synthetic clusianone (29) tested on HeLa, MCF7 and MiAPaca-2 carcinoma cells using resazurin assay showed IC_{50} values in the range of 5.0-8.0 $\mu\text{g/mL}$ (Simpkins *et al.*, 2012). However, the IC_{50} of the resazurin assay were analysed after 72 hours of synthetic clusianone (29) treatment. This indicates clusianone (29) exhibited good anticancer activity in A549 cells within 48 hours of treatment in the present MTT assay conducted. It was reported that 7-epiclusianone (30) was tested against non-small lung cancer (NCI- 460) and numerous cancer cell lines using SRB assay showed IC_{50} values of more than 5 μM after 48 hours treatment (Murata *et al.*, 2010). Further to this, 7-epiclusianone (30) was tested against non-small lung cancer (A549) using MTS assay. The IC_{50} value was above 15 μM . In comparison to its epimer (30), clusianone (29) definitely has exhibited higher cytotoxicity activity at a lower dosage in non-small lung cancer cells.

Clusianone (29) derivatives were tested using MTT assay in order to study the structure-activity relationship of these derivatives on both carcinoma and normal cell lines. Based on the results (**Table 5.7**), several findings were summarized. First, compound CMet (53) bioactivity against carcinoma cells A549 and HK1 cells had decreased with IC_{50} value of 86.70 μM and 64.45 μM respectively. It was noticed that the methylation has decreased the cytotoxicity effects of CMet (53) on both cancer and normal cells by 30 fold at least. Compound CMet (53) was also less toxic to normal cells in terms of the concentration which was lethal to 50% of the cells population. Upon hydrogenation of tetraprenylated group of CMet (53) leads to a more lipophilic domain of this compound which has indeed decreased the cytotoxicity effect of CHyd (54) by 20 folds. The IC_{50} values for A549 and HK1 cells were 59.70 μM

and 65.50 μM . In terms of solubility of the compound CMet (53) and CHyd (54) in DMSO, both compounds were vortexed and further sonicated for 15 minutes at 30°C since both methylation and hydrogenation of clusianone (29) have made the compounds to possess less polarity or perhaps lipophilic characteristics which made these compounds less soluble in DMSO.

In contrast, to compound CMet (53) and CHyd (54), compound CMxA (55), CMeA (56) and CEtA (57) were easily dissolved in DMSO without much vortex force since these compounds possess both hydroxyl and amine groups which were highly polar compounds. The cytotoxicity results of compounds CMxA (55), CMeA (56) and CEtA (57) indicates good activity since IC_{50} value was in the range of 3.0 to 20.0 μM . Compound CMxA (55) demonstrated potential anticancer activity on both A549 and HK1 cells with IC_{50} value of 2.82 μM and 5.12 μM respectively. However, compound CMxA (55) has cytotoxicity which affects the normal cells more significantly than the carcinoma cells. The plausible reason to these could be due to the presence of N-O bond in CMxA (55) which was linked to its low bond dissociation energy. As such, this weak bond with electron rich N-O group was susceptible to nucleophilic attack by proteins in biochemical assays resulting in false positives (Rishton, 2003; Axerio-Cilies *et al.*, 2009).

Remarkably, compound CMeA (56) exhibited good activity on both A549 and HK1 cells with IC_{50} values of 4.09 μM and 3.43 μM . Most importantly, compound CMeA (56) suppressed the growth rate of MRC5 and NP69 normal cells at a higher concentration above 10.0 μM indicating more than 50% less cytotoxicity to normal cells compared to carcinoma cells. As for

compounds CEtA (57), IC_{50} values were all beyond 10.0 μ M for both normal and carcinoma cells indicating moderate effect on the normal cell lines.

Antimicrotubule drug docetaxol (18) was used as control drug since type B PPAP compounds have been demonstrated to exhibit inhibitory activity of tubulin assembly of carcinoma cells (Roux *et al.*, 2000). The effect of docetaxol (18) was 500 times potent in inhibiting the cells from proliferating when being compared to clusianone (29). Among the six compounds, CMeA (56) was chosen for further study due to less cytotoxicity effect on normal cells and most importantly for the good anticancer activity below 5.0 μ M concentration against cancer cells (Boik, 2001). Clusianone (29) and compound CMeA (56) were further studied for morphology studies since both compounds have shown interesting anticancer activity as a result of MTT assay.

5.2 Morphology changes in treated A549 and HK1 cells

The effects of clusianone (29) in different concentration were tested on both the A549 and HK1 cells by cell morphology observation under inverted phase microscope. In addition to this, cell morphology studies were carried out for compound CMeA (56) which displayed significant cytotoxicity activity against the A549 and HK1 cells while having moderate effect on the normal cells. The selections of both the compounds were made based on characteristics set by Boik. (2001), whereby IC_{50} values of pure compounds should be less than $5.0\ \mu\text{M}$. The reason for this criterion was that these compounds will have a better efficacy in the *in vivo* test and less chances of toxicity which can cause adverse effect (Boik, 2001). Since cytotoxicity test using MTT assay was only able to show cell-killing property without demonstrating the specific cell death mechanism, further studies such as morphology observation of the treated cells under inverted phase microscope were crucial in understanding the mechanism of action of both clusianone (29) and compound CMeA (56) against A549 and HK1 cells.

Cell death occurrence happens in two main mechanisms known as apoptosis and necrosis. Apoptosis is a programmed cell death which is physiological process by which unwanted cells are eliminated during either development stage or during the course of any other biological process in the cells. On the other hand, necrosis is cell death process triggered by a pathological process, which usually occurs when cells are exposed to serious physical or chemical affront (Eisel *et al.*, 1998).

There were several distinct morphological changes cells go through during apoptosis. These features include cell shrinkage, chromatin aggregation, cytoplasmic fragmentation and formation of membrane bound vesicles which eventually forms apoptotic bodies. In contrast to apoptosis, necrosis begins with the loss of membrane integrity which leads to the swelling of cytoplasm and mitochondria and ends with total cell lysis (Eisel *et al.*, 1998).

Cell morphology of A549 cells cell treated with clusianone (29) indicated cell death *via* apoptosis since cell shrinkage and apoptotic bodies predominated at both IC₅₀ and 5 µg/mL (**Figure 5.7**). Images from the clusianone (29) treated HK1 cells morphology experiments shows evident signs of apoptosis such as cell shrinkage and pyknotic body both IC₅₀ and 5 µg/mL (**Figure 5.7**). There was also a decline in the number of cells in both A549 and HK1 cells clusianone (29) treated at IC₅₀ and 5 µg/mL due to adherent cell detachment. This cell detachment phenomena occurs *via* two major events of either apoptosis which causes loss of cellular adhesion or necrosis which causes the disruption of the plasma membrane (Rello *et al.*, 2005).

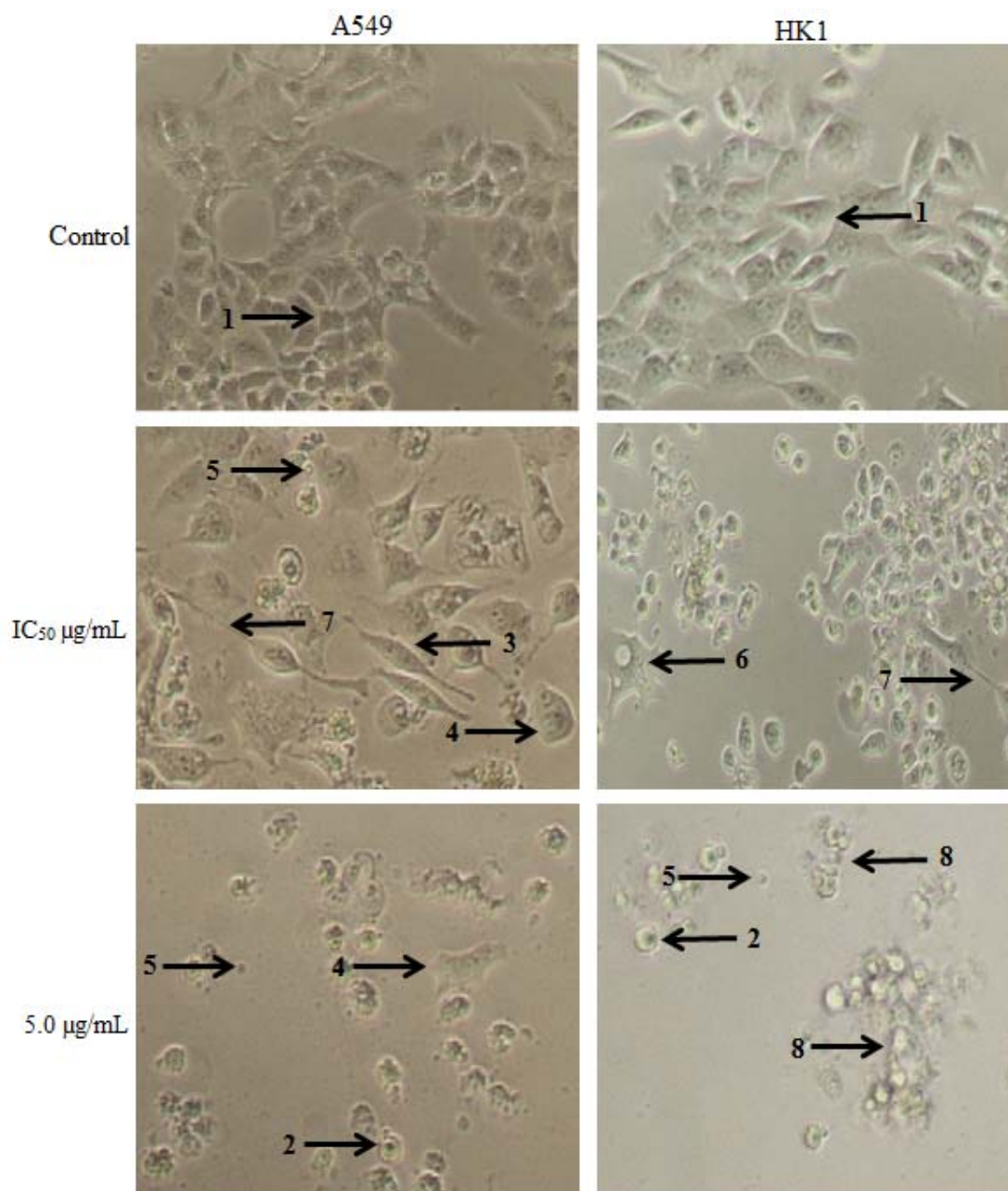


Figure 5.7 Morphology changes of carcinoma cell A549 (top to bottom left) and HK1 (top to bottom right) cells treated with clusianone (29). Cells were treated with clusianone (29) for 48 hours and imaged by inverted phase contrast microscope (magnification 200×). The arrow indicates (1) control cell, (2) condensed nuclei, (3) cell shrinkage, (4) membrane blebbing, (5) apoptotic body, (6) cell lysis/blistering (7) echinoid spikes and (8) pyknotic body.

In contrast to the control cells, clusianone (29) treated cells showed decline in cell number since apoptotic bodies no longer possess cellular adhesion and most of these cells eventually detached from the surface of tissue culture plates (**Figure 5.7**). This apoptotic characteristic inducing early detachment occurrence of monolayer cells from their basal cell membrane are also known as anoikis (Rahman *et al.*, 2013).

As for the A549 cells treated with compound CMeA (56), majority cell showed cell shrinkage characteristics which indicated apoptosis typical appearance at IC₅₀ concentration. On the contrary, domination of cell lysis characteristic which was distinctive necrosis appearance occurred at 5 µg/mL (**Figure 5.8**). The effect of compound CMeA (56) against HK1 cells at IC₅₀ concentration showed that majority cells attributed membrane blebbing appearances (**Figure 5.8**). Decline in the number of cell are observed in both cells as the CMeA (56) treatment was increased from 0-5 µg/mL. Generally, membrane blistering was common in both A549 and HK1 cells treated with CMeA (56) at 5 µg/mL which reveals cell death *via* necrosis (Rello *et al.*, 2005).

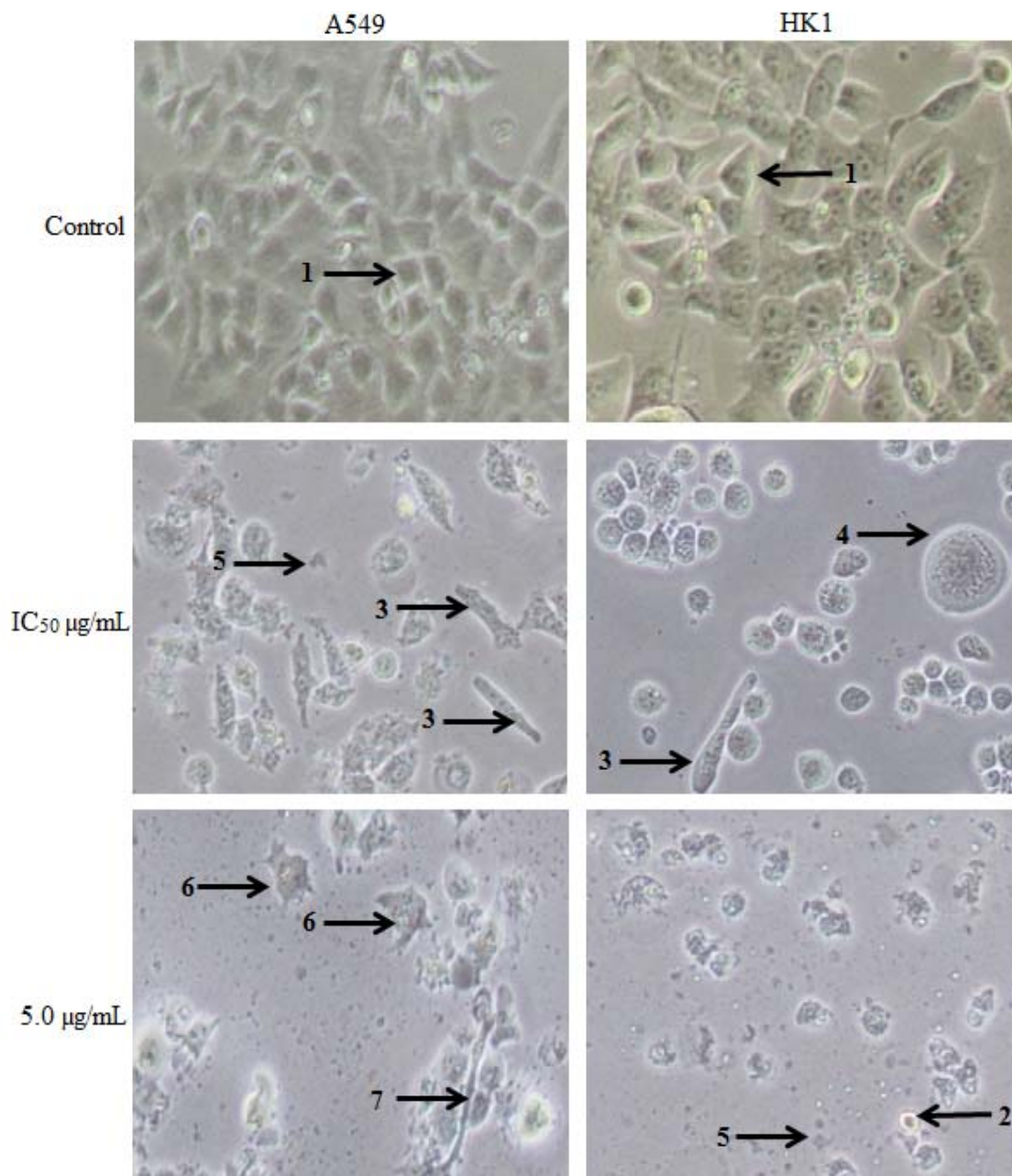


Figure 5.8 Morphology changes of carcinoma cell A549 (top to bottom left) and HK1 (top to bottom right) cells treated with CMeA (56). Cells were treated with CMeA (56) for 48 hours and imaged by inverted phase contrast microscope (magnification 200×). The arrow indicates (1) control cell, (2) condensed nuclei, (3) cell shrinkage, (4) membrane blebbing, (5) cytoplasmic contents, (6) cell lysis/blistering and (7) echinoid spikes.

The HK1 cells treated at 5 µg/mL showed necrosis characteristic. Cell lysis occurrence was observed with compound CMeA (56) treated on HK1 cells which were a prominent attribution of cell death *via* necrosis. One of the most distinctive morphology of cell death *via* necrosis observed was cellular swelling due to the loss of membrane integrity. During this stage, water influx through plasma membrane occurs causing the cell to appear vacuolated. Consequently, this will cause membrane blebbing which will finally lead to cell lysis whereby all cell cytosolic contents including non-functional organelles are spilled out (Eisel *et al.*, 1998).

5.3 Mode of action pathway studies of clusianone (29) and CMeA (56) treated against A549 and HK1 cells through immunostaining

Immunostaining technique became an important tool in order to further study the inhibition effect of clusianone (29) and compound CMeA (56) against A549 and HK1 cell lines. This technique emphasizes antibody utilization to detect specific protein in samples also known as immunohistochemistry. There are several immunostaining methods such as flow cytometry, Western blot, enzyme linked-immunosorbent assay, microarrays and electron microscopy (Hughes *et al.*, 2014). However, Western blot was employed as the best methodology for this study since the technique has broad cell heterogeneity as compared to flow cytometry (Kornblau *et al.*, 2005). Western blot detects the specific proteins in cell sample in tissue homogenate or extract form (Kurien & Scofield, 2003). The method has been used for both qualitative and quantitative analysis over the past decades and has been an important analytical tool in specific protein detection research field (Taylor & Posch, 2014).

Cytotoxicity assay using the MTT assay revealed that clusianone (29) and compound CMeA (56) prevailed significant antiproliferative activity against both A549 and HK1 cells showing IC_{50} values below 5 $\mu\text{g/mL}$. This prompted further pathway studies of clusianone (29) and CMeA (56) as potential antimicrotubule agent or antimitotic agent by observing the expression of β -tubulin and cell check point cycle regulators cyclin B1/Cdk1 complex at different time point (8, 16, 24 and 48 hours) of the treated carcinoma cells by immunostaining. The cells were treated with respective IC_{50} concentration determined from MTT test since these concentrations were considered

proapoptotic dose which caused at least 50% of cell death population (Berridge *et al.*, 1996).

Based on the results of Western blot analysis as shown in (**Figure 5.9**), clusianone (29) exhibited profound dysregulation in the β -tubulin protein expressed in A549 cells. The downregulation of protein can be observed across the different time treatment as compared to the control untreated cells protein blots. The expression of β -tubulin protein mainly declined after 16 hours (43.18%) of treatment with about 50% downregulation was estimated compared to cell treated at 8 hours (102.02%). From this observation, it can be deduced that only after 16 hours of treatment the onset of apoptosis rapidly occurred in A549 cells. The β -tubulin protein decreased gradually and finally after 48 hours of treatment, it was observed only 10.72% β -tubulin proteins were expressed. On an account of this, both the cell cycle regulator Cdk-1 and cyclin B1 protein expression were also downregulated from 16 hours onwards.

Overall, the decrease in the protein band intensity was noticed after 16 hours of treatment and clusianone (29) has a strong inhibitory effect on both β -tubulin and Cdk-1 activity. Cdk-1 are important cell cycle regulators which also phosphorylates β -tubulin (Fourest-Lieuvin *et al.*, 2006). Hence, clusianone (29) showed signs of interference with mitotic phase related proteins and it could be postulated that the mechanism of action of clusianone (29) consequently causes cell cycle arrest at G2/M phase in A549 cells. The plausible reason could be the antimicrotubule effect by clusianone (29) consequently leading to dysregulation of cell cycle regulators (Nurse, 1990; Lindqvist *et al.*, 2007).

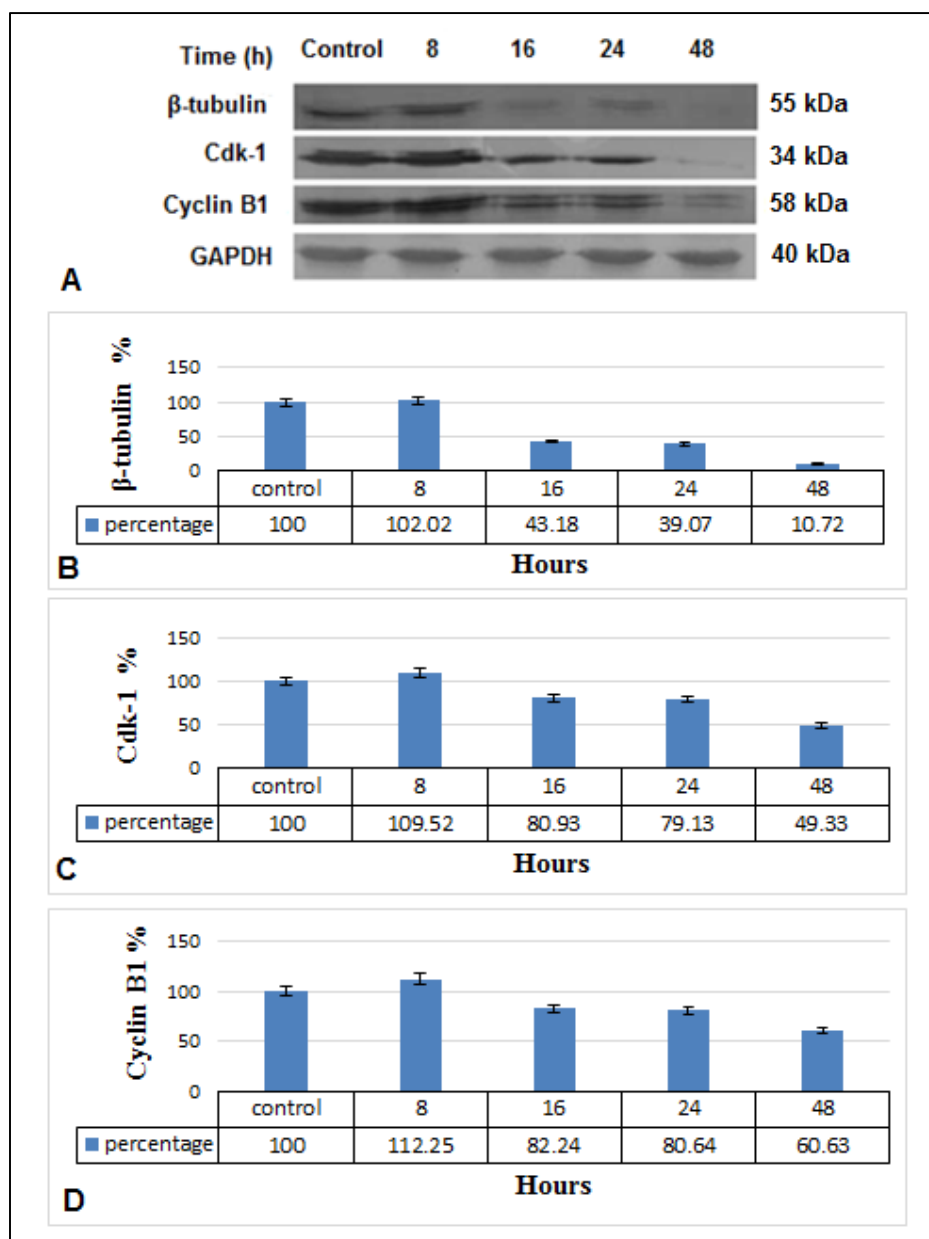


Figure 5.9 A549 cells treated at IC_{50} of clusianone (29) and protein extraction harvested after 8, 16, 24 and 48 hours for western blot analysis. A. β -tubulin, Cdk-1 and Cyclin B1 were immunoprecipitated with appropriate antibodies and GAPDH level was used as an internal loading control for protein amount. Western blot densitometry quantification results: B. Percentage of β -tubulin protein; C. Percentage of Cdk-1 protein; D. Percentage of Cyclin B1 protein at 8, 16, 24 and 48 hours of treated A549 cells compared to the control (untreated A549 cells harvested after 48 hours). Results are presented as mean \pm SD from two independent experiments.

Meanwhile, similar pattern of protein expression was not observed for HK1 cells treated with clusianone (29) specifically referring to cell cycle regulator protein expressions as time progressed from 8 hours to 48 hours of treatments (**Figure 5.10**). Both Cdk-1 and cyclin B1 protein expression in HK1 cells were not affected by clusianone (29). It was clear that β -tubulin downregulation occurs after 24 hours (79.0%) treatments and interestingly less detection of β -tubulin protein after 48 hours (39.37%) treatment. Arising out of this was the doubling time for HK1 cells which was probably more than 30 hours as compared to A549 cells which have a doubling time less than 24 hours (Huang *et al.* 1980; Chan *et al.*, 2012). Under these circumstances, the cells indicate late apoptosis and cells cycle regulators of cell division progression were not affected at even at 48 hours treatment. Nonetheless, it remains to be further investigated to the increase in Cdk-1 protein expressions after 48 hours treatment with 107.63% protein expressed compared to control untreated cells.

This result suggests that clusianone (29) has interfered with the microtubule system since β -tubulin protein has declined abruptly in HK1 cells after 48 hours treatment with clusianone (29) (Ohishi *et al.*, 2007; Jirásek *et al.*, 2009; Narvi *et al.*, 2013). Conversely, consistent expressions of both Cdk-1 and cyclin B1 protein levels indicate that clusianone (29) was not contributing to cell cycle arrest at G2/M phase. However, the cell death occurrence could possibly happen at a later stage of mitotic phase since the expression of β -tubulin protein has been altered after 48 hours treatment with clusianone (29) (Allan & Clarke, 2007; Clute & Pines, 1999).

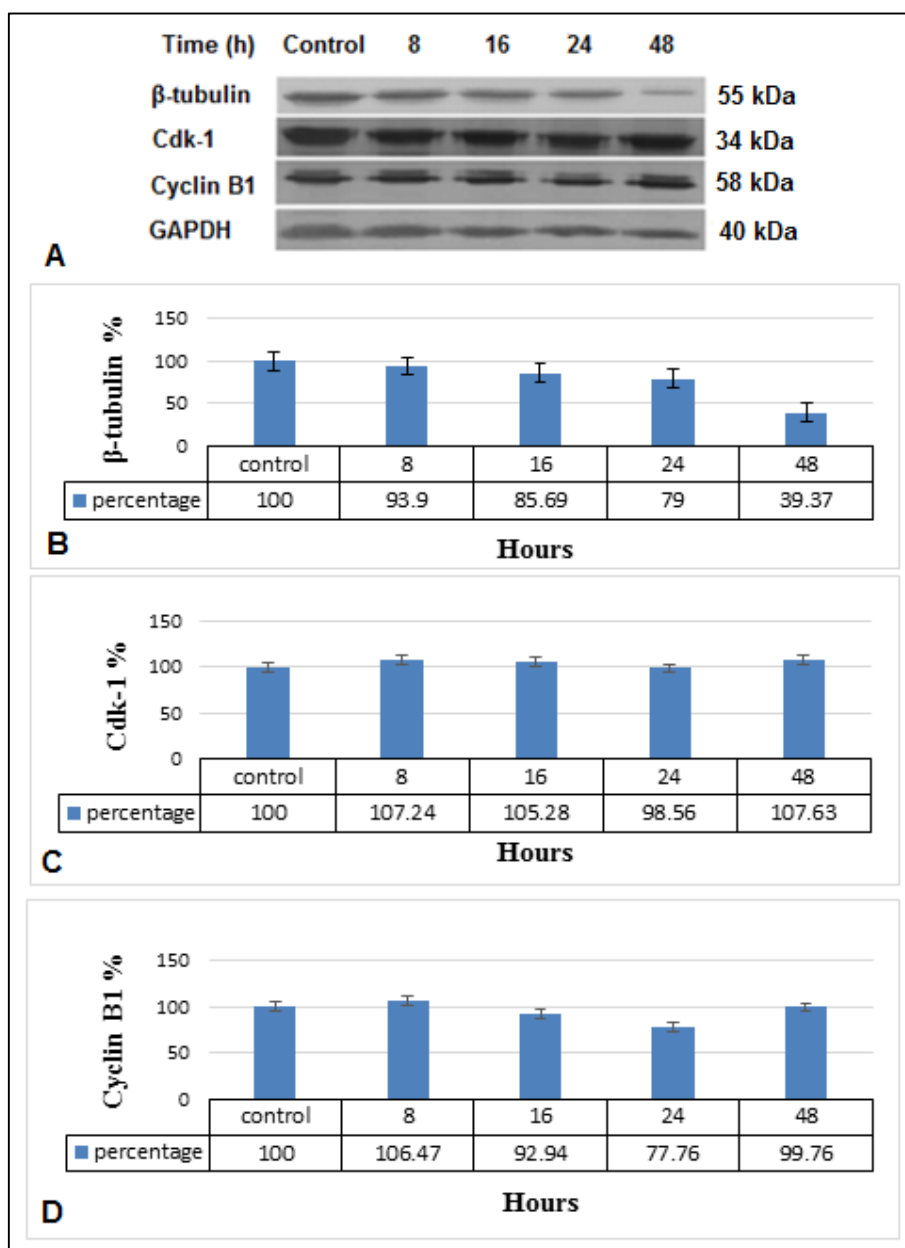


Figure 5.10 HK1 cells treated at IC_{50} of clusianone (29) and protein extraction harvested after 8, 16, 24 and 48 hours for western blot analysis. A. β -tubulin, Cdk-1 and Cyclin B1 were immunoprecipitated with appropriate antibodies and GAPDH level was used as an internal loading control for protein amount. Western blot densitometry quantification results: B. Percentage of β -tubulin protein; C. Percentage of Cdk-1 protein; D. Percentage of Cyclin B1 protein at 8, 16, 24 and 48 hours of treated HK1 cells compared to the control (untreated HK1 cells harvested after 48 hours). Results are presented as mean \pm SD from two independent experiments.

Next, CMeA (56) was tested against A549 cells and results are shown in (**Figure 5.11**). Interestingly, all three proteins blots indicated decline in protein expression in a time dependent manner. In particular, after 48 hours treatment, the decline in β -tubulin protein (0%) was linked to the decline in Cdk-1 protein (54.59%). Meanwhile, decrease in cyclin B1 (0%) protein was more marked compared to the Cdk-1 protein. This was a clear indication of cell cycle arrest in the progression of cell division since all proteins required for mitosis phase progression are downregulated significantly especially after 24 hours treatment (Taguchi *et al.*, 2007). Nevertheless, A549 cells doubling time is around 22 hours which indicates that the downregulations of these proteins occurred during the mitosis stage of the cells.

The decrease in the level of cyclin B1 has affected the level of Cdk-1. Consequently, the reduction in Cdk-1 protein has disrupted the level of β -tubulin level since Cdk-1 is responsible for the phosphorylation of tubulins (Fourest-lieuvin *et al.*, 2006). Most importantly all three protein levels were reduced, demonstrating high possibility of cell death through cell cycle arrest at G2/M phase including mitotic catastrophe probably arising from the microtubule spindle formation (Nurse, 1990; Lindqvist *et al.*, 2007).

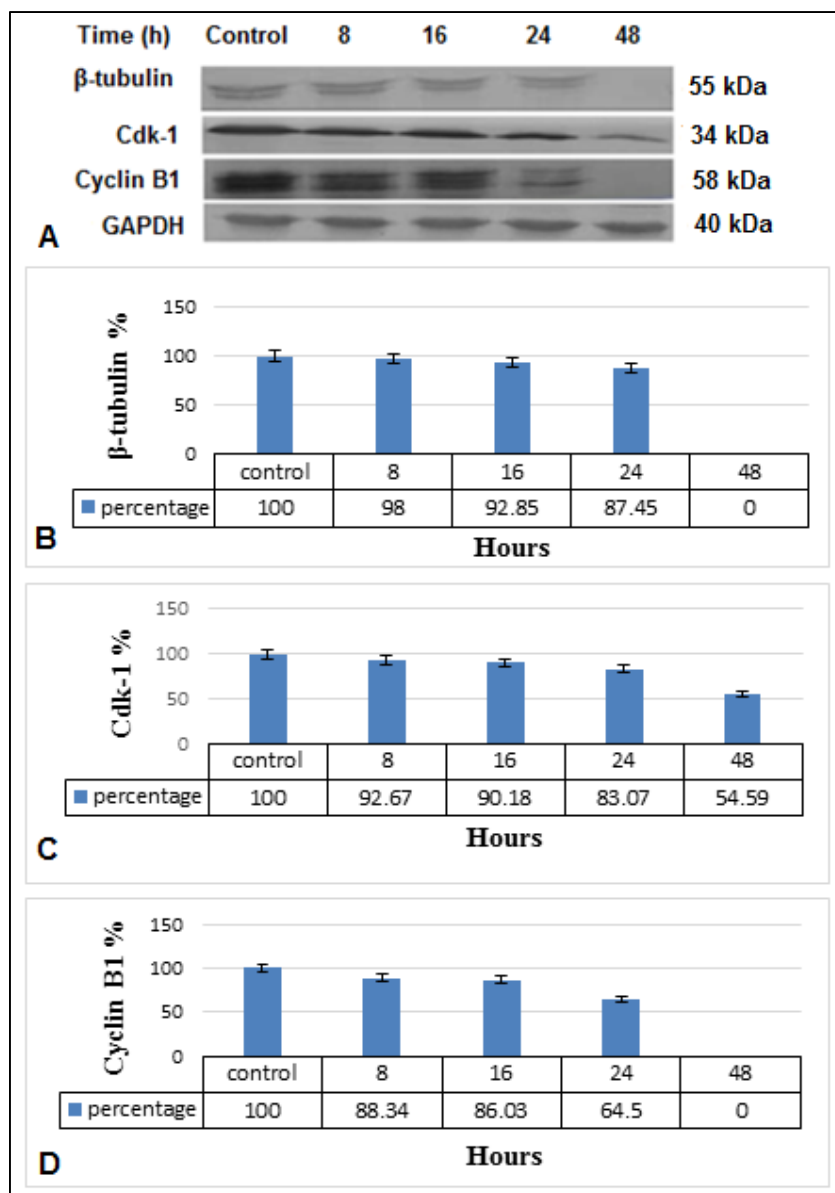


Figure 5.11 A549 cells treated at IC_{50} of compound CMeA (56) and protein extraction harvested after 8, 16, 24 and 48 hours for western blot analysis. A. β -tubulin, Cdk-1 and Cyclin B1 were immunoprecipitated with appropriate antibodies and GAPDH level was used as an internal loading control for protein amount. Western blot densitometry quantification results: B. Percentage of β -tubulin protein; C. Percentage of Cdk-1 protein; D. Percentage of Cyclin B1 protein at 8, 16, 24 and 48 hours of treated A549 cells compared to the control (untreated A549 cells harvested after 48 hours). Results are presented as mean \pm SD from two independent experiments.

Subsequent time dependent treatment of CMeA (56) against HK1 cells revealed similar downregulation of proteins pattern with CMeA (56) time dependent treatment against A549 cells. The decrease in β -tubulin (19.28%), Cdk-1 (46.5%) and cyclin B1 (51.16%) were notable especially after 48 hours treatment (**Figure 5.12**). Besides, the decline in the level of Cdk-1 and cyclin B1 proteins were most probably following the onset of apoptosis which was initiated after 16 hours treatment (Allan & Clarke, 2007; Clute & Pines, 1999). Mitosis rapidly occurs in actively proliferating cells, particularly in HK1 cell lines have doubling time within 25-30 hours. Therefore, any failure in cell cycle check point regulations within this period culminates in unrestricted cell division and eventually leading to cell death.

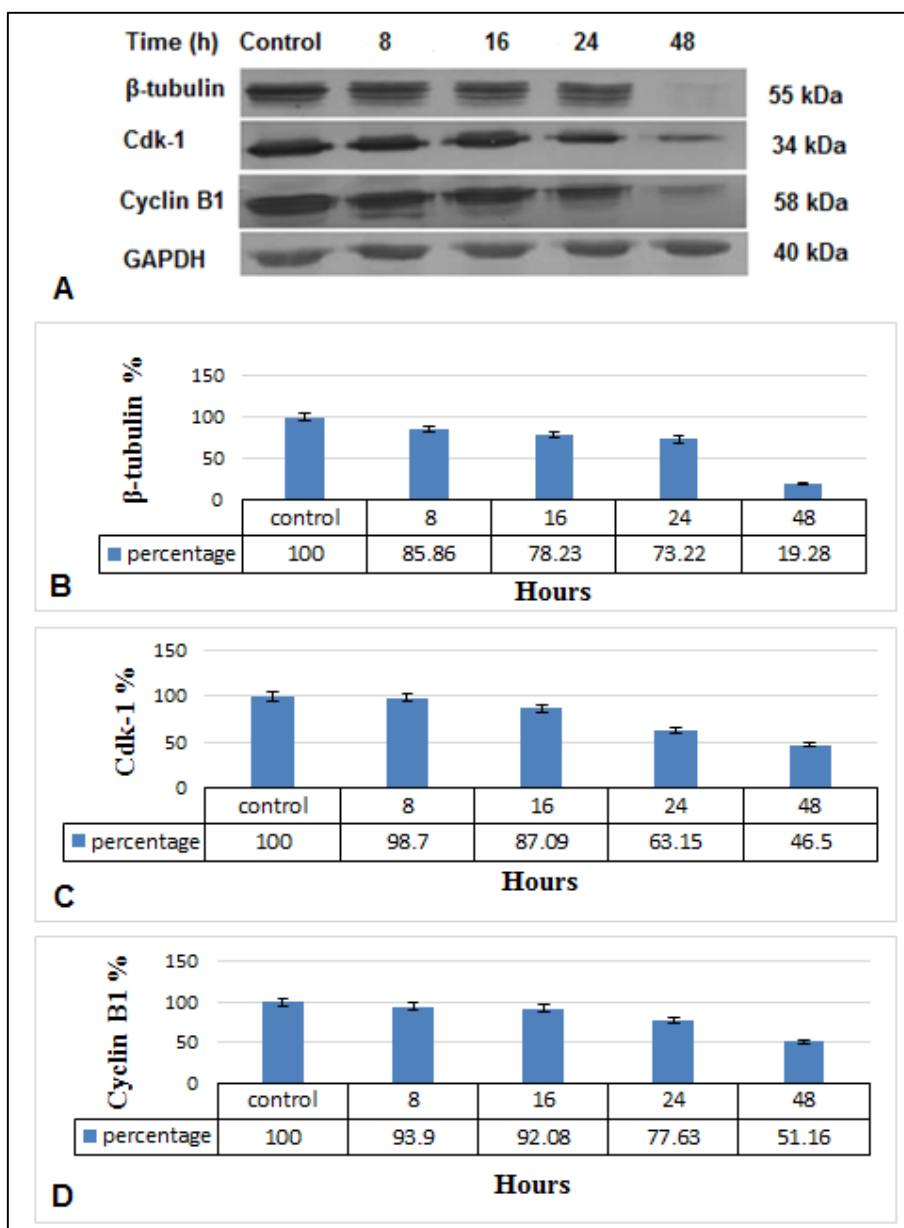


Figure 5.12 HK1 cells treated at IC_{50} of compound CMeA (56) and protein extraction harvested after 8, 16, 24 and 48 hours for western blot analysis. A. β -tubulin, Cdk-1 and Cyclin B1 were immunoprecipitated with appropriate antibodies and GAPDH level was used as an internal loading control for protein amount. Western blot densitometry quantification results: B. Percentage of β -tubulin protein; C. Percentage of Cdk-1 protein; D. Percentage of Cyclin B1 protein at 8, 16, 24 and 48 hours of treated HK1 cells compared to the control (untreated HK1 cells harvested after 48 hours). Results are presented as mean \pm SD from two independent experiments.

To date, experiments using isolated mitochondrial from mouse liver tissues and the research revealed that cyclin B1/Cdk1 complex proteins were found to relocate in the matrix of mitochondria and an increased influx of mitochondrial cyclin B1/Cdk1 complex was associated with elevated mitochondrial bioenergetics in G2/M transition. Noteworthy, mitochondria-targeted cyclin B1/Cdk1 complex increases mitochondrial respiration with enhanced oxygen consumption and ATP generation which provides cells with efficient bioenergy for G2/M transition and shortens overall cell-cycle time (Wang *et al.*, 2014). In the present study, both Cdk1 and Cyclin B1 was markedly downregulated in clusianone (29) treated A549 cells possibly decreasing mitochondrial bioenergetics in G2/M transition eventually leading to the occurrence of cell death. This was also relevant to the discovery that revealed clusianone (29) at low micromolar concentration depletes the ATP level of mitochondria in HepG2 cells leading to cell death (Reis *et al.*, 2014).

Previous anticancer pathway study of clusianone (29) was tested against HepG2 cells which were estrogen receptor (*ER*) positive cells. It was also postulated that clusianone (29) interaction with estrogen receptor may have contributed to apoptosis *via* intrinsic pathway in HepG2 cells (Reis *et al.*, 2014). According to the report by Reis *et al.* (2014), clusianone (29) possessing hydroxyl group may have the binding activity that is similar to estradiol which binds to estragon receptor sites leading to signalling cascade of cell death pathway. However in this research, male derived lung cells A549 and nasopharyngeal cells HK1 were examined and these cells expressed almost insignificant estrogen receptors compared to cells derived from female cells. The A549 and HK1 cells overexpresses human growth factor receptor (*EGFR*)

(Stabile *et al.*, 2005; Ma *et al.*, 2010). This fact suggests less probability of clusianone (29) and CMeA (56) causing cell death by binding to estrogen receptors (ER) of A549 and HK1 cells. It is plausible that clusianone (29) and CMeA (56) are micromolar inhibitors of human growth factor receptor (EGFR).

In silico studies have proven that interaction between C7 hydroxyl groups in taxol interferes with polar cluster region (Thr276, Ser277 and Arg278) of β - tubulin protein structure (**Figure 2.7**). Consequently, this leads to the stabilization of microtubule structure and preventing disassembly of microtubule for the next stage of mitosis phase progression to occur. Similarly, clusianone (29) possessing hydroxyl group is postulated to interact with polar cluster region (Thr276, Ser277 and Arg278) of β - tubulin protein structure. Interestingly, CMeA (56) possessing both hydroxyl and amine compound is postulated to have exerted a greater interaction with β -tubulin protein based on the cytotoxicity immunostaining results. The presence of lone pair on amine group could be the main contributor in the interaction between CMeA (56) and microtubule receptor which leads to microtubule disruption. This theory postulated was supported by the fact shown in molecular modelling studies using taxol interaction with β -tubulin protein. In this study, benzamido group having lone pairs on amide group was occupied by Asp26. There were also hydrogen bonds reported between this groups which enhance the interaction (Renzulli *et al.*, 2006).

In conclusion, clusianone (29) and compound CMeA (56) have exhibited antimicrotubule activity since expression of β -tubulin, Cdk1 and cyclin B1 complex has declined especially after 48 hours treatment.

CHAPTER 6 CONCLUSIONS & RECOMMENDATIONS FOR FUTURE STUDIES

6.1 Conclusions

The isolation of clusianone (29) from the leaves of *G. parvifolia* (Miq.) Miq., has led to attain 500 mg of clusianone (29) crystals. The optimization of clusianone (29) *via* recrystallization afforded x-ray diffraction quality crystals which allowed the single x-ray analysis of clusianone (29) crystal obtained in $P2_12_12_1$ polymorph form. Synthesis of clusianone (29) derivatives led to structural-activity relationship (SAR) of clusianone (29) against lung and nasopharyngeal carcinoma including cytotoxicity effect on normal lung and nasopharyngeal cell lines.

Eight derivatives of clusianone (29) were obtained from five types of chemical reactions. These clusianone (29) derivatives were routinely prepared on a scale of 10-100 mg and purified using column chromatography. Clusianone (29) was methylated, hydrogenated, added with oxime and primary amines functional groups and alkylated to install additional prenyl chain and geranyl chain. Compound CMet (53) afforded crystals through slow evaporation of methanol evaporation crystal and seeding technique which were further characterized using single crystal X-ray crystallography analysis.

The overall MTT assay data confirmed that CMeA (56) exhibited better inhibitory against the A549 and HK1 respiratory carcinoma cells compared to other derivatives. Focusing on the structural requirements based on SAR study of this research, CPryl (58) and CGeryl (59) were developed to unravel the potency of clusianone (29) derivatives with additional prenyl and geranyl chain

as antimicrotubule agent. However, due to low yield and time restraint the biological activities of these two compounds have not been tested.

Morphology studies using inverted phase microscopy were selectively analysed on treated A549 cells and HK1 cells. Clusianone (29) and compound CMeA (56) were treated at different concentration (0-5 $\mu\text{g/mL}$) to these cells and visualized under the inverted phase microscopy after 48 hours treatment. It was observed that clusianone (29) induces cell death of both A549 and HK1 cells *via* apoptotic manner with majority cells displaying cell shrinkage and apoptotic bodies. Conversely, A549 cells and HK1 cells treated with CMeA (56) showed cell morphology predominated by necrosis characteristics.

Based on the Western Blot results, both clusianone (29) and CMeA (56) lead to mitotic cell death (MCD) which is essential during cell division with β -tubulin being hallmark for the inhibitory effect Cdk1 and cyclin B1 have been identified as the checkpoint checkmate in the cell death occurrences in both A549 and HK1 cells treated with clusianone (29) and CMeA (56). Thus, suggesting validity to further the study of both clusianone (29) and CMeA (56) on tumour cells, since tumour cells undergo unrestricted growth as compared to normal cells dividing rate. Despite being the shortest phase of the cell cycle, the mitotic phase has been a target for both clusianone (29) and CMeA (56). β -tubulin and Cdk1 are targets for small molecule inhibitors which leads to mitotic cell death (MCD) pathway.

The introduction of nitrogen element into the core of CMeA (56) bicyclo [3.3.1] nonane-2,4,9-trione structure provides added values to the overall anticancer activity against respiratory carcinoma cell. First hypothesis arising based on the increased antimicrotubule activity is that the nitrogen lone pair

provides binding ability to the specific microtubule binding sites. This hypothesis is also supported by the fact the imine derivatives have high water solubility properties because the nitrogen elements exist as acid salts in water (Yamazaki *et al.*, 2012).

There was no information about the mechanism of action of clusianone (29) as antimicrotubule agent in the literature. Most importantly, the SAR studies from this research providently indicate the fundamental of hydroxyl, prenyl and imine groups which were postulated to be interacting in the microtubule binding domains. This eventually culminates in cell death of the A549 and HK1 respiratory carcinoma cells. In this research, the mode of action of clusianone (29) and its potent derivative CMeA (56) as the potential antimicrotubule agent have been successfully studied and will be reported and published in due course.

Naturally occurring PPAP compounds are found in a number of edible and medicinal plants. As such, there are many publications emphasizing the various biological activities of PPAP compounds and many PPAP natural product researchers have conducted *in vivo* animal model test including some under clinical trials. More information in these *in vivo* test warrants the effect of PPAP compounds in human (Wu *et al.*, 2014). However, there was lack of literature on understanding the function of different moieties present in PPAP compounds through concise SAR studies for in-depth understanding of their the molecular targets and mechanism of action.

Therefore, the SAR studies arising from this research were thought to provide valuable information about the desirable and undesirable moieties which accounts for the PPAP compound's cytotoxicity activity and antimicrotubule

inhibitor characteristics. Nonetheless, the study provides insight molecular mechanism that could potentially further clusianone (29) to be tested for *in vivo* studies specifically aimed to treat lung adenocarcinoma and squamous nasopharynx carcinoma.

6.2 Recommendation for future studies

This research successfully synthesized eight clusianone (29) derivatives. Providentially, clusianone (29) and compound CMeA (56) demonstrated good cytotoxicity activity against both A549 cells and HK1 cells. In addition, extended protein works *via* Western blot analysis has indicated that clusianone and compound CMeA (56) indeed inhibit cancer cell progression through mitotic cell death. There are several recommendations that could be carried out to further the studies. Since both clusianone (29) and compound CMeA (56) has hydroxyl groups and compound CMeA (56) has an amine group, more clusianone (29) derivatives possessing hydroxyl and amine group should be prepared.

Following this approach, *in silico* test utilizing molecular docking studies to determine the interaction between clusianone (29) and compound CMeA (56) in the β -tubulin protein domain. The studies will determine the functional groups responsible for stabilizing the microtubule polymerization or perhaps absolute orientation and position in β -tubulin domain. Besides β -tubulin protein, since clusianone (29) and compound CMeA (56) downregulate Cdk1 cell cycle regulators expressions, molecular modelling should also emphasize the possibility of interaction between these compounds and Cdk1 protein.

Tubulin assembly assay has been a topic of interest for researchers working with type B PPAP. In the course of the present work, it was found that

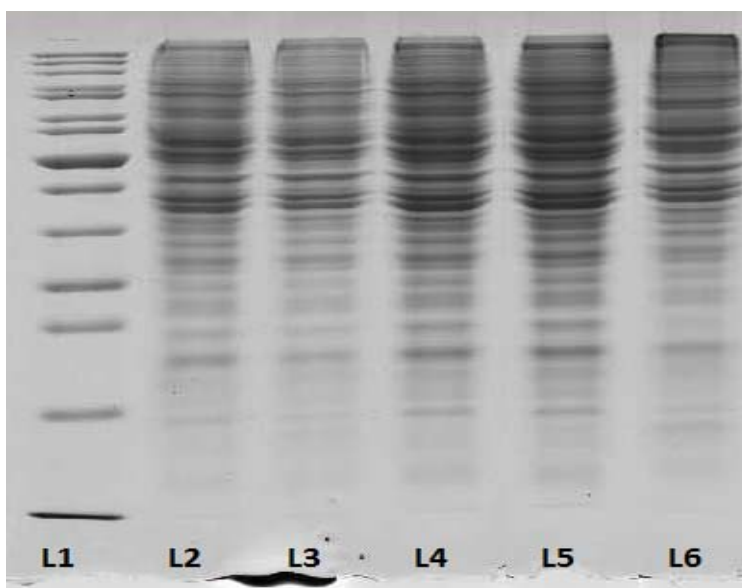
both clusianone (29) and compound CMeA (56) downregulate β -tubulin expression particularly after 48 hours treatment. Theoretically, the results suggest that both compounds exhibit microtubule dynamics disruption by interfering with tubulin assembly dynamics. However, the rate of binding of clusianone (29) and compound CMeA (56) to enhance polymerization of tubulin has not been explored. To date, with the availability of microtubule cytoskeleton assay kits containing tubulins isolated from animal cells makes this kinetic profiling studies possible. In addition, the assay kit includes positive control drugs such as paclitaxel should be used to compare the rate of activity of compound's tested against tubulin assembly activity.

Selection of ideal drug involves various physicochemistry test and most importantly preclinical trials on animal models have been compulsory from regulatory point of view. Therefore, clusianone (29) and compound CMeA (56) which have been tested for biological activity on *in vitro* scale should be tested and validated using *in vivo* experiments. *In vivo* test is crucial to further understand the efficacy of clusianone (29) and compound CMeA (56) through absorption, distribution, metabolism and excretion (ADME) studies. Nevertheless, *in vivo* test determines the dosage of the compound which are safe for both animal and human through toxicity assessments. With reference to this, proper lead compound formulation can be developed together with in depth pharmacokinetic and pharmacodynamics analysis.

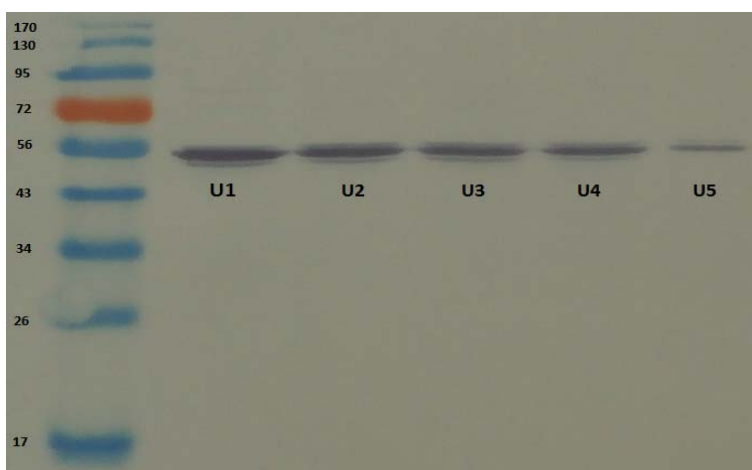
Over the past decades, the paradigm of clinical cancer treatment has evolved from just depending on chemotherapy solely to combining both targeted therapy and chemo drugs for better prognosis for cancer patients. Chemo drugs rapidly kill dividing cells but drawbacks related narrow therapeutic value and

toxicity side effects often becomes an issue or perhaps remains uncertain. Hence, the use of targeted therapy in conjunction with chemotherapy has been preferred by clinicians. On account of this, clusianone (29) and compound CMeA (56) can be tested for synergistic effect between other targeted therapy drugs such as Gefinitib, Erlotinib and Afabtinib. These drugs specifically targets *EGFR* for inhibitory effects in cancer cell lines and since both A549 and HK1 cells highly express *EGFR*, this synergistic approach has a promising therapeutic effect.

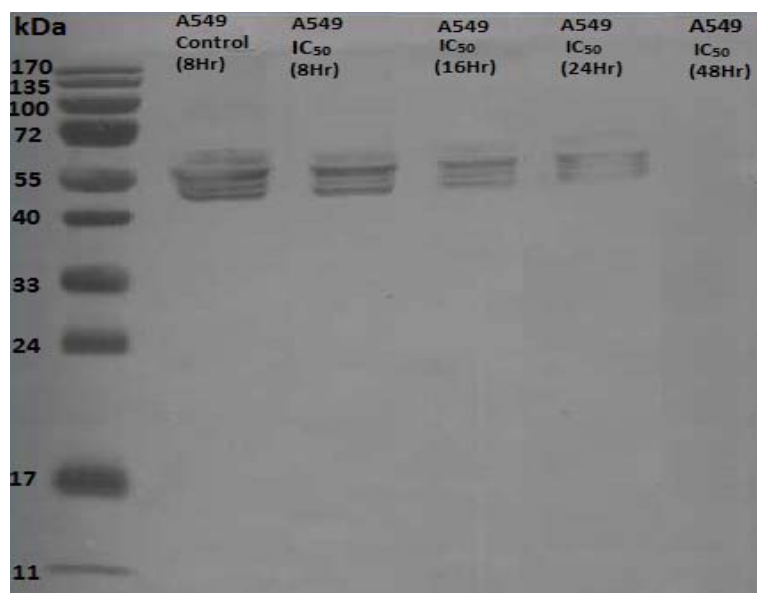
APPENDICES



Appendix A: 12% SDS-PAGE showing protein bands of A549 cells stained with Coomassie Blue. Lanes L1: Molecular weight marker, L2: 8 hours treatment with compound CMeA (56), L3: 16 hours treatment with compound CMeA (56), L4: 24 hours treatment with compound CMeA (56) and L5: 48 hours treatment with compound CMeA (56).



Appendix B: Proteins transferred from SDS-PAGE to nitrocellulose membrane and incubated with β -tubulin monoclonal antibody. Less background of the protein bands are noticed upon staining with TMB substrate. Lanes, U1: Control HK1 cells (Untreated), U2: 8 hours treatment with compound clusianone (29), U3: 16 hours treatment with compound clusianone (29), U4: 24 hours treatment and U5: 48 hours treatment with compound clusianone (29).



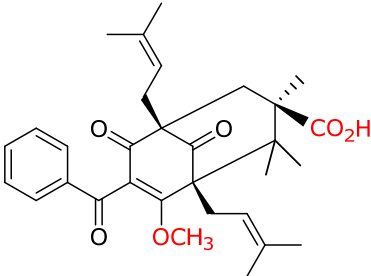
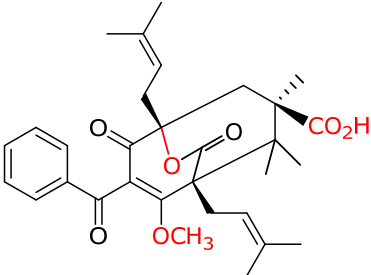
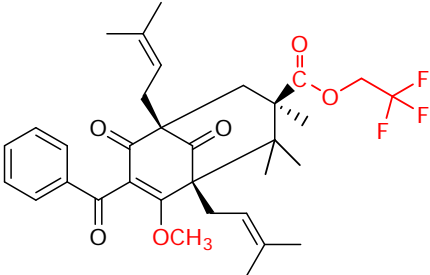
Appendix C: A549 cells treated with compound CMeA (56) and proteins transferred from SDS-PAGE to nitrocellulose membrane and incubated with β -tubulin polyclonal antibody. High background of the protein bands are noticed upon staining with TMB substrate.



Treatment	Density 1	Density 2	Mean	Standard deviation	Percentage %
Control	152.11	148.19	150.15	2.771858582	100
8	142.13	139.93	141.03	1.555634919	93.9
16	129.99	127.32	128.655	1.887975106	85.69
24	119.38	117.84	118.61	1.088944443	79
48	60.11	58.12	59.115	1.407142495	39.37

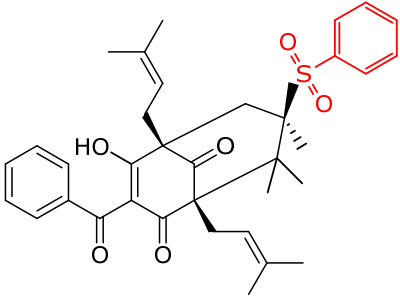
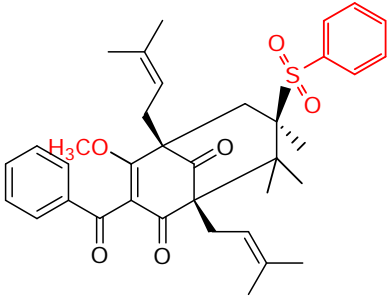
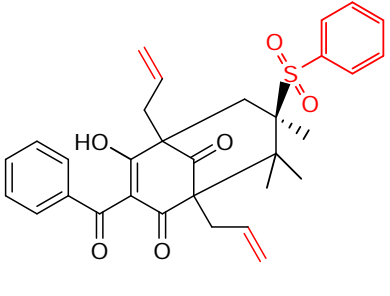
Appendix D: Protein quantification method using Quantity One Bio-Rad software and further statistical analysis to quantify total protein stains based on optical density value. Lanes, U1: Control HK1 cells (Untreated), U2: 8 hours treatment with clusianone (29) , U3: 16 hours treatment with compound clusianone (29), U4: 24 hours treatment and U5: 48 hours treatment with compound clusianone (29).

Appendix E: Table of total synthetic clusianone (29) derivatives by other synthetic research group and the derivatives tested for anticancer activities.

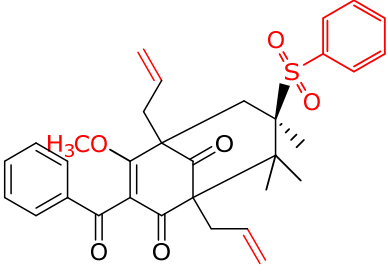
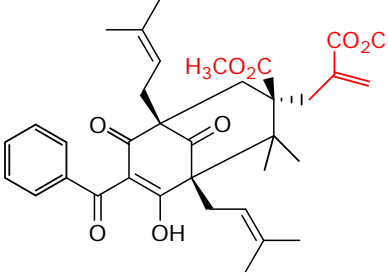
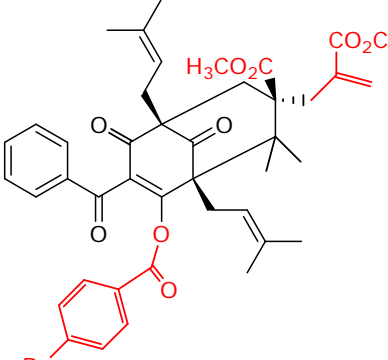
Total synthetic derivatives of clusianone (29) (Red formula indicates new functional group installed)	Anticancer activity	Reference
 <p>JQ-101 (61)</p>	^a MTS assay against lung carcinoma cells H460 (IC ₅₀ = 30 μM) A549 (IC ₅₀ = 40 μM) ^b SIRT1 activity assay (IC ₅₀ = 30 μM)	(Qi & Porco, 2007) (Zhu <i>et al.</i> , 2014)
 <p>JQ-02 (62)</p>	^b SIRT1 activity assay (IC ₅₀ = > 90 μM) Loss of activity	(Qi & Porco, 2007) (Zhu <i>et al.</i> , 2014)
 <p>JQ-08 (63)</p>	^b SIRT1 activity assay (IC ₅₀ = > 90 μM) Loss of activity	(Qi & Porco, 2007) (Zhu <i>et al.</i> , 2014)

^a MTS assay : 3-(4,5-dimethylthiazol-2-yl)-5-(3-carboxymethoxyphenyl)-2-(4-sulfophenyl)-2Htetrazolium assay to assess cell viability.

^b SIRT1 assay : Nicotinamide adenine dinucleotide (NAD)-dependent histone deacetylase inhibitory assay as preliminary anticancer test.

Total synthetic derivatives of clusianone (29) (Red formula indicates new functional group installed)	Anticancer activity	Reference
 <p>JQ-11 (64)</p>	^b SIRT1 activity assay (IC ₅₀ = > 90 μM) Loss of activity	(Qi & Porco, 2007) (Zhu <i>et al.</i> , 2014)
 <p>JQ-05 (65)</p>	^b SIRT1 activity assay (IC ₅₀ = > 90 μM) Loss of activity	(Qi & Porco, 2007) (Zhu <i>et al.</i> , 2014)
 <p>JQ-34 (66)</p>	^b SIRT1 activity assay (IC ₅₀ = > 90 μM) Loss of activity	(Qi & Porco, 2007) (Zhu <i>et al.</i> , 2014)

^b SIRT1 assay : Nicotinamide adenine dinucleotide (NAD)-dependent histone deacetylase inhibitory assay as preliminary anticancer test.

Total synthetic derivatives of clusianone (29) (Red formula indicates new functional group installed)	Anticancer activity	Reference
 <p>JQ-32 (67)</p>	^b SIRT1 activity assay (IC ₅₀ = > 90 μM) Loss of activity	(Qi & Porco, 2007) (Zhu <i>et al.</i> , 2014)
 <p>JQ-10 (68)</p>	^b SIRT1 activity assay (IC ₅₀ = > 90 μM) Loss of activity	(Qi & Porco, 2007) (Zhu <i>et al.</i> , 2014)
 <p>JQ-04 (69)</p>	^b SIRT1 activity assay (IC ₅₀ = > 90 μM) Loss of activity	(Qi & Porco, 2007) (Zhu <i>et al.</i> , 2014)

^b SIRT1 assay : Nicotinamide adenine dinucleotide (NAD)-dependent histone deacetylase inhibitory assay as preliminary anticancer test.



Acta Crystallographica Section E

Structure Reports

Online

ISSN 1600-5368

A $P2_12_12_1$ polymorph of (+)-clusianoneSree Vaneesa Nagalingam,^a Janet Wong Pik Ching,^a
Mohammed Khaleel bin Break,^b M. Ibrahim M. Tahir^c and
Teng-Jin Khoo^{a*}^aCentre for Natural and Medicinal Product Research, School of Pharmacy, Faculty of Science, University of Nottingham Malaysia Campus, Jalan Broga, 43500 Semenyih, Selangor, Malaysia, ^bSchool of Chemical Sciences and Food Technology, Universiti Kebangsaan Malaysia, 43600 Bangi, Malaysia, and ^cDepartment of Chemistry, Faculty of Science, Universiti Putra Malaysia, Malaysia
Correspondence e-mail: tengjin.khoo@nottingham.edu.my

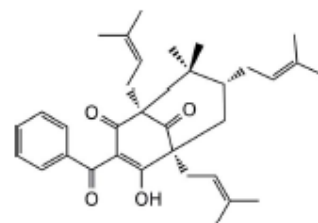
Received 25 October 2013; accepted 12 November 2013

Key indicators: single-crystal X-ray study; $T = 100$ K; mean $\sigma(\text{C}-\text{O}) = 0.002$ Å; R factor = 0.034; wR factor = 0.084; data-to-parameter ratio = 16.4.

The title compound, $\text{C}_{33}\text{H}_{42}\text{O}_4$ [systematic name: (1*S*,5*S*,7*R*)-3-benzoyl-4-hydroxy-8,8-dimethyl-1,5,7-tris(3-methylbut-2-enyl)bicyclo[3.3.1]nona-3-ene-2,9-dione], has a central bicyclo[3.3.1]nonane-2,4,9-trione surrounded by tetraprenylated and benzoyl groups. The compound was recrystallized several times in methanol using both a slow evaporation method and with a crystal-seeding technique. This subsequently produced diffraction-quality crystals which crystallize in the orthorhombic space group $P2_12_12_1$, in contrast to a previous report of a structure determination in the $Pna2_1$ space group [McCandlish *et al.* (1976). *Acta Cryst. B* **32**, 1793–1801]. The title compound has a melting point of 365–366 K, and a specific rotation $[\alpha]^{20}$ value of +51.94°. A strong intramolecular $\text{O}-\text{H}\cdots\text{O}$ hydrogen bond is noted. In the crystal, molecules are assembled in the *ab* plane by weak $\text{C}-\text{H}\cdots\text{O}$ interactions.

Related literature

For related structural studies, see: McCandlish *et al.* (1976); Santos *et al.* (1998, 2001). For background to *Clusiaceae* metabolites, see: Monache *et al.* (1991); de Oliveira *et al.* (1996). For discussion of polycyclic polyprenylated acylphloroglucinols, including their biological properties, see: Piccinelli *et al.* (2005); Garnsey *et al.* (2011); Simpkins (2013).



Experimental

Crystal data

$\text{C}_{33}\text{H}_{42}\text{O}_4$ $V = 2844.96$ (10) Å³
 $M_r = 502.69$ $Z = 4$
 Orthorhombic, $P2_12_12_1$ $\text{Cu K}\alpha$ radiation
 $a = 9.2035$ (2) Å $\mu = 0.59$ mm⁻¹
 $b = 13.4629$ (2) Å $T = 100$ K
 $c = 22.9607$ (5) Å $0.21 \times 0.14 \times 0.08$ mm

Data collection

Oxford Diffraction Gemini diffractometer 39826 measured reflections
 Absorption correction: multi-scan 5498 independent reflections
 (CrysAlis PRO; Oxford Diffraction, 2002) 5269 reflections with $I > 2\sigma(I)$
 $R_{int} = 0.034$
 $T_{min} = 0.86$, $T_{max} = 0.95$

Refinement

$R[F^2 > 2\sigma(F^2)] = 0.034$ $\Delta\rho_{max} = 0.24$ e Å⁻³
 $wR(F^2) = 0.084$ $\Delta\rho_{min} = -0.18$ e Å⁻³
 $S = 0.96$ Absolute structure: Hach (1983),
 2383 Friedel pairs
 335 reflections Absolute structure parameter:
 H-atom parameters constrained -0.04 (15)

Table 1
Hydrogen-bond geometry (Å, °).

$D-H\cdots A$	$D-H$	$H\cdots A$	$D\cdots A$	$D-H\cdots A$
O11—H11 ¹ —O1	0.98	1.48	2.4277 (14)	158
C27—H27 ³ —O1 ¹	0.99	2.63	3.330 (2)	128
C36—H36 ³ —O1 ¹	0.94	2.67	3.523 (2)	151
C8—H8 ¹ —O11 ⁴	0.95	2.62	3.300 (2)	129
C21—H21 ¹ —O17 ⁴	0.96	2.70	3.610 (2)	158

Symmetry codes: (i) $x-1, y, z$; (ii) $-x+2, y+\frac{1}{2}, z+\frac{1}{2}$; (iii) $-x+2, y-\frac{1}{2}, z+\frac{1}{2}$; (iv) $-x+1, y+\frac{1}{2}, z+\frac{1}{2}$.

Data collection: *CrysAlis PRO* (Agilent, 2011); cell refinement: *CrysAlis PRO*; data reduction: *CrysAlis PRO*; program(s) used to solve structure: *SUPERFLIP* (Palatinus & Chapuis, 2007); program(s) used to refine structure: *CRYSTALS* (Betteridge *et al.*, 2003; Cooper *et al.*, 2010); molecular graphics: *CAMERON* (Watkin *et al.*, 1996) and *Mercury* (Macrae *et al.*, 2006); software used to prepare material for publication: *publCIF* (Westrip, 2010).

The authors would like to thank the Ministry of Science, Technology and Innovation in Malaysia (MOSTI 02-02-12-SF0055) for providing a grant for this study. Professor C. Moody is thanked for access to instrumentation at the University of Nottingham, UK.

Supplementary data and figures for this paper are available from the IUCr electronic archives (Reference: TK5270).

References

- Agilent (2011). *CrysAlis PRO*. Agilent Technologies UK Ltd, Yarnton, England.
- Betteridge, P. W., Carruthers, J. R., Cooper, R. I., Prout, K. & Watkin, D. J. (2003). *J. Appl. Cryst.* **36**, 1487.
- Cooper, R. I., Thompson, A. L. & Watkin, D. J. (2010). *J. Appl. Cryst.* **43**, 1100–1107.
- Flack, H. D. (1983). *Acta Cryst. A* **39**, 876–881.
- Garnsey, M. R., Matous, J. A., Kwiek, J. J. & Coltart, D. M. (2011). *Bioorg. Med. Chem. Lett.* **21**, 2406–2409.
- Macrae, C. F., Edgington, P. R., McCabe, P., Pidcock, E., Shields, G. P., Taylor, R., Towler, M. & van de Streek, J. (2006). *J. Appl. Cryst.* **39**, 453–457.
- McCandlish, L. E., Hanson, J. C. & Stout, G. H. (1976). *Acta Cryst.* **B32**, 1793–1803.
- Monache, F. D., Monache, G. D. & Gacs-Baltz, E. (1991). *Physicochemistry*, **30**, 2008–2005.
- Oliveira, C. M. A. de, Porto, A. M., Bittich, V., Vencato, I. & Marsaloli, A. J. (1996). *Tetrahedron Lett.* **37**, 6427–6430.
- Oxford Diffraction (2002). *CrysAlis CCD and CrysAlis RED*. Oxford Diffraction Ltd, Abingdon, Oxfordshire, England.
- Palatinus, L. & Chapuis, G. (2007). *J. Appl. Cryst.* **40**, 786–790.
- Piccinelli, A. L., Cuesta-Rubio, O., Chica, M. B., Mahmood, N., Pagano, B., Pavone, M., Barone, V. & Rastrelli, L. (2005). *Tetrahedron*, **61**, 8206–8211.
- Santos, M. H., Nagem, T. J., Braz-Filho, R., Lula, I. S. & Speziali, N. L. (2008). *Magn. Reson. Chem.* **39**, 155–159.
- Santos, M. H., Speziali, N. L., Nagem, T. J. & Oliveira, T. T. (1998). *Acta Cryst. C* **54**, 1990–1992.
- Simpkins, N. S. (2013). *Chem. Commun.* **49**, 1042–1051.
- Watkin, D. J., Prout, C. K. & Pearce, L. J. (1996). *CAMERON*. Chemical Crystallography Laboratory, Oxford, England.
- Westrip, S. P. (2010). *J. Appl. Cryst.* **43**, 920–925.

filtered, evaporated and then dried using a rotary evaporator under reduced pressure at 40 °C. The hexane extract of the leaves (9.7 g) was then chromatographed on silica gel (70-230 mesh) and eluted with diethyl ether and evaporated. This fraction of the extract which contains a major portion of chlorophyll compounds was then mixed with silica gel:activated charcoal in proportion of 1:3:1, respectively, and placed in a column with a porous frit. The material was eluted with hexane (500 ml) followed by dichloromethane (500 ml) with the aid of vacuum pressure. To isolate the compound, the dichloromethane dried fractions (4.8 g) was further chromatographed on silica gel (70-230 mesh) and eluted with mixtures of cyclohexane/chloroform and chloroform/methanol of increasing polarity. A total of 122 fractions were collected in 20 ml vials and fractions from F51—F60 were crystallized *via* slow methanol evaporation. Growth of diffraction quality crystals were obtained through several recrystallizations in methanol using both slow evaporation method and crystal seeding technique over a period of 10 days. Yellow cubic crystals (119 mg) were obtained and the melting point was 365–366 K and the specific optical rotation $[\alpha]^{20}$ was +51.94 °. The specific optical rotation was measured using an ADP-440 Perkin Elmer digital polarimeter using a sodium lamp at 589 nm. The melting point was recorded on Stuart's melting point apparatus SMP100. All the data analysis relevant to melting point, specific rotation and X-ray diffraction analysis were repeated three times to determine the reproducibility of the data and various parameters.

2.2. Refinement

Crystal data, data collection and structure refinement details are summarized in Table 1. The H atoms were all located in a difference map, but those attached to carbon atoms were repositioned geometrically. The H atoms were initially refined with soft restraints on the bond lengths and angles to regularize their geometry (C—H in the range 0.93–0.98 and O—H = 0.82 Å) and $U_{eq}(H)$ (in the range 1.2–1.5 times U_{eq} of the parent atom), after which the positions were refined with riding constraints except the hydroxyl hydrogen which were refined freely (Cooper *et al.*, 2010).

Computing details

Data collection: *CrysAlis PRO* (Agilent, 2011); cell refinement: *CrysAlis PRO* (Agilent, 2011); data reduction: *CrysAlis PRO* (Agilent, 2011); program(s) used to solve structure: *SUPERFLIP* (Palatinus & Chapuis, 2007); program(s) used to refine structure: *CRYSTALS* (Betteridge *et al.*, 2003; Cooper *et al.*, 2010); molecular graphics: *CAMERON* (Watkin *et al.*, 1996) and *Mercury* (Macrae *et al.*, 2006); software used to prepare material for publication: *publCIF* (Westrip, 2010).

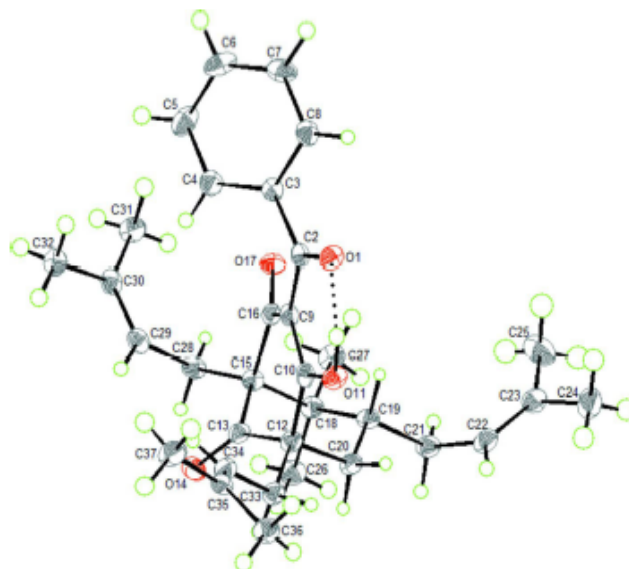
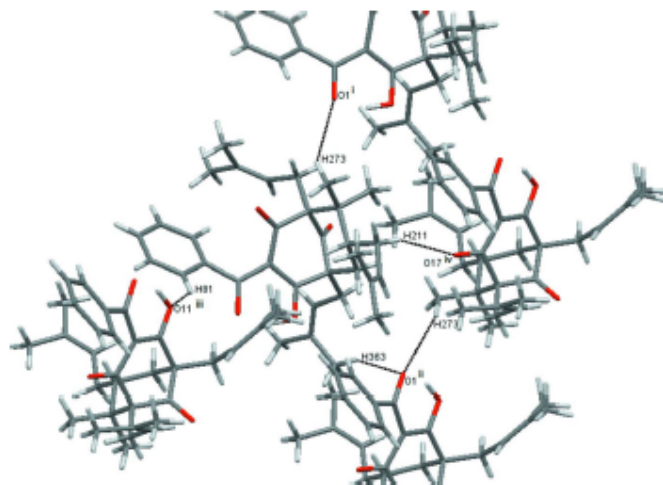


Figure 1

The title compound with displacement ellipsoids drawn at the 50% probability level. H atoms are shown as spheres of arbitrary radius. View of the molecule showing intramolecular hydrogen bond.

**Figure 2**

Partial packing diagram showing the C—H...O intermolecular interactions. Symmetry codes: (i) $x - 1, y, z$; (ii) $-x + 2, y + 1/2, -z + 3/2$; (iii) $-x + 2, y - 1/2, -z + 3/2$; (iv) $-x + 1, y + 1/2, -z + 3/2$.

(1*S*,5*S*,7*R*)-3-Benzoyl-4-hydroxy-8,8-dimethyl-1,5,7-tris(3-methylbut-2-enyl)bicyclo[3.3.1]nona-3-ene-2,9-dione

Crystal data

$C_{20}H_{28}O_4$

$M_r = 502.69$

Orthorhombic, $P2_12_12_1$

Hall symbol: $P\ 2ac\ 2ab$

$a = 9.2035\ (2)\ \text{\AA}$

$b = 13.4629\ (2)\ \text{\AA}$

$c = 22.9607\ (5)\ \text{\AA}$

$V = 2844.96\ (10)\ \text{\AA}^3$

$Z = 4$

$F(000) = 1088$

$D_x = 1.174\ \text{Mg m}^{-3}$

Melting point: 365 K

Cu $K\alpha$ radiation, $\lambda = 1.54180\ \text{\AA}$

Cell parameters from 19011 reflections

$\theta = 3\text{--}71^\circ$

$\mu = 0.59\ \text{mm}^{-1}$

$T = 100\ \text{K}$

Prismatic, colourless

$0.21 \times 0.14 \times 0.08\ \text{mm}$

Data collection

Oxford Diffraction Gemini
diffractometer

Radiation source: Cu $K\alpha$

Graphite monochromator

ω scans

Absorption correction: multi-scan

(*CrysAlis PRO*; Oxford Diffraction, 2002)

$T_{\text{min}} = 0.86, T_{\text{max}} = 0.95$

39826 measured reflections

5498 independent reflections

5269 reflections with $I > 2.0\sigma(I)$

$R_{\text{int}} = 0.034$

$\theta_{\text{max}} = 71.6^\circ, \theta_{\text{min}} = 3.8^\circ$

$h = -11 \rightarrow 11$

$k = -16 \rightarrow 16$

$l = -28 \rightarrow 28$

Refinement

Refinement on F^2

Least-squares matrix: full

$R[F^2 > 2\sigma(F^2)] = 0.034$

$wR(F^2) = 0.084$

supplementary materials

$S = 0.96$
 5498 reflections
 335 parameters
 0 restraints
 Primary atom site location: other
 Hydrogen site location: difference Fourier map
 H-atom parameters constrained
 Method = Modified Sheldrick $w = 1/[\sigma^2(F^2) + (0.04P)^2 + 1.02P]$,
 where $P = (\max(F_o^2, 0) + 2F_c^2)/3$
 $(\Delta\sigma)_{\max} = 0.001$
 $\Delta\rho_{\max} = 0.24 \text{ e } \text{\AA}^{-3}$
 $\Delta\rho_{\min} = -0.18 \text{ e } \text{\AA}^{-3}$
 Absolute structure: Flack (1983), 2383 Friedel
 pairs
 Absolute structure parameter: $-0.04 (15)$

Special details

Experimental. The crystal was placed in the cold stream of an Oxford Cryosystems open-flow nitrogen cryostat with a nominal stability of 0.1 K.

Fractional atomic coordinates and isotropic or equivalent isotropic displacement parameters (\AA^2)

	x	y	z	$U_{\text{eq}}^*/U_{\text{eq}}$
O1	1.01156 (11)	0.23087 (8)	0.70014 (5)	0.0254
H1	0.9976	0.3386	0.7123	0.0500*
C2	0.89022 (15)	0.21427 (11)	0.67631 (6)	0.0196
C3	0.87580 (15)	0.11723 (10)	0.64619 (6)	0.0196
C4	0.81066 (17)	0.10926 (12)	0.59161 (7)	0.0252
C5	0.81469 (18)	0.01993 (13)	0.56225 (7)	0.0333
C6	0.87951 (19)	-0.06283 (13)	0.58714 (8)	0.0364
C7	0.94348 (19)	-0.05514 (12)	0.64160 (8)	0.0338
C8	0.94353 (17)	0.03472 (11)	0.67054 (7)	0.0260
C9	0.78010 (15)	0.29113 (10)	0.67650 (6)	0.0189
C10	0.82224 (15)	0.38637 (11)	0.69421 (6)	0.0200
O11	0.95023 (11)	0.40387 (7)	0.71561 (4)	0.0244
C12	0.72277 (16)	0.47533 (10)	0.69123 (6)	0.0207
C13	0.60033 (16)	0.45383 (10)	0.64825 (6)	0.0204
O14	0.56632 (12)	0.51181 (7)	0.61064 (5)	0.0285
C15	0.51798 (15)	0.35827 (10)	0.66056 (6)	0.0198
C16	0.62421 (15)	0.26982 (10)	0.66719 (6)	0.0187
O17	0.57659 (11)	0.18581 (7)	0.66667 (5)	0.0232
C18	0.43562 (16)	0.37607 (10)	0.72158 (6)	0.0215
C19	0.55121 (16)	0.40042 (10)	0.76906 (6)	0.0211
C20	0.64960 (16)	0.48756 (11)	0.75201 (6)	0.0220
C21	0.48510 (17)	0.42104 (11)	0.83005 (7)	0.0255
C22	0.59687 (18)	0.41885 (11)	0.87765 (7)	0.0268
C23	0.61287 (19)	0.35035 (12)	0.91878 (7)	0.0297
C24	0.7280 (2)	0.36145 (15)	0.96492 (8)	0.0415
C25	0.5211 (2)	0.25871 (14)	0.92400 (9)	0.0454
C26	0.32752 (17)	0.46277 (12)	0.71414 (7)	0.0286
C27	0.35104 (16)	0.28311 (12)	0.73993 (7)	0.0275
C28	0.41309 (16)	0.33433 (10)	0.60982 (6)	0.0227
C29	0.48887 (16)	0.31514 (11)	0.55260 (7)	0.0234
C30	0.48971 (16)	0.23037 (11)	0.52250 (6)	0.0235
C31	0.41774 (19)	0.13577 (11)	0.54147 (7)	0.0297
C32	0.56841 (18)	0.22262 (12)	0.46514 (7)	0.0286
C33	0.80586 (17)	0.57064 (11)	0.67524 (6)	0.0238

supplementary materials

C34	0.90501 (18)	0.55841 (11)	0.62358 (6)	0.0269
C35	1.03353 (17)	0.60074 (10)	0.61558 (6)	0.0242
C36	1.10148 (18)	0.67277 (11)	0.65730 (7)	0.0283
C37	1.1235 (2)	0.57708 (12)	0.56262 (7)	0.0336
H41	0.7629	0.1648	0.5747	0.0322*
H51	0.7720	0.0154	0.5245	0.0408*
H61	0.8767	-0.1239	0.5662	0.0448*
H71	0.9882	-0.1120	0.6603	0.0423*
H81	0.9888	0.0410	0.7073	0.0323*
H191	0.6141	0.3413	0.7739	0.0240*
H201	0.7285	0.4939	0.7814	0.0255*
H202	0.5948	0.5492	0.7515	0.0250*
H211	0.4404	0.4855	0.8298	0.0302*
H212	0.4098	0.3724	0.8376	0.0308*
H221	0.6650	0.4724	0.8783	0.0333*
H241	0.7808	0.4252	0.9604	0.0629*
H242	0.6826	0.3587	1.0029	0.0630*
H243	0.7968	0.3064	0.9624	0.0633*
H251	0.4774	0.2571	0.9626	0.0712*
H252	0.4405	0.2558	0.8975	0.0712*
H253	0.5783	0.1996	0.9203	0.0711*
H261	0.2489	0.4460	0.6869	0.0435*
H262	0.3726	0.5228	0.7009	0.0443*
H263	0.2793	0.4760	0.7516	0.0424*
H271	0.2827	0.2989	0.7720	0.0415*
H272	0.4133	0.2300	0.7529	0.0415*
H273	0.2935	0.2588	0.7065	0.0413*
H281	0.3488	0.3913	0.6046	0.0275*
H282	0.3528	0.2790	0.6214	0.0274*
H291	0.5415	0.3699	0.5369	0.0295*
H311	0.3450	0.1161	0.5121	0.0463*
H312	0.3641	0.1421	0.5785	0.0443*
H313	0.4882	0.0812	0.5462	0.0471*
H321	0.5028	0.1978	0.4355	0.0443*
H322	0.6530	0.1781	0.4687	0.0436*
H323	0.6061	0.2878	0.4517	0.0438*
H331	0.8619	0.5902	0.7093	0.0268*
H332	0.7355	0.6225	0.6683	0.0297*
H341	0.8682	0.5150	0.5937	0.0329*
H361	1.1371	0.7325	0.6379	0.0438*
H362	1.1884	0.6436	0.6753	0.0454*
H363	1.0391	0.6926	0.6877	0.0428*
H371	1.1424	0.6355	0.5392	0.0501*
H372	1.0793	0.5284	0.5373	0.0518*
H373	1.2186	0.5520	0.5739	0.0518*

Atomic displacement parameters (\AA^2)

	U^{11}	U^{22}	U^{33}	U^{12}	U^{13}	U^{23}
O1	0.0188 (5)	0.0295 (5)	0.0279 (5)	0.0028 (4)	-0.0055 (4)	-0.0029 (4)

supplementary materials

C2	0.0186 (7)	0.0247 (7)	0.0157 (6)	-0.0013 (6)	0.0009 (5)	0.0033 (5)
C3	0.0143 (6)	0.0228 (7)	0.0216 (7)	0.0013 (6)	0.0031 (5)	0.0010 (5)
C4	0.0223 (7)	0.0281 (8)	0.0250 (7)	0.0033 (6)	-0.0014 (6)	-0.0008 (6)
C5	0.0277 (8)	0.0415 (9)	0.0307 (8)	0.0014 (7)	-0.0041 (7)	-0.0124 (7)
C6	0.0330 (9)	0.0281 (8)	0.0480 (10)	0.0050 (7)	0.0038 (8)	-0.0156 (7)
C7	0.0331 (9)	0.0251 (7)	0.0432 (9)	0.0107 (7)	0.0017 (7)	0.0014 (7)
C8	0.0231 (7)	0.0299 (8)	0.0251 (7)	0.0045 (6)	-0.0002 (6)	0.0012 (6)
C9	0.0199 (7)	0.0209 (7)	0.0160 (6)	0.0006 (5)	0.0006 (5)	0.0015 (5)
C10	0.0192 (6)	0.0250 (7)	0.0157 (6)	-0.0026 (6)	0.0016 (5)	0.0013 (5)
O11	0.0215 (5)	0.0246 (5)	0.0270 (5)	-0.0021 (4)	-0.0028 (4)	-0.0040 (4)
C12	0.0222 (7)	0.0186 (7)	0.0215 (7)	-0.0026 (5)	0.0020 (6)	-0.0015 (5)
C13	0.0213 (7)	0.0186 (6)	0.0214 (7)	0.0034 (6)	0.0024 (6)	-0.0028 (5)
O14	0.0349 (6)	0.0215 (5)	0.0291 (6)	0.0015 (4)	-0.0056 (5)	0.0039 (4)
C15	0.0170 (6)	0.0196 (6)	0.0227 (7)	0.0005 (5)	-0.0002 (5)	-0.0006 (5)
C16	0.0194 (6)	0.0199 (6)	0.0169 (6)	0.0011 (5)	0.0005 (5)	-0.0007 (5)
O17	0.0195 (5)	0.0185 (5)	0.0318 (6)	-0.0007 (4)	0.0004 (4)	-0.0005 (4)
C18	0.0181 (7)	0.0214 (7)	0.0248 (7)	0.0010 (6)	0.0026 (6)	-0.0010 (5)
C19	0.0213 (7)	0.0179 (6)	0.0242 (7)	0.0021 (5)	0.0028 (6)	-0.0005 (5)
C20	0.0236 (7)	0.0200 (7)	0.0223 (7)	0.0000 (6)	0.0018 (6)	-0.0023 (5)
C21	0.0270 (7)	0.0222 (7)	0.0272 (7)	0.0026 (6)	0.0057 (6)	-0.0009 (6)
C22	0.0305 (8)	0.0241 (7)	0.0259 (7)	-0.0004 (6)	0.0081 (6)	-0.0059 (6)
C23	0.0340 (8)	0.0285 (8)	0.0267 (8)	0.0077 (7)	0.0078 (7)	-0.0029 (6)
C24	0.0491 (11)	0.0477 (10)	0.0278 (9)	0.0143 (9)	0.0009 (8)	-0.0037 (8)
C25	0.0507 (12)	0.0352 (10)	0.0503 (11)	0.0003 (9)	0.0050 (10)	0.0126 (8)
C26	0.0232 (7)	0.0291 (8)	0.0335 (8)	0.0066 (6)	0.0013 (7)	-0.0016 (7)
C27	0.0225 (8)	0.0293 (8)	0.0306 (8)	-0.0031 (6)	0.0043 (6)	-0.0013 (7)
C28	0.0178 (7)	0.0214 (6)	0.0290 (8)	0.0030 (5)	-0.0052 (6)	-0.0002 (6)
C29	0.0196 (7)	0.0252 (7)	0.0254 (7)	-0.0011 (6)	-0.0056 (6)	0.0039 (6)
C30	0.0187 (7)	0.0283 (7)	0.0235 (7)	0.0022 (6)	-0.0060 (6)	0.0012 (6)
C31	0.0312 (8)	0.0258 (7)	0.0322 (8)	0.0000 (7)	0.0025 (7)	-0.0028 (6)
C32	0.0283 (8)	0.0328 (8)	0.0247 (7)	-0.0003 (7)	-0.0015 (6)	0.0001 (6)
C33	0.0282 (8)	0.0199 (7)	0.0232 (7)	-0.0041 (6)	0.0019 (6)	-0.0015 (6)
C34	0.0381 (9)	0.0209 (6)	0.0217 (7)	-0.0045 (6)	0.0022 (7)	-0.0021 (6)
C35	0.0327 (8)	0.0173 (6)	0.0227 (7)	0.0020 (6)	0.0033 (6)	0.0028 (5)
C36	0.0280 (8)	0.0250 (7)	0.0317 (8)	-0.0024 (6)	0.0034 (6)	-0.0012 (6)
C37	0.0409 (9)	0.0267 (8)	0.0332 (9)	-0.0057 (7)	0.0124 (8)	-0.0030 (6)

Geometric parameters (Å, °)

O1—C2	1.2635 (17)	C23—C24	1.506 (3)
H1—O11	0.984	C23—C25	1.500 (3)
C2—C3	1.4842 (19)	C24—H241	0.992
C2—C9	1.448 (2)	C24—H242	0.968
C3—C4	1.393 (2)	C24—H243	0.977
C3—C8	1.391 (2)	C25—H251	0.974
C4—C5	1.379 (2)	C25—H252	0.960
C4—H41	0.950	C25—H253	0.958
C5—C6	1.387 (3)	C26—H261	0.983
C5—H51	0.953	C26—H262	0.958
C6—C7	1.386 (3)	C26—H263	0.984

supplementary materials

C6—H61	0.953	C27—H271	0.992
C7—C8	1.380 (2)	C27—H272	0.964
C7—H71	0.969	C27—H273	0.988
C8—H81	0.945	C28—C29	1.510 (2)
C9—C10	1.400 (2)	C28—H281	0.975
C9—C16	1.479 (2)	C28—H282	0.967
C10—O11	1.2979 (17)	C29—C30	1.334 (2)
C10—C12	1.509 (2)	C29—H291	0.953
C12—C13	1.526 (2)	C30—C31	1.500 (2)
C12—C20	1.5582 (19)	C30—C32	1.507 (2)
C12—C33	1.5381 (19)	C31—H311	0.987
C13—O14	1.2054 (18)	C31—H312	0.987
C13—C15	1.5198 (19)	C31—H313	0.986
C15—C16	1.5482 (19)	C32—H321	0.969
C15—C18	1.6110 (19)	C32—H322	0.986
C15—C28	1.5469 (19)	C32—H323	0.993
C16—O17	1.2131 (17)	C33—C34	1.506 (2)
C18—C19	1.558 (2)	C33—H331	0.973
C18—C26	1.543 (2)	C33—H332	0.966
C18—C27	1.533 (2)	C34—C35	1.326 (2)
C19—C20	1.5328 (19)	C34—H341	0.964
C19—C21	1.552 (2)	C35—C36	1.500 (2)
C19—H191	0.990	C35—C37	1.505 (2)
C20—H201	0.994	C36—H361	0.977
C20—H202	0.971	C36—H362	0.982
C21—C22	1.501 (2)	C36—H363	0.943
C21—H211	0.961	C37—H371	0.969
C21—H212	0.969	C37—H372	0.966
C22—C23	1.328 (2)	C37—H373	0.973
C22—H221	0.955		
O1—C2—C3	115.88 (13)	C22—C23—C25	124.43 (16)
O1—C2—C9	119.39 (13)	C24—C23—C25	114.94 (15)
C3—C2—C9	124.59 (12)	C23—C24—H241	110.9
C2—C3—C4	121.69 (13)	C23—C24—H242	109.1
C2—C3—C8	118.39 (13)	H241—C24—H242	109.8
C4—C3—C8	119.53 (14)	C23—C24—H243	109.8
C3—C4—C5	119.68 (15)	H241—C24—H243	109.4
C3—C4—H41	120.4	H242—C24—H243	107.7
C5—C4—H41	119.9	C23—C25—H251	108.9
C4—C5—C6	120.70 (15)	C23—C25—H252	114.7
C4—C5—H51	119.3	H251—C25—H252	104.9
C6—C5—H51	120.0	C23—C25—H253	111.5
C5—C6—C7	119.63 (15)	H251—C25—H253	106.8
C5—C6—H61	118.2	H252—C25—H253	109.5
C7—C6—H61	122.1	C18—C26—H261	111.8
C6—C7—C8	120.00 (15)	C18—C26—H262	113.2
C6—C7—H71	121.4	H261—C26—H262	108.1
C8—C7—H71	118.6	C18—C26—H263	109.3

supplementary materials

C3—C8—C7	120.41 (14)	H261—C26—H263	105.5
C3—C8—H81	119.0	H262—C26—H263	108.7
C7—C8—H81	120.6	C18—C27—H271	110.6
C2—C9—C10	117.48 (13)	C18—C27—H272	112.9
C2—C9—C16	122.67 (13)	H271—C27—H272	107.8
C10—C9—C16	119.24 (13)	C18—C27—H273	109.2
C9—C10—O11	121.85 (13)	H271—C27—H273	108.0
C9—C10—C12	123.08 (13)	H272—C27—H273	108.3
O11—C10—C12	115.06 (12)	C15—C28—C29	113.75 (11)
H1—O11—C10	102.2	C15—C28—H281	107.9
C10—C12—C13	109.07 (11)	C29—C28—H281	107.9
C10—C12—C20	107.79 (11)	C15—C28—H282	108.1
C13—C12—C20	106.27 (11)	C29—C28—H282	111.9
C10—C12—C33	111.80 (12)	H281—C28—H282	107.0
C13—C12—C33	111.78 (12)	C28—C29—C30	126.86 (14)
C20—C12—C33	109.91 (11)	C28—C29—H291	115.6
C12—C13—O14	122.17 (13)	C30—C29—H291	117.5
C12—C13—C15	114.12 (11)	C29—C30—C31	124.98 (14)
O14—C13—C15	123.50 (13)	C29—C30—C32	120.98 (14)
C13—C15—C16	110.76 (11)	C31—C30—C32	114.03 (13)
C13—C15—C18	105.69 (11)	C30—C31—H311	109.2
C16—C15—C18	109.03 (11)	C30—C31—H312	113.4
C13—C15—C28	110.33 (11)	H311—C31—H312	105.8
C16—C15—C28	107.93 (11)	C30—C31—H313	112.0
C18—C15—C28	113.10 (11)	H311—C31—H313	108.7
C15—C16—C9	118.54 (12)	H312—C31—H313	107.4
C15—C16—O17	119.21 (13)	C30—C32—H321	109.7
C9—C16—O17	122.20 (13)	C30—C32—H322	110.4
C15—C18—C19	108.57 (11)	H321—C32—H322	110.0
C15—C18—C26	108.64 (12)	C30—C32—H323	112.3
C19—C18—C26	111.01 (12)	H321—C32—H323	107.7
C15—C18—C27	110.89 (12)	H322—C32—H323	106.7
C19—C18—C27	109.04 (12)	C12—C33—C34	113.47 (12)
C26—C18—C27	108.70 (12)	C12—C33—H331	107.3
C18—C19—C20	112.70 (11)	C34—C33—H331	110.0
C18—C19—C21	113.66 (12)	C12—C33—H332	108.0
C20—C19—C21	108.97 (11)	C34—C33—H332	110.8
C18—C19—H191	108.0	H331—C33—H332	107.0
C20—C19—H191	107.4	C33—C34—C35	127.09 (14)
C21—C19—H191	105.7	C33—C34—H341	114.5
C19—C20—C12	113.78 (11)	C35—C34—H341	118.4
C19—C20—H201	108.9	C34—C35—C36	124.15 (14)
C12—C20—H201	107.5	C34—C35—C37	120.78 (14)
C19—C20—H202	110.5	C36—C35—C37	115.06 (14)
C12—C20—H202	107.7	C35—C36—H361	112.4
H201—C20—H202	108.2	C35—C36—H362	110.5
C19—C21—C22	112.63 (12)	H361—C36—H362	104.3
C19—C21—H211	108.9	C35—C36—H363	113.8
C22—C21—H211	108.4	H361—C36—H363	108.0

supplementary materials

C19—C21—H212	108.7	H362—C36—H363	107.3
C22—C21—H212	110.3	C35—C37—H371	112.1
H211—C21—H212	107.8	C35—C37—H372	113.5
C21—C22—C23	127.39 (15)	H371—C37—H372	106.9
C21—C22—H221	116.5	C35—C37—H373	110.7
C23—C22—H221	116.1	H371—C37—H373	105.5
C22—C23—C24	120.62 (16)	H372—C37—H373	107.6

Hydrogen-bond geometry (Å, °)

<i>D</i> —H··· <i>A</i>	<i>D</i> —H	H··· <i>A</i>	<i>D</i> ··· <i>A</i>	<i>D</i> —H··· <i>A</i>
O11—H1···O1	0.98	1.48	2.4227 (14)	158
C27—H273···O1 ⁱ	0.99	2.63	3.330 (2)	128
C36—H363···O1 ⁱⁱ	0.94	2.67	3.523 (2)	151
C8—H81···O11 ⁱⁱⁱ	0.95	2.62	3.300 (2)	129
C21—H211···O17 ^{iv}	0.96	2.70	3.610 (2)	158

Symmetry codes: (i) $x-1, y, z$; (ii) $-x+2, y+1/2, -z+3/2$; (iii) $-x+2, y-1/2, -z+3/2$; (iv) $-x+1, y+1/2, -z+3/2$.



Structural Derivatization of Clusianone and *In Vitro* Cytotoxicity Evaluation Targeting Respiratory Carcinoma Cells

Sree Vaneesa Nagalingam, Kok Wai-Ling, Khoo Teng-Jin
Centre for Natural and Medicinal Product Research, School of Pharmacy, Faculty of Science, University of Nottingham Malaysia Campus, Semenyih, Selangor, Malaysia

Abstract

Clusianone (1) was isolated from *Garcinia parvifolia* and structurally modified using semisynthetic methods to obtain compounds 2–4. The structural derivatization included methylation (2), hydrogenation (3), and the addition of a methylamine group [(4) to (1)]. Cytotoxic effects of these compounds were assessed on MRC5 fibroblasts, A549 lung adenocarcinoma, HK1 squamous nasopharynx carcinoma, and NP69 normal nasopharyngeal epithelial cell lines. Clusianone (1) showed cytotoxic activity against A549 cells with an IC_{50} value of 3.06 μ M. Compound (4) showed cytotoxic activities against both A549 and HK1 cells with IC_{50} values of 4.09 μ M and 3.43 μ M, respectively. The results of the cytotoxicity assay provide a correlation on the structure activity relationship of clusianone against HK1 and A549 cells, which can be further investigated as a potential antiproliferative compound.

Key words

Garcinia parvifolia • Clusiaceae • clusianone analogues • semisynthetic methods • cytotoxic activity

Supporting information available online at
<http://www.thieme-connect.de/products>

Natural clusianone belongs to compounds classified as type B polyprenylated polycyclic acylphloroglucines (PPAPs) that are found in plants of the Clusiaceae (Guttiferae) family [1,2]. To date, natural clusianone has been found in various parts of the targeted Clusiaceae plants, including fruits [3], flowers [4,5], leaves [6], roots [7], stems, and bark [8,9]. Naturally occurring 1 has shown potential anticancer activity [9] and further investigations of clusianone-treated HepG2 hepatocarcinoma cells revealed cytotoxic effects by mitochondrial impairment [10]. In the last decade, clusianone (1) has gained substantial interest from the synthetic community leading to a breakthrough in total synthesis of this compound [11–14]. Synthetic clusianone was tested for cytotoxicity in several cancer cell lines: HeLa (cervix carcinoma), MIA-PaCa-2 (pancreatic carcinoma), and MCF7 (breast adenocarcinoma). The IC_{50} values ranged from 3.0 μ M to 8.3 μ M for the three cancer cell lines [15,16].

In our studies, we extracted clusianone using a previously published method [6]. The isolation and abundance of clusianone from the leaves of *Garcinia parvifolia* (Miq.) Miq. has made chemical modifications readily attainable as compared to clusianone isolated from the dried stem bark of *Garcinia assigu* [9] and the roots of *Hypericum hypericoides* (L.) Crantz [7]. X-ray crystallography was identical in previous reports, and a detailed comparison of our and previously reported NMR data [8] was established.

This method provided a quantity of over 0.5 g (0.05% yield) of 1 to be used as starting material for synthesizing sufficient quantities of clusianone derivatives (2–4). All products were purified via column chromatography. The products 1–4 exhibited the predicted fragmentation and mass m/z when analyzed by ESI-MS (○ Fig. 1). In addition, further characterizations of 1–4 were conducted utilizing 1H NMR and ^{13}C NMR spectroscopy to characterize both tautomers (a/b) present. Data on clusianone and analogues are available as Supporting Information. Furthermore, clusianone derivatives (2–4) were produced in less than two reactions steps, with yields over 75% (○ Fig. 2).

A bioassay involving the (MTT) tetrazolium dye reduction assay revealed that the cytotoxic effects of all four compounds (1–4) against normal (MRC5 & NP69) and carcinoma (A549 & HK1) respiratory cells lines were profound. The IC_{50} values after 48 h were averaged from three sets of experiments (○ Table 1). The IC_{50} values were determined from the resulting dose response plot by using the interpolation methods in GraphPad Prism 6. Cytotoxicity screening tests were also performed against normal cell lines to validate the compound inhibitory activity in cancer cells without significantly affecting the viability of normal cells. Based on these results, several findings can be summarized: The methoxylation of OH has decreased the cytotoxic effects of 2 on both cancer and normal cells by 30-fold. Compound 2 is also less toxic to normal cells in terms of concentration, which is lethal to 50% of the cells. Upon hydrogenation, the tetraprenylated group of 2 leads to a more lipophilic domain of this compound, which has indeed decreased the cytotoxic effect of 3 by 20-fold. The cytotoxicity result of compound 4 is rather significant since the IC_{50} value is in the range of 3.0 to 5.0 μ M. Interestingly, compound 4 suppressed the growth rate of MRC5 and NP69 at concentrations above 10.0 μ M. Compound 4 showed significant cytotoxic activities against both A549 and HK1 cells with IC_{50} values of 4.09 μ M and 3.43 μ M, respectively. Apart from this, clusianone (1) showed a significant IC_{50} value of 3.06 μ M against A549 cells and thus affects less MRC5 cells. Cytotoxicity results prevail that a hydroxyl group on clusianone is crucial in preventing the cell division progression to occur. Similarly, compound 4 possessing both hydroxyl and amine is postulated to exert a greater interaction with carcinoma cells since 4 suppressed carcinoma cell growth better than 1. This indicates that compounds 1 and 4 both exhibit antiproliferative characteristics. The antimicrotubule drug docetaxol was used as a control since type B PPAP compounds have been demonstrated to exhibit an inhibitory activity of the tubulin assembly of carcinoma cells [17]. In conclusion, 1 and 4 have potential for development as anticancer candidates, and future works to study their modes of action as antimicrotubule agents should be emphasized.

Material and Methods

Isolation and optimization of clusianone

Leaves of *G. parvifolia* (University of Nottingham Malaysia Campus 45) were collected from trees in a reserved forest in Sungai Congkak, Selangor. The plant authenticity was verified and a voucher specimen (herbarium number PID 271210–13) was deposited at the School of Pharmacy of the University of Nottingham Malaysia Campus and Forest Research Institute Malaysia (FRIM). Dried and powdered *G. parvifolia* leaves (1000 g) were extracted by maceration. A total of 80 g of hexane extract was obtained from the 1000 g of powdered leaves macerated. Successive

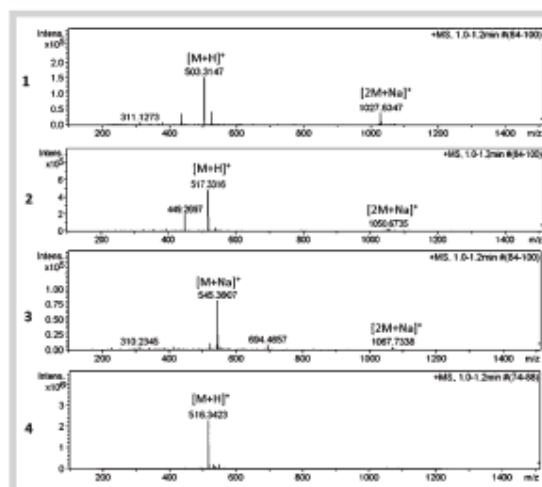


Fig. 1 ESI-MS analysis of clusianone and its derivatives (1–4) demonstrating the parent mass of the compounds and dimer formations with adducts H^+ and Na^+ .

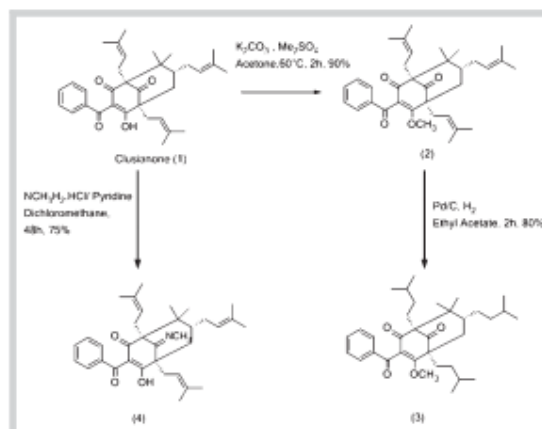


Fig. 2 Semisynthesis of clusianone (1).

column chromatography, including chlorophyll removal steps, was carried out as previously reported in a larger scale to obtain clusianone (1) [6].

Preparation of clusianone derivatives

Three clusianone (1) derivatives [methylated (2), hydrogenated (3), and amine added (4)] were synthesized on a 10 to 100 mg scale and purified using column chromatography. All derivatives were synthesized from clusianone except for 3, which was syn-

thesized from 2 intermediately. Detailed synthesis steps and ESI-MS, 1H NMR, and ^{13}C NMR characterizations of the four compounds are available as Supporting Information.

Compounds

Clusianone ($C_{33}H_{42}O_4$): Yellow crystals; m.p. 90–92°C; ESI-MS m/z , $[M + H]^+$: 503.3147 calcd. for 503.3167 (rel. int. %) = 503 (100), 435 (23), 379 (4.5), 343 (1.9), 311 (4.6), 235 (1.7). For 1H NMR and ^{13}C NMR of 1 (a/b), see Tables S1 and S2, Supporting Information.

Compound	MRC5	A549	NP69	HK1
Clusianone (1)	4.16 ± 0.85	3.06 ± 1.00	3.66 ± 0.94	5.35 ± 0.91
2	120.38 ± 2.98	86.70 ± 1.60	101.02 ± 2.92	62.70 ± 2.52
3	47.15 ± 2.05	57.70 ± 1.93	68.80 ± 2.01	65.55 ± 1.74
4	10.20 ± 0.82	4.09 ± 0.61	10.02 ± 0.52	3.43 ± 0.57
Docetaxel ^a	0.006	0.006	0.006	0.006

^aDocetaxel control; MRC5 (lung fibroblast) [19], A549 (lung adenocarcinoma) [20], NP69 (immortalized nasopharyngeal epithelial cell) [21], HK1 (squamous carcinoma of the nasopharynx) [22].

Table 1 Cytotoxicity IC₅₀ ± SD (μM) of clusianone and its derivatives against MRC5, A549, HK1, and NP69 cells.

Compound 2 (C₃₄H₄₄O₄): White crystals; m.p. 108–110 °C; ESI-MS *m/z*, [M + H]⁺: 517.3316 calcd. for 517.3318 (rel. int. %) = 517 (100), 449 (40.6), 393 (5.3), 357 (4.2), 325 (4.0). For ¹H NMR and ¹³C NMR of 2 (a/b), see Tables S3 and S4, Supporting Information.

Compound 3 (C₃₄H₄₄O₄): Brown wax; ESI-MS *m/z*, [M + Na]⁺: 545.3607 calcd. for 545.3607 (rel. int. %) = 545 (100), 523 (13.4), 429 (2.8), 413 (5.5), 385 (3.4), 341 (3.3), 310 (6.0), 226 (4.0). For ¹H NMR and ¹³C NMR of 3 (a/b), see Tables S5 and S6, Supporting Information.

Compound 4 (C₃₄H₄₄NO₂): Colorless wax; ESI-MS *m/z*, [M + H]⁺: 516.3423 calcd. for 516.3423 (rel. int. %) = 517 (100), 498 (1.7), 490 (2.0), 448 (1.1). For ¹H NMR and ¹³C NMR of 4 (a/b), see Table S7, Supporting Information.

Cytotoxicity assay

All stock cultures, except for the NP69 cultures, were grown in T25 flasks with Rosewell Park Memorial Institute medium (RPMI) containing 10% fetal bovine serum (FBS). NP69 cultures were grown in keratinocyte-SFM together with a supplement of bovine pituitary extract (BPE) and human recombinant (EGF). Freshly trypsinized cells were seeded into 96-well plates at densities of 10,000 cells in 100 μL medium per well. After one day of culture, each of the wells was subjected to different concentrations of the compounds, from 0–200 μg/mL. The compounds were dissolved in dimethyl sulfoxide (DMSO) and diluted further with RPMI medium for all cultures, except for NP69, which was diluted with keratinocyte-SFM that serves as a stock solution. The DMSO concentration used was not higher than 0.1%. Different concentrations of the compounds (1–4) were prepared through a serial dilution of the stock solution. The plates were then incubated for 48 h to test their cytotoxicity levels. Docetaxol (Fresenius Kabi Oncology Ltd.), with a purity of 99%, was used as a positive control. The docetaxol was dissolved in sodium chloride buffer. After 48 h of treatment, the MTT [3-(4,5-dimethylthiazol-2-yl)-2,5-diphenyltetrazolium bromide] assay was performed [18]. Absorbance readings were set at 540 nm using a microplate reader. The absorbance was further analyzed as described in the Supporting Information.

Supporting information

A detailed description of the semisynthesis process, spectral data of clusianone and its analogues, and absorbance data are available as Supporting Information.

Acknowledgements

We would like to thank Dr. Alan Khoo Soo-Beng from the Institute of Medical Research and Prof. Tsao George Sai-Wah from the University of Hong Kong for providing the NP69 and HK1 cells. The authors would like to thank the Ministry of Higher Education (MOHE) for providing a grant for the study.

Conflict of Interest

All authors declare no conflicts of interest.

References

- Ciochini R, Grossman RR. Polycyclic polyphenylated acylphloroglucinols. *Chem Rev* 2006; 106: 3963–3986.
- Biber N, Mišić K, Plettker B. The total synthesis of hyperpappanone, hyperbione L, epi-clusianone and oblongibillin A. *Nat Chem* 2011; 3: 938–942.
- Piccinelli AL, Cuesta-Rubio O, Chica MR, Mahmood N, Pagano B, Puvone M, Barone V, Rastrelli L. Structural revision of clusianone and 7-epi-clusianone and anti-HIV activity of polyisoprenylated benzophenones. *Tetrahedron* 2005; 61: 8206–8211.
- Porto AL, Machado SM, de Oliveira CM, Bittrich V, Amaral MC, Marsilioli AJ. Polyisoprenylated benzophenones from *Clusia floral* resins. *Phytochemistry* 2000; 55: 755–768.
- Da Silva MCA, Heringer AP, Figueiredo MR, de Paula SR. Separation of clusianone from *Clusia fluminensis* Planch. and Triana (Clusiaceae) by high speed counter current chromatography (HSCCC). *J Liq Chromatogr Relat Technol* 2012; 35: 2313–2321.
- Nagalingam SV, Ching WP, Break MK, Tahir MM, Khoo TJ. A P₂(2)₂ polymorph of (+)-clusianone. *Acta Crystallogr Sect E Struct Rep Online* 2013; 69: 1799–1800.
- Christian OE, McLean S, Reynolds WF, Jacobs H. Prenylated benzophenones from *Hypericum hypericoides*. *Nat Prod Commun* 2008; 3: 1781–1786.
- McCandlish LE, Hanson JC, Stout GH. The structures of two derivatives of bicyclo[3.3.1]nonane-2, 4, 9-trione. A natural product: clusianone, C₃₄H₄₄O₄, and trimethylated catechinic acid, C₃₄H₄₀O₆. *Acta Crystallogr B* 1976; 32: 1793–1801.
- Ito C, Inagawa M, Miyamoto Y, Onoda S, Rao KS, Mukainaka T, Tokuda H, Nishino H, Furukawa H. Polyphenylated benzophenones from *Garcinia assigu* and their potential cancer chemopreventive activities. *J Nat Prod* 2003; 66: 206–209.
- Reis FH, Purdo-Andreu GL, Nuñez-Figueroa Y, Cuesta-Rubio O, Murin-Pardo J, Uyemura SA, Curti C, Alberici LC. Clusianone, a naturally occurring nemorosone regioisomer, uncouples rat liver mitochondria and induces HepG2 cell death. *Chem Biol Interact* 2014; 212: 20–29.
- Rodeschini V, Ahmad NM, Simpkins NS. Synthesis of (+)-clusianone: high-yielding bridgehead and diketone substitutions by regioselective lithiation of enol ether derivatives of bicyclo[3.3.1]nonane-2, 4, 9-triones. *Org Lett* 2006; 8: 5283–5285.
- Qi J, Porco JA Jr. Rapid access to polyphenylated phloroglucinols via alkylative dearomatization-annulation: total synthesis of (+)-clusianone (1). *J Am Chem Soc* 2007; 129: 12682–12683.
- Nuhanić P, David M, Pouplin T, Delpech B, Maruizano C. Alpha, alpha'-annulation of 2, 6-prenyl-substituted cyclohexanone derivatives with malonyl chloride: application to a short synthesis of (+)-clusianone. Formation and rearrangement of a biogenetic-like intermediate. *Org Lett* 2007; 9: 14200–14201.
- Garnsey MR, Lim D, Yost JM, Coltart DM. Development of a strategy for the asymmetric synthesis of polycyclic polyphenylated acylphloroglucinols via N-amino cyclic carbamate hydrazones: application to the total synthesis of (+)-clusianone. *Org Lett* 2010; 12: 5234–5237.
- Simpkins NS, Holtrup F, Rodeschini V, Taylor JD, Wolf R. Comparison of the cytotoxic effects of enantiopure PPAPs, including nemorosone and clusianone. *Bioorg Med Chem Lett* 2012; 22: 6144–6147.
- Simpkins NS. Adventures in bridgehead substitution chemistry: synthesis of polycyclic polyphenylated acylphloroglucinols (PPAPs). *Chem Commun (Camb)* 2013; 49: 1042–1051.

- 17 Roux D, Hadi HA, Thoret S, Guénard D, Thoison O, Puls M, Sévener T. Structure-activity relationship of poly(isoprenyl) benzophenones from *Garcinia pyrifera* on the tubulin/microtubule system. *J Nat Prod* 2000; 63: 1070–1076
- 18 Mosmann T. Rapid colorimetric assay for cellular growth and survival: application to proliferation and cytotoxicity assays. *J Immunol Methods* 1983; 65: 55–63
- 19 Jacobs JP, Jones CM, Ruffe JP. Characteristic of human diploid cell designated MRC-5. *Nature* 1970; 227: 168–170
- 20 Giard DJ, Aaronson SA, Todaro GJ, Arnstein P, Kersey JH, Parks WP. In vitro cultivation of human tumors: establishment of cell lines derived from a series of solid tumors. *J Natl Cancer Inst* 1973; 51: 1417–1423
- 21 Tsao SW, Wong X, Liu Y, Cheung YC, Feng H, Zheng Z, Wong N, Yuen PW, Lo AK, Wong YC, Huang DP. Establishment of two immortalized nasopharyngeal epithelial cell lines using SV40 large T and HPV16E6/E7 viral oncogenes. *Biochim Biophys Acta* 2002; 1590: 150–158
- 22 Huang DP, Ho JH, Poon YF, Chew EC, Saw D, Lai M Li CL, Mok LS, Lai SH, Lau WH. Establishment of a cell (NPC/HK1) from a differentiated squamous carcinoma of the nasopharynx. *Int J Cancer* 1980; 26: 127–132

received July 29, 2015
revised November 19, 2015
accepted December 18, 2015

Bibliography
DOI <http://dx.doi.org/10.1055/s-0035-1568332>
Planta Med Lett
© Georg Thieme Verlag KG Stuttgart · New York ·
ISSN 2199-157X

Correspondence
Khoo Yong-jin
School of Pharmacy, Faculty of Science
Room 8A35 Block B
University of Nottingham Malaysia Campus
Jalan Broga
43500 Semenyih, Selangor Darul Ehsan
Malaysia
Phone: + 6(03) 89 24 82 13
Fax: + 6(03) 89 24 80 18
tengj.khoo@nottingham.edu.my



REFERENCES

- Acuña, U. M., Jancovski, N. and Kennelly, E. J. (2009). Polyisoprenylated benzophenones from *Clusiaceae*: potential drugs and lead compounds. *Curr. Top. Med. Chem.*, **9**: 1560–1580.
- Adam, P., Arigoni, D., Bacher, A. and Eisenreich, W. (2002). Biosynthesis of Hyperforin in *Hypericum perforatum*. *J. Med. Chem.*, **45**: 4786–4793.
- Ahmad, N. M., Rodeschini, V., Simpkins, N. S., Ward, S. E. and Blake, A. J. (2007). Synthesis of polyprenylated acylphloroglucinols using bridgehead lithiation: the total synthesis of racemic clusianone and a formal synthesis of racemic garsubellin A. *J. Org. Chem.*, **72**: 4803–4815.
- Aldridge, G. M., Podrebarac, D. M., Greenough, W. T. and Weiler, I. J. (2009). The use of total protein stains as loading controls: an alternative to high-abundance single protein controls in semi-quantitative immunoblotting. *J. Neurosci. Methods*, **172**: 250–254.
- Allan, L. A. and Clarke, P. R. (2007). Phosphorylation of caspase-9 by CDK1/cyclin B1 protects mitotic cells against apoptosis. *Mol. Cell.*, **26**: 301–310.
- Axerio-Cilies, P., Castañeda, I. P., Mirza, A. and Reynisson, J. (2009). Investigation of the incidence of “undesirable” molecular moieties for high-throughput screening compound libraries in marketed drug compounds. *Eur. J. Med. Chem.*, **44**: 1128–1134.
- Baloglu, E. and Kingston, D. G. (1999). A new semisynthesis of paclitaxel from baccatin III. *J. Nat. Prod.*, **62**: 1068–1071.
- Bareschino, M. A., Schettino, C. and Rossi, A. (2011). Treatment of advanced non-small cell lung cancer. *J. Thoracic. Dis.*, **3**: 122–133.
- Bauer, J. F. (2008). Polymorphism- A critical Consideration in Pharmaceutical Development, Manufacturing and Stability. *J. Valid. Tech.*, **14**: 15-23.
- Beerhues, L. (1996). Benzophenone synthase from cultured cells of *Centaureum erythraea*. *FEBS Lett.*, **383**: 264–266.
- Bergfors, T. (2003). Seeds to crystals. *J. Struct. Biol.*, **142**: 66–76.
- Berridge, M. V., Tan, A. N. S., McCoy, K.D. and Wang, R. U. I. (1996). The Biochemical and Cellular Basis of Cell Proliferation Assays That Use Tetrazolium Salts. *Biochemica.*, **4**: 14–19.
- Biber, N., Mows, K. and Plietker, B. (2011). The total synthesis of hyperpappuanone, hyperibone L, epi-clusianone and oblongifolin. *Nat. Chem.*, **3**: 938–942.
- Bissery, M. C., Guénard, D., Guéritte-Voegelein, F. and Lavelle, F. (1991). Experimental antitumor activity of taxotere (RP 56976, NSC 628503), a taxol analogue. *Cancer Res.*, **51**: 4845–4852.

- Bittrich, V., Amaral, C. E. and Marsaioli, A. J. (2000). Polyisoprenylated benzophenones from *Clusia floral* resins. *Phytochem.*, **55**: 755–768.
- Blatt, A. H. (1939). The addition of β -methoxyamine to unsaturated ketones and the rearrangement of β -methoxyaminoketones. *J. Am. Chem. Soc.*, **63**: 3494–3499.
- Boik, J. (2001). *Natural Compounds in Cancer Therapy*. Minnesota: Oregon Medical Press. pp. 8-9.
- Boubakir, Z., Beuerle, T., Liu, B. and Beerhues L. (2005). The first prenylation step in hyperforin biosynthesis. *Phytochem.*, **66**: 51–57.
- Boyce, J. H. and Porco, J. A. (2014). Asymmetric, Stereodivergent Synthesis of (-)-Clusianone Utilizing a Biomimetic Cationic Cyclization. *Angew. Chem. Int. Ed.*, **53**: 1–7.
- Boyd, M. R. (1995). *The NCI In Vitro Anticancer Drug Discovery Screen*. pp. 23-42.
- Bradford, M. (1976). A rapid and sensitive method for the quantitation of microgram quantities of protein utilizing the principle of the protein-dye binding. *Anal. Biochem.*, **72**: 248–254.
- Brennan, B. (2006). Nasopharyngeal carcinoma. *Orphan. J. Rare. Diseas.*, **1**: 1-5.
- Burkhart, C. A., Kavallaris, M. and Horwitz, S. B. (2001). The role of beta-tubulin isotypes in resistance to antimitotic drugs. *Biochim. Biophys. Acta.*, **1471**: O1–O9.
- Bystrov, N. S., Chernov, B. K., Dobrynin, V. N. and Kolosov, M. N. (1975). The structure of hyperforin. *Tetrahedron*, **16**: 2791–2794.
- Camargo, M. S., Prieto Resende, F. A., Boldrin, P. K., Cardoso, C. R. P., Fernández, M. R., Molina, J. M. M., Olea, N., Vilegas, W., Cuesta-Rubio, O. and Varanda, E. A. (2013). Evaluation of estrogenic, antiestrogenic and genotoxic activity of nemorosone, the major compound found in brown Cuban propolis. *BMC Complemen. Altern. Med.*, **13**: 1-8.
- Cancer Research UK. (2011). CancerStats – Cancer Worldwide. *IARC*, **9**: 1–8.
- Cang, S., Ma, Y., Chiao, J. W. and Liu, D. (2014). Phenethyl isothiocyanate and paclitaxel synergistically enhanced apoptosis and alpha-tubulin hyperacetylation in breast cancer cells. *Exp. Hematol. Oncol.*, **3**: 1–6.
- Caplow, M. and Shanks, J. (1996). Evidence that a single monolayer tubulin-GTP cap is both necessary and sufficient to stabilize microtubules. *Mol. Biol. Cell.*, **7**: 663–675.
- Caplow, M. and Shanks, J. (1995). Induction of microtubule catastrophe by formation of tubulin-GDP and apotubulin subunits at microtubule ends. *Biochemistry*, **34**: 15732–15741.

- Chan A. T. (2010). Nasopharyngeal carcinoma. *Ann Oncol.*, **21**: 308-312.
- Chan, K. S., Koh, C. G. and Li, H. Y. (2012). Mitosis-targeted anti-cancer therapies: where they stand. *Cell Death Dis.*, **3**: e411.
- Chen, Y. (2012). Lung Cancer. (Accessed date 17/4/2012). Available from: <http://www.ncbi.nlm.nih.gov/pubmedhealth/PMH0004529/>.
- Chernayaev, G. A., Barkova, T. I., Egorova, V. V., Sorokina, I. B., Ananchenko, S. N., Mataredza, G. D., Sokolova, N. A. and Rozan, V. B. (1975). A series of optical, structural and isomeric analogs of estradiol: A comparative study of the biological activity and affinity to cytosol receptor of rabbit uterus. *J. Steroid Biochem.*, **6**: 1483-1488.
- Chippendale, T. W. E., Hu, B., Haj, A. J. E. and Smith, D. (2012). A study of enzymatic activity in cell cultures *via* the analysis of volatile biomarkers. *Analyst.*, **137**: 4677-4685.
- Chou, Y. H., Ngais, K. L. and Goldman, R. (1991). The Regulation of Intermediate Filament Reorganization in Mitosis. *J. Biol. Chem.*, **266**: 7325-7328.
- Christian, O. E., Reynolds, R. F. and Jacob, H. (2008). Prenylated Benzophenones from *Hypericum hypericoides*. *Nat. Prod. Comm.*, **3**: 1781-1786.
- Christian, O. E., Christian, O. E., Fronczek, F. R., Ky, K., Pradhan, S., Manandhar, A. and Richmond, C. (2012). Redetermination and absolute configuration of (+)-7-epiclusianone. *Acta Crystallogr., Sect. E: Struct. Rep. Online.*, **68**: o3222-3230.
- Ching, J. W. P. (2013). *3-Hydroxy-3-Methylglutaryl coenzyme A (HMG- CoA) Reductase Inhibitors from Plant Secondary Metabolites as Hypercholestromic Lowering Agent*. Ph.D. thesis, University of Nottingham Malaysia Campus.
- Ciochina, R. and Grossman, R. B. (2006). Polycyclic polyprenylated acylphloroglucinols. *Chem. Rev.*, **106**: 3963-3986.
- Clute, P, Pines, J. (1999). Temporal and spatial control of cyclin B1 destruction in metaphase. *Nat. Cell Biol.*, **1**: 82-87.
- Cogliano, V. J., Baan, R., Straif, K., Grosse, Y., Lauby-Secretan, B., Ghissassi, F. E., Bouvard, V., Benbrahim-Tallaa, L., Guha, N., Freeman, C., Galichet, L. and Wild, C. P. (2011). Preventable exposures associated with human cancers. *J. Natl. Cancer Inst.*, **103**: 1827-1839.
- Cragg, G. M. and Newman, D. J. (2013). Natural products: a continuing source of novel drug leads. *Biochim. Biophys. Acta.*, **1830**: 3670-3695.

- Cuesta-Rubio, O., Velez-Castro, H., Frontana-Urbe, B. A. and Cárdenas, J. (2001). Nemorosone, the major constituent of floral resins of *Clusia rosea*. *Phytochem.*, **57**: 279–283.
- Deharo, E. and Ginsburg, H. (2011). Analysis of additivity and synergism in the anti-plasmodial effect of purified compounds from plant extracts. *Malar. J.*, **10**: S1-S5.
- Díaz-Carballo, D., Malak, S., Bardenheuer, W., Freistuehler, M. and Reusch, H. P. (2008). Cytotoxic activity of nemorosone in neuroblastoma cells. *J. Cell. Mol. Med.*, **12**: 2598–2608.
- Draviam, V. M., Orrechia, S., Lowe, M., Pardi, R. and Pines, J. (2001). The localization of human cyclins B1 and B2 determines CDK1 substrate specificity and neither enzyme requires MEK to disassemble the Golgi apparatus. *J. Cell Biol.*, **152**: 945–958.
- Dumontet, C. and Jordan, M. A. (2010). Microtubule-binding agents: a dynamic field of cancer therapeutics. *Nat. Rev. Drug discovery*, **9**: 790–803.
- Ee, G. C. L., Ng, S. H., Goh, J. K., Sukari, M. A. and Rahmani, M. (2009). Chemical constituents of *Garcinia parvifolia* (Guttiferae). *Malays. J. Sci.*, **28**:105–110.
- Eisel, D., Fertig, G., Fischer, B., Manzow, S. and Schmelig, K. eds. (1998). *Apoptosis and Cell Proliferation*. (Second edition). Germany: Boehringer Mannheim. pp. 2-5.
- Eric, L. M., Rozendaal, V. and Lelyveld, G. P. (2000). Screening of the needles of different yew species and cultivars for paclitaxel and related taxoids. *Phytochem.*, **53**: 383–389.
- Fourest-lieuvain, A., Peris, L., Gache, V., Garcia-Saez, I., Juillan-Binard, C., Lantéz, V. and Job, D. (2006). Microtubule Regulation in Mitosis: Tubulin Phosphorylation by the Cyclin-dependent Kinase Cdk1. *Mol. Biol. Cell.*, **17**: 1041–1050.
- Fu, Y., Li, S., Zu, Y., Yang, G., Yang, Z., Luo, M., Jiang, S., Wink, M. and Efferth, T. (2009). Medicinal chemistry of paclitaxel and its analogues. *Curr. Med. Chem.*, **16**: 3966–3985.
- Furuno, N., Elzen, N. D. and Pines, J. (1999). Human cyclin A is required for mitosis until mid-prophase. *The J. Cell Biol.*, **147**: 295–306.
- Garnsey, M. R., Matous, J. A., Kwiek, J.J. and Coltart, D. M. (2011). Asymmetric total synthesis of (+)- and (-)-clusianone and (+)- and (-)-clusianone methyl enol ether via ACC alkylation and evaluation of their anti-HIV activity. *Bioorg. Med. Chem. Lett.*, **21**: 2406–2409.

- Gartner, M., Müller, T., Simon, J.C., Giannis, A. and Sleeman, J.P. (2005). Aristoforin, a novel stable derivative of hyperforin, is a potent anticancer agent. *ChemBiochem.*, **6**: 171–177.
- Gavet, O. and Pines, J. (2010). Activation of cyclin B1-Cdk1 synchronizes events in the nucleus and the cytoplasm at mitosis. *J. Cell Biol.*, **189**: 247–59.
- Gerlier, D. and Thomasset, N. (1986). Use of MTT colorimetric assay to measure cell activation. *J. Immunol. Methods*, **94**: 57–63.
- Giard, D. J., Aaronson, S. A., Todaro, G. J., Arnstein, P., Kersey, J. H. and Parks, W. P. (1973). *In Vitro* Cultivation of Human Tumors: Establishment of Cell Lines Derived From. *J. Natl. Cancer Inst.*, **51**: 1417– 1423.
- Gligorov, J. and Lotz, J. P. (2004). Preclinical pharmacology of the taxanes: implications of the differences. *The Oncol.*, **9**: 3–8.
- Goulart, B. H., Martins, R. G. and Lynch, T. J. (2001). Twenty-two years of phase III trials for patients with advanced non-small-cell lung cancer: sobering results. *J Clin. Oncol.*, **19**: 4089.
- Grenning, A. J., Boyce, J. H. and Porco, J. A. (2014). Rapid Synthesis of Polyprenylated Acylphloroglucinol Analogs via Dearomative Conjugative Allylic Annulation. *J. Am. Chem. Soc.*, **136**: 11799–11804.
- Guideline, I. C. H. H. T. (2009). *Pharm. Dev.*
- Gustafsson, M. H. G., Bittrich, V. and Stevens, P. F. (2014). Phylogeny of Clusiaceae Based on rbc L sequences. *Int. J. Plant Sci.*, **163**: 1045–1054.
- Hamed, W., Brajeul, S., Mahuteau-Betzer, F., Thoison, O., Mons, S., Delpech, B., Nguyen, V. H., Sévenet, T. and Marazano, C. (2006). Oblongifolins A-D, Polyprenylated Benzoylphloroglucinol Derivatives from *Garcinia oblongifolia*. *J. Nat. Prod.*, **69**: 774–777.
- Hamid, R., Rotshteyn, Y., Rabadi, L., Parikh, R. and Bullock, P. (2004). Comparison of alamar blue and MTT assays for high through-put screening. *Toxicol. In Vitro*, **18**: 703–710.
- Haumeil, J. C. C. and Rnaud, P. A. (2002). Evaluation of the Cytotoxicity Effect of Dimethyl Sulfoxide (DMSO) on Caco2 / TC7 Colon Tumor Cell Cultures. *Biol. Pharm. Bull.*, **25**: 1600–1603.
- Herbst, R. S. and Khuri, F. R. (2003). Mode of action of docetaxel – a basis for combination with novel anticancer agents. *Cancer Treat. Rev.*, **29**: 407–415.
- Hochegger, H., Takeda, S. and Hunt, T. (2008). Cyclin-dependent kinases and cell- cycle transitions: does one fit all? *Nature*, **9**: 910-916.

Hong, J., Kwon S. J., Sang, S., Ju, J., Zhou, J. N., Ho, C. T., Huang, M. T. and Yang C. S. (2007). Effects of garcinol and its derivatives on intestinal cell growth: Inhibitory effects and autoxidation-dependent growth-stimulatory effects. *Free Rad. Biol. Med.*, **42**: 1211–1221.

Horeischi, F., Guttroff, C. and Plietker, B. (2015). The enantioselective total synthesis of (+)-clusianone. *Chem. Comm.*, **1**: 1–3.

Hsieh, H. P., Liou, J. P., Lin, Y. T., Mahindro, N., Chang, J. Y., Yang, Y. N., Chern, S. S., Tan U. K., Chang C. W., Chen T. W., Lin C. H., Chang, Y. Y. and Wang, C. C. (2003). Structure-activity and crystallographic analysis of benzophenone derivatives-the potential anticancer agents. *Bioorg. Med. Chem. Lett.*, **13**: 101–105.

Huang, D. P., Ho, J. H., Poon, Y. F., Chew, E. C., Saw, D., Lui, M., Li, C. L., Mak, L. S., Lai, S. H. and Lau, W. H. (1980). Establishment of a cell (NPC/HK1) from a differentiated squamous carcinoma of the nasopharynx. *Int. J. Cancer*, **26**: 127–132.

Hughes, A. J. (2014). Single-cell Western blotting. *Nat. Methods*, **11**: 749–755.

Ito, C., Itoigawa, M., Miyamoto, Y., Onoda, S., Rao, K. S., Mukainaka, T., Tokuda, H., Nishino, H. and Furukawa, H. (2003). Polyprenylated benzophenones from *Garcinia assigu* and their potential cancer chemopreventive activities. *J. Nat. Prod.*, **66**: 206–209.

Jacobs, J., Jones, C. M. and Baille, J.P. (1970). Characteristic of Human Diploid Cell Designated MRC-5. *Nature*, **227**: 168–170.

Janke, C. and Bulinski, J. C. (2011). Post-translational regulation of the microtubule cytoskeleton: mechanisms and functions. *Nat. Rev. Mol. Cell Biol.*, **12**: 773–786.

Jirásek, T., Cipro, S., Musilová, A., Kubecová, M. and Mandys, V. (2009). Expression of class III beta-tubulin in colorectal carcinomas: an immunohistochemical study using TU-20 & TuJ-1 antibody. *Indian J. Med. Res.*, **129**: 89–94.

Jordan, M. A. and Wilson, L. (2004). Microtubule as target for anticancer drug. *Nat. Rev. Drug Discovery*, **4**: 253–265.

Kalyuzhny, A. E. ed. (2011). *Signal Transduction Immunohistochemistry Methods and Protocols*. Heidelberg, Germany: Humana Press-Springer. pp. 55-67.

Kardono, L. B. S. (2006). Bioactive Constituents of *G. porrecta* and *G. parvifolia* Grown in Indonesia. *Pak. J. Biol. Sci.*, **9**: 483–486.

Kavallaris, M. 2010. Microtubules and resistance to tubulin-binding agents. *Nature Rev. Cancer*, **10**: 194–204.

- Keepers, Y. P., Pizao, P. E., Peters G. F., Ark-Otte, J. V., Winograd, B. and Pinedo, M. H. (1991). Comparison of the Sulforhodamine B Protein and Tetrazolium (MTT) Assays for *in vitro* Chemosensitivity Testing. *Eur. J. Cancer*, **27**: 879–900.
- Khodjakov, A. and Rieder, C. L. (2009). The nature of cell-cycle checkpoints: facts and fallacies Cyclin B-Cdk active. *J. Biol.*, **8**: 1-5.
- Klein, J. and Grummt, I. (1999). Cell cycle-dependent regulation of RNA polymerase I transcription: the nucleolar transcription factor UBF is inactive in mitosis and early G1. *Proc. Natl. Acad. Sci. USA.*, **96**: 6096–6101.
- Kornblau, S. M., Womble, M., Cade, J. S., Lemker, E. and Qiu, Y. H. (2005). Comparative analysis of the effects of sample source and test methodology on the assessment of protein expression in acute myelogenous leukemia. *Nat. Leukemia*, **19**: 1550–1557.
- Kufe, D. W., Raphael, E. P., Weichselbaum, R. R., Robert, C. B., Gansler, T. S., Holland, J. F. and Frei, E. eds. (2003). *Cancer Medicine*. (Sixth edition). Hamilton: BC Decker. pp. 1-149.
- Kurien, B. T. and Scofield, R. H. (2003). Protein blotting: a review. *J. Immunol. Methods*, **274**: 1–15.
- Lalla, J. K. S., Achhra, C.V., Shah, M. and Parmar, D. (2008). *Cancer Int. J. Res. Pharm. Chem.*, **3**: 26–33.
- Leandro-García, L. J., Leskelä, S., Landa, I., Montero-Conde, C., López-Jiménez, E., Letón, R., Cascón, A., Robledo, M. and Rodríguez-Antona, C. (2010). Tumoral and tissue-specific expression of the major human beta-tubulin isotypes. *Cytoskeleton*, **67**: 214–223.
- Liakopoulos, D., Kusch, J., Grava, S., Vogel, J. and Barral, Y. (2003). Asymmetric loading of Kar9 onto spindle poles and microtubules ensures proper spindle alignment. *Cell*, **112**: 561–574.
- Lim, T. K. (2012). *Edible Medicinal And Non-Medicinal Plants: Volume 2, Fruit*. (Twelfth edition) Dordrecht: Springer Netherlands. pp. 1-79.
- Lin, E., Kalunta, C. I., Chen, F. S., Nguyen, T. T., Kaptein, J. S. and Lad, P. M. (1995). Dimethyl Sulfoxide Suppresses Apoptosis in Burkitts Lymphoma Cells. *Exp. Cell Res.*, **216**: 403–410.
- Lindqvist, A., Zon, W. V., Rosenthal C. K. and Wolthuis, R. M. F. (2007). Cyclin B1-Cdk1 activation continues after centrosome separation to control mitotic progression. *PLoS Biol.*, **5**: e123 (1127-1137).
- Liu, B, Falkenstein-Paul, H. and Schmidt, W. Ã. L. B. (2003). Benzophenone synthase and chalcone synthase from *Hypericum androsaemum* cell cultures:

cDNA cloning, functional expression and site-directed mutagenesis of two polyketide synthases. *Plant J.*, **34**: 847–855.

Lowe, M., Rabouille, C., Nakamura, N., Watson, R., Jackman, M., Jämsä, E., Rahman, D., Pappin, D. J. and Warren G. (1998). Cdc2 kinase directly phosphorylates the cis-Golgi matrix protein GM130 and is required for Golgi fragmentation in mitosis. *Cell*, **94**: 783–793.

Lucas, C. L. and Moody, C. J. (2010). *Advances in Heterocyclic Chemistry Volume 100*. Elsevier. pp. 53-74.

Ludueno R. F. (1998). Multiple forms of tubulin. *Int. Rev. Cytol.*, **178**: 207–275.

Ma, B. B., Lui, V. W., Poon, F. F., Wong, S. C., To, K. F., Wong, E., Chen, H., Lo, K. W., Tao, Q., Chan, A. T., Ng, M. H. and Cheng, S. H. (2010). Preclinical activity of gefitinib in non-keratinizing nasopharyngeal carcinoma cell lines and biomarkers of response. *Invest. New Drugs.*, **28**: 326–333.

Maccari, L., Manetti, F., Corelli, F. and Botta, M. (2003). 3D QSAR studies for the β - tubulin binding site of microtubule-stabilizing anticancer agents (MSAAs). *Il Farmaco*, **58**: 659–668.

Mackeen, M., Ali, A. M., Lajis, N. H., Kawazu, K., Hassan, Z., Amran, M., Habsah, M., Mooi, L. Y. and Mohamed, S. M. (2000). Antimicrobial, antioxidant, antitumour- promoting and cytotoxic activities of different plant part extracts of *Garcinia atroviridis* Griff. Ex T. Anders. *J. Ethnopharmacol.*, **72**: 395–402.

MacPhee, D. J. (2010). Methodological considerations of improving Western blot analysis. *J. Pharmacol. Toxicol. Methods*, **61**: 171–177.

Maeda, E., Akahane, M., Kiryu, S., Kato, N., Yoshikawa, T., Hayashi, N., Aoki, S., Minami, M., Uozaki, H., Fukayama, M. and Ohtomo, K. (2009). Spectrum of Epstein-Barr virus-related diseases: a pictorial review. *Jp. J. Radiol.*, **27**: 4–19.

Magnani, M., Ortuso, F., Soro, S., Alcaro, S., Tramontano, A. and Botta, M. (2006). The betaI/betaIII-tubulin isoforms and their complexes with antimitotic agents. Docking and molecular dynamics studies. *FEBS J.*, **273**: 3301–3310.

Matsumoto, K., Akao, Y., Kobayashi, E., Ito, T., Ohguchi, K., Tanaka, T., Linuma, M. and Nozawa, Y. (2003). Cytotoxic Benzophenone Derivatives from *Garcinia* Species Display a Strong Apoptosis- Inducing Effect against. *Biol. Pharm. Bull.*, **26**: 569–571.

McCandlish, L. E., Hanson, J. C. and Stout, G. H. (1976). The structures of two derivatives of bicyclo[3.3.1]nonane-2,4,9-trione. A natural product: clusianone, C₃₃H₄₂O₄ and trimethylated catechinic acid, C₁₈H₂₀O₆. *Acta Crystallogr., Sect. A: Found. Adv.*, **B32**: 1793–1801.

- McChesney, J. D., Venkataraman, S. K. and Henri, J. T. (2007). Plant natural products: back to the future or into extinction? *Phytochem.*, **68**: 2015–2022.
- McCormack, V. A. and Boffetta, P. (2011). Today's lifestyles, tomorrow's cancers: trends in lifestyle risk factors for cancer in low- and middle-income countries. *Ann Oncol.*, **22**: 2349–2357.
- Missailidis, S. ed. (2008). *Anticancer Therapeutics*. London: John Wiley & Sons, Ltd.
- Monache, F. D., Monache, G. D. and Gacs-Batz, E. (1991). Prenylated Benzophenones from *Clusia Sandiensis*. *Phytochem.*, **30**: 2003– 2005.
- Moongkarndi, P., Kosem, N., Kaslungka, S., Luanratana, O., Pongpan, N. and Neungton, N. (2004). Antiproliferation, antioxidation and induction of apoptosis by *Garcinia mangostana* (mangosteen) on SKBR3 human breast cancer cell line. *J. Ethnopharmacol.*, **90**: 161–166.
- Moore, J. K. and Miller, R. K. (2007). The Cyclin-dependent Kinase Cdc28p Regulates Multiple Aspects of Kar9p Function in Yeast, *Mol. Biol. Cell*, **18**: 1187–1202.
- Morgan, D. O. (1997). Cyclin-dependent kinases: engines, clocks, and microprocessors. *Annu. Rev. Cell Dev. Biol.*, **13**: 261–291.
- Mosmann, T. (1983). Rapid colorimetric assay for cellular growth and survival: application to proliferation and cytotoxicity assays. *Journal of immunological method*, **65**: 55–63.
- Munier, R. (1953). Separation of alkaloids from their N-oxides by paper chromatography. *Bull. Soc. Chem. Biol.*, **35**: 1225–1231.
- Murata, R. M., Yatsuda, R., Santos, M. H., Kohn, L. K., Martins, F. T., Nagem, T. J., Alencar, S. M., Carvalho, J. E. D. and Rosalen, P. L. (2010). Antiproliferative Effect of Benzophenones and their Influence on Cathepsin Activity. *Phytother. Res.*, **24**: 379–383.
- Nagalingam, S. V., Ching, J. W. P., Break, K. B., Tahir, M. I. M. and Jin, K. T. (2013). A $P2_12_12_1$ polymorph of (+)-clusianone. *Acta Crystallogr., Sect. E: Struct. Rep. Online*, **69**: o1799– o1800.
- Nagalingam, S. V., Ling, K. W. and Jin, K. T. (2016). Structural Derivatization of Clusianone and *In Vitro* Cytotoxicity Evaluation Targeting Respiratory Carcinomas. *Planta Med Lett*, **3**: e10-e13.
- Narvi, E., Jaakkola, K., Winsel, S., Oetken-Lindholm, C., Halonen, P., Kallio, L. and Kallio, M. J. (2013). Altered TUBB3 expression contributes to the epothilone response of mitotic cells. *Br. J. Cancer*, **108**: 82–90.

Nettles, J. H., Li, H., Cornett, B., Krahn, J. M., Snyder, J. P. and Downing, K. H. (2004). The binding mode of epothilone A on alpha, beta-tubulin by electron crystallography. *Science*, **305**: 866–869.

Nigg, E.A. (2001). Mitotic kinases as regulators of cell division and its checkpoints. *Nat. Rev. Mol. Cell Biol.*, **2**: 21–32.

Njardarson, J. T. (2012). Synthetic Efforts Toward [3.3.1] Bridged Bicyclic Phloroglucinol Natural Products. *Tetrahedron*, **67**: 7631–7666.

Nuhant, P., David, M., Pouplin, T., Delpech, B. and Marazano, C. (2007). A, α' -Annulation of 2,6-Prenyl-Substituted Cyclohexanone Derivatives with Malonyl Chloride: Application to a Short Synthesis of Rearrangement of a Biogenetic-Like Intermediate., *Org. Lett.*, **9**: 14200–14201.

Nurse, P. (1990). Universal control mechanism regulating onset of M-phase. *Nature*, **344**: 503–508.

O'Connor, C. (2008). *Cell Division*. Boston: Nature Education. pp. 123-298.

Ohishi, Y., Oda, Y., Basaki, Y., Kobayashi, H., Wake, N., Kuwano, M. and Tsuneyoshi, M. (2007). Expression of beta-tubulin isotypes in human primary ovarian carcinoma. *Gynecol. Oncol.*, **105**: 586–592.

Oliveira, C. M. A., Portol, A. M., Bittrich, V., Vencato, I. and Marsaioli, A. J. (1996). Floral resins of *clusia* spp: Chemical composition and biological function. *Tetrahedron*, **37**: 6427–6430.

Padhye, S., Ahmad, A., Oswal, N. and Sarkar, F. H. (2009). Emerging role of Garcinol, the antioxidant chalcone from *Garcinia indica* Choisy and its synthetic analogs. *J. Oncol. Hematol*, **2**: 1-3.

Pan, M. H., Chang, W. L., Lin-Shiau, S. Y., Ho, C. T. and Lin, J. K. (2001). Induction of apoptosis by garcinol and curcumin through cytochrome c release and activation of caspases in human leukemia HL-60 cells. *J. Agric. Food Chem*, **49**: 1464–1474.

Pardo-Andreu, G. L., Nuñez-Figueredo, Y., Tudella, V. G., Cuesta-Rubio, O., Rodrigues, F. P., Pestana, C. R., Uyemura, S. A., Leopoldino, A. M., Alberici L. C. and Curti, C. (2011). The anti-cancer agent nemorosone is a new potent protonophoric mitochondrial uncoupler. *Mitochondrion*, **11**: 255–263.

Parkin, D. M., Bray, F., Ferlay, J. and Pisani, P. (2002). Global cancer statistics 2002. *CA Cancer J. Clin*, **55**: 74–108.

Parthiban, P., Balasubramanian, S., Aridoss, G. and Kabilan, S. (2008). Synthesis and NMR spectral studies of some 2,6-diarylpiperidin-4-one O-benzyloximes. *Spectrochimica Acta. Part A*, **70**: 11–24.

- Piccinelli, A. L., Cuesta-Rubio, O., Chica, M. B., Mahmood, N., Pagano, B., Pavone, M., Barone, V. and Rastrelli, L. (2005). Structural revision of clusianone and 7-epi-clusianone and anti-HIV activity of polyisoprenylated benzophenones. *Tetrahedron*, **61**: 8206–8211.
- Pineda, O., Farràs, J., Maccari, L., Manetti, F., Botta, M., Vilarrasa, J. (2004). Computational comparison of microtubule-stabilising agents laulimalide and peloruside with taxol and colchicine. *Bioorg. Med. Chem. Lett.*, **14**: 4825–4829.
- Preisinger, C., Körner, R., Wind, M., Lehmann, W. D., Kopajtich, R. and Barr, F. (2005). Plk1 docking to GRASP65 phosphorylated by Cdk1 suggests a mechanism for Golgi checkpoint signalling. *EMBO J.*, **24**: 753–765.
- Protiva, P., Hopkins, M. E., Baggett, S., Yang, H., Lipkin, M., Holt, P. R., Kennelly, E. J. and Bernard, W. I. (2008). Growth inhibition of colon cancer cells by polyisoprenylated benzophenones is associated with induction of the endoplasmic reticulum response. *Int. J. Cancer*, **123**: 687–694.
- Provencio, M., Isla, D., Sánchez, A. and Cantos, B. (2011). Inoperable stage III non- small cell lung cancer: Current treatment and role of vinorelbine. *J. Thorac. Dis.*, **3**: 197–204.
- Qi, J. and Porco, J. A. (2007). Rapid Access to Polyprenylated Phloroglucinols via Alkylative Dearomatization-Annulation: Total Synthesis of (±)-Clusianone. *J. Am. Chem. Soc.*, **129**: 12682– 12683.
- Rahman, S. N. S. A., Wahab, N. A. and Malek, S. N. A. (2013). *In Vitro* Morphological Assessment of Apoptosis Induced by Antiproliferative Constituents from the Rhizomes of *Curcuma zedoaria*. *J. Evid. Based Complementary Altern.*, 1–14.
- Rao, S., He, L., Ojima, I. and Orr G. A. (1999). Characterization of the Taxol Binding Site on the Microtubule: Identification of Arg282 in β -tubulin as the site of photoincorporation of a 7-benzophenone analogue of taxol. *J. Biol. Chem.*, **274**: 37990–37994.
- Rao, S., Krauss, N. E., Heerding, J. M., Swindell, C. S., Ringel, I., Orr, G.A. and Horwitz, S. B. (1994). Photolabels the N-terminal 31 Amino Acids of β -Tubulin, *Am. Soc. Mol. Biol.*, 3132–3134.
- Rates, S. M. (2001). Plants as source of drugs. *Toxicon*, **39**: 603–613.
- Reis, F. H. Z., Pardo-Andreu, G. L., Nuñez-Figueredo, Y., Cuesta-Rubio, O., Marín Prida, J., Uyemura, S. A., Curti, C. and Alberici, L. C. (2014). Clusianone, a naturally occurring nemorosone regioisomer, uncouples rat liver mitochondria and induces HepG2 cell death. *Chem. Biol. Interact.*, **212**: 20–29.
- Rello, S., Stockert, J. C., Moreno, V., Gámez, A., Pacheco, M., Juarranz, A., Cañete, M. and Villanueva, A. (2005). Morphological criteria to distinguish

cell death induced by apoptotic and necrotic treatments. *Apoptosis*. **10**: 201–208.

Renzulli, M. L., Rocheblave, L., Stanislava, I., Avramova, Galletti, E., Castagnolo, D., Maccari, L., Forli, S., Manetti, F., Corelli, F. and Botta, M. (2006). A pharmacophore modeling approach to design new taxol mimics: towards the synthesis of potential anticancer and MDR-reversing agent. *Iss. Ital.-Swiss. Med. Chem. Meet.*, **8**: 111–130.

Richard, J. A. (2014). Chemistry and Biology of the Polycyclic Polyprenylated Acylphloroglucinol Hyperforin. *Eur. J. Org. Chem.*, 273–299.

Rishton, G. M. (2003). Nonleadlikeness and leadlikeness in biochemical screening. *Drug Discov. Today*, **8**: 86–96.

Rosen, A. L., Moravek, R. T. and Carlton, J. K. (1952). Streak reagents for chromatography. *Anal. Chem.*, **24**: 1335–1336.

Roux, D., Hadi, H. A., Thoret, S., Guénard, D., Thoison, O., Païs, M. and Sévenet, T. (2000). Structure-activity relationship of polyisoprenyl benzophenones from *Garcinia pyrifera* on the tubulin/microtubule system. *J. Nat. Prod.*, **63**: 1070–1076.

Rukachaisirikul, V., Trisuwan, K., Sukpondma, Y. and Phongpaichit, S. (2008). A new Benzoquinone derivative from the leaves of *Garcinia parvifolia*. *Arch. Pharm. Res.*, **31**: 17–20.

Rullah, K., Aluwi, M. F. F. M., Yaminb, B. M., Bahari, M. N. A., Weid, L. S., Ahmad, S., Abas, F., Ismail, N. H., Jantan, I. and Wai, L. K. (2014). Inhibition of prostaglandin E2 production by synthetic minor prenylated chalcones and flavonoids : Synthesis , biological activity, crystal structure, and in silico evaluation. *Bioorg. Med. Chem. Lett.*, **24**: 3826–3834.

Santos, M. H., Nagem, T. J., Lula, I. S. and Speziali, N. L. (2001). Complete assignment of the ^1H and ^{13}C NMR spectra of the tetraisoprenylated benzophenone 15-epiclusianone. *Magn. Reson. Chem.*, **39**: 155–159.

Santos, M. H., Speziali, N. L., Nagem, T. J. and Oliveira, T. T. (1998). Epiclusianone: a New Natural Product Derivative of Bicyclo[3.3.1]nonane-2,4,9-trione. *Acta Crystallogr., Sect. C: Struct. Chem.*, **54**: 1990–1992.

Sargenti, S. R. and Vichnewski, W. (2000). Sonication and Liquid Chromatography as a Rapid Technique for Extraction and Fractionation of Plant Material. *Phytochem. Anal.*, **73**: 69–73.

Satyajit, D., Sarker, Latif, Z. and Gray, A. I.eds. (2006). *Natural Products Isolation* (Second edition). Humana Press. pp. 1-515.

- Satyanarayana, A. and Kaldis, P. (2009). Mammalian cell-cycle regulation: several Cdks, numerous cyclins and diverse compensatory mechanisms. *Oncogene*, **28**: 2925–2939.
- Schempp, C. M., Kirkin, V., Simon-Haarhaus, B., Kersten, A., Kiss, J., Termeer, C. C., Gilb, B., Kaufmann, T., Borner, C., Sleeman, J. P. and Simon, J. C. (2002). Inhibition of tumour cell growth by hyperforin, a novel anticancer drug from St. John's Wort that acts by induction of apoptosis. *Nat. Onco.*, **6**: 1242–1250.
- Shoemaker, R. H. (2006). The NCI60 human tumour cell line anticancer drug screen. *Nat. Rev. Cancer*, **6**: 813–823.
- Silva, M. C. A., Heringer, A. P., Figueiredo, M. R. and Paiva, S. R. (2012). Separation of clusianone from *Clusia Fluminensis* Planch and Triana (Clusiaceae) by high speed counter current chromatography (HSCCC). *J. Liq. Chromatogr. Relat. Technol.*, **35**: 2313–2321.
- Simpkins, N. S., Holtrup, F., Rodeschini, V., Taylor, J. D. and Wolf, R. C. (2012). Comparison of the cytotoxic effects of enantiopure PPAPs, including nemorosone and clusianone. *Bioorg. Med. Chem. Lett.*, **22**: 6144–6147.
- Sirri, V., Hernandez-Verdun, D., Roussel, P. (2002). Cyclin-dependent kinases govern formation and maintenance of the nucleolus. *J. Cell Biol.*, **156**: 969–981.
- Snyder, J. P., Nettles, J. H., Cornett, B., Downing, K. H. and Nogales, E. (2001). The binding conformation of Taxol in β -tubulin: A model based on electron crystallographic density. *PNAS*, **98**: 5312–5316.
- Soejarto, D. D., Fong, H. H. and Tan, G. T. (2005). Ethnobotany/ethnopharmacology and mass bioprospecting: issues on intellectual property and benefit-sharing. *J. Ethnopharmacol.*, **100**: 15–22.
- Stabile, L. P., Lyker, J. S., Gubish, C. T., Zhang, W., Grandis, J. R. and Siegfried, J. M. (2005). Combined Targeting of the Estrogen Receptor and the Epidermal Growth Factor Receptor in Non – Small Cell Lung Cancer Shows Enhanced Antiproliferative Effects. *Cancer Res.*, **4**: 1459–1471.
- Sunagawa, I. (2005). *Crystals Growth, Morphology and Perfection*. Cambridge University Press. pp. 147-166.
- Sweeney, P. W. (2008). Phylogeny and Floral Diversity in the Genus *Garcinia* (Clusiaceae) and Relatives. *Int. J. Plant Sci.*, **169**: 1288–1303.
- Sweet, S. and Singh, G. (1999). Changes in mitochondrial mass, membrane potential, and cellular adenosine triphosphate content during the cell cycle of human leukemic (HL-60) cells. *J. Cell. Physio.*, **180**: 91–96.

- Syamsudin, K. S. and Sutaryo, B. (2007). Screening of Some Extracts from *Garcinia parvifolia* Miq. (Guttifera) for Antiplasmodial, Antioxidant, Cytotoxicity and Antibacterial Activities. *Asian J. Plant. Sci.*, **6**: 972–976.
- Taguchi, N., Ishihara, N., Jofuku, A., Oka, T. and Mihara K. (2007). Mitotic phosphorylation of dynamin-related GTPase Drp1 participates in mitochondrial fission. *J. Biol. Chem.*, **282**: 11521–11529.
- Taylor, S. C. and Posch, A. (2014). The design of a quantitative Western Blot experiment. *Bio. Med. Res. Int.* 1-9.
- Tsao, S. W., Wang, X., Liu, Y., Cheung, Y. C., Feng, H., Zheng, Z., Wong, N., Yuen, P. W., Lo A. K., Wong, Y. C. and Huang, D. P. (2002). Establishment of two immortalized nasopharyngeal epithelial cell lines using SV40 large T and HPV16E6/E7 viral oncogenes. *Biochim. Biophys. Acta, Mol. Cell Res.*, **1590**: 150–158.
- Tsukano, C., Siegel, D. R. and Danishefsky, S. J. (2007). Differentiation of nonconventional “carbanions”-the total synthesis of nemorosone and clusianone. *Angew. Chem. Int. Ed.*, **46**: 8840–8844.
- Vasquez, R. J., Gard, D. L. and Cassimeris, L. (1999). Phosphorylation by CDK1 regulates XMAP215 function in vitro. *Cell Motil. Cytoskeleton*, **43**: 310–321.
- Verdier-Pinard, P., Pasquier, E., Xiao, H., Burd, B., Villard, C., Lafitte, D., Miller, L. M., Angeletti, R. H., Horwitz, S. B. and Braguer, D. (2009). Tubulin proteomics: towards breaking the code. *Anal. Biochem*, **384**: 197–206.
- Visvader, J. E. (2011). Cells of origin in cancer. *Nature*, **469**: 314–322.
- Wang, C. C., Lin, S. Y., Lai, Y. H., Liu, Y. J., Hsu, Y. L. and Chen, J. J. (2012). Dimethyl sulfoxide promotes the multiple functions of the tumor suppressor HLJ1 through activator protein-1 activation in NSCLC cells. *PloS one*, **7**: 1-10.
- Wang, Y., Seemann, J., Pypaert, M., Shorter, J. and Warren, G. (2003). A direct role for GRASP65 as a mitotically regulated Golgi stacking factor. *EMBO*, **22**: 3279–3290.
- Wang, Z., Fan, M., Candas, D., Zhang, T. Q., Qin, L., Eldridge, A., Wachsmann, Hogiu, S., Ahmed, K. M., Chromy. B. A., Nantajit, D., Duru, N., He, F., Chen, M., Finkel, T., Weinstein, L. S. and Li, J. J. (2014). Cyclin b1/cdk1 coordinates mitochondrial respiration for cell-cycle G2/M progression. *Dev. Cell*. **29**: 217–232.
- Weng, J. R., Tsao, L. T., Wang, J. P., Wu, R. R. and Lin, C. N. (2004). Anti-inflammatory phloroglucinols and terpenoids from *Garcinia subelliptica*. *J. Nat. Prod.*, **67**: 1796–1799.

- Williams, G. H. and Stoeber, K. (2012). The cell cycle and cancer. *J. Pathol.*, **226**: 352–364.
- Witherup, K. M., Look, S. A., Stasko, M. W., Ghiorzi, T. J., Muschik, G. M. and Cragg, G. M. (1990). Taxus Spp. Needles contain amounts of Taxol comparable to the bark of *Taxus brevifolia*: analysis and isolation. *J. Nat. Prod.*, **53**: 1249–1255.
- Wu, S. B., Long, C. and Kenelly, E. J. (2014). Structural diversity and bioactivities of natural benzophenones. *Nat. Prod. Rep.*, **31**: 1158–1174.
- Wu, C. C., Lu Y. H., Wei, B. L., Yang, S. C., Won, S. J. and Lin, C. N. (2008). Phloroglucinols with Prooxidant Activity from *Garcinia subelliptica*. *J. Nat. Prod.*, **71**: 246–250.
- Wusteman, F. S., Dodgson, K. S., Lloyd, A. G., Rose, F. A. and Tudball, N. (1964). Thin- layer chromatography in the study of ester sulphates. *J. Chromatogr. A*, **16**: 334–339.
- Xu, Y. J., Chiang, P. Y., Lai, Y. H., Vittal, J. J., Wu, X. H., Tan, B. K., Imiyabir, Z., Goh, S. H. (2000). Cytotoxic prenylated depsidones from *Garcinia parvifolia*. *J. Nat. Prod.*, **63**: 1361–1363.
- Yamaguchi, T., Goto, H., Yokohama, T., Siljie, H., Hanisch, A., Uldschmid, A., Takai, Y., Oguri, T., Nigg, E. A. and Inagaki M. (2005). Phosphorylation by Cdk1 induces Plk1-mediated vimentin phosphorylation during mitosis. *J. Cell Biol.*, **171**: 431–436.
- Yamashiro, S., Chern, H., Yamakita, Y. and Matsumura, F. (2001). Mutant Caldesmon lacking cdc2 phosphorylation sites delays M-phase entry and inhibits cytokinesis. *Mol. Biol. Cell*, **12**: 239–250.
- Yamashiro, S., Yamakita, Y., Hosoya, H. and Matsumura, F. (1991). Phosphorylation of non-muscle caldesmon by p34cdc2 kinase during mitosis. *Nature*, **349**: 169–172.
- Yamazaki, Y., Tanaka, K., Nicholson, B., Deyanat, G., Potts, B., Yoshida, T., Oda, A., Kitagawa, T., Orikasa, S., Kiso, Y., Yasui, H., Akamatsu, Miki., Chinen, T., Usui, T., Shinozaki, Y., Neuteboom, S., Palladino, M., Kanoh, K., Kenneth, Lloyd. and Hayashi, Y. (2012). Synthesis and Structure-Activity Relationship Study of Antimicrotubule Agents Phenylahistin Derivatives with a idehydropiperazine-2,5-dione Structure. *J. Med. Chem.*, **55**: 1056–1071.
- Zhang, L. J., Chiou, C. T., Cheng, J. J., Huang, H. C., Kuo, L. M., Liao, C. C., Bastow, K. F., Lee, K. H. and Kuo, Y. H. (2011). Cytotoxic Polyisoprenyl Benzophenonoids from *Garcinia subelliptica*. *J. Nat. Prod.*, **73**: 557–562.

Zhu, L., Chiao C. Y., Zhang, Q., Porco, J. A. Faller, D. V. and Dai, Y. (2014). Identification of a novel polyprenylated acylphloroglucinol-derived SIRT1 inhibitor with cancer-specific anti-proliferative and invasion-suppressing activities. *Int. J. Oncol.*, **45**: 2128-2136.

Zu, Y. G., Fu, Y., Li, S., Sun, R., Li, Q. and Schwarz, G. (2008). Rapid separation of four main taxoids in *Taxus* species by combined LLP-SPE-HPLC (PDA) procedure. *J. Chromatogr. A*, **1177**: 77–86.